Existence of Different Solitary Structures in Magnetized Nonthermal Dusty Plasma

by

Debdatta Debnath

THESIS SUBMITTED IN FULFILLMENT
OF THE REQUIREMENTS FOR THE DEGREE OF
DOCTOR OF PHILOSOPHY (SCIENCE)

at

JADAVPUR UNIVERSITY

188, RAJA S. C. MALLICK ROAD, KOLKATA - 700 032
WEST BENGAL, INDIA

FEBRUARY, 2022

Existence of Different Solitary Structures in Magnetized Nonthermal Dusty Plasma

by

Debdatta Debnath

THESIS SUBMITTED IN FULFILLMENT OF THE REQUIREMENTS FOR THE DEGREE OF DOCTOR OF PHILOSOPHY (SCIENCE)

at

JADAVPUR UNIVERSITY
188, RAJA S. C. MALLICK ROAD, KOLKATA - 700 032
WEST BENGAL, INDIA
FEBRUARY, 2022

যাদবপুর বিশ্ববিদ্যালয়

FACULTY OF SCIENCE
DEPARTMENT OF MATHEMATICS

JADAVPUR UNIVERSITY
Kolkata-700 032, India
Telephone : 91 (33) 2414 6717

CERTIFICATE FROM THE SUPERVISOR

This is to certify that the thesis entitled "**Existence of Different Solitary Structures in Magnetized Nonthermal Dusty Plasma"** submitted by Ms. **Debdatta Debnath** who got her name registered on **November 03, 2015** for the award of Ph.D. (Science) degree of Jadavpur University, is absolutely based upon her own work under the supervision of **Prof. Anup Bandyopadhyay**, Department of Mathematics, Jadavpur University, Kolkata, India and that neither this thesis nor any part of it has been submitted for either any degree / diploma or any other academic award anywhere before.

Anup Bandyopadhyay
15/02/2022

Prof. Anup Bandyopadhyay

(Signature of the Supervisor date with Official seal)

PROFESSOR
Dept. of Mathematics, Jadavpur University
Kolkata
700032

Dedicated to my parents:

Dipen Debnath

&

Rita Debnath

Table of Contents

Acknowledgements

Foremost, I would like to thank Prof. K. P. Das (retired), Department of Applied Mathematics, University of Calcutta, for his advice and helpful suggestions at different stages of my research work. I have been benefitted very much from his advice and enlightening comments.

Next, I would like to express my sincere gratitude to my guide, Prof. Anup Bandyopadhyay for the continuous support of my Ph.D. study and research, for his patience, motivation, enthusiasm and immense knowledge. His guidance helped me in all the time of research and writing of this thesis. I shall remain grateful forever to him for his affection, inspiration and valuable advice.

I would like to convey my thanks to Prof. Basudev Ghosh, Department of Physics, Jadavpur University, for his valuable comments on my work.

I would like to thank the members of the Centre for Plasma Studies, Jadavpur University. I have learnt a lot from them.

My sincere thanks also goes to the Heads of the Department of Mathematics, Jadavpur University, for giving me adequate facilities during the tenure of my research works. They rendered their support whenever it was needed. I also shall remain indebted to the teachers and staffs for their kind help, despite many adverse circumstances.

I would like to express my deep gratitude to Mrs. Jaba Bandyopadhyay and my fellow labmates, Sankirtan Sardar, Ashesh Paul, Sandip Dalui, Paltu Halder, Kushal Guha Bakshi, Ritwika Mondal, Sayeedul Islam, Sabiruddin Molla, Monsur Rahaman, for their constant encouragement and fruitful discussions which helped me to complete this work.

My very special thanks goes to Nupur Paul and Hiya Mondal, not only for their continuous support in various stages of my research work, but also for standing beside me in all my ups and downs during this Ph.D. tenure.

Last but not the least, I would like to thank my family: my father, Dipen Debnath, my mother, Rita Debnath, my elder sister, Debarati Debnath and my brother-in-law, Subhramanium Biswas, for their endless love and support at every step of my life.

I greatly appreciate the financial support offered by INSPIRE Fellowship Scheme, Department of Science and Technology, Government of India.

Debdatta Debnath.
15/02/2022

Date : February 15, 2022
Place : Jadavpur, Kolkata

Debdatta Debnath

List of published / accepted / communicated papers

1. *Ion acoustic solitary structures in a magnetized nonthermal dusty plasma*

   D. Debnath, A. Bandyopadhyay and K. P. Das

   ***Phys. Plasmas* 25**, Article No. 033704 (13 pages) (2018)

   https://doi.org/10.1063/1.5021127

2. *Combined effect of Kappa and Cairns distributed electrons on ion acoustic solitary structures in a collisionless magnetized dusty plasma*

   D. Debnath and A. Bandyopadhyay

   ***Astrophys. Space Sci.* 365**, Article No. 72 (18 pages) (2020)

   https://doi.org/10.1007/s10509-020-03786-6

3. *Ion acoustic solitary structures at the acoustic speed in a collisionless magnetized nonthermal dusty plasma*

   D. Debnath and A. Bandyopadhyay

   ***Zeitschrift fr Naturforschung A*, 76**, pp. 985-1005 (2021)

   https://doi.org/10.1515/zna-2021-0120

4. *Small amplitude ion acoustic solitary waves in a collisionless magnetized dusty plasma*

   D. Debnath, S. Sardar and A. Bandyopadhyay

   To be communicated

5. *Arbitrary amplitude ion acoustic solitary structures in a collisionless magnetized dusty plasma consisting of nonthermal electrons and isothermal positrons*

   D. Debnath and A. Bandyopadhyay

   To be communicated

Abstract

In this thesis, we have considered the following problems on the existence of ion acoustic (IA) solitary structures including double layers and supersolitons in a magnetized nonthermal dusty plasma.

Problem-1: Here, we have used Sagdeev potential technique to investigate the arbitrary amplitude IA solitary structures in a collisionless magnetized dusty plasma consisting of negatively charged static dust grains, adiabatic warm ions and nonthermal electrons. The present system supports both positive and negative potential solitary waves, coexistence of solitary waves of both polarities, and negative potential double layers. The system does not support any positive potential double layer. Although the system supports negative potential double layers, but these double layer solutions cannot restrict the occurrence of all solitary structures of same polarity. In fact, there exists a parameter regime for which the negative potential double layer is unable to restrict the occurrence of negative potential solitary waves, and in this region of the parameter space, there exist negative potential solitary waves after the formation of negative potential double layer. Consequently, negative potential supersolitons have been observed and the Mach number M corresponding to a negative potential supersoliton is restricted by the inequality $M_{NPDL} < M < M_{cr}$, but this supersoliton structure reduces to a conventional solitary wave of same polarity if $M \geq M_{cr}$, where M_{NPDL} is the Mach number corresponding to a negative potential double layer and M_{cr} is a critical value of M. Thus, we have seen a transition process of negative potential solitary structures, viz., soliton $\rightarrow$ double layer $\rightarrow$ supersoliton $\rightarrow$ soliton. Different solitary structures have been investigated with the help of compositional parameter spaces and the phase portraits of the dynamical system describing the nonlinear behaviour of IA waves. The mechanism of transition of a negative potential supersoliton to a conventional soliton after the formation of double layer of same polarity has been discussed with the help of phase portraits.

Problem-2: Here, we have considered the same plasma system as mentioned in **Problem-1**, but we have investigated the existence of IA solitary structures including double layers and supersolitons at the acoustic speed. At the acoustic speed, for negative polarity, the

system supports solitons, double layers, supersoliton structures after the formation of double layer, supersoliton structures without the formation of double layer, solitons after the formation of double layer whereas the system supports solitons and supersolitons without the formation of double layer for the case of positive polarity. But it is not possible to get the coexistence of solitary structures (including double layers and supersolitons) of opposite polarities. For negative polarity, we have observed an important transformation, viz., soliton before the formation of double layer $\rightarrow$ double layer $\rightarrow$ supersoliton $\rightarrow$ soliton after the formation of double layer whereas for both positive and negative polarities, we have observed the transformation from solitons to supersolitons without the formation of double layer. There does not exist any negative (positive) potential solitary structures within $0 < \mu < \mu_c$ ($\mu_c < \mu < 1$) and the amplitude of the positive (negative) potential solitary structure decreases for increasing (decreasing) μ and the solitary structures of both polarities collapse at $\mu = \mu_c$, where μ_c is a critical value of μ, the ratio of unperturbed number density of electrons to that of ions. Similarly, there exists a critical value β_{e2} of the nonthermal parameter β_e such that the solitons of both polarities collapse at $\beta_e = \beta_{e2}$.

Problem-3: This problem is an extension of **Problem-1** in the following direction: (1) Starting from one dimensional Kappa distribution for electrons, we have systematically developed the combined Kappa-Cairns distribution, (2) we have found the effective bounds of both nonthermal parameters κ and β_e for the combined Kappa-Cairns distribution. This distribution can generate more highly energetic particles in comparison with both Kappa and Cairns distributions. We have investigated IA solitary structures in a collisionless magnetized plasma composed of negatively charged static dust grains, adiabatic warm ions and a population of highly energetic electrons generated from the combined Kappa-Cairns distribution. Sagdeev pseudo potential technique has been considered to investigate the arbitrary amplitude steady state solitary structures including double layers and supersolitons. We have developed a computational scheme to draw the existence domains showing the nature of existence of different solitary structures. Different solitary structures of both positive and negative polarities have been observed for different values of κ and β_e . We have seen two important transitions of solitary structures for negative polarity, viz., soliton before the formation of double layer $\rightarrow$ double layer $\rightarrow$ supersoliton $\rightarrow$ soliton after the formation of double layer, and soliton before the formation of supersoliton $\rightarrow$ supersoliton

$\rightarrow$ soliton. For the second case, we have a supersoliton structure without the formation of double layer and this case is completely new one for magnetized plasma. Different solitary structures supported by the system have been investigated with the help of compositional parameter spaces and the phase portraits of the dynamical systems describing different solitary structures.

Problem-4: Here, the plasma system is same as the plasma system as defined in **Problem-3**, but here we have considered the Poisson equation instead of quasi-neutrality condition along with the different conservation equations to describe the nonlinear behaviour of IA waves. In this problem, we have derived a KdV-ZK (Korteweg-de Vries-Zakharov-Kuznetsov) equation to investigate the oblique propagation of weakly nonlinear and weakly dispersive IA waves in a collisionless magnetized plasma consisting of warm adiabatic ions, static negatively charged dust grains and combined Kappa-Cairns distribution of electrons. It is found that a factor (B_1) of the coefficient of the nonlinear term of the KdV-ZK equation vanishes along different families of curves in different parameter planes. In this situation, i.e., when $B_1 = 0$, we have derived a modified KdV-ZK (MKdV-ZK) equation to describe the nonlinear behaviour of IA waves. We have investigated the solitary wave solutions of these evolution equations propagating obliquely to the direction of the magnetic field. We have also discussed the effect of different parameters of the present plasma system on the amplitude of these solitary wave solutions.

Problem-5: The present problem is an extension of **Problem-1** in the following direction: instead of considering three-component collisionless magnetized plasma consisting of adiabatic warm ions, nonthermal electrons and static negatively charged dust grains, we have considered a collisionless magnetized four-component plasma consisting of adiabatic warm ions, nonthermal electrons, isothermal positrons and static negatively charged dust grains immersed in a static uniform magnetic field directed along a fixed direction. Arbitrary amplitude IA solitary structures have been investigated in the present plasma system. We have observed that the system supports positive potential solitary waves, negative potential solitary waves, coexistence of solitary waves of both polarities, negative potential double layers, negative potential supersolitons, positive potential supersolitons for different values of the parameters of the system. We have investigated the effect of different parameters of the system on the solitary structures.

Introduction

This thesis contains some problems on the existence of Ion Acoustic (IA) solitary structures including double layers and supersolitons in a collisionless magnetized multi-species plasma consisting of adiabatic warm ions, nonthermal electrons, negatively charged dust grains with or without positrons. Here, we have considered two types of nonthermal electron species. In some problems, we have considered the nonthermal distribution of electrons as prescribed by Cairns *et al.* [1] whereas with the aim of producing more energetic particles in a collisionless magnetized plasma system, we have considered the combined effect of Kappa and Cairns distributions. In fact, we have modified the Kappa distribution by imposing the nonthermal characteristics of Cairns distribution thereon. We have discussed different properties of this type of velocity distribution of energetic particles. In the introduction, we have presented the overall scenario of the thesis by considering the key points of each chapter. To begin the main topics of different chapters presented in this thesis, we have considered the following points:

- A brief review of the development of solitary waves
- Kappa distribution and Cairns distribution
- Combined Kappa-Cairns distribution
- Satellite observations
- Different methods used in the present thesis
- Overview of each chapter

A Brief Review of the Development of Solitary Waves

The early history of solitary waves began in the science of hydrodynamics. J. E. Allen [2] reported that in August 1834, while the Victorian Engineer and Naval Architect John Scott Russell [3] was inspecting the Union Canal at the outskirts of Edinburgh, he observed "a most beautiful and extraordinary phenomenon". Here we describe this discovery in his own words: "I was observing the motion of a boat which was rapidly drawn along a narrow channel by a pair of horses, when the boat suddenly stopped − not so the mass of water in the channel which it had put in motion; it accumulated round the prow of the vessel in a state of violent agitation, then suddenly leaving it behind, rolled forward with great velocity, assuming the form of a large solitary elevation, a round, smooth and well-defined heap of water, which continued its course along the channel apparently without change of form or diminution of speed. I followed it on a horseback, and overtook it still rolling on at a rate of some eight or nine miles an hour, preserving its original figure some thirty feet long and a foot to a foot and a half in height. Its height gradually diminished, and after a chase of one or two miles I lost it in the windings of the channel. Such, in the month of August 1834, was my first chance interview with that singular and beautiful phenomenon which I have called the Wave of Translation". Allen [2] also reported that Scott Russell had described his observations to Sir John Herschel, a leading scientist of those days and he was not impressed. Later on, Scott Russell carried out laboratory experiments and succeeded to reproduce the phenomenon of solitary waves. He performed this by having a small reservoir with a movable side at the end of a trough. On removing the partition, the water formed a solitary wave. Later on, several authors [4, 5] have theoretically investigated the solitary wave. Korteweg & deVries [6] gave a definite theory of solitary waves in 1895, working in Amsterdam. These authors were successful to deduce a nonlinear equation regarding

the solitary wave which is well-known as Korteweg-de Vries (KdV) equation. The subject of solitary waves was reborn in Plasma Physics in 1958 by Adlam & Allen [7] who discovered solitary waves in a collisionless magnetized plasma.

In 1949, Walter H. Munk [8] investigated and summarized the useful relationships derived by means of the solitary wave theory and plotted those relations using dimensionless parameters. Zabusky & Kruskal [9] discovered, by numerical investigation, that solitary waves retain their identity after colliding and these particle-like behaviour led the authors to introduce the term soliton replacing the term solitary wave. Washimi & Tanuiti [10] showed the one-dimensional long-time asymptotic behaviour of small but finite amplitude ion acoustic waves. Sagdeev [11] elucidated that the equations governing the dynamics of nonlinear ion acoustic waves can be written in the form of the energy integral of a classical particle in a potential well. Shukla & Yu [12] considered the problem of nonlinear ion acoustic waves in a magnetized plasma and found that the waves can propagate as a soliton whose motion is oblique to the external magnetic field. The authors found a relation between the angle of propagation, the speed and the amplitude of the soliton. The authors also presented an exact analytical formula for the electric field in the small amplitude limit. Bona *et al.* [13] examined the interaction of solitary wave solutions of a model equation for long waves in dispersive media numerically. They found that the waves do not emerge from the interaction unscathed, and two new solitary waves of slightly different amplitudes from the original waves, together with a small dispersive tail are generated as a result of interaction. Considering isothermal electrons, several authors [14–16] investigated the existence and stability of solitary waves in magnetized plasmas. On the other hand, several authors [17–24] studied the existence and stability of small amplitude solitary waves in a magnetized plasma by considering Cairns [1] distributed nonthermal electrons. Malfliet [25] proposed a method for obtaining traveling wave solutions of nonlinear wave equations that are essentially of a localized nature, based

on the fact that most solutions are functions of a hyperbolic tangent. Cairns *et al.* [26] investigated obliquely propagating ion acoustic solitons in a magnetized plasma composed of warm adiabatic ions and nonthermal electrons. The authors employed the reductive perturbation method to derive the Kortweg-de Vries equation which admits a solitary wave solution for small amplitude limit. They also studied the highly nonlinear situation by the numerical solution of the fully nonlinear system of equations. The authors reported that the presence of nonthermal electrons changes the nature of ion acoustic solitons. The soliton may change from compressive to rarefactive in the small amplitude limit, whereas the fully nonlinear equations may allow rarefactive and compressive solitary waves to coexist. The effects of external magnetic field, obliqueness and ion temperature on the amplitude and width of the compressive and rarefactive solitons have also been discussed. Yan & Zhang [27] presented a generalized transformation based on the Riccati-equation and applied it to solve Whitham-Broer Kaup (WBK) equation in shallow water, and as a result, they obtained many explicit exact solutions, which contain new solitary wave solutions, periodic wave solutions and combinations thereof. Mamun & Shukla [28] considered the nonlinear propagation of electron acoustic waves in a plasma consisting of a cold electron fluid, hot electrons obeying a trapped/vortex-like distribution and stationary ions. The authors studied the properties of small but finite amplitude electron acoustic solitary waves by employing the reductive perturbation method and the properties of arbitrary amplitude electron acoustic solitary waves have been investigated by means of the pseudo potential approach. Mamun & Shukla [29] investigated the properties of cylindrical and spherical dust ion acoustic solitary waves in an unmagnetized dusty plasma composed of inertial ions, Boltzmann electrons and stationary dust particles by employing the reductive perturbation technique. The authors derived the modified Kortweg-deVries equation and also obtained its numerical solutions. The

authors reported that the properties of dust ion acoustic solitary waves in a nonplanar cylindrical or spherical geometry differ from those in a planar one-dimensional geometry. Ghosh [30] investigated the role of negative ions on small but finite amplitude dust acoustic solitary wave including the effects of high and low charging rates of dust grains compared to the dust oscillation frequency in electronegative dusty plasma. The author has reported that the solitary wave is governed by Korteweg-de Vries (KdV) equation in case of high charging rate and it is governed by KdV equation with a linear damping term in case of low charging rate. The author has also reported that the soliton width decreases (increases) with the increase of negative ion number density (temperature). Dubinov *et al.* [31] proved a possibility of stationary solitary electrostatic waves with large amplitude in symmetric unmagnetized symmetric pair plasmas. Bandyopadhyay *et al.* [32] investigated the excitation and propagation of finite amplitude low frequency solitary waves in an argon plasma impregnated with kaolin dust particles. El-Awady & Moslem [33] studied the generation of nonlinear ion acoustic waves in a plasma having nonextensive electrons and positrons.

Kappa distribution and Cairns distribution

Alfvén [34] reported that the velocity distribution functions in many cosmic plasmas are non-Maxwellian as well as highly anisotropic due to the presence of an excess of highly energetic particles. But, there is no general mechanism to construct the velocity distribution function of energetic particles in the space plasma, consequently different non-Maxwellian velocity distribution functions have been constructed in phase space to describe the behaviour of the energetic particles on the basis of the assumption that the relaxation time of the energetic particles is not so small to reach thermal equilibrium [35]. Kappa distribution and the nonthermal velocity distribution of Cairns *et al.* [1] are two widely used non-Maxwellian models for energetic particles.

There are enormous evidence for the existence of a population of highly energetic electrons in space plasmas, resulting in a long high-energy tailed non-Maxwellian distribution [36]. Such a population of suprathermal electrons is generally modelled by a Kappa distribution which has the property that the number of particles in phase space far away from the point $v = 0$ is much greater than the number of particles in the same region for the case of a Maxwellian - Boltzmann distribution, where v is the velocity of the particle in phase space, and consequently the number of highly energetic particles is much larger in Kappa distribution in comparison with Maxwellian - Boltzmann distribution. Decades ago, Binsack [37] used Kappa distribution in his Ph.D. thesis where he mentioned that actually Kappa distribution was introduced by Prof. S. Olbert in his studies of plasmas on IMP-1 [38]. By the same time Vasyliunas [39] also used this distribution. Later, Kappa distribution was considered by many authors in various studies of plasma physics [40–57].

On the other hand, motivated by the observations of solitary structures with density depletion by the Freja satellite [58], Cairns *et al.* [1] reported that in presence of nonthermally distributed electrons with an excess of energetic particles, the nature of ion sound solitary structures changes its character and it is possible to obtain solutions with density depletion. A similar result was reported by Nishihara & Tajiri [59] for a two-electron-temperature plasma. In fact, for Cairns distributed nonthermal velocity distribution function of the energetic electrons [1], it can be easily checked that for increasing values of the nonthermal parameter (β_e), the distribution function develops wings, symmetrical with respect to the vertical axis $v = 0$, which become stronger as β_e increases, and consequently, nonthermal velocity distribution generates energetic particles for increasing values of β_e in finite region of phase space in the neighbourhood of $v = 0$. Therefore, for increasing β_e, distribution function develops wings, which become stronger as β_e increases, and at the same time the center density in phase space drops, the latter is a result of the normalization of the area under

the integral. Consequently, one cannot take values of $\beta_e > 4/7$ as that stage might stretch the credibility of the Cairns model too far [60]. Therefore, nonthermal velocity distribution of Cairns *et al.* [1] produces flattening at moderate values of v. So, Cairns distribution of nonthermal electrons [1] can describe the flattening of the distribution with respect to Maxwell - Boltzmann distribution as the background distribution. Cairns distribution [1] has been used by several authors to discuss different wave structures in various plasma systems [17, 61–78].

Combined Kappa-Cairns distribution

Kappa distribution has the property that the number of particles in phase space far away from the point $v = 0$ is much greater than the number of particles in the same region for the case of a Maxwellian - Boltzmann distribution whereas Cairns [1] distributed nonthermal velocity distribution function can be regarded as a modified Maxwellian - Boltzmann distribution which has the property that the number of particles in phase space in the neighbourhood of the point $v = 0$ is much smaller than the number of particles in phase space in the neighbourhood of the point $v = 0$ for the case of Maxwellian - Boltzmann distribution of the energetic electrons. So, Cairns distribution [1] describes the flattening of the distribution in phase space in the neighbourhood of the point $v = 0$ whereas Kappa distribution describes the flattening of the distribution in phase space far away from the point $v = 0$. Therefore, to consider the flattening of the Kappa distribution in the neighbourhood of $v = 0$, one can develop Cairns distribution with respect to Kappa distribution as the background distribution. The combined Kappa-Cairns distribution is aimed to describe the possible deviation from Kappa distribution in the neighbourhood of $v = 0$. So, in the combined Kappa-Cairns distribution, we have considered Kappa distribution as the background electron distribution and the deviation of this background distribution can be described by Cairns distribution. Therefore, our aim is to consider

the combined Kappa-Cairns distribution in those heliospheric environments in which flattening of the distribution can be discussed by Cairns distribution with respect to Kappa distribution as the background distribution. Figure 3.1 of Chapter-3 shows the flattening of the combined Kappa-Cairns distribution described by the nonthermal Cairns distribution with respect to Kappa distribution as the background distribution. In Chapter-3, starting from one dimensional Kappa distribution for electrons, we have systematically developed the combined Kappa-Cairns distribution. The effective bounds of both nonthermal parameters κ and β_e for the combined Kappa-Cairns distribution have been derived. This distribution can generate more highly energetic particles in comparison with both Kappa and Cairns distributions. This combined Kappa-Cairns distribution reduces to the one dimensional Kappa distribution when $\beta_e = 0$ whereas the combined Kappa-Cairns distribution reduces to nonthermal distribution of Cairns *et al.* [1] if $\kappa \to \infty$. On the other hand, if $\beta_e = 0$ and $\kappa \to \infty$, the combined Kappa-Cairns distribution is simplified to the isothermal Maxwellian - Boltzmann distribution.

Numerous studies have shown that Kappa distributions (or combinations thereof) are frequently observed in several space, geophysical and other plasmas, where the deviation from Maxwell is more evident in the high-energy tails of the observed distributions. Kappa distributions have been employed to describe space plasma population in the inner heliosphere, including solar wind [79, 80], the planetary magnetospheres, including magnetosheath [37–39], the outer heliosphere and inner heliosheath [81] etc. which can be described by the combined Kappa-Cairns distributions for even better accuracy.

High-energy tailed distributions (κ distributions) do not show major temperature anisotropies but this property of high-energy tailed κ distributions is not consistent with various space plasma observations [82]. In fact, the space plasma observations indicate the major temperature anisotropy in astrophysical environments. Again,

Pierrard *et al.* [83] reported that the electron temperatures are generally higher in the slow solar wind than in high-speed stream. An excess of parallel temperature has been observed to dominate the observations and it is significantly larger in high-speed streams than in the slower solar wind, while an excess of perpendicular temperature is more common in low-speed and high-density conditions. In both the cases, the temperature anisotropy is high and Kappa distribution cannot describe such particle population. The Combined Kappa-Cairns distribution is a more generalized distribution which may be relevant to serve this purpose.

Satellite Observations

Magnetized dusty plasma naturally occurs in numerous astrophysical environments, e.g., the planetary rings, asteroid zones, comets, the interstellar medium, the Earth's ionosphere and the Earth's magnetosphere [84–91]. Nonthermally distributed energetic particles in dusty plasmas are observed in a number of astrophysical environments [58, 92–107]. Specifically, the observations of electric field structures by the FAST [98–100, 103, 107] satellite, Viking satellite [94, 96], Freja satellite [58], GEOTAIL [97] and POLAR [101, 102, 107] missions in the Earth's magnetosphere, indicate the presence of fast energetic electrons. The electrostatic wave structures observed by the Freja satellite [58] can be described by Cairns [1] distributed nonthermal electrons.

The satellite observations by Vela 2 and Vela 3 [39] indicate that the plasma sheet electrons typically have a broad quasi-thermal energy spectrum, peaked anywhere between a few hundred electronvolt (ev) and a few kiloelectronvolt (kev), with a non-Maxwellian high-energy tail [108]. Now, the particle distribution in the neighbourhoods of the peaks can be well described by Cairns distribution whereas the particle population along the tail can be described by Kappa distribution. Alongside, there are many space plasma environments where the linear and nonlinear plasma phenomena [1, 39, 54, 109, 110] cannot be precisely described by Cairns distribution

or any such non-Maxwellian distribution.

Cairns distribution [1] can explain both positive and negative polarity structures observed in space plasmas. In fact, Cairns *et al.* [1] used this one dimensional non-thermal model to study the existence of nonlinear structures like those observed by the Freja [58] and Viking satellite [94, 96]. It was shown that this distribution can describe the existence of both positive and negative density perturbations, which could not be prevailed with Maxwellian electrons or κ distributed electrons. More specifically, the electric field structures observed by the FAST [98–100, 103, 107] satellite and Viking satellite [94, 96] in the auroral zone together with the Freja satellite [58] observations in the auroral zone of the upper ionosphere and the observations by GEOTAIL [97] and POLAR [101, 102, 107] missions in the Earth's magnetosphere indicate the existence of fast energetic electrons. In a number of astrophysical environments [58, 92–107], one can use Cairns distribution for lighter species.

Different Methods Used in the Present Thesis

We have used Sagdeev Pseudo Potential technique, Reductive Perturbation method and various methods of Applied Mathematics to solve the different problems presented in this thesis.

Overview of Each Chapter

Chapter-1

In this chapter, we have considered a collisionless magnetized dusty plasma system consisting of warm adiabatic ions, static negatively charged dust grains and non-thermal electrons, immersed in a uniform static magnetic field directed along a fixed direction. The nonlinear behaviour of IA waves can be described by the continuity equation of ions, the equation of motion of ion fluid and the pressure equation of ions. But instead of Poisson equation, we have used the quasi-neutrality condition to make

a closed and consistent system of equations. The quasi-neutrality condition is considered on the basis of the assumption that the length scale of the solitary structure is greater than the Debye length or the gyroradius [90, 111]. In this plasma system, IA solitary structures including double layers and supersolitons have been investigated with special emphases on the following points:

- Lifting the equation of continuity, equation of motion and the pressure equation for ion fluid in the wave frame moving with a constant velocity M normalized by C_s (ion acoustic speed) along a direction having direction cosines (l_x, l_y, l_z), using the appropriate boundary conditions for the solitary structures together with the condition that the electrostatic potential vanishes at infinity, the energy integral is derived. The Sagdeev pseudo potential function [11] associated with this energy integral is analysed to find the nature of existence of different solitary structures with respect to the basic parameters of the system and the Mach number M.

- For the first time, in the magnetized plasma, an analytic theory is presented to find the upper bound M_{pmax} (M_{nmax}) of M for the existence of all positive (negative) potential solitary structures, i.e., one can get positive (negative) potential solitary structures for $M_c < M < M_{pmax}$ ($M_c < M < M_{nmax}$), where M_c is the lower bound of M for the existence of solitary structures, i.e., solitary structures start to exist for $M > M_c$.

- For the first time, in the magnetized plasma, an analytic theory is presented to find the Mach number M_{PPDL} (M_{NPDL}) corresponding to a positive (negative) potential double layer [PPDL (NPDL)] solution of the energy integral, i.e., one can get a PPDL (NPDL) solution of the energy integral for $M = M_{PPDL}$ ($M = M_{NPDL}$).

- With the help of the different bounds of M for the existence of different solitary structures, we draw qualitatively different compositional parameter spaces which show the nature of existence of different solitary structures with respect to any parameter of the system.

- The regions of existence of different solitary structures in a compositional parameter space have been clearly indicated. The compositional parameter space shows the existence of negative potential solitons after the formation of NPDL and consequently formation of negative potential supersolitons (NPSSs) is confirmed. The description of solitary structures after the formation of double layer of same polarity through the compositional parameter space is helpful for investigating the existence of supersoliton structures in comparison with the study of supersoliton structures at some discrete points of the compositional parameter spaces. But still now supersoliton structures in magnetized plasma have been discussed at some discrete points of the compositional parameter spaces without giving a proper reason for the existence of the supersoliton structures at those points of the compositional parameter spaces. This is purely based on the trial and error method. But if we can draw the existence domains for the different solitary structures, then these existence domains clearly indicate the region of existence of solitons after the formation of NPDL, which gives an idea regarding the existence domain of NPSSs in the compositional parameter spaces. But of course, this compositional parameter space cannot clearly indicate the upper bound of M for the existence of NPSSs.

- We have analyzed the formation of supersoliton structures and their limitations with the help of phase portraits of the dynamical system describing the nonlinear behaviour of IA waves. This analysis determines the exact bound of M for the existence of NPSSs.

- For the first time, in the magnetized plasma, the mechanism of transition from the NPSS to a negative potential conventional soliton (soliton before the formation of double layer of same polarity) after the formation of double layer of same polarity has been investigated through the phase portrait analysis.

Chapter-2

In this chapter, we have considered the same plasma system as mentioned in Chapter-1 but here, we have investigated the existence and the nature of different ion acoustic solitary structures including double layers and supersolitons **at the acoustic speed** giving special emphases on the following points:

- Lifting the hydrodynamic equations in the wave frame moving with a constant velocity M normalized by the ion acoustic speed C_s along the direction having unit vector $\widehat{L} = l_x\widehat{x} + l_y\widehat{y} + l_z\widehat{z}$, we have derived the energy integral with $V(M, \phi)$ being the Sagdeev pseudo potential and for $M = M_c$, one can analyze $V(M, \phi)(= V(M_c, \phi))$ to investigate the existence and the nature of different solitary structures at the acoustic speed.

- At the acoustic speed, the Mach number M is given by the equation : $M = M_c = l_z M_s$, where M_s is a function of $\gamma(= 5/3)$, σ_{ie}, β_e and μ, i.e., $M_s = M_s(\gamma,\ \sigma_{ie},\ \beta_e,\ \mu)$. So, one can take the variation of M_s with respect to β_e or μ because $\gamma(= 5/3)$ is a fixed parameter and σ_{ie} can also be taken as fixed for specific plasma system. So, in the present work, we want to investigate the existence and the nature of different solitary structures along the curve $M = M_c$.

- For the first time, in the magnetized plasma, we have critically discussed the criteria for the existence of different solitary structures at the acoustic speed, i.e., at $M = M_c$. We have seen that the criteria for the existence of different

solitary structures at the acoustic speed depend on $V(M_c, \phi)$ but the polarity of different solitary structures depends on the sign of the derivative of $V(M_c, \phi)$ with respect to ϕ at $\phi = 0$.

- We have found that $V(M_c, 0) = 0$, $V'(M_c, 0) = 0$, $V''(M_c, 0) = 0$ and in this case, the polarity of the solitary structures depends on the sign of $V'''(M_c, 0)$. In particular, $V'''(M_c, 0) < 0$ implies that the system may support positive potential soliton structures including positive potential double layers and positive potential supersolitons at the acoustic speed whereas $V'''(M_c, 0) > 0$ implies that the system may support negative potential soliton structures including negative potential double layers and negative potential supersolitons at the acoustic speed. If $V'''(M_c, 0) = 0$, then one can discuss the nature of the solitary structure by considering the sign of $V^{iv}(M_c, 0)$.

- For the first time, in the magnetized plasma, we have investigated different ion acoustic solitary structures at the acoustic speed. In fact, we have observed the existence of the following solitary structures at the acoustic speed, i.e., at $M = M_c$: (a) positive potential solitary waves (PPSWs), (b) negative potential solitary waves (NPSWs), (c) negative potential double layers (NPDLs), (d) negative potential supersoliton (NPSS) structures after the formation of NPDL, (e) NPSS structures without the formation of NPDL, (f) NPSW structures after the formation of NPDL, (g) positive potential supersoliton (PPSS) structures without the formation of positive potential double layer (PPDL).

- At the acoustic speed, we have observed that it is not possible to get (a) coexistence of both PPSW and NPSW structures, (b) coexistence of both PPDL and NPDL structures, (c) coexistence of both PPSS and NPSS structures. In fact, for the first time in the magnetized plasma, we have observed that there is

no coexistence of solitary structures of opposite polarities at the acoustic speed which supports an important result (THEOREM 5) derived by Das *et al.* [70].

- At the acoustic speed, we have observed that the amplitude of negative potential soliton decreases with increasing β_e whereas the amplitude of positive potential soliton decreases with decreasing β_e and both negative and positive potential solitons collapse at the critical value β_{e2} of β_e such that $V'''(M_c, 0) = 0$ at $\beta_e = \beta_{e2}$. At this point of the compositional parameter space of $V'''(M_c, 0)$ with respect to β_e, we have $V^{iv}(M_c, 0) > 0$ which indicates that it is impossible to get any solitary structure at $\beta_e = \beta_{e2}$.

- At the acoustic speed, we have seen that the amplitude of negative potential soliton increases with increasing μ whereas the amplitude of positive potential soliton decreases with increasing μ and both negative and positive potential solitons collapse at the critical value μ_c of μ such that $V'''(M_c, 0) = 0$ at $\mu = \mu_c$. At this point of the compositional parameter space $V'''(M_c, 0)$ with respect to μ, we have $V^{iv}(M_c, 0) > 0$ which indicates that it is impossible to get any solitary structure at $\mu = \mu_c$.

- For the first time, in the magnetized plasma, phase portraits corresponding to the different solitary structures have been drawn at the acoustic speed to make a clear difference between the conventional soliton structures, double layer structures and supersoliton structures that we have obtained for the present plasma system.

- For the first time, in the magnetized plasma, the transformation process of different negative potential solitary structures has been investigated at the acoustic speed, viz., NPSW (before the formation of NPDL) $\rightarrow$ NPDL $\rightarrow$ NPSS $\rightarrow$ NPSW (after the formation of NPDL). In fact, we have investigated the

transformation of different negative potential solitary structures at the acoustic speed just before and just after the formation of double layer.

- For the first time, in the magnetized plasma, the transformation process of NPSW structures has also been considered at the acoustic speed without the formation of double layer structure of same polarity, viz., NPSW $\rightarrow$ NPSS, i.e., here we have investigated the transformation of different negative potential solitary structures at the acoustic speed just before the formation of NPSS. Similar process of transformation from PPSW structure to PPSS structure at the acoustic speed can also be verified when there is no double layer of same polarity.

Chapter-3

This chapter can be regarded as an extension of Chapter-1 in the following direction: we have considered the combined Kappa-Cairns distribution of electrons instead of taking Cairns [1] distributed nonthermal electrons. In this chapter, we have systematically investigated the combined Kappa-Cairns distribution to produce more energetic particles in comparison with both Kappa and Cairns distributions. In fact, we modify the Kappa distribution by imposing the nonthermal characteristics of Cairns distribution thereon. We have discussed different important properties of this new distribution and finally, we have investigated ion acoustic solitary structures in a collisionless magnetized dusty plasma consisting of negatively charged static dust grains, adiabatic warm ions and combined Kappa-Cairns distributed electrons giving special emphases on the following points. This problem is completely new in literature.

- We have systematically derived combined Kappa-Cairns distribution and this distribution reduces to the one dimensional Kappa distribution as defined by several authors [43, 110, 112] when $\beta_e = 0$. On the other hand, if $\kappa \rightarrow \infty$, the combined Kappa-Cairns distribution reduces to nonthermal distribution of

Cairns *et al.* [1] whereas if $\beta_e = 0$ and $\kappa \to \infty$, the combined Kappa-Cairns distribution is simplified to the isothermal distribution.

- For combined effect of Kappa and Cairns distributions, we have found the lower bound of the parameter κ for which combined effect of Kappa and Cairns distributions is well defined as a velocity distribution in phase space.

- We have analytically studied the dependence of the upper bound (β_{eT}) of β_e as a function of κ, i.e., we have shown that β_e is restricted by the inequality $0 \leq \beta_e \leq \beta_{eT}$, where β_{eT} is a function of κ.

- We have shown that as κ tends to ∞, the upper bound β_{eT} of β_e is equal to $4/7$, i.e., when the combined distribution reduces to the nonthermal distribution, the maximum value of the nonthermal parameter is $4/7$ which has already been reported by Verheest & Pillay [60].

- We have derived the expression of the number density of electron species that follows the combined Kappa-Cairns velocty distribution in phase space.

- For the first time in magnetized plasma, we have considered the combined effect of Kappa and Cairns distributions on the solitary structures of the ion acoustic wave in a collisionless magnetized dusty plasma.

- For the first time in magnetized plasma, considering the number density of electrons for combined Kappa-Cairns distribution, we have used Sagdeev pseudo potential method to investigate the arbitrary amplitude ion acoustic solitary structures in a collisionless magnetized dusty plasma.

- For the present plasma system, considering different bounds of Mach number, we have presented different compositional parameter spaces with respect to the nonthermal parameter β_e. These compositional parameter spaces clearly show

the existence domains of different types of solitary structures for different values of κ and other parameters of the system.

- From the different compositional parameter spaces with respect to the non-thermal parameter β_e, we have seen the existence of different solitary structures, viz., negative potential solitary waves (NPSWs), positive potential solitary waves (PPSWs), negative potential double layers (NPDLs), coexistence of positive and negative potential solitary waves and negative potential solitary waves after the formation of NPDL for different ranges of β_e and κ. But the existence of negative potential solitary waves after the formation of NPDL confirms the existence of negative potential supersolitons (NPSSs) also. For large values of Kappa, the above mentioned solitary structures are qualitatively same as observed in Chapter-1. In this connection, we would like to mention that Dubinov & Kolotkov [113] first elaborately investigated supersoliton structures in unmagnetized plasma. After that several authors [69, 71–77, 114–120] investigated supersoliton structures in different unmagnetized and magnetized plasma systems.

- For the first time in magnetized plasma, we have observed both types of negative potential supersolitons, viz., negative potential supersoliton after the formation of negative potential double layer and negative potential supersoliton without the formation of double layer. Although in an unmagnetized plasma, Verheest *et al.* [114] have shown the existence of supersoliton without the formation of double layer of same polarity.

- For the first time in magnetized plasma, we have analyzed a new transition of solitary structures: soliton $\rightarrow$ supersoliton $\rightarrow$ soliton. This type of transition

was not found in Chapter-1 where we considered only Cairns distributed non-thermal electrons. We have also found the well known transition of solitary structures: soliton → double layer → supersoliton → soliton in the present plasma system.

Chapter-4

In this chapter, we have considered the same plasma system as mentioned in Chapter-3 but we have considered the Poisson equation instead of quasi-neutrality condition along with the different conservation equations as described in Chapter-3 to investigate the nonlinear behaviour of small amplitude ion acoustic waves giving special emphases on the following points:

- To discuss the nonlinear behaviour of the small amplitude ion acoustic waves in a collisionless magnetized plasma consisting of warm adiabatic ions, static negatively charged dust grains and combined Kappa-Cairns distribution of electrons, we have derived the following Korteweg-de Vries-Zakharov-Kuznetsov (KdV - ZK) equation:

$$\frac{\partial \phi^{(1)}}{\partial \tau} + AB_1\phi^{(1)}\frac{\partial \phi^{(1)}}{\partial \zeta} + \frac{1}{2}A\frac{\partial^3 \phi^{(1)}}{\partial \zeta^3} + \frac{1}{2}AD\frac{\partial}{\partial \zeta}\left(\nabla^2_{\perp\xi}\phi^{(1)}\right) = 0, \tag{1}$$

  where B_1, A and D are functions of the parameters of the plasma system.

- We have observed that a factor (B_1) of the coefficient of the nonlinear term of the KdV-ZK equation vanishes along a family of curves in different parameter planes and for this case, following modified KdV-ZK (MKdV-ZK) equation can effectively describe the nonlinear behaviour of the ion acoustic wave:

$$\frac{\partial \phi^{(1)}}{\partial \tau} + AB_2(\phi^{(1)})^2\frac{\partial \phi^{(1)}}{\partial \zeta} + \frac{1}{2}A\frac{\partial^3 \phi^{(1)}}{\partial \zeta^3} + \frac{1}{2}AD\frac{\partial}{\partial \zeta}\left(\nabla^2_{\perp\xi}\phi^{(1)}\right) = 0, \tag{2}$$

  where B_2 is a function of the parameters of the plasma system.

- We have derived the solitary wave solutions of both KdV - ZK and MKdV - ZK equations propagating obliquely to the direction of the magnetic field. Again it is easy to check that the MKdV-ZK equation admits the coexistence of both negative and positive potential solitary waves because $\phi^{(1)}$ is a solution of the MKdV-ZK equation $\Leftrightarrow -\phi^{(1)}$ is also a solution of the same MKdV-ZK equation.

For KdV solitons, we have observed the following points:

- The amplitude of the negative potential soliton decreases with increasing β_e whareas the amplitude of the positive potential soliton increases with increasing β_e, where β_e is the nonthermal parameter associated with Cairns [1] distribution.

- The amplitude of the negative potential soliton increases with increasing κ whareas the amplitude of the positive potential soliton decreases with increasing κ, where κ is the parameter associated with κ distribution.

- The amplitude of the negative potential soliton decreases with increasing δ and also the amplitude of the positive potential soliton decreases with increasing δ, where δ is the angle between the direction of propagation of the wave and direction of the magnetic field.

For MKdV solitons, we have observed the following points:

- The amplitude of the soliton increases with increasing β_e for both positive potential and negative potential solitons.

- The amplitude of the soliton decreases with increasing κ for both positive potential and negative potential solitons.

- The amplitude of the soliton decreases with increasing δ for both positive potential and negative potential solitons.

Chapter-5

This chapter can be regarded as an extension of Chapter-1 in the following direction: In this chapter, we have considered a collisionless magnetized four-component plasma consisting of adiabatic warm ions, nonthermal electrons, isothermal positrons and static negatively charged dust grains immersed in a static uniform magnetic field directed along a fixed direction instead of considering three-component collisionless magnetized plasma consisting of adiabatic warm ions, nonthermal electrons and static negatively charged dust grains. So, in the present plasma system, we have considered isothermal positron species along with adiabatic warm ions, nonthermal electrons, isothermal positrons and static negatively charged dust grains.

We have used the Sagdeev pseudo potential method to determine and analyze the nonlinear behaviour of the ion acoustic wave. We have observed that the system supports NPSWs, NPDLs, NPSSs, NPSWs after the formation of NPDL, PPSWs, coexistence of PPSS and NPSW, PPSS, coexistence of PPSW and NPSW. The phase portrait of the dynamical system describing the nonlinear behaviour of ion acoustic wave has been drawn to confirm the existence of NPSS.

The parameters of the system are μ, p, β_e, l_z and M. We have observed the nature of the solitary structures with respect to each of the parameters of the system. For NPSWs,

- the amplitude of NPSW increases with increasing p,
- the amplitude of NPSW decreases with increasing β_e,
- the amplitude of NPSW increases with increasing μ,
- the amplitude of NPSW decreases with increasing l_z and
- the amplitude of NPSW increases with increasing M.

We have also examined the variations of the amplitude of negative potential supersolitons (NPSS) with respect to β_e and μ individually. We have seen that the amplitude of NPSS decreases with increasing β_e whereas the amplitude of NPSSs increases with increasing μ.

We have studied the variations of the amplitude of PPSWs with respect to μ, p and l_z for both isothermal electrons and isothermal positrons, i.e., we have considered $\beta_e = 0$. For PPSWs,

- the amplitude of PPSW increases for increasing μ,
- the amplitude of PPSW increases with increasing p and
- the amplitude of PPSW decreases with increasing l_z.

We have also determined a critical value p_c of positron concentration p such that the system supports only positive potential solitary structures and no negative potential solitary structures for $p > p_c$. For $\mu = 0.6, \beta_e = 0.235, l_z = 0.6, M = 0.9$, the value of p_c is 0.00002.

Chapter 1

Ion acoustic solitary structures in a magnetized nonthermal dusty plasma *

In this chapter, we have used Sagdeev potential technique to investigate the arbitrary amplitude ion acoustic solitary structures in a collisionless magnetized dusty plasma consisting of negatively charged static dust grains, adiabatic warm ions and nonthermal electrons. The present system supports both positive and negative potential solitary waves, coexistence of solitary waves of both polarities, and negative potential double layers. The system does not support any positive potential double layer. Although the system supports negative potential double layers, but these double layer solutions cannot restrict the occurrence of all solitary structures of same polarity. In fact, there exists a parameter regime for which the negative potential double layer is unable to restrict the occurrence of negative potential solitary waves, and in this region of the parameter space, there exist negative potential solitary waves after the formation of negative potential double layer. Consequently, negative potential supersolitons have been observed and the Mach number M corresponding to a negative potential supersoliton is restricted by the inequality $M_{NPDL} < M < M_{cr}$, but this supersoliton structure reduces to a conventional solitary wave of same polarity if $M \geq M_{cr}$, where M_{NPDL} is the Mach number corresponding to a negative potential double layer and M_{cr} is a critical value of M. Thus, we have seen a transition process of negative potential solitary structures, viz., soliton $\rightarrow$ double layer $\rightarrow$ supersoliton $\rightarrow$ soliton. Different solitary structures have been investigated with the help of compositional parameter spaces and the phase portraits of the dynamical system describing the nonlinear behaviour of ion acoustic waves. The mechanism of transition of a negative potential supersoliton to a conventional soliton after the formation of double layer of same polarity has been discussed with the help of phase portraits.

*This chapter has been published in ***Physics of Plasmas*** **25**, 033704 (2018); https://doi.org/10.1063/1.5021127

1.1 Introduction

Magnetized dusty plasma naturally occurs in a number of astrophysical environments such as the planetary rings, asteroid zones, comets, the interstellar medium, the Earth's ionosphere and the Earth's magnetosphere [84–91]. Acoustic wave modes in unmagnetized or magnetized dusty plasma have received a great deal of attention since the last few decades. There can exist two or more acoustic waves in a typical dusty plasma depending on different time scales. Dust acoustic [86] (DA) and dust ion acoustic [121] (DIA) waves are two such acoustic waves in a collisionless unmagnetized plasma containing electrons, ions, and charged dust grains. For the first time, Shukla & Silin [121] reported that a collisionless unmagnetized dusty plasma supports low-frequency DIA waves with phase velocity much smaller (larger) than electron (ion) thermal velocity. For long wavelength plane wave perturbation, the dispersion relation of DIA wave is similar to that of ion acoustic (IA) wave for a plasma with $T_i << T_e$ and n_{e0}/n_{i0} is of moderate magnitude for dusty plasma system, where T_i (T_e) is the average ion (electron) temperature and n_{e0} (n_{i0}) is the unperturbed number density of electrons (ions). For the case of usual two-component electron - ion plasma, the above two conditions are modified as follows: $T_i << T_e$ and $n_{e0} = n_{i0}$. Thus, IA waves in dusty plasmas are basically IA waves modified by the presence of heavy dust particulates. In the present chapter, we have investigated IA solitary structures in a collisionless magnetized dusty plasma system consisting of warm adiabatic ions, static negatively charged dust grains and nonthermal electrons, immersed in a uniform static magnetic field directed along a fixed direction.

Yinhua & Yu [122] have investigated ion acoustic (IA) solitary waves propagating obliquely to an external uniform static magnetic field in presence of heavy dust particulates. They have found the existence of small amplitude IA solitary waves. Choi *et al.* [90] have studied IA solitary waves obliquely propagating to an external magnetic field in a collisionless magnetized dusty plasma. Later, Choi *et al.*[111] have

studied the effect of ion temperature on the IA solitary waves by considering the isothermal ion pressure. Maitra & Roychoudhury [123] have studied the IA solitary waves in a collisionless magnetized dusty plasma, but they have used Poisson equation instead of taking quasi-neutrality condition. In the above mentioned papers, the authors have used Sagdeev potential formalism. But finally, they have expanded the Sagdeev potential in a Taylor series up to a finite order of an appropriate dependent variable to investigate small but finite amplitude solitary structures. Several authors [69, 124–140] have studied DIA / IA solitary structures in different unmagnetized / magnetized dusty plasmas. Some authors [69, 130, 136, 138–140] considered the nonthermal electrons in different unmagnetized or magnetized dusty plasmas.

Nonthermally distributed energetic particles in dusty plasmas are observed in a number of astrophysical environments [58, 92–107]. Specifically, the observations of electric field structures by the FAST [98–100, 103, 107] Satellite, Viking Satellite [94, 96], Freja Satellite [58] and GEOTAIL [97] and POLAR [101, 102, 107] missions in the Earth's magnetosphere, indicate the existence of fast energetic electrons. The electrostatic wave structures observed by the Freja Satellite [58] can be described by Cairns [1] distributed nonthermal electrons. Following Cairns *et al.* [1], the number density of nonthermal energetic electrons can be written as

$$n_e = \int_{-\infty}^{\infty} f_{e0}\left(v^2 - \frac{2e}{m_e}\phi\right)dv, \tag{1.1.1}$$

where $-e$ is the charge of an electron, m_e is the mass of an electron, ϕ is the electrostatic potential and $f_{e0}(v^2)$ is given by

$$f_{e0}(v^2) = \frac{n_{e0}\left[1 + \alpha_e\left(\frac{v}{v_{te}}\right)^4\right]}{(1+3\alpha_e)\sqrt{2\pi}v_{te}} \exp\Big[-\frac{v^2}{2v_{te}^2}\Big], \tag{1.1.2}$$

with $v_{te} = \sqrt{(K_B T_e)/m_e}$, $\alpha_e \geq 0$ and K_B is the Boltzmann constant.
From (1.1.1) and (1.1.2), we get

$$\frac{n_e}{n_{e0}} = \Big(1 - \beta_e\frac{e\phi}{K_B T_e} + \beta_e\frac{e^2\phi^2}{K_B^2 T_e^2}\Big)\exp\Big[\frac{e\phi}{K_B T_e}\Big], \tag{1.1.3}$$

Here $\beta_e = 4\alpha_e/(1+3\alpha_e)$ with $\alpha_e \geq 0$ and for $\alpha_e = 0$ ($\alpha_e = 0 \Leftrightarrow \beta_e = 0$), we get the usual isothermal distribution of electrons. It is simple to check that β_e is an increasing function of α_e. Here β_e (or α_e) is the nonthermal parameter that determines the proportion of the fast energetic particles. Using the inequality $\alpha_e \geq 0$, it is simple to check that $0 \leq \beta_e < 4/3$. However, we cannot take the entire region of β_e ($0 \leq \beta_e < 4/3$). In fact, if we plot the nonthermal velocity distribution ($f_{e0}(v^2)$) against its velocity (v) in phase space, then we see that for increasing β_e, distribution function develops wings which become stronger as β_e increases. At the same time the center density in phase space drops, consequently we should not take values of $\beta_e > 4/7$, since that stage might stretch the credibility of the Cairns model too far [60]. In fact, for $\beta_e > 4/7$, the nonthermal velocity distribution function of Cairns *et al.* [1] attains three maximum values at three different points $v = -v_{te} \times \sqrt{2 + \sqrt{7 - 4(\beta_e)^{-1}}}$, $v = 0$ and $v = v_{te} \times \sqrt{2 + \sqrt{7 - 4(\beta_e)^{-1}}}$ in phase space and consequently this property of the nonthermal velocity distribution function of Cairns *et al.* [1] is qualitatively different from Maxwellian velocity distribution function because Maxwell - Boltzmann velocity distribution function has only one maximum at $v = 0$. For example, for $\beta_e = 0.58 > 4/7(\approx 0.571429)$, the nonthermal velocity distribution function of Cairns *et al.* [1] has three maxima at the points $v = -1.52369 \times v_{te}$, $v = 0$ and $v = 1.52369 \times v_{te}$. But here our aim is to construct a distribution function which can produce more energetic particles in comparison with the Maxwell - Boltzmann velocity distribution function without changing the qualitative behaviour, i.e., the distribution function has only one maximum. So, we see that the nonthermal distribution of Cairns *et al.* [1] describes the non isothermal distribution having a deviation from the Maxwell - Boltzmann distribution if β_e is restricted by the inequality $0 \leq \beta_e \leq 4/7$. So, the effective range of β_e is $0 \leq \beta_e \leq 4/7$. As $4/7 \approx 0.571429$, in the present chapter, we take $0 \leq \beta_e \leq 0.57$.

In the present chapter, we have considered a collisionless magnetized dusty plasma system consisting of warm adiabatic ions, static negatively charged dust grains and

nonthermal electrons , immersed in a uniform static magnetic field directed along a fixed direction. The nonlinear behaviour of IA waves can be described by the continuity equation of ions, the equation of motion of ion fluid and the pressure equation of ions. But instead of Poisson equation, we have used the quasi-neutrality condition to make a closed and consistent system of equations. The quasi-neutrality condition is considered on the basis of the assumption that the length scale of the solitary structure is greater than the Debye length or the gyroradius [90, 111]. In this plasma system, IA solitary structures including double layers and supersolitons have been investigated with special emphases on the following points:

- Lifting the equation of continuity, equation of motion and the pressure equation for ion fluid in the wave frame moving with a constant velocity M normalized by C_s (ion acoustic speed) along a direction having direction cosines (l_x, l_y, l_z), using the appropriate boundary conditions for the solitary structures together with the condition that the electrostatic potential vanishes at infinity, an energy integral is derived. The Sagdeev pseudo potential function [11] associated with this energy integral is analysed to find the nature of existence of different solitary structures with respect to the basic parameters of the system.

- For the first time, in the magnetized plasma, an analytic theory is presented to find the upper bound M_{pmax} (M_{nmax}) of M for the existence of all positive (negative) potential solitary structures, i.e., one can get positive (negative) potential solitary structures for $M_c < M < M_{pmax}$ ($M_c < M < M_{nmax}$), where M_c is the lower bound of M for the existence of solitary structures, i.e., solitary structures start to exist for $M > M_c$.

- For the first time, in the magnetized plasma, an analytic theory is presented to find the Mach number M_{PPDL} (M_{NPDL}) corresponding to a positive (negative) potential double layer [PPDL (NPDL)] solution of the energy integral, i.e., one can get a PPDL (NPDL) solution of the energy integral for $M = M_{PPDL}$

$(M = M_{NPDL})$.

- With the help of the different bounds of M for the existence of different solitary structures, we draw qualitatively different compositional parameter spaces which show the nature of existence of different solitary structures with respect to any parameter of the system.

- The regions of existence of different solitary structures in a compositional parameter space have been clearly indicated. The compositional parameter space shows the existence of negative potential solitons after the formation of NPDL and consequently formation of negative potential supersolitons (NPSSs) is confirmed. The description of solitary structures after the formation of double layer of same polarity through the compositional parameter space is helpful for investigating the existence of supersoliton structures in comparison with the study of supersoliton structures at some discrete points of the compositional parameter spaces. But still now supersoliton structures in magnetized plasma have been discussed at some discrete points of the compositional parameter spaces without giving a proper reason for the existence of the supersoliton structures at those points of the compositional parameter spaces. This is purely based on the trial and error method. But if we can draw the existence domains for the different solitary structures, then these existence domains clearly indicate the region of existence of solitons after the formation of NPDL, which gives an idea regarding the existence domain of NPSSs in the compositional parameter spaces. But of course, this compositional parameter space cannot clearly indicate the upper bound of M for the existence of NPSSs.

- We have analyzed the formation of supersoliton structures and their limitations with the help of phase portraits of the dynamical system describing the nonlinear behaviour of IA waves. This analysis determines the exact bound of M for the existence of NPSSs.

- For the first time, in the magnetized plasma, the mechanism of transition from the NPSS to a negative potential conventional soliton (soliton before the formation of double layer of same polarity) after the formation of double layer of same polarity has been investigated through the phase portrait analysis.

1.2 Basic Equations

Here we consider a dusty plasma system consisting of warm adiabatic ions, static negatively charged dust grains and nonthermal electrons immersed in a uniform (space independent) static (time independent) magnetic field ($\overrightarrow{B} = B_0\widehat{z}$) directed along $z-$axis. The nonlinear behaviour of IA waves can be described by the continuity equation, the equation of motion and the pressure equation of ion fluid together with the quasi-neutrality condition:

$$\frac{\partial n_i}{\partial t} + \overrightarrow{\nabla} \cdot (n_i \overrightarrow{u}_i) = 0, \tag{1.2.1}$$

$$\Big(\frac{\partial}{\partial t} + \overrightarrow{u}_i \cdot \overrightarrow{\nabla}\Big)\overrightarrow{u}_i + \frac{\sigma_{ie}}{n_i}\overrightarrow{\nabla} p_i = -\overrightarrow{\nabla}\phi + \overrightarrow{u}_i \times \widehat{z}, \tag{1.2.2}$$

$$\frac{\partial p_i}{\partial t} + (\overrightarrow{u}_i \cdot \overrightarrow{\nabla}) p_i + \gamma p_i (\overrightarrow{\nabla} \cdot \overrightarrow{u}_i) = 0, \tag{1.2.3}$$

$$n_i = n_e + 1 - \mu, \tag{1.2.4}$$

The equations (1.2.1) - (1.2.3) are supplemented by following equilibrium charge neutrality condition:

$$\frac{Z_d n_{d0}}{n_{i0}} = 1 - \mu. \tag{1.2.5}$$

Here n_i, n_e, $\overrightarrow{u}_i = (u_{ix}, u_{iy}, u_{iz})$, p_i, ϕ, (x, y, z), and t are, respectively, the ion number density, the electron number density, the ion fluid velocity, the ion fluid pressure, the electrostatic potential, the spatial variables and time, and they have been nomalized

by n_{i0} (unperturbed ion number density), n_{i0}, C_s $(= \sqrt{\frac{K_B T_e}{m_i}})$, $n_{i0} K_B T_i$, $\frac{K_B T_e}{e}$, $r_g = C_s/\omega_c$ and $(\omega_c)^{-1}$ respectively. It is important to note that each spatial variable is normalized by ion gyroradius (r_g) and time is normalized by the inverse of ion gyrofrequency $((\omega_c)^{-1})$. Here m_i is the mass of an ion, n_{d0} and Z_d are, respectively, the unperturbed dust number density and the number of electrons residing on the dust grain surface, $\gamma(= \frac{5}{3})$ is the adiabatic index, $\sigma_{ie} = \frac{T_i}{T_e}$, $\mu = \frac{n_{e0}}{n_{i0}}$.

Under the above mentioned normalization of the field variables, the number density (n_e) as given by the equation (1.1.3) of nonthermal electrons [1] can be written as

$$n_e = \mu\big(1 - \beta_e\phi + \beta_e\phi^2\big)e^{\phi}. \tag{1.2.6}$$

The linear dispersion relation for low frequency $(\omega << \omega_c)$ IA waves obtained from the original system of equations (without any normalization of the independent and dependent variables) corresponding to the equations (1.2.1) - (1.2.6) can be written as

$$\frac{(\omega/\omega_c)}{r_g k_z} = \Big\{M_s^{-2} + (r_g k_\perp)^2\Big\}^{-1/2}, \tag{1.2.7}$$

where

$$M_s = \sqrt{\gamma\sigma_{ie} + \frac{1}{\mu(1-\beta_e)}}, \tag{1.2.8}$$

$k_\perp^2 = k_x^2 + k_y^2$, and we have assumed that all the perturbed dependent variables vary as $\exp[i(k_x x + k_y y + k_z z - \omega t)]$.

If we use the normalized variables, i.e., if we use the system of equations (1.2.1) - (1.2.6), the dimensionless linear dispersion relation for low frequency $(\omega/\omega_c << 1)$ IA waves can be written as

$$\frac{\omega}{k_z} = \Big\{\frac{\mu(1-\beta_e)}{1 + \gamma\sigma_{ie}\mu(1-\beta_e)} + k_\perp^2\Big\}^{-1/2}. \tag{1.2.9}$$

Here ω is normalized by ω_c and k_x, k_y, k_z are normalized by $1/r_g$, i.e., replacing ω/ω_c by ω, $r_g k_z$ by k_z and $r_g k_\perp$ by $k_\perp$ in equation (1.2.7), we get the equation (1.2.9).

The dimensionless linear dispersion relations (5) of Yinhua & Yu [122], (9) of Choi *et al.* [90] and (10) of Choi *et al.* [111] can be easily obtained from the dimensionless linear dispersion relation (1.2.9) of this chapter by considering appropriate values of the parameters. For example, the dispersion relation (1.2.9) is exactly same as the dispersion relation (10) of Choi *et al.* [111] if we take $\beta_e = 0$, $\gamma = 1$, $\sigma_{ie} = \sigma$ and $k_y = 0$.

Using (1.2.1), the pressure equation of ion fluid (1.2.3) can be written as $p_i = n_i^{\gamma}$. Using this expression of p_i, the equation (1.2.2) can be simplified as

$$\Big(\frac{\partial}{\partial t} + \overrightarrow{u}_i \cdot \overrightarrow{\nabla}\Big)\overrightarrow{u}_i + \gamma\sigma_{ie}(n_i)^{\gamma-2}\overrightarrow{\nabla} n_i = -\overrightarrow{\nabla}\phi + \overrightarrow{u}_i \times \widehat{z}. \tag{1.2.10}$$

Again, using (1.2.6), equation (1.2.4) can be written as

$$n_i = \mu\big(1 - \beta_e\phi + \beta_e\phi^2\big)e^{\phi} + 1 - \mu. \tag{1.2.11}$$

We have used the equations (1.2.1), (1.2.10) and (1.2.11) to derive the energy integral.

1.3 Energy Integral

To study the arbitrary amplitude time independent IA solitary structures, we suppose that all the dependent variables depend only on a single variable $\xi = l_x x + l_y y + l_z z - Mt$ with $l_x^2 + l_y^2 + l_z^2 = 1$, where M is independent of x, y, z and t. Therefore, lifting the equation (1.2.1) and each component of the momentum equation (1.2.10) in the wave frame moving with a constant velocity M normalized by C_s along a direction having direction cosines (l_x, l_y, l_z), we get the following equations:

$$\frac{d}{d\xi}\Big(n_i\Psi\Big) = 0, \tag{1.3.1}$$

$$\Psi\frac{du_{ix}}{d\xi} + l_x\frac{dH}{d\xi} - u_{iy} = 0, \tag{1.3.2}$$

$$\Psi\frac{du_{iy}}{d\xi} + l_y\frac{dH}{d\xi} + u_{ix} = 0, \tag{1.3.3}$$

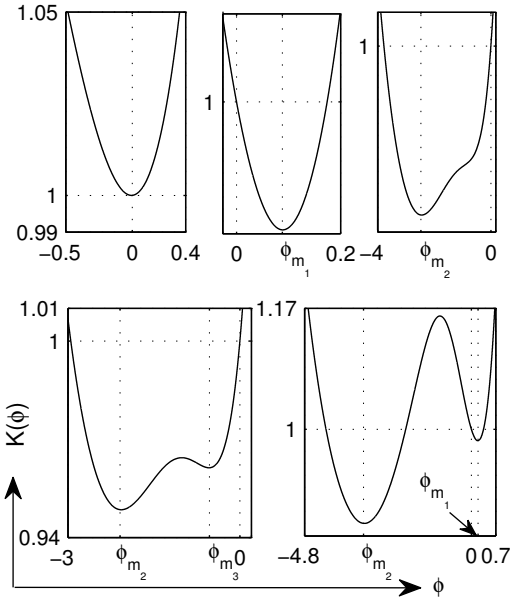

Figure 1.1: $K(\phi)$ is plotted against ϕ for $\gamma = 5/3$ with (a) $\sigma_{ie} = 0.01$, $\mu = 0.5$, $\beta_e = 0.18$, (b) $\sigma_{ie} = 0.01$, $\mu = 0.5$, $\beta_e = 0.2$, (c) $\sigma_{ie} = 0.1$, $\mu = 0.6$, $\beta_e = 0.2$, (d) $\sigma_{ie} = 0.01$, $\mu = 0.6$, $\beta_e = 0.2$, (e)$\sigma_{ie} = 0.01$, $\mu = 0.6$, $\beta_e = 0.3$.

$$\Psi \frac{du_{iz}}{d\xi} + l_z \frac{dH}{d\xi} = 0, \tag{1.3.4}$$

where we have used the following notations:

$$\Psi = -M + l_x u_{ix} + l_y u_{iy} + l_z u_{iz}, \tag{1.3.5}$$

$$H = H(\phi) = \frac{\gamma \sigma_{ie}}{\gamma - 1}(n_i)^{\gamma - 1} + \phi. \tag{1.3.6}$$

From (1.3.1), we get the following expression of Ψ:

$$\Psi = -\frac{M}{n_i}, \tag{1.3.7}$$

where we have used the following boundary conditions:

$$\Big(n_i, u_{ix}, u_{iy}, u_{iz}, \phi, \frac{d\phi}{d\xi}\Big) \to \big(1, 0, 0, 0, 0, 0\big) \text{ as } |\xi| \to \infty. \tag{1.3.8}$$

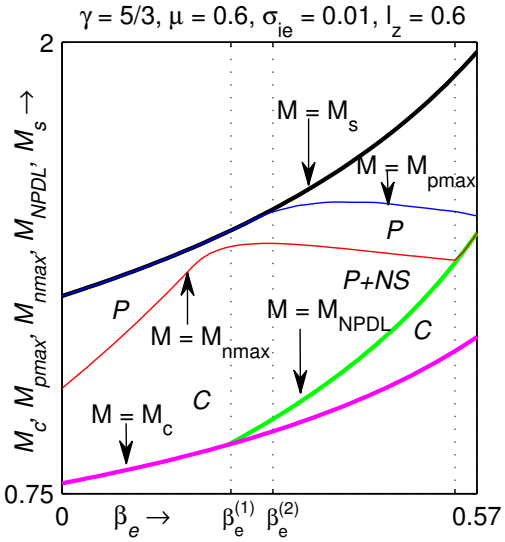

Figure 1.2: M_c, M_s, M_{pmax}, M_{nmax} and M_{NPDL} are plotted against β_e. The magenta line, black line, blue line, red line and green line correspond to the curves $M = M_c$, $M = M_s$, $M = M_{pmax}$, $M = M_{nmax}$ and $M = M_{NPDL}$ respectively. This figure shows the existence of NPSWs after the formation of NPDL along with other solitary structures.

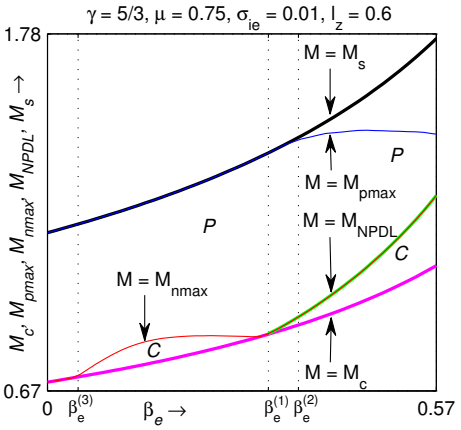

Figure 1.3: M_c, M_s, M_{pmax}, M_{nmax} and M_{NPDL} are plotted against β_e. The magenta line, black line, blue line, red line and green line correspond to the curves $M = M_c$, $M = M_s$, $M = M_{pmax}$, $M = M_{nmax}$ and $M = M_{NPDL}$ respectively. This figure shows that there does not exist any NPSW after the formation of NPDL.

Substituting this expression of Ψ as given by (1.3.7) in the equation (1.3.4), integrating the resulting equation and finally using the boundary condition (1.3.8) to find the integration constant, we get the following equation:

$$u_{iz} = \frac{l_z}{M} G(\phi), \tag{1.3.9}$$

where

$$G = G(\phi) = \sigma_{ie}\{(n_i)^{\gamma} - 1\} + \int_0^{\phi} n_i d\phi. \tag{1.3.10}$$

From equations (1.3.5), (1.3.7) and (1.3.9), we get the following expression of $l_x u_{ix} + l_y u_{iy}$:

$$l_x u_{ix} + l_y u_{iy} = M - \frac{M}{n_i} - \frac{l_z^2}{M} G(\phi). \tag{1.3.11}$$

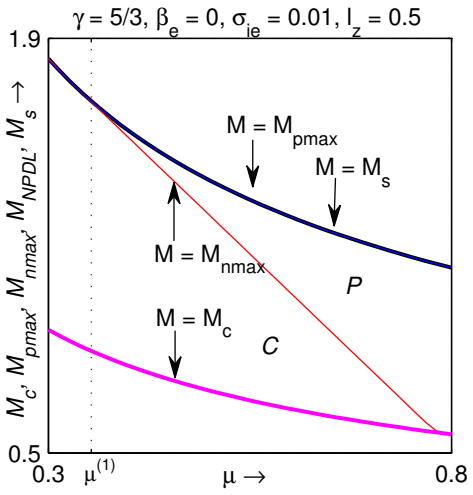

Figure 1.4: M_c, M_s, M_{pmax}, M_{nmax} and M_{NPDL} are plotted against μ for $\beta_e = 0$. The magenta line, black line, blue line, red line and green line correspond to the curves $M = M_c$, $M = M_s$, $M = M_{pmax}$, $M = M_{nmax}$ and $M = M_{NPDL}$ respectively. As there is no green line corresponding to the curve $M = M_{NPDL}$ then there does not exist any NPDL solution for $\beta_e = 0$.

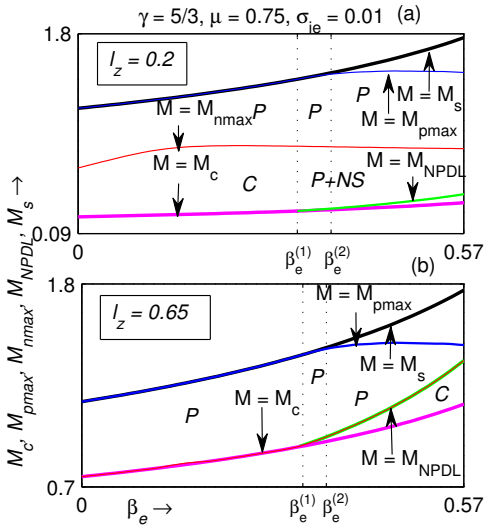

Figure 1.5: M_c, M_s, M_{pmax}, M_{nmax} and M_{NPDL} are plotted against β_e for different l_z. The magenta line, black line, blue line, red line and green line correspond to the curves $M = M_c$, $M = M_s$, $M = M_{pmax}$, $M = M_{nmax}$ and $M = M_{NPDL}$ respectively. There is a qualitative difference between (a) and (b). For (a), the system supports coexistence of PPSWs and NPSWs after the formation of NPDL as indicated by P+NS, whereas figure (b) shows that the system does not support any NPSW after NPDL.

Substituting the expression of Ψ as given by (1.3.7) in the equations (1.3.2) and (1.3.3), we get

$$-\frac{M}{n_i}\frac{du_{ix}}{d\xi} + l_x\frac{dH}{d\xi} - u_{iy} = 0, \tag{1.3.12}$$

$$-\frac{M}{n_i}\frac{du_{iy}}{d\xi} + l_y\frac{dH}{d\xi} + u_{ix} = 0. \tag{1.3.13}$$

Multiplying (1.3.12) by l_x and (1.3.13) by l_y, finally, adding the resulting equations, we get

$$l_y u_{ix} - l_x u_{iy} = -\frac{dP}{d\xi}, \tag{1.3.14}$$

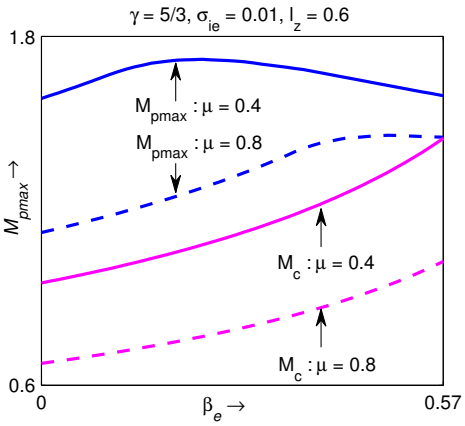

Figure 1.6: M_c, M_{pmax} are plotted against β_e for different values of μ. There is no considerable change in the area of the existence regions of PPSWs for increasing μ.

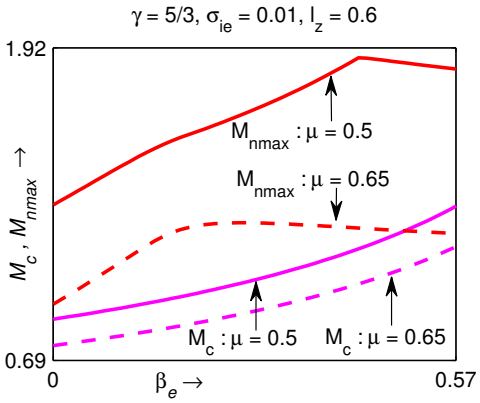

Figure 1.7: M_c, M_{nmax} are plotted against β_e for different values of μ. The region of existence of NPSWs decreases for increasing μ.

where we have used (1.3.11) and

$$P = \frac{M^2}{2(n_i)^2} + \frac{\gamma\sigma_{ie}}{\gamma-1}(n_i)^{\gamma-1} + \phi. \tag{1.3.15}$$

Solving the equations (1.3.11) and (1.3.14) for the unknowns u_{ix} and u_{iy}, we get

$$u_{ix} = \frac{l_x\left\{M - \frac{M}{n_i} - \frac{l_z^2}{M}G(\phi)\right\} - l_y\frac{dP}{d\xi}}{l_x^2 + l_y^2}, \tag{1.3.16}$$

$$u_{iy} = \frac{l_y\left\{M - \frac{M}{n_i} - \frac{l_z^2}{M}G(\phi)\right\} + l_x\frac{dP}{d\xi}}{l_x^2 + l_y^2}. \tag{1.3.17}$$

Substituting these two values of u_{ix} and u_{iy} in (1.3.12) or in (1.3.13), we get the following equation:

$$\frac{d^2P}{d\xi^2} = f(\phi) = n_i - 1 - \frac{l_z^2}{M^2}n_iG(\phi). \tag{1.3.18}$$

This equation can be written as

$$\frac{dQ}{d\phi} + \frac{2}{R}\frac{dR}{d\phi}Q = \frac{2}{R}f(\phi), \tag{1.3.19}$$

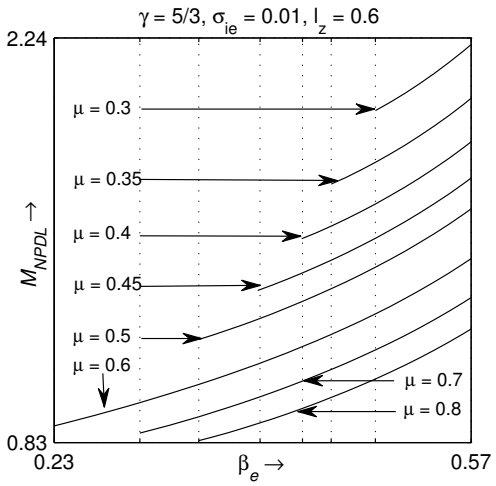

Figure 1.8: M_{NPDL} is plotted against β_e for different values of μ. This figure shows that for increasing μ, NPDLs start to exist for lower values of β_e up to $\mu = 0.6$ and after this value of μ, NPDLs start to exist for higher values of β_e.

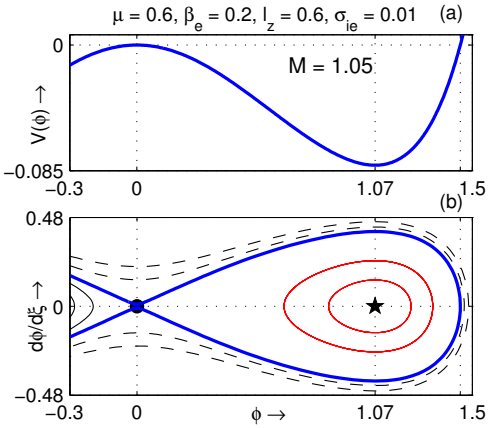

Figure 1.9: (a) $V(\phi)$ and (b) the phase portrait of the system have been drawn on the same ϕ-axis. This figure shows that the the curve $V(\phi)$ of the upper panel (a) corresponds to the separatrix of the of the phase portrait of the dynamical system (1.5.1) as shown by heavy blue line. Each maximum (minimum) point of $V(\phi)$ corresponds to a saddle (non-saddle) fixed point of the dynamical system (1.5.1). This figure confirms the existence of PPSW.

where $Q = \left(\frac{d\phi}{d\xi}\right)^2$ and $R = \frac{dP}{d\phi}$.

The equation (1.3.19) is a first order and first degree linear differential equation in Q and the general solution of (1.3.19) can be written as

$$\left(\frac{d\phi}{d\xi}\right)^2 \times \left(\frac{dP}{d\phi}\right)^2 = \int 2\frac{dP}{d\phi} f(\phi) d\phi + C_1, \tag{1.3.20}$$

where C_1 is a integration constant. Using the boundary condition (1.3.8), we get

$$0 = \int 2\frac{dP}{d\phi} f(\phi) d\phi \Big|_{\phi=0} + C_1. \tag{1.3.21}$$

Using the equation (1.3.21), the equation (1.3.20) can be put in the following form:

$$\frac{1}{2}\left(\frac{d\phi}{d\xi}\right)^2 + V(\phi) = 0, \tag{1.3.22}$$

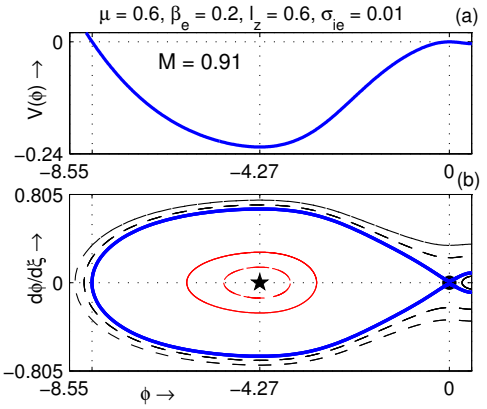

Figure 1.10: (a) $V(\phi)$ and (b) the phase portrait of the system have been drawn on the same ϕ-axis. This figure also shows that the the curve $V(\phi)$ of the upper panel (a) corresponds to the separatrix of the of the phase portrait of the dynamical system (1.5.1) as shown by heavy blue line. Each maximum (minimum) point of $V(\phi)$ corresponds to a saddle (non-saddle) fixed point of the dynamical system (1.5.1). This figure confirms the existence of NPSW.

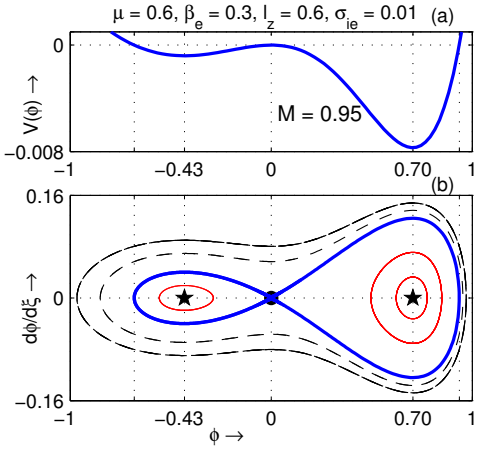

Figure 1.11: (a) $V(\phi)$ and (b) the phase portrait of the system have been drawn on the same ϕ-axis. This figure confirms the coexistence of both PPSW and NPSW.

where

$$V(\phi) = V(M, \phi) = -\frac{\int_0^{\phi} \frac{dP}{d\phi} f(\phi) d\phi}{\left(\frac{dP}{d\phi}\right)^2}. \tag{1.3.23}$$

The equation (1.3.22) is the well known energy integral with Sagdeev pseudo potential $V(\phi)(= V(M, \phi))$ given in (1.3.23). According to the mechanical analogy of Sagdeev [11], the system supports a positive (negative) potential solitary wave [PPSW] ([NPSW]) solution of (1.3.22) if (i) $\phi = 0$ is the position of unstable equilibrium of a particle of unit mass associated with the energy integral (1.3.22), i.e., $V(0) = V'(0) = 0$ and $V''(0) < 0$; (ii) the condition for the oscillation of the particle within the interval $\min\{0, \phi_m\} < \phi < \max\{0, \phi_m\}$ holds good when the particle is slightly displaced from its unstable position of equilibrium ($\phi = 0$), i.e., $V(\phi_m) = 0$,

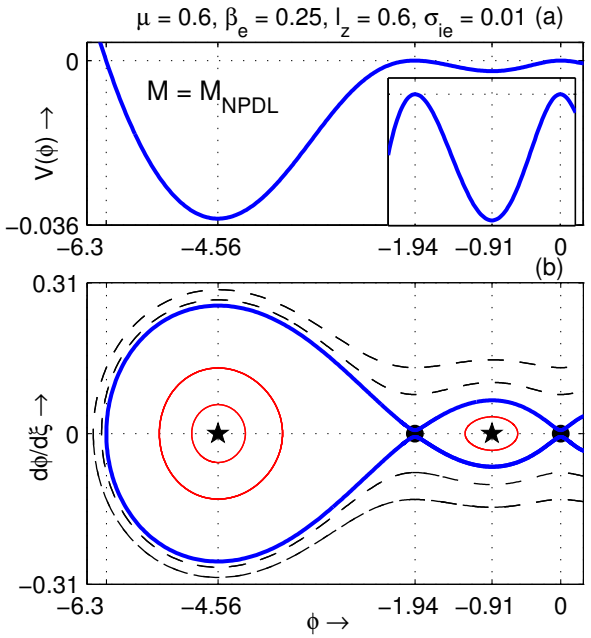

Figure 1.12: (a) $V(\phi)$ and (b) the phase portrait have been drawn on the same ϕ for $M = M_{NPDL}$. The portion of $V(\phi)$ included within $-1.94 \leq \phi \leq 0$ has been shown in the inset. We see that the separatrix (as shown by heavy blue line) of the phase portrait appears to pass through two saddle points corresponding to two maximum values of $V(\phi)$ at $\phi = 0$ and at $\phi = -1.94$ (approximately). This figure confirms the existence of NPDL.

$V'(\phi_m) > 0$ ($V'(\phi_m) < 0$) for some $\phi_m > 0$ ($\phi_m < 0$); (iii) the energy integral (1.3.22) is well defined within the interval $\min\{0, \phi_m\} < \phi < \max\{0, \phi_m\}$, i.e., $V(\phi) < 0$ for all $\min\{0, \phi_m\} < \phi < \max\{0, \phi_m\}$. On the other hand, the system supports a PPDL (NPDL) solution of (1.3.22) if the second condition is replaced by $V(\phi_m) = 0$, $V'(\phi_m) = 0$, $V''(\phi_m) < 0$ for some $\phi_m > 0$ ($\phi_m < 0$), which states that the particle cannot be reflected back from the point $\phi = \phi_m$ to the point $\phi = 0$. The physical interpretation for the existence of different solitary structures has been given in details in the paper of Das *et al.*[141]. Using this mechanical analogy of Sagdeev [11], we present analytical theories to determine different bounds of M for the existence of different solitary structures, and also to find the Mach numbers M_{PPDL} and

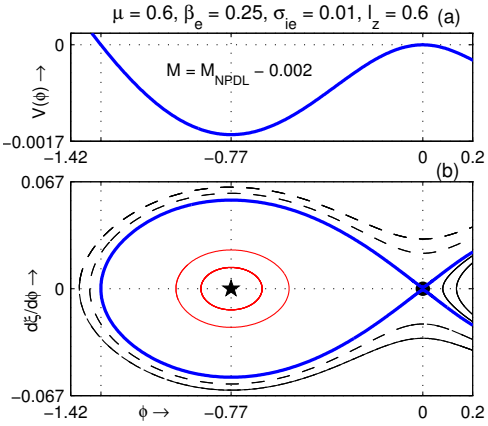

Figure 1.13: (a) $V(\phi)$ and (b) the phase portrait of the system have been drawn on the same ϕ-axis for $M = M_{NPDL} - 0.002$. Existence of NPSW is confirmed before the formation of double layer.

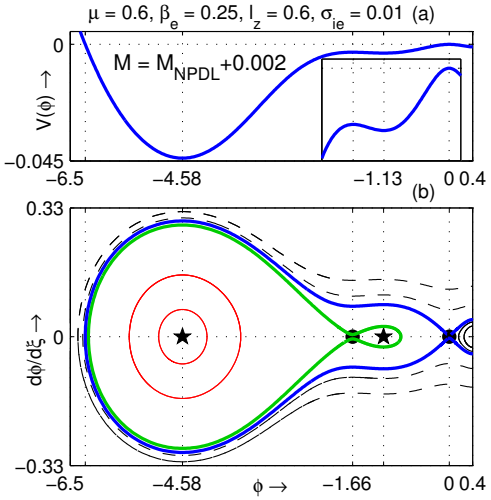

Figure 1.14: (a) $V(\phi)$ and (b) the phase portrait of the system have been drawn on the same ϕ-axis for $M = M_{NPDL} + 0.002$. Here we see that the separatrix of the of the phase portrait of the dynamical system (1.5.1) which appears to pass through the saddle $(0, 0)$ contains more than one non-saddle fixed points and another separatrix through the non-zero saddle $(-1.66, 0)$. Consequently, the separatrix that appears to pass through the saddle $(0, 0)$ corresponds to a supersoliton. Therefore, this figure confirms the existence of supersoliton after the formation of double layer.

M_{NPDL} corresponding to a PPDL and NPDL solution respectively in the following two subsections.

1.3.1 Different Bounds of M: M_c, M_{pmax} & M_{nmax}

Differentiating the equation (1.3.15) with respect to ϕ, we get

$$\frac{dP}{d\phi} = -M_s^2 n_i^{-3}\left(\frac{dn_i}{d\phi}\right)\left[\frac{M^2}{M_s^2} - K(\phi)\right], \tag{1.3.24}$$

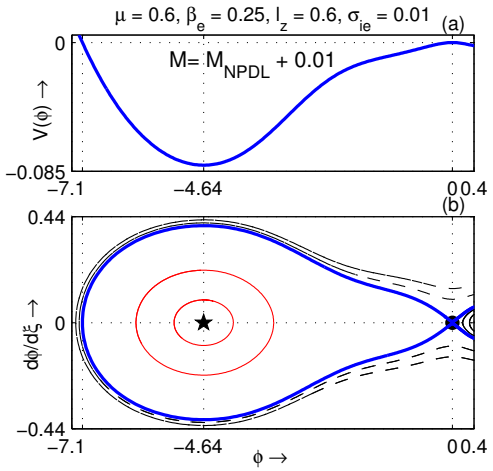

Figure 1.15: (a) $V(\phi)$ and (b) the phase portrait of the system have been drawn on the same ϕ-axis for $M = M_{NPDL} + 0.01$. The separatrix of lower panel of this figure corresponds to a conventional soliton.

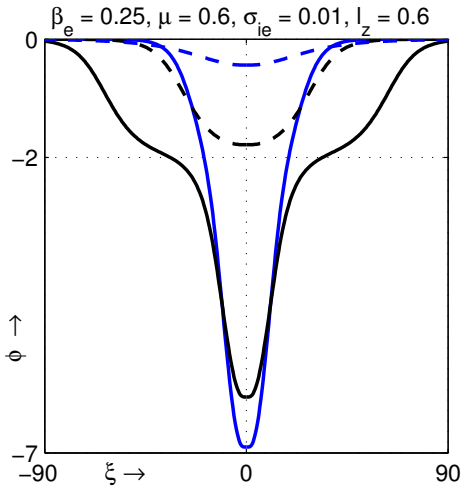

Figure 1.16: ϕ is plotted against ξ for (a) $M = M_{NPDL} + 0.0001$ (solid black curve), (b) $M = M_{NPDL} - 0.0001$ (dashed black curve), (c) $M = M_{NPDL} + 0.01$ (solid blue curve), and (d) $M = M_{NPDL} - 0.01$ (dashed blue curve). This figure clearly indicates the jump type discontinuity between the amplitudes of solitons before and after the formation of double layer.

where

$$K(\phi) = \frac{1}{M_s^2}\Big[\gamma\sigma_{ie}n_i^{\gamma+1} + n_i^3\Big(\frac{dn_i}{d\phi}\Big)^{-1}\Big]. \tag{1.3.25}$$

Now it is simple to check that n_i, $\dfrac{dn_i}{d\phi}$ and $K(\phi)$ are strictly positive functions of ϕ, i.e., $n_i > 0$, $\dfrac{dn_i}{d\phi} > 0$ and $K(\phi) > 0$ for any value of ϕ and for any set of values of the parameters of the system. Again, one can easily check that $K(0) = 1$.

It is simple to check that $V(0) = 0$, $V'(0) = 0$ and $V''(0) < 0$ gives the following bounds for M:

$$M_c < M < M_s, \tag{1.3.26}$$

where $M_c = l_z M_s$ and we have assumed the condition $\left.\frac{dP}{d\phi}\right|_{\phi=0} \neq 0$.

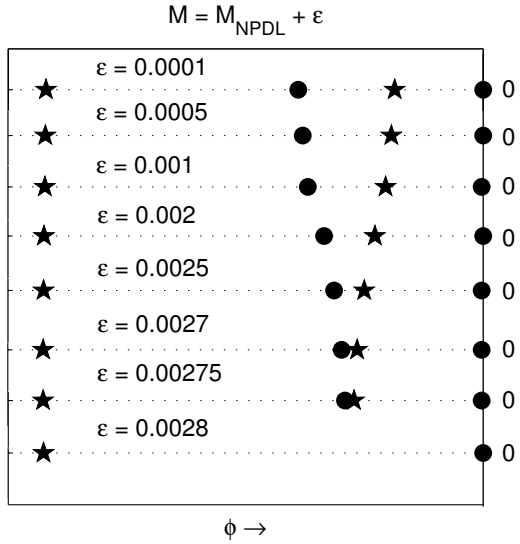

Figure 1.17: Saddle points (small solid circles) and equilibrium points other than saddle points (small solid stars) for the dynamical system (1.5.1) have been drawn on ϕ - axis for different values of $M = M_{NPDL} + \epsilon$. This figure clearly shows the transition from supersoliton structures to conventional soliton.

Therefore, the solitary structures start to exist for $M > M_c$. Although $M < M_s$ for the existence of the solitary structures, but M_s is not necessarily the exact upper bound of M for the existence of the solitary structures. To find the exact upper bound of M, we consider the equation $\frac{dP}{d\phi} = 0$ along with the inequality $M < M_s$. In fact, the inequality $M < M_s$ states that $\frac{dP}{d\phi} \neq 0$ at $\phi = 0$, but to consider the exact bounds of M it is necessary to consider $\frac{dP}{d\phi} \neq 0$ throughout the entire possible range of ϕ where $V(\phi)$ is well defined.

Instead of considering $\frac{dP}{d\phi} \neq 0$, one can consider $\frac{dP}{d\phi} = 0$, and this equation gives

$$\frac{M^2}{M_s^2} = K(\phi). \tag{1.3.27}$$

Obviously the equation (1.3.27) is well defined only when $K(\phi) > 0$ for all ϕ. From equation (1.3.25), using (1.2.4) and (1.2.6), we see that $K(\phi)$ is independent of M.

Therefore, $\frac{dP}{d\phi} = 0$ holds good only when M assumes the value $M_s\sqrt{K(\phi)}$ and consequently for the existence of positive (negative) potential solitary structure, M cannot exceed the value $M_s\sqrt{K(\phi_m)}$, where $K(\phi)$ attains its global minimum at $\phi = \phi_m$ in the positive (negative) side of ϕ - axis, i.e., for $\phi_m \geq 0$ ($\phi_m \leq 0$). Now we explain the phrase 'global minimum' with the help of the figure 1.1. We have already stated that $K(\phi) > 0$ for any value of ϕ and for any set of physically admissible values of the parameters. Plotting $K(\phi)$ against ϕ for different values of the parameters of the system, it is simple to check that $K(\phi) > 0$ for all ϕ. In figures 1.1(a) - 1.1(e), $K(\phi)$ is plotted against ϕ for different values of the parameters. These figures indicate five qualitatively different curves of $K(\phi)$ against ϕ. Figure 1.1(a) shows that the minimum value of $K(\phi)$ in the positive side of ϕ - axis ($\phi \geq 0$) as well as in the negative side of ϕ - axis ($\phi \leq 0$) is equal to $K(0)$. Figure 1.1(b) shows that $K(\phi)$ has only one minimum at $\phi = \phi_{m_1}(> 0)$ such that $0 < K(\phi_{m_1}) < 1$ and the minimum value of $K(\phi)$ in the negative side of ϕ - axis ($\phi \leq 0$) is equal to $K(0)$. Figure 1.1(c) shows that $K(\phi)$ has only one minimum at $\phi = \phi_{m_2}(< 0)$ such that $0 < K(\phi_{m_2}) < 1$ and the minimum value of $K(\phi)$ in the positive side of ϕ - axis ($\phi \geq 0$) is equal to $K(0)$. Figure 1.1(d) shows that $K(\phi)$ has two minima at $\phi = \phi_{m_2}(< 0)$ and at $\phi = \phi_{m_3}(< 0)$ such that $0 < K(\phi_{m_2}),\ K(\phi_{m_3}) < 1$ and the minimum value of $K(\phi)$ in the positive side of ϕ - axis ($\phi \geq 0$) is equal to $K(0)$. Figure 1.1(e) shows that $K(\phi)$ has two minima at $\phi = \phi_{m_1}(> 0)$ and at $\phi = \phi_{m_2}(< 0)$ such that ϕ_{m_1} lies on the positive side of ϕ - axis ($\phi \geq 0$), ϕ_{m_2} lies on the negative potential side of ϕ - axis ($\phi \leq 0$) and $0 < K(\phi_{m_1}), K(\phi_{m_2}) < 1$. Now, our aim is to minimize $K(\phi_{m_1})$ and / or $K(\phi_{m_2})$ in order to obtain the global minimum in the positive and / or in the negative potential side(s). By the phrase 'global minimum', we would like to mean the minimum of the minimum values of $K(\phi)$. For example, for figure 1.1(d), global minimum of $K(\phi)$ is $\min\{K(\phi_{m_2}),\ K(\phi_{m_3})\} = K(\phi_{m_2})$ on the negative side of ϕ - axis ($\phi \leq 0$), whereas global minimum of $K(\phi)$ is $K(0)$ on the positive side of ϕ - axis ($\phi \geq 0$), i.e., we can say that $K(\phi)$ attains the global minimum value at $\phi = \phi_m = \phi_{m_2}$ on the negative side

of ϕ - axis ($\phi \leq 0$), whereas $K(\phi)$ attains the global minimum value at $\phi = \phi_m = 0$ on the positive side of ϕ - axis ($\phi \geq 0$). On either side of the ϕ - axis including $\phi = 0$, there always exists a ϕ_m such that $K(\phi)$ attains the global minimum value at $\phi = \phi_m$. If K^+ and K^- respectively, denote the global minimum of $K(\phi)$ on the positive and on the negative potential sides, then $K^+ = K(\phi_m)$ with $\phi_m \geq 0$ and $K^- = K(\phi_m)$ with $\phi_m \leq 0$. For example, $K^+ = K(\phi_m)$ with $\phi_m = \phi_{m1}$ and $K^- = K(\phi_m)$ with $\phi_m = 0$ for figure 1.1(b), whereas $K^+ = K(\phi_m)$ with $\phi_m = 0$ and $K^- = K(\phi_m)$ with $\phi_m = \phi_{m_2}$ for figure 1.1(d). From the above discussions, it is clear that both K^+ and K^- exist finitely, and consequently for the existence of positive (negative) potential solitary structure, M is restricted by the inequality $M_c < M < M_s \times \sqrt{K^+}$ ($M_c < M < M_s \times \sqrt{K^-}$). The above analysis can be illustrated in the following paragraphs.

Let M_{pmax} (M_{nmax}) be the upper bound of M for the existence of the positive (negative) potential solitary structures, i.e., for the existence of the positive (negative) potential solitary structures, we must have $M_c < M < M_{pmax}$ ($M_c < M < M_{nmax}$). Now we have the following two cases: (I) $K(\phi) > 1$ and (II) $0 \leq K(\phi) \leq 1$.

(I) If $K(\phi) > 1$ for all $\phi \geq 0$ ($\phi \leq 0$) then the upper bound of M for the existence of the positive (negative) potential solitary structures is given by $M_{pmax} = M_s$ ($M_{nmax} = M_s$). Again, there does not exist any $\phi(\geq 0)$ ($\phi \leq 0$) for which M assumes the value $M_s\sqrt{K(\phi)}$ because $M = M_s\sqrt{K(\phi)} \Rightarrow \frac{M}{M_s} = \sqrt{K(\phi)} > 1 \Rightarrow M > M_s$ which contradicts the fact $M_c < M < M_s$ and consequently $\frac{dP}{d\phi} \neq 0$ for $\phi \neq 0$. So, $V(\phi)$ is well defined as a real valued function of ϕ if it is well defined at $\phi = 0$. Therefore, the upper bound of M for the existence of the positive (negative) potential solitary structures is given by the inequality (1.3.26).

(II) If $0 \leq K(\phi) \leq 1$ for some ϕ, then let $K(\phi)$ attain its global minimum at $\phi = \phi_m$ such that $0 \leq K(\phi_m) \leq 1$. Therefore, $M = M_s\sqrt{K(\phi_m)}$ is a minimum value of M at which there is a singularity of $V(\phi)$ at $\phi = \phi_m$, i.e., $\left.\frac{dP}{d\phi}\right|_{\phi=\phi_m} = 0$ when $M = M_s \times \sqrt{K(\phi_m)}$.

The above discussions guide us to take $M_{pmax} = M_s \times \sqrt{K^+}$ and $M_{nmax} = M_s \times \sqrt{K^-}$.

1.3.2 Mach Numbers M_{PPDL} & M_{NPDL} Corresponding to a PPDL & NPDL

Let us use the notation $V(M, \phi)$ instead of $V(\phi)$. Using this notation, the conditions for the existence of a PPDL (NPDL) solution of the energy integral (1.3.22) are (i) $V(M, 0) = 0$, $V'(M, 0) = 0$, $V''(M, 0) < 0$; (ii) $V(M, \phi_m) = 0$, $V'(M, \phi_m) = 0$, $V''(M, \phi_m) < 0$ for some $\phi_m > 0$ ($\phi_m < 0$); (iii) $V(M, \phi) < 0$ for all $0 < \phi < \phi_m$ ($\phi_m < \phi < 0$). We have used condition (i) to find the lower bound and a rough idea about the upper bound for the existence of any solitary structure including double layers of any polarity. Condition (iii) is necessary to define the energy integral (1.3.22) within the interval $\min\{0, \phi_m\} < \phi < \max\{0, \phi_m\}$. Now we use condition (ii) to find the Mach number corresponding to a PPDL and / or NPDL solution of the energy integral (1.3.22). Let M_{dl} and $\phi_{dl} \neq 0$ be the solutions of the equations $V(M, \phi_m) = 0$ and $V'(M, \phi_m) = 0$ for the unknowns M and ϕ_m. It is important to note that $\phi = 0$ is a solution of the equations $V(M, \phi_m) = 0$ and $V'(M, \phi_m) = 0$ for any value of M in view of condition (i). Therefore, we have $V(M_{dl}, \phi_{dl}) = 0$ and $V'(M_{dl}, \phi_{dl}) = 0$ for non-zero ϕ_{dl} and consequently M_{dl} corresponds to a Mach number M_{PPDL} (M_{NPDL}) for a PPDL (NPDL) solution of the energy integral (1.3.22) if $\phi_{dl} > 0$ ($\phi_{dl} < 0$) and ϕ_{dl} is the smallest (largest) real satisfying the conditions $V(M_{dl}, \phi_{dl}) = 0$ and $V'(M_{dl}, \phi_{dl}) = 0$.

Equations $V(M_{dl}, \phi_{dl}) = 0$ and $V'(M_{dl}, \phi_{dl}) = 0$ give the following expression of M_{dl}:

$$M_{dl} = \sqrt{\frac{l_z^2 n_i(\phi_{dl}) G(\phi_{dl})}{n_i(\phi_{dl}) - 1}}, \tag{1.3.28}$$

where $G(\phi)$ is given by the equation (1.3.10). The equation $V(M_{dl}, \phi_{dl}) = 0$ gives the

following equation:

$$\int_0^{\phi_{dl}} P'(M_{dl},\phi) f(M_{dl},\phi) d\phi = 0, \tag{1.3.29}$$

where $P' = \frac{dP}{d\phi}$. Substituting (1.3.28) in (1.3.29), we get an equation for the unknown ϕ_{dl}. Solving this equation for the unknown ϕ_{dl} at least numerically and putting this solution in the equation (1.3.28), one can get the value of M_{dl}. If $V''(M_{dl},\phi_{dl}) < 0$, then this M_{dl} corresponds to the Mach number M_{PPDL} (M_{NPDL}) of a PPDL (NPDL).

Now M_{nmax} (M_{pmax}) can restrict the existence of all NPSWs (PPSWs). But if both M_{nmax} (M_{pmax}) and $M = M_{NPDL}$ ($M = M_{PPDL}$) exist for fixed values of the parameters, then we must have $M_c < M_{NPDL} < M_{nmax}$ ($M_c < M_{PPDL} < M_{pmax}$). For this case, we can split the entire range of M into two disjoint sub-intervals $M_c < M < M_{NPDL}$ ($M_c < M < M_{PPDL}$) and $M_{NPDL} < M < M_{nmax}$ ($M_{PPDL} < M < M_{pmax}$). For $M_c < M < M_{NPDL}$ ($M_c < M < M_{PPDL}$), we get a sequence of NPSWs (PPSWs) converging to the NPDL (PPDL) solution at $M = M_{NPDL}$ ($M = M_{PPDL}$). In other words, the NPDL (PPDL) solution at $M = M_{NPDL}$ ($M = M_{PPDL}$) can restrict the occurrence of all NPSWs (PPSWs) for all M lying within the interval $M_c < M < M_{NPDL}$ ($M_c < M < M_{PPDL}$), whereas for $M_{NPDL} < M < M_{nmax}$ ($M_{PPDL} < M < M_{pmax}$), we get NPSWs (PPSWs) after the formation of NPDL (PPDL) at $M = M_{NPDL}$ ($M = M_{PPDL}$) and consequently the existence of supersolitons [142] or dias - type solitons [69] are confirmed. These type of solitons have been recently reported by many authors [71, 74, 114–116, 118, 119, 138–140].

1.4 Existence Domains

Here we draw different regions bounded by the curves $M = M_c$, $M = M_s$, $M = M_{pmax}$, $M = M_{nmax}$, $M = M_{NPDL}$, $M = M_{PPDL}$ with respect to any parameter of the system. These regions essentially describe the existence domains of different

solitary structures bounded by different curves. For example, the region bounded by the curves $M = M_c$ and $M = M_{pmax}$ ($M = M_{nmax}$) represents the domain of existence of all PPSWs (NPSWs) including all PPDLs (NPDLs). At each point along the curve $M = M_{NPDL}$ ($M = M_{PPDL}$), one can get an NPDL (a PPDL). The region bounded by the curves $M = M_c$ and $M = M_{NPDL}$ ($M = M_{PPDL}$) represents the domain of existence of all NPSWs (PPSWs) before the formation of NPDL (PPDL). If $M_c < M_{NPDL} < M_{nmax}$, then the region bounded by the curves $M = M_{NPDL}$ and $M = M_{nmax}$ represents the domain of existence of all NPSWs after the formation of NPDL. We have used the following notations and terminologies: C – Region of coexistence of both NPSWs and PPSWs, N – Region of existence of NPSWs, P – Region of existence of PPSWs and NS – Region of existence of negative potential solitons after the formation of NPDL. The curves $M = M_c$, $M = M_s$, $M = M_{pmax}$, $M = M_{nmax}$ and $M = M_{NPDL}$ have been shown in the heavy magenta line, heavy black line, blue line, red line and heavy green line respectively.

Now we define the following three cut off values of β_e which help us to study the different existence regions. (i) $\beta_e^{(1)}$ is a cut off value of β_e such that NPDL solutions start to exist for $\beta_e \geq \beta_e^{(1)}$. (ii) $\beta_e^{(2)}$ is a cut off value of β_e such that $M = M_{pmax}$ coincides with M_s for $0 \leq \beta_e \leq \beta_e^{(2)}$, i.e., for $\beta_e > \beta_e^{(2)}$, $M = M_{pmax}$ is different from M_s. (iii) $\beta_e^{(3)}$ is a cut off value of β_e such that $M = M_{nmax}$ starts to differ from M_c for $\beta_e > \beta_e^{(3)}$, i.e. for $0 \leq \beta_e \leq \beta_e^{(3)}$, $M = M_{nmax}$ coincides with M_c.

Based on the above mentioned notations and terminologies, the existence domains are self-explanatory. For example, figure 1.2 shows the existence domain or the compositional paramater space with respect to β_e. From this figure, we have the following observations. (i) The system supports PPSWs (NPSWs) for admissible values of β_e whenever M lies within the interval $M_c < M < M_{pmax}$ ($M_c < M < M_{nmax}$). (ii) The system supports coexistence of solitary waves of both polarities and the region of coexistence is bounded by the curves $M = M_c$ and $M = M_{nmax}$. This figure also shows that the existence region of negative potential solitary structures is a subset of

the existence region of positive potential solitary structures. (iii) The system starts to support NPDL along the curve $M = M_{NPDL}$ whenever $\beta_e \geq \beta_e^{(1)}$. (iv) Now, for $\beta_e \geq \beta_e^{(1)}$, we observe that $M_{NPDL} \leq M_{nmax}$. Consequently, for $\beta_e \geq \beta_e^{(1)}$, the curve $M = M_{NPDL}$ cannot bound the existence region of NPSWs and there exist two types of NPSWs. The first type of NPSWs are restricted by $M_c < M < M_{NPDL}$ and the second type of NPSWs are restricted by $M_{NPDL} < M < M_{nmax}$ and there exists a jump type discontinuity in the amplitudes of the NPSWs just before and just after the formation of double layer. In other words, the NPDL solution is unable to restrict the occurence of NPSWs and there exist NPSWs after the formation of double layer and such NPSWs are bounded by the curves $M = M_{NPDL}$ and $M = M_{nmax}$. Therefore, the existence of NPSWs after the formation of NPDL confirms the existence of a sequence of NPSSs. (v) The system does not support any PPDL and consequently it does not support any positive potential supersoliton (PPSS).

Figures 1.3 - 1.5 are self-explanatory. From figure 1.2 and figure 1.3, we have the following observations. (i) There is no effective change in the area of the existence region of PPSWs for increasing μ. (ii) The existence region of NPSWs decreases as μ increases. (iii) With the increment in μ, the value of $\beta_e^{(1)}$ increases, i.e., with the increment in μ, the system starts to support NPDLs as well as NPSSs for higher nonthermality of electrons. (iv) The existence region of NS decreases for increasing values of μ and ultimately, the system does not support any NS.

Figure 1.4 shows the existence domain with respect to μ for isothermal electrons, i.e., for $\beta_e = 0$. From this figure, we have the following observations. (i) M_{nmax} coincides with M_s for $0 < \mu \leq \mu^{(1)}$, i.e., M_{nmax} starts to differ from M_s for $\mu > \mu^{(1)}$. (ii) The system supports the coexistence of both NPSWs and PPSWs. (iii) The system does not support double layer of any polarity. (iv) This figure also shows that the existence region of NPSWs is smaller than the existence region of PPSWs.

Figure 1.5 shows that the qualitative behaviour of IA solitary structures is very

much sensible on the angle of propagation of the solitary structures with the uniform static magnetic field. In fact, figure 1.5 (a) shows the coexistence of PPSWs and NPSWs after the formation of NPDL , whereas figure 1.5 (b) shows that the coexistence of PPSWs and NPSWs after the formation of NPDL is impossible.

In figure 1.6, M_{pmax} and M_c are plotted against β_e for two different values of μ. This figure shows that there is no effective change in the area of the existence region of PPSWs for increasing μ. In figure 1.7, M_{nmax} and M_c are plotted against β_e for two different values of μ. This figure shows that the region of existence of NPSWs decreases for increasing μ. In figure 1.8, M_{NPDL} is plotted against β_e for different values of μ. In this figure, we see that the interval of β_e for the existence of NPDLs increases for increasing values of μ if $\mu \leq \mu^{(cr)}$, and if μ exceeds $\mu^{(cr)}$, interval of β_e for the existence of NPDLs decreases for increasing values of μ, where $\mu^{(cr)}$ is a critical value of μ. On the other hand, the region of existence of NPSWs before the formation of NPDLs increases for increasing values of μ whenever $\mu \leq \mu^{(cr)}$, whereas the region of existence of NPSWs before the formation of NPDLs decreases for increasing values of μ for $\mu > \mu^{(cr)}$. For the values of the parameters as mentioned in the figure 1.8, the value of $\mu^{(cr)}$ is approximately equal to 0.6.

1.5 Phase Portraits

In section 1.4, we have seen that the system supports the following IA solitary structures: (i) NPSWs, (ii) PPSWs, (iii) coexistence of NPSWs and PPSWs (iv) NPDLs, (v) coexistence of PPSWs and NPDLs, (vi) NPSWs after the formation of NPDLs, and (vii) coexistence of PPSWs and NPSWs after the formation of NPDLs. From the compositional parameter spaces or existence domains of different IA solitary structures, it is impossible to find the upper bound of the Mach number for the existence of NPSSs, although it is simple to check that there is a finite jump between the amplitudes of solitons just before and just after the formation of double layer which

confirms the existence of NPSSs. So, it is not possible to investigate the existence of a critical value (M_{cr}) of M such that the phase portraits of the solitons after the formation of double layer ($M > M_{cr}(> M_{NPDL})$) are qualitatively same as the conventional solitons before the formation of double layer ($M_c < M < M_{NPDL}$). Consequently, for the existence of NPSSs, we have $M_{NPDL} < M < M_{cr}$. So, there must be a transition of solitary structures, viz., soliton $\rightarrow$ double layer $\rightarrow$ supersoliton $\rightarrow$ soliton after the formation of double layer of same polarity. To discuss this transition process, it is important to know the phase portraits of the dynamical system describing the different IA solitary structures.

Now, differentiating the energy integral (1.3.22) with respect to ϕ, we can write the resulting equation in the following two coupled differential equations:

$$\frac{d\phi_1}{d\xi} = \phi_2, \ \frac{d\phi_2}{d\xi} = -V'(\phi_1), \quad \text{where} \ \ \phi_1 = \phi. \tag{1.5.1}$$

The equilibrium point of (1.5.1) is (ϕ_1^*, ϕ_2^*), where $\phi_2^* = 0$ and ϕ_1^* is given by $V'(\phi_1^*) = 0$. The equation $V'(\phi_1^*) = 0$ gives the value(s) of ϕ_1^* as a function of the parameters of the system along with M, i.e., $\phi_1^* = \phi_1^*(M, \gamma, \mu, \beta_e, \sigma_{ie}, l_z)$. Therefore, the values of the parameters γ, μ, β_e, σ_{ie} and l_z are not sufficient to determine ϕ_1^*. To get ϕ_1^*, it is necessary to know the value of M. But one can get the value of M by considering the existence domain with respect to any parameter of the system. For example, if the values of γ, μ, σ_{ie} and l_z are given, then by drawing the existence domain with respect to β_e, one can get the value of β_e and the corresponding value of M for the existence of the required solitary structure.

To describe the existence and the shape of NPSSs, and the coexistence of solitons of both polarities, we consider figures 1.9 - 1.15, where we have used the existence domain as shown in figure 1.2 to determine the Mach numbers for the formation of different solitary structures including NPSSs.

Figures 1.9 (b) - 1.15 (b) are, respectively, the phase portraits of PPSW, NPSW,

coexistence of solitary waves of both polarities, NPDL, NPSW just before the formation of NPDL (NPSS), NPSW after the formation of double layer. In the upper panel (or marked as (a)) of each figure of figures 1.9 - 1.15, $V(\phi)$ is plotted against ϕ, whereas the lower panel (or marked as (b)) of each figure shows the phase portrait of the system (1.5.1). The curve $V(\phi)$ and the phase portrait have been drawn on the same horizontal axis $\phi(= \phi_1)$. The small solid circle and the small solid star correspond to a saddle point and an equilibrium point other than saddle point of the system (1.5.1) respectively. From figures 1.9 - 1.15, we see that each maximum (minimum) point of $V(\phi)$ corresponds to a saddle point (an equilibrium point other than a saddle point) of the system (1.5.1).

The one-one correspondence between the separatrix of the phase portrait (as shown with a heavy bold line) in the lower panel with the curve $V(\phi)$ against ϕ of the upper panel has been explained elaborately in the recently published paper of Paul *et al.* [140] The origin $(0, 0)$ is always a saddle point of the system (1.5.1) and the separatrix corresponding to a solitary structure appears to start and end at the saddle point (0,0). The separatrix corresponding to a solitary structure is shown with a heavy bold blue line, whereas other separatrices (if any) are shown by heavy bold green lines. The phase portrait of the dynamical system corresponding to a conventional soliton contains only one separatrix that appears to start and end at the origin enclosing only one non-saddle fixed point and there does not exist any other separatrix within the first one. Again, Paul *et al.* [140] reported that the trajectory corresponding to the separatrix approaches the origin as $\xi \to \pm\infty$, and a separatrix corresponding to a solitary structure does not correspond to a periodic solution because for this case, the trajectory takes forever trying to reach a saddle point which proves an important result that a pseudo particle associated with the energy integral (1.3.22) takes an infinite long time to move away from its unstable position of equilibrium and it continues its motion until ϕ takes the value ϕ_m and again, it takes an infinite long time to come back its unstable position of equilibrium [104, 141],

where $V(\phi_m) = 0$ and $V'(\phi_m) > 0$ ($V'(\phi_m) < 0$) for $\phi_m > 0$ ($\phi_m < 0$). The closed curve about an equilibrium point (other than a saddle point) contained in at least one separatrix indicates the possibility of the periodic wave solution about that fixed point.

Figure 1.11(b) shows the phase portrait of the dynamical system (1.5.1) corresponding to the coexistence of solitary waves of both polarities and in figure 1.11(a), $V(\phi)$ is plotted against ϕ which shows the coexistence of solitary waves of both polarities. Here from the phase portrait, we see that there is only one separatrix that appears to start and end at the saddle point $(0, 0)$, but it encloses two non-saddle fixed points - one lies on the positive side of ϕ -axis, viz., $(0.7, 0)$ and the other fixed point lies on the negative side of ϕ -axis, viz., $(-0.43, 0)$. As one separatrix that appears to start and end at the origin $(0, 0)$ (saddle point) encloses two non-saddle fixed points lying on the opposite direction of ϕ - axis, we have a coexistence of solitary waves of both polarities.

Figure 1.12(b) shows the phase portrait of the dynamical system corresponding to an NPDL and this figure shows that the separatrix corresponding to the double layer solution appears to start and end at the saddle $(0, 0)$ and again, it appears to pass through the saddle point at $(-1.94, 0)$ enclosing the non-saddle fixed point $(-0.91, 0)$. In figure 1.12(a), $V(\phi)$ is plotted against ϕ. Figure 1.12(a) and figure 1.12(b) together give a one-one correspondence between the separatrix of the phase portrait as shown with a heavy blue line in the lower panel with the curve $V(\phi)$ against ϕ of the upper panel. This mechanism holds good for the formation of PPSWs and also for the formation of NPSWs. Therefore, figure 1.12(b) shows that the separatrix corresponding to the double layer solution appears to pass through two saddle points and it encloses other two fixed points. If both the saddle points exist after a small increment of M from $M = M_{NPDL}$, then the separatrix through the origin encloses an inner separatrix through a non-zero saddle and at least two equilibrium points as shown in figure 1.14(b) for $M = M_{NPDL} + 0.002$. So, according to the definition of

supersoliton as prescribed by Dubinov and Kolotkov [142], figure 1.14(b) corresponds to an NPSS. But for $M = M_{NPDL} + 0.01$, we get figure 1.15.

From the figures 1.10(b), 1.11(b) (part of phase portrait corresponding to NPSW), 1.13(b), and the figure 1.15(b), we observe that there is no qualitative difference between these four phase portraits. For all four phase portraits, there exist a saddle at the origin, a non-saddle fixed point lying on the negative ϕ - axis, and we have only one separatrix which appears to start and end at the saddle point (0,0) enclosing the non-saddle fixed point lying on the negative ϕ - axis. Therefore, figure 1.15 indicates the existence of an NPSW after the formation of NPDL and the phase portrait corresponding to this NPSW looks like a phase portrait corresponding to a conventioal NPSW. But the blue solid curve and blue dashed curve of figure 1.16 shows that there is a finite jump between the amplitudes of solitons for $M = M_{NPDL} - 0.01$ and $M = M_{NPDL} + 0.01$. This is not only true for $M = M_{NPDL} - 0.01$ and $M = M_{NPDL} + 0.01$, this result is also true for $M = M_{NPDL} - \epsilon$ and $M = M_{NPDL} + \epsilon$, i.e., there is a finite jump between the amplitudes of solitons for $M = M_{NPDL} - \epsilon$ and $M = M_{NPDL} + \epsilon$, and this has been shown by the black solid curve and black dashed curve of figure 1.16 for $\epsilon = 0.0001$. Thus, we get a sequence of supersolitons for increasing values of $M(> M_{NPDL})$, but if M exceeds a cut-off value M_{cr}, then the solitons after the formation of double layer simply reduce to conventional solitons, i.e., there exists a transition from supersoliton to soliton with the increment of M after the formation of double layer. To understand this transition process, we draw the saddle and other equilibrium points of the system (1.5.1) on the $\phi(= \phi_1)$-axis for increasing values of M starting from $M = M_{NPDL} + 0.0001$ in figure 1.17. This figure shows that the distance between the non-zero saddle and the non-saddle fixed point nearest to it decreases for increasing values of M and ultimately both of them disappear from the system. Finally, the system contains only one saddle at the origin and a non-saddle equilibrium point. Consequently, only one separatrix enclosing the non-saddle fixed point is possible that appears to pass through the saddle at the

origin. So, the existence of a soliton after the formation of a double layer confirms the existence of a sequence of supersolitons and there exists a critical value M_{cr} of M such that for the existence of supersolitons, we must have $M_{NPDL} < M < M_{cr}$, whereas for $M_{cr} \leq M < M_{nmax}$, we get soliton like structures after the formation of a double layer. Thus, figure 1.17 clearly shows the transition from supersoliton to soliton structures after the formation of a double layer.

1.6 Conclusions

IA solitary structures have been investigated in a collisionless magnetized dusty plasma system consisting of warm adiabatic ions, static negatively charged dust grains and nonthermal electrons. A complete set of equation of continuity in three dimension, equation of motion in three dimension and the pressure equation in three dimension for ion fluid has been considered to describe nonlinear behaviour of IA waves. Instead of Poisson equation, the quasi-neutrality condition is assumed to close the system of equations.

A complete analytic theory is presented to find the upper bounds M_{pmax} (M_{nmax}) of the Mach number M for the existence of all PPSWs (NPSWs). Again, we have also investigated an analytic theory to find the Mach numbers M_{PPDL} (M_{NPDL}) corresponding to a PPDL (NPDL) solution of the energy integral. With the help of these two analytic theories, one can easily develop appropriate algorithms to determine M_{pmax}, M_{nmax}, M_{PPDL} and M_{NPDL}. These Mach numbers help us to draw the compositional parameter space which shows the nature of existence of different solitary structures with respect to any parameter of the system.

We have seen that the description of solitary structures after the formation of the double layer of same polarity is helpful for investigating the existence of supersoliton structures of same polarity in comparison with the study of supersoliton structures at some discrete points of the compositional parameter spaces. The mechanism of

transition from the NPSS to a negative potential soliton after the formation of double layer of same polarity has been investigated through the phase portrait analysis of the dynamical system describing the nonlinear behaviour of IA waves. We have analyzed the formation of supersoliton structures and their limitations with the help of phase portraits. This is another important aspect of this chapter. In fact, this analysis determines the exact bound M for the existence of NPSSs.

It is observed that the system supports PPSWs, NPSWs, coexistence of solitary waves of both polarities, NPDLs, NPSWs after the formation of NPDLs and NPSSs. The qualitative behaviour of IA solitary structures is independent of the intensity of the magnetic field because the Sagdeev potential $V(\phi)$ is free from the intensity of the magnetic field. But the qualitative behaviour of IA solitary structures is very much sensible on the angle of propagation of the solitary structures with the uniform static magnetic field. In fact, $V(\phi)$ depends on $l_z = \cos\delta$, but does not depend on l_x and l_y, where δ is the angle between the direction of solitary structure and the direction of the external uniform static magnetic field.

The region of existence of PPSWs increases for increasing values of μ, whereas the region of existence of NPSWs decreases for increasing values of μ. The interval of β_e for the existence of NPDLs increases for increasing values of μ if $\mu \leq \mu^{(cr)}$, whereas if μ exceeds $\mu^{(cr)}$, interval of β_e for the existence of NPDLs decreases for increasing values of μ, where $\mu^{(cr)}$ is a critical value of μ. The region of existence of NPSWs before the formation of NPDLs increases for increasing values of μ whenever $\mu \leq \mu^{(cr)}$, whereas the region of existence of NPSWs before the formation of NPDLs decreases for increasing values of μ for $\mu > \mu^{(cr)}$.

Chapter 2

Ion acoustic solitary structures at the acoustic speed in a collisionless magnetized nonthermal dusty plasma †

In this chapter, we have investigated the existence of ion acoustic solitary structures including double layers and supersolitons at the acoustic speed in a collisionless magnetized plasma consisting of negatively charged static dust grains, adiabatic warm ions and nonthermal electrons. At the acoustic speed, for negative polarity, the system supports solitons, double layers, supersoliton structures after the formation of double layer, supersoliton structures without the formation of double layer, solitons after the formation of double layer whereas the system supports solitons and supersolitons without the formation of double layer for the case of positive polarity. But it is not possible to get the coexistence of solitary structures (including double layers and supersolitons) of opposite polarities. For negative polarity, we have observed an important transformation, viz., soliton before the formation of double layer $\rightarrow$ double layer $\rightarrow$ supersoliton $\rightarrow$ soliton after the formation of double layer whereas for both positive and negative polarities, we have observed the transformation from solitons to supersolitons without the formation of double layer. There does not exist any negative (positive) potential solitary structures within $0 < \mu < \mu_c$ ($\mu_c < \mu < 1$) and the amplitude of the positive (negative) potential solitary structure decreases for increasing (decreasing) μ and the solitary structures of both polarities collapse at $\mu = \mu_c$, where μ_c is a critical value of μ, the ratio of unperturbed number density of electrons to that of ions. Similarly, there exists a critical value β_{e2} of the nonthermal parameter β_e such that the solitons of both polarities collapse at $\beta_e = \beta_{e2}$.

†This chapter has been published in ***Zeitschrift fr Naturforschung A***, **76**, pp. 985-1005, 2021; https://doi.org/10.1515/zna-2021-0120

2.1 Introduction

Several authors [1, 12, 35, 56, 62, 67, 69, 71–73, 75, 77, 90, 111, 113, 119, 123, 127, 143–166] investigated solitary structures and/or double layers and/or supersolitons for the supersonic speed of the waves, i.e., for $M > M_c$, where M is the velocity of the wave frame normalized by linearized speed of the respective wave in the plasma system and M_c is the critical value of M such that $M > M_c$ indicates supersonic speed of the wave, $M < M_c$ indicates subsonic speed of the wave and $M = M_c$ indicates that the wave is moving at the acoustic speed. Therefore, M_c is the lower bound of the Mach number M for the existence of solitary structures including double layers and supersolitons, and consequently solitary structures including double layers and supersolitons begin to exist for $M > M_c$. For the first time, in the magnetized plasma, we have invstigated solitary structures including double layers and supersolitons at the acoustic speed.

For the first time, Verheest and Hellberg [167] observed the positive potential dust acoustic solitary structure at the acoustic speed in a collisionless unmagnetized plasma consisting of negatively charged dust paticulates and different species of ions at different temperatures. After that Baluku *et al.* [49] have also observed dust ion acoustic solitary structure at the acoustic speed in a collisionless unmagnetized dusty plasma consisting of cold dust particles, adiabatic warm ions and κ distributed electrons. They have also considered all the three cases, viz., $M = M_c$ (sonic case), $M < M_c$ (subsonic case) and $M > M_c$ (supersonic case) (see figures 4(c) - 4(f) in Baluku *et al.* [49]). They have shown the existence of solitary structures for both the cases $M = M_c$ (sonic case) and $M > M_c$ (supersonic case). In a later paper, Baluku *et al.* [168] have also observed ion acoustic solitary structure at the acoustic speed in

a collisionless unmagnetized plasma consisting of two different species of electrons at different temperatures. The numerical observations [49, 167, 168] of the existence of solitary structure at the acoustic speed ($M = M_c$) influenced Das *et al.*[70] to investigate the analytical theory for the existence of solitary structures including double layers at the acoustic speed, and finally they have proved three important results to confirm the existence of different solitary structures in plasma systems. They have applied these results to investigate the existence of dust acoustic solitary structures including double layers at the acoustic speed in a nonthermal dusty plasma, where ion species follows nonthermal Cairns distribution [1], electron species is isothermal with negatively charged dust grains. In 2015, Verheest & Hellberg [169] have shown the existence of double layers and supersolitons at the acoustic speed in a plasma consisting of cold positive and negative ions, in presence of Cairns distributed [1] nonthermal electrons. Recently, Paul *et al.* [170] have used the results of Das *et al.*[70] to investigate dust ion acoustic solitary structures at the acoustic speed in a collisionless unmagnetized four component dusty plasma system consisting of nonthermal [1] electrons, isothermal positrons, adiabatic warm ions and negatively charged static dust grains. They have also considered the case when there is no positron in the system. In this case, they have found the existence of negative potential double layer (NPDL) and negative potential supersoliton (NPSS) at the acoustic speed. Finally, they have also investigated the transformation of different negative potential solitary structures at the acoustic speed just before and just after the formation of double layer.

In Chapter-1, we have investigated the arbitrary amplitude ion acoustic solitary structures including double layers and supersolitons in a collisionless magnetized dusty plasma consisting of adiabatic warm ions, negatively charged static dust grains and

nonthermal [1] electrons. Although the method of construction of the distribution function of energetic particles in astrophysical plasmas is a very difficult problem when the particles are not in thermal equilibrium, different non-Maxwellian distributions have been used to describe the behaviour of the energetic particles. One of the widely used non-Maxwellian distributions is the κ distribution. Long years ago, Binsack [37] , Olbert [38] , Vasyliunas [39] used this distribution to describe a population of fast energetic particles along the long tail of one humped symmetrical distribution about $v = 0$, where v is the velocity of electron in phase space. So, using this κ distribution, one cannot describe a population of fast energetic electrons in a finite region of the phase space in the neighbourhood of $v = 0$. However, Cairns *et al.* [1] modelled the following velocity distribution to describe the effect of fast energetic electrons together with a population of Maxwellian distributed electrons:

$$f_{ce0}(v^2) = \frac{n_{e0}}{\sqrt{2\pi}} \frac{1 + \alpha_e \Big(\frac{v}{v_{te}}\Big)^4}{(1 + 3\alpha_e) v_{te}} \exp\left[- \frac{v^2}{2v_{te}^2} \right], \tag{2.1.1}$$

where $\alpha_e (\geq 0)$ is a nonthermal parameter, n_{e0} is the unperturbed number density of electrons and $v_{te} = \sqrt{K_B T_e / m_e}$ with T_e is the average temperature of electrons, K_B is the Boltzmann constant and m_e is the mass of an electron. Instead of α_e, one can consider β_e as the nonthermal parameter which determines the proportion of fast energetic electrons, where

$$\beta_e = \frac{4\alpha_e}{1 + 3\alpha_e}. \tag{2.1.2}$$

As $\alpha_e \geq 0$, it is simple to check the following restriction on β_e: $0 \leq \beta_e < \frac{4}{3}$. Now, this distribution can be regarded as a modified Maxwellian having the following properties: **(a)** In the neighbourhood of the point $v = 0$, the number of electrons is much smaller than the number of electrons for the case of a Maxwellian distribution.

(b) In the neighbourhood of the point $v = 0$, the number of electrons decreases with increasing β_e for $0 \leq \beta_e < \frac{4}{3}$ and for $\beta_e \to \frac{4}{3}$, the number of electrons almost vanishes in a small neighbourhood of $v = 0$. For $\beta_e = 0$, Cairns distribution reduces to the Maxwellian isothermal distribution.

(c) For $\beta_e > 4/7$, in Chapter-1, we have reported clearly that the distribution function has three local maxima at three different points $v = -V$, $v = 0$ and $v = V$ in phase space, where

$$V = v_{te} \times \sqrt{2 + \sqrt{7 - 4(\beta_e)^{-1}}}. \tag{2.1.3}$$

This property of the Cairns distribution is qualitatively different from Maxwellian distribution or κ distibution because Maxwellian distribution and κ distibution are both one humped symmetrical distributions about $v = 0$.

(d) For $0 \leq \beta_e \leq 4/7$, the distribution function is a one humped symmetrical distribution about $v = 0$ which is qualitatively similar to the Maxwell - Boltzmann distribution or κ distribution. Consequently, β_e is restricted by the following inequality: $0 \leq \beta_e \leq 4/7$. This restriction on β_e has already been reported by Verheest & Pillay [60].

(e) The mean speed $\langle v \rangle$ and the root - mean - square - velocity $\sqrt{\langle v^2 \rangle}$ are respectively given by

$$\langle v \rangle = 0 \text{ and } \sqrt{\langle v^2 \rangle} = \sqrt{1 + 3\beta_e}\ v_{te}. \tag{2.1.4}$$

For $\beta_e = 0$, the root - mean - square - velocity is same as that for the Maxwellian distribution.

(f) This Cairns distribution [1] includes a ring structure. This distribution can explain both positive and negative polarity structures observed in space plasma. In fact,

Cairns *et al.* [1] used this one-dimensional nonthermal model to study the existence of nonlinear structures like those observed by the Freja [58] and Viking Satellites [94, 96]. It was shown that this distribution can describe the existence of both positive and negative density perturbations, which could not be prevailed with Maxwellian electrons or κ distributed electrons. More specifically, the electric field structures observed by the FAST [98–100, 103, 107] and Viking Satellite [94, 96] in the auroral zone together with the Freja Satellite [58] observations in the auroral zone of the upper ionosphere and the observations by GEOTAIL [97] and POLAR [101, 102, 107] missions in the Earth's magnetosphere indicate the existence of fast energetic electrons. In a number of astrophysical environments [58, 92–107], one can use Cairns distribution for lighter species.

In Chapter-1, we have used the Sagdeev pseudo potential technique to investigate the existence and the nature of both positive and negative potential solitary waves, coexistence of solitary waves of both polarities, negative potential double layers and negative potential supersolitons for the Mach number $M > M_c$. In the present chapter, we have considered the same collisionless magnetized nonthermal dusty plasma to study the ion acoustic solitary structures at the acoustic speed $M = M_c$. In general, solitary structures including double layer and supersoliton are nonlinear wave structures. Using the mechanical analogy of Sagdeev [11], the solitary structure can be explained by considering one-dimensional motion of a pseudo particle of unit mass under the action of a definite force field. Because of the particle-like behaviour of the solitary structure, its shape and size remain unchanged during its propagation. In several papers, Paul and his co-workers [73, 75, 77, 165] reported that the double layers are responsible to accelerate the charged particles and the formation of double layer

is helpful to study the possible causes of acceleration of energetic particles in several space plasma environments. In this regard, it can be noted that the phenomenon of acceleration of the particles in auroral zone of the atmosphere is due to double layers which are often generated in the magnetosphere of the earth [171]. However, we have considered the particle-like behaviour of the solitary structures at the acoustic speed in Section 2.4 whereas we have studied different solitary structures by considering the separatrices of a dynamical system described by a system of coupled equations in Section 2.6.

The basic hydrodynamic equations describing these nonlinear behaviours of the ion acoustic waves are the equation of continuity of ions, equation of motion of ions, equation of pressure of ions. These hydrodynamic equations are supplemented by the quasi-neutrality condition, where we have assumed that the length scale of the solitary structure is greater than the Debye length or the ion-gyroradius [90, 111]. With the help of these equations, we want to study the existence and the nature of the different ion acoustic solitary structures including double layers and supersolitons at the acoustic speed giving special emphases on the following points:

- Lifting the hydrodynamic equations in the wave frame moving with a constant velocity M normalized by the ion acoustic speed C_s along the direction having unit vector $\widehat{L} = l_x\widehat{x} + l_y\widehat{y} + l_z\widehat{z}$, we have derived the energy integral with $V(M, \phi)$ being the Sagdeev pseudo potential and for $M = M_c$, one can analyze $V(M, \phi)(= V(M_c, \phi))$ to investigate the existence and the nature of different solitary structures at the acoustic speed.

- At the acoustic speed, the Mach number M is given by the equation : $M = M_c = l_z M_s$, where M_s is a function of $\gamma(= 5/3)$, σ_{ie}, β_e and μ, i.e., $M_s =$

$M_s(\gamma,\ \sigma_{ie},\ \beta_e,\ \mu)$. So, one can take the variation of M_s with respect to β_e or μ because $\gamma(= 5/3)$ is a fixed parameter and σ_{ie} can also be taken as fixed for specific plasma system. So, in the present work, we want to investigate the existence and the nature of different solitary structures along the curve $M = M_c$.

- For the first time, in the magnetized plasma, we have critically discussed the criteria for the existence of different solitary structures at the acoustic speed, i.e., at $M = M_c$. We have seen that the criteria for the existence of different solitary structures at the acoustic speed depend on $V(M_c, \phi)$ but the nature of different solitary structures depends on the sign of the derivative of $V(M_c, \phi)$ with respect to ϕ at $\phi = 0$.

- We have found that $V(M_c, 0) = 0$, $V'(M_c, 0) = 0$, $V''(M_c, 0) = 0$ and in this case, the nature of the solitary structures depends on the sign of $V'''(M_c, 0)$. In particular, $V'''(M_c, 0) < 0$ implies that the system may support positive potential soliton structures including positive potential double layers and positive potential supersolitons at the acoustic speed whereas $V'''(M_c, 0) > 0$ implies that the system may support negative potential soliton structures including negative potential double layers and negative potential supersolitons at the acoustic speed. If $V'''(M_c, 0) = 0$, then one can discuss the nature of the solitary structure by considering the sign of $V^{iv}(M_c, 0)$.

- For the first time, in the magnetized plasma, we have investigated different ion acoustic solitary structures at the acoustic speed. In fact, we have observed the existence of the following solitary structures at the acoustic speed, i.e., at

$M = M_c$: (a) positive potential solitons (PPSWs), (b) negative potential solitons (NPSWs), (c) negative potential double layers (NPDLs), (d) negative potential supersoliton (NPSS) structures after the formation of NPDL, (e) NPSS structures without the formation of NPDL, (f) NPSW structures after the formation of NPDL, (g) positive potential supersoliton (PPSS) structures without the formation of positive potential double layer (PPDL).

- At the acoustic speed, we have observed that it is not possible to get (a) coexistence of both PPSW and NPSW structures, (b) coexistence of both PPDL and NPDL structures, (c) coexistence of both PPSS and NPSS structures. In fact, for the first time in the magnetized plasma, we have observed that there is no coexistence of solitary structures of opposite polarities at the acoustic speed which supports an important result (THEOREM 5) derived by Das *et al.* [70].

- At the acoustic speed, we have seen that the amplitude of negative potential soliton decreases with increasing β_e whereas the amplitude of positive potential soliton decreases with decreasing β_e and both negative and positive potential solitons collapse at the critical value β_{e2} of β_e such that $V'''(M_c, 0) = 0$ at $\beta_e = \beta_{e2}$. At this point of the compositional parameter space of $V'''(M_c, 0)$ with respect to β_e, we have $V^{iv}(M_c, 0) > 0$ which indicates that it is impossible to get any solitary structure at $\beta_e = \beta_{e2}$.

- At the acoustic speed, we have seen that the amplitude of negative potential soliton increases with increasing μ whereas the amplitude of positive potential soliton decreases with increasing μ and both negative and positive potential solitons collapse at the critical value μ_c of μ such that $V'''(M_c, 0) = 0$ at $\mu = \mu_c$.

At this point of the compositional parameter space $V'''(M_c, 0)$ with respect to μ, we have $V^{iv}(M_c, 0) > 0$ which indicates that it is impossible to get any solitary structure at $\mu = \mu_c$.

- For the first time, in the magnetized plasma, phase portraits corresponding to the different solitary structures have been drawn at the acoustic speed to make a clear difference between the conventional soliton structures, double layer structures and supersoliton structures that we have obtained in the present plasma system.

- For the first time, in the magnetized plasma, the transformation process of different negative potential soliton structures has been investigated at the acoustic speed, viz., NPSW (before the formation of NPDL) $\rightarrow$ NPDL $\rightarrow$ NPSS $\rightarrow$ NPSW (after the formation of NPDL). In fact, we have investigated the transformation of different negative potential solitary structures at the acoustic speed just before and just after the formation of double layer.

- For the first time, in the magnetized plasma, the transformation process of NPSW structures has also been considered at the acoustic speed without the formation of double layer structure of same polarity, viz., NPSW $\rightarrow$ NPSS, i.e., here we have investigated the transformation of different negative potential solitary structures at the acoustic speed just before the formation of NPSS. Similar process of transformation from PPSW structure to PPSS structure at the acoustic speed can also be verified when there is no double layer of same polarity.

In this chapter, we have used the same set of hydrodynamic equations (1.2.1) - (1.2.3) of **Chapter-1** consisting of the continuity equation, the equation of motion and the pressure equation of ion fluid along with the same quasi-neutrality condition (1.2.4) of **Chapter-1**, but for easy readability of this chapter the complete set of basic equations has been given in the next section of this chapter also.

2.2 Basic Equations

The present plasma system is collisionless, magnetized and nonthermal one, which contains negatively charged static dust particulates, nonthermal electrons and adiabatic warm ions. The system is under the action of constant magnetic field directed along $z-$axis. We have considered the same basic hydrodynamic equations as given in Chapter-1, although for the convenience of the reader, we restate those equations:

$$\frac{dn_i}{dt} + n_i(\overrightarrow{\nabla} \cdot \overrightarrow{u}_i) = 0, \tag{2.2.1}$$

$$\frac{d\overrightarrow{u}_i}{dt} + \frac{\sigma_{ie}}{n_i}\overrightarrow{\nabla} p_i = -\overrightarrow{\nabla}\phi + \overrightarrow{u}_i \times \widehat{z}, \tag{2.2.2}$$

$$\frac{dp_i}{dt} + \gamma p_i(\overrightarrow{\nabla} \cdot \overrightarrow{u}_i) = 0, \tag{2.2.3}$$

where (2.2.1) is the continuity equation of ion fluid, (2.2.2) describes the conservation of momentum for ions, (2.2.3) is the pressure equation of ion fluid. These hydrodynamic equations are supplemented by the following quasi-neutrality condition on the basis of the assumption that the length scale of the solitary structure is greater than the Debye length or the gyroradius [90, 111]:

$$n_i = n_e + 1 - \mu. \tag{2.2.4}$$

Here

$$\frac{d}{dt} = \frac{\partial}{\partial t} + \overrightarrow{u}_i \cdot \overrightarrow{\nabla}, \tag{2.2.5}$$

$$\frac{Z_d n_{d0}}{n_{i0}} = 1 - \mu, \tag{2.2.6}$$

$$n_e = \mu\big(1 - \beta_e\phi + \beta_e\phi^2\big)e^{\phi}, \tag{2.2.7}$$

where we have used the equilibrium charge neutrality condition (2.2.6) to get (2.2.4), the equation (2.2.7) describes the number density of Cairns distributed [1] nonthermal electrons, $\mu = n_{e0}/n_{i0}$ with n_{e0}, n_{i0} and n_{d0} are, respectively, the unperturbed electron, ion and dust number densities, Z_d is the number of electrons residing on a dust grain surface, each spatial variable is normalized by ion gyroradius $r_g(= C_s/\omega_c)$ and time is normalized by the inverse of ion gyrofrequency $(\omega_c)^{-1}$, where $C_s = \sqrt{K_B T_e/m_i}$ and ω_c is the ion gyrofrequency. Again, the quantities n_i, n_e, $\overrightarrow{u}_i = (u_{ix}, u_{iy}, u_{iz})$, p_i and ϕ are, respectively, the ion number density, the electron number density, the ion fluid velocity vector, the ion fluid pressure and the electrostatic potential, and these quantities have been nomalized by n_{i0}, n_{i0}, C_s, $n_{i0}K_BT_i$, K_BT_e/e respectively. Here $\gamma(= 5/3)$ is the adiabatic index, m_i is the mass of an ion, and $\sigma_{ie} = T_i/T_e$.

Again, using (2.2.7), equation (2.2.4) can be written as

$$n_i = \mu\big(1 - \beta_e\phi + \beta_e\phi^2\big)e^{\phi} + 1 - \mu. \tag{2.2.8}$$

In Chapter-1, we have already analyzed the linear dispersion relation for low frequency IA waves obtained from the system of equations (2.2.1) - (2.2.3) and (2.2.8). Lifting the equations (2.2.1) - (2.2.3) in the wave frame moving with a constant dimensionless velocity M normalized by C_s (ion acoustic speed) along a direction having direction cosines (l_x, l_y, l_z), in Chapter-1, we have already investigated the existence of different solitary structures for $M > M_c$, where M is the normalized velocity or dimensionless velocity of the wave frame and M_c is the lower bound of M for the existence of solitary structures, i.e., solitary structures begin to exist for

$M > M_c$. The Mach number M or the constant velocity M normalized by C_s can also be defined as follows:

$$M = \frac{U}{C_s}, \tag{2.2.9}$$

where U is the actual velocity of the wave frame.

Specifically, in Chapter-1, we have presented an analytic theory to find the upper bound M_{pmax} (M_{nmax}) of M for the existence of all positive (negative) potential solitary structures, i.e., one can get positive (negative) potential solitary structures for $M_c < M < M_{pmax}$ ($M_c < M < M_{nmax}$). But they have not investigated the ion acoustic solitary structures when $M = M_c$ or $U = M_c C_s$. This is the first problem in magnetized plasma where we have investigated the existence of different solitary structures at $M = M_c$, i.e., at the lower bound of the Mach number. In this chapter, we have used the equations (2.2.1) - (2.2.3) and (2.2.8) to study the existence of different solitary structures at $M = M_c$.

2.3 Energy Integral

Assuming that all the dependent variables depend only on a single variable $\xi = l_x x + l_y y + l_z z - Mt$ with $l_x^2 + l_y^2 + l_z^2 = 1$, where M is independent of x, y, z and t, in order to study the arbitrary amplitude time independent IA solitary structures, and lifting the equations (2.2.1) - (2.2.3) in the wave frame moving with a constant velocity M normalized by C_s along the direction $\widehat{L} = l_x\widehat{x} + l_y\widehat{y} + l_z\widehat{z}$, we get the following equations:

$$\Big(-M+u\Big)\frac{dn_i}{d\xi} + n_i\frac{du}{d\xi} = 0, \tag{2.3.1}$$

$$\Big(-M+u\Big)\frac{d\overrightarrow{u}_i}{d\xi} + \Big(\frac{\sigma_{ie}}{n_i}\frac{dp_i}{d\xi} + \frac{d\phi}{d\xi}\Big)\widehat{L} = \overrightarrow{u}_i \times \widehat{z}, \tag{2.3.2}$$

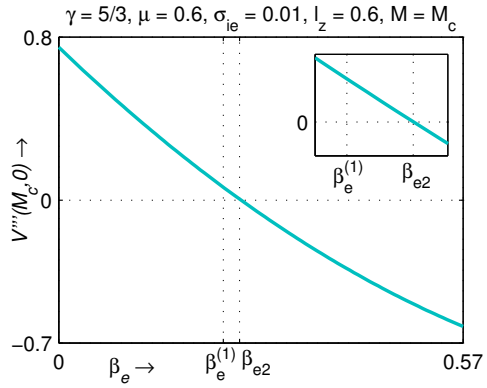

Figure 2.1: $V'''(M_c, 0)$ is plotted against β_e. This figure shows the sign of $V'''(M_c, 0)$ with respect to β_e.

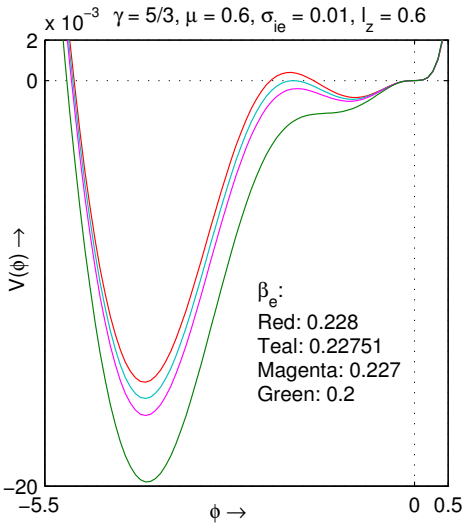

Figure 2.2: $V(\phi)$ is plotted against ϕ for different values of β_e at $M = M_c$. Here red curve corresponds to a conventioal NPSW structure before the formation of NPDL structure for $\beta_e = 0.228$, teal curve corresponds to a NPDL structure for $\beta_e = 0.22751$, magenta curve corresponds to a NPSS structure for $\beta_e = 0.227$ and green curve corresponds to a conventioal NPSW structure after the formation of NPDL structure for $\beta_e = 0.225$.

$$\Big(- M + u \Big) \frac{dp_i}{d\xi} + \gamma p_i \frac{du}{d\xi} = 0, \tag{2.3.3}$$

where we have used the following notations:

$$u = l_x u_{ix} + l_y u_{iy} + l_z u_{iz}. \tag{2.3.4}$$

Eliminating $\dfrac{du}{d\xi}$ from the equations (2.3.1) and (2.3.3), we get the following equation:

$$n_i \frac{dp_i}{d\xi} - \gamma p_i \frac{dn_i}{d\xi} = 0. \tag{2.3.5}$$

This equation can be simplified as follows:

$$\frac{d}{d\xi} \Big[p_i n_i^{-\gamma} \Big] = 0. \tag{2.3.6}$$

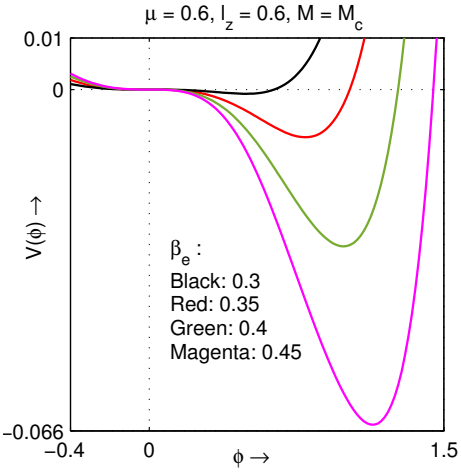

Figure 2.3: $V(\phi)$ is plotted against ϕ in the positive direction of ϕ - axis for different values of β_e at $M = M_c$. Here black curve ($\beta_e = 0.3$), red curve ($\beta_e = 0.35$), green curve ($\beta_e = 0.4$) and magenta curve ($\beta_e = 0.45$) correspond four different PPSWs with increasing amplitude.

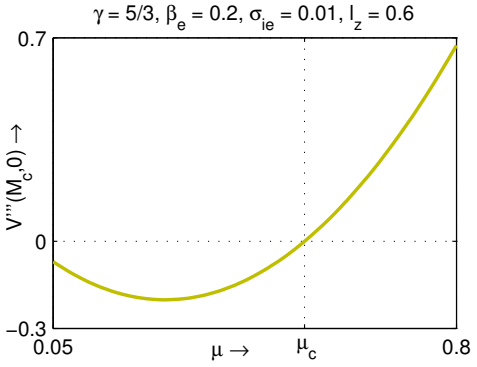

Figure 2.4: $V'''(M_c, 0)$ is plotted against μ for fixed values of the other parameters as mentioned in the figure. This figure shows that $V'''(M_c, 0) < 0$ for $\mu < \mu_c (\approx 0.5175)$, $V'''(M_c, 0) = 0$ for $\mu = \mu_c$ and $V'''(M_c, 0) > 0$ for $\mu > \mu_c$.

Integrating the above equation with respect to ξ and using the boundary conditions:

$$\left(n_i, p_i, u_{ix}, u_{iy}, u_{iz}, \phi, \frac{d\phi}{d\xi}\right) \to \left(1, 1, 0, 0, 0, 0, 0\right) \quad \text{as} \quad |\xi| \to \infty, \tag{2.3.7}$$

we get the following adiabatic law for ion pressure p_i:

$$p_i = n_i^{\gamma}. \tag{2.3.8}$$

Using equation (2.3.8), the coefficient of $\widehat{L}$ as given in the second term of left hand side of (2.3.2) can be simplified as follows

$$\frac{\sigma_{ie}}{n_i}\frac{dp_i}{d\xi} + \frac{d\phi}{d\xi} = \frac{dH}{d\xi} \tag{2.3.9}$$

where

$$H = H(\phi) = \frac{\gamma\sigma_{ie}}{\gamma - 1}(n_i)^{\gamma-1} + \phi, \tag{2.3.10}$$

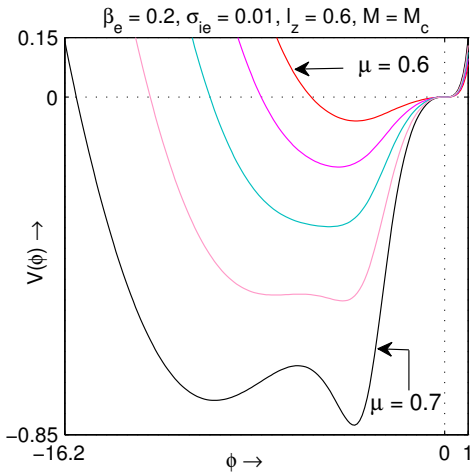

Figure 2.5: $V(\phi)$ is plotted against ϕ for different values of μ at $M = M_c$. Here red curve ($\mu = 0.6$), magenta curve ($\mu = 0.625$), green curve ($\mu = 0.65$) all correspond to conventional NPSW structures whereas pink curve ($\mu = 0.675$) and black curve ($\mu = 0.7$) indicate the formation of NPSS structures without the formation of NPDL structure.

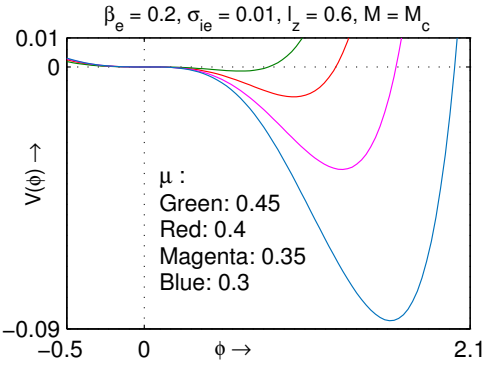

Figure 2.6: $V(\phi)$ is plotted against ϕ for different values of μ at $M = M_c$. Here green curve ($\mu = 0.45$), red curve ($\mu = 0.4$), magenta curve ($\mu = 0.35$) and blue curve ($\mu = 0.3$) all correspond to conventional PPSW structures.

and consequently x-component, y-component and z-component of (2.3.2) can be written in the following form:

$$\Big(-M+u\Big)\frac{du_{ix}}{d\xi}+l_x\frac{dH}{d\xi}-u_{iy}=0, \tag{2.3.11}$$

$$\Big(-M+u\Big)\frac{du_{iy}}{d\xi}+l_y\frac{dH}{d\xi}+u_{ix}=0, \tag{2.3.12}$$

$$\Big(-M+u\Big)\frac{du_{iz}}{d\xi}+l_z\frac{dH}{d\xi}=0. \tag{2.3.13}$$

Writing the equation (2.3.1) in the form

$$\frac{d}{d\xi}\Big[\Big(-M+u\Big)n_i\Big]=0, \tag{2.3.14}$$

and integrating this equation with respect to ξ, we get the following expression of u:

$$u=M\Big(1-\frac{1}{n_i}\Big), \tag{2.3.15}$$

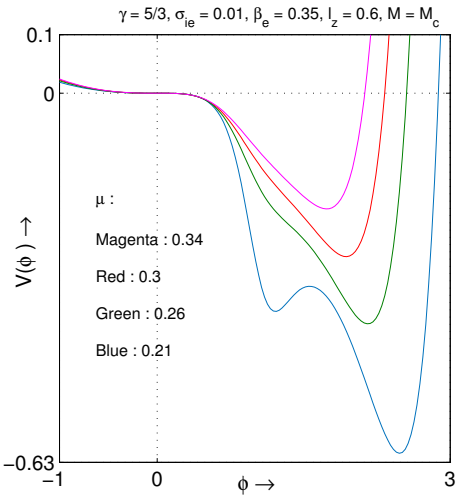

Figure 2.7: $V(\phi)$ is plotted against ϕ for different values of μ at $M = M_c$. Here magenta curve ($\mu = 0.34$), red curve ($\mu = 0.3$), green curve ($\mu = 0.26$) indicate the existence of PPSWs and blue curve ($\mu = 0.21$) indicates the PPSS without the formation of PPDL structure.

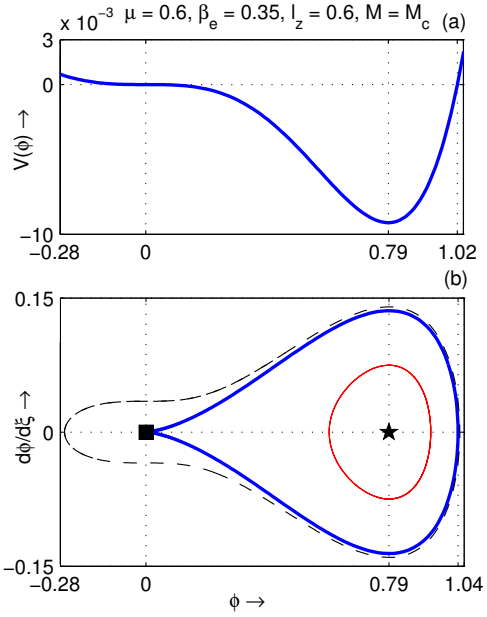

Figure 2.8: (a) $V(\phi)$ and (b) the phase portrait of the system are drawn on the same ϕ-axis for $\mu = 0.6$, $\beta_e = 0.35$, $l_z = 0.6$ and at the corresponding M_c. The separatrix of lower panel of this figure as shown in blue curve corresponds to a PPSW.

where the condition (2.3.7) has been used to find the integration constant.

Using (2.3.15), the equation (2.3.13) can be written as follows:

$$\frac{d}{d\xi}\Big[u_{iz} - \frac{l_z}{M}\Big(\sigma_{ie} n_i^{\gamma} + \int n_i d\phi\Big)\Big] = 0. \tag{2.3.16}$$

The derivation of (2.3.16) is given in Appendix - A.

Integrating the equation (2.3.16) with respect to ξ and using the boundary condition (2.3.7) to obtain the constant of integration, we get the following equation:

$$u_{iz} = \frac{l_z}{M} G(\phi), \tag{2.3.17}$$

where

$$G = G(\phi) = \sigma_{ie}\{(n_i)^{\gamma} - 1\} + \int_0^{\phi} n_i d\phi. \tag{2.3.18}$$

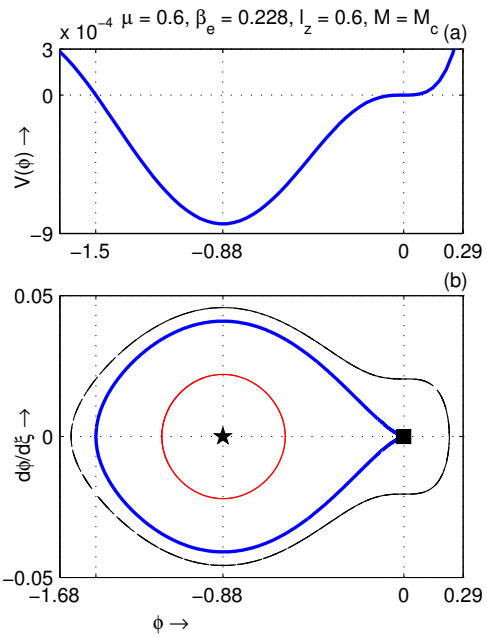

Figure 2.9: (a) $V(\phi)$ and (b) the phase portrait of the system are drawn on the same ϕ-axis for $\mu = 0.6$, $\beta_e = 0.228$, $l_z = 0.6$, $M = M_c$. The separatrix of lower panel of this figure as shown in blue curve corresponds to an NPSW.

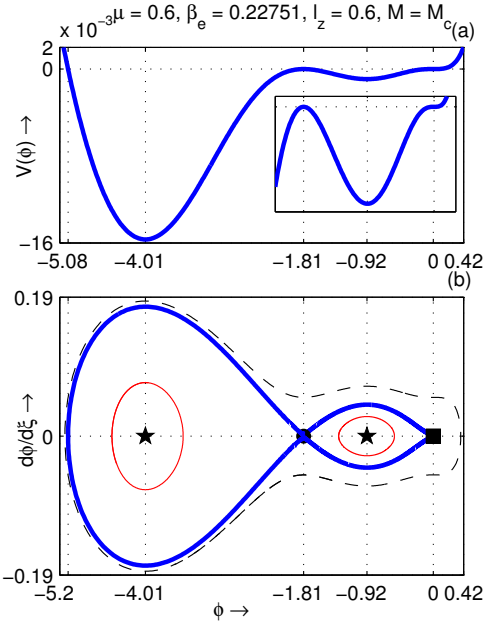

Figure 2.10: (a) $V(\phi)$ and (b) the phase portrait of the system are drawn on the same ϕ-axis for $\mu = 0.6$, $\beta_e = 0.22751$, $l_z = 0.6$, $M = M_c$. The separatrix of lower panel of this figure as shown in blue curve corresponds to an NPDL.

From equation (2.3.4), we get the following expression of $l_x u_{ix} + l_y u_{iy}$:

$$l_x u_{ix} + l_y u_{iy} = M - \frac{M}{n_i} - \frac{l_z^2}{M} G(\phi), \tag{2.3.19}$$

where we have used the equations (2.3.15) and (2.3.17) to eliminate u and u_{iz} from the resulting equation.

Multiplying (2.3.11) by l_x and (2.3.12) by l_y, finally, adding these equations, we get

$$\Big(- M + u\Big) \frac{d}{d\xi} \Big(l_x u_{ix} + l_y u_{iy} \Big) + \Big(l_x^2 + l_y^2 \Big) \frac{dH}{d\xi} + l_y u_{ix} - l_x u_{iy} = 0. \tag{2.3.20}$$

Using the expression of u as given in equation (2.3.15) and the expression of $l_x u_{ix} + l_y u_{iy}$ as given in equation (2.3.19), the equation (2.3.20) can be written in the following

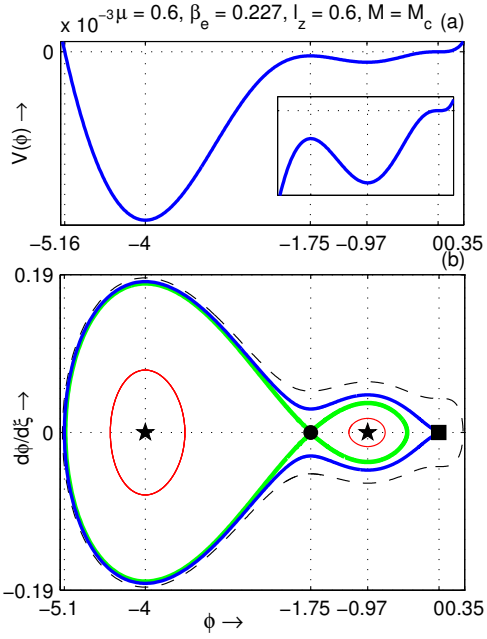

Figure 2.11: (a) $V(\phi)$ and (b) the phase portrait of the system are drawn on the same ϕ-axis for $\mu = 0.6$, $\beta_e = 0.227$, $l_z = 0.6$, $M = M_c$. The separatrix of lower panel of this figure as shown in blue curve contains another separatrix as shown in green curve and this separatrix (shown in blue curve) corresponds to a NPSS.

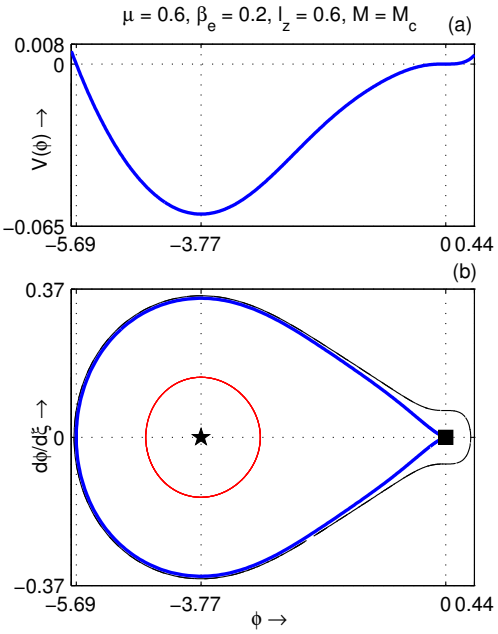

Figure 2.12: (a) $V(\phi)$ and (b) the phase portrait of the system are drawn on the same ϕ-axis for $\mu = 0.6$, $\beta_e = 0.2$, $l_z = 0.6$, $M = M_c$. The separatrix of lower panel of this figure corresponds to a conventional NPSW after the formation of NPDL.

form:

$$l_y u_{ix} - l_x u_{iy} = -\frac{dP}{d\xi}, \tag{2.3.21}$$

where

$$P = \frac{M^2}{2(n_i)^2} + H, \tag{2.3.22}$$

and we have used the condition $l_x^2 + l_y^2 + l_z^2 = 1$.

Solving the linear equations (2.3.19) and (2.3.21) for the unknown variables u_{ix}

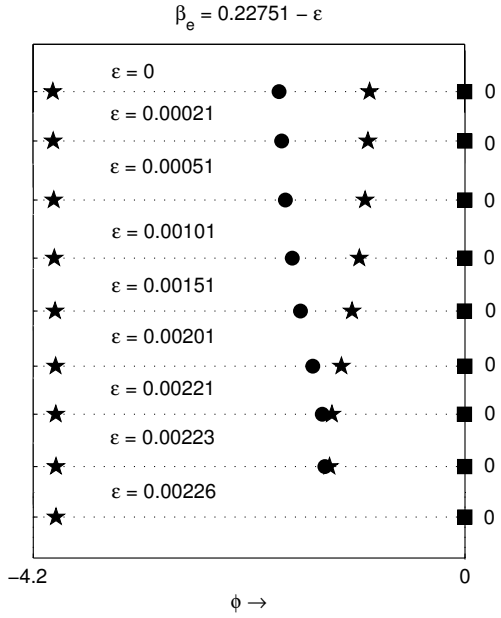

Figure 2.13: Point of inflexion (small solid square), unstable fixed point (small solid circle) and stable fixed point (small solid star) for the dynamical system (2.6.2) are drawn on the $\phi-$axis for different values of $\beta_e = 0.22751-\epsilon$ where $\epsilon = 0$ corresponds to NPDL. This figure shows the smooth transformation process in different negative potential soliton structures, viz., NPSW (before the formation of NPDL) $\rightarrow$ to NPDL $\rightarrow$ to NPSS $\rightarrow$ to conventional NPSW (after the formation of NPDL).

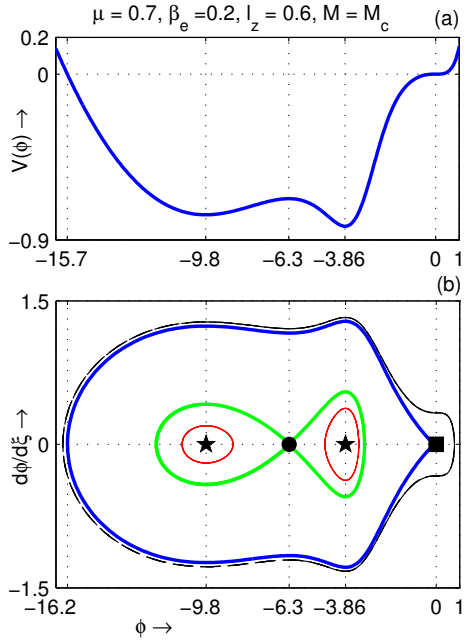

Figure 2.14: (a) $V(\phi)$ and (b) the phase portrait of the system are drawn on the same ϕ-axis at $M = M_c$. The separatrix of lower panel of this figure as shown in blue curve contains another separatrix as shown in green curve and this separatrix (shown in blue curve) corresponds to a NPSS.

and u_{iy}, we get

$$u_{ix} = \frac{l_x\left\{M - \frac{M}{n_i} - \frac{l_z^2}{M}G(\phi)\right\} - l_y\frac{dP}{d\xi}}{l_x^2 + l_y^2}, \tag{2.3.23}$$

$$u_{iy} = \frac{l_y\left\{M - \frac{M}{n_i} - \frac{l_z^2}{M}G(\phi)\right\} + l_x\frac{dP}{d\xi}}{l_x^2 + l_y^2}. \tag{2.3.24}$$

Substituting these two values of u_{ix} and u_{iy} in (2.3.11) or in (2.3.12), we get the

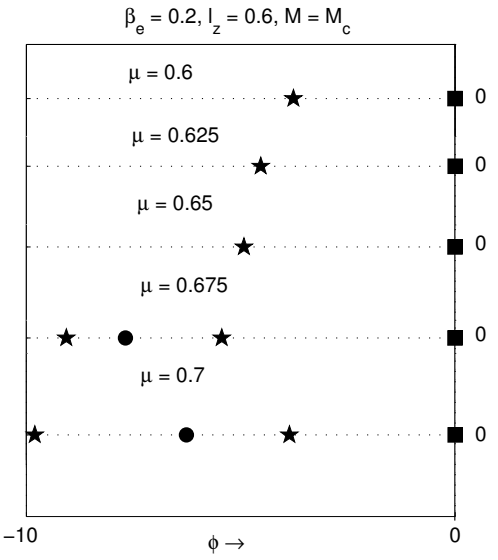

Figure 2.15: Point of inflexion (small solid square), unstable fixed point (small solid circle) and stable fixed point (small solid star) for the dynamical system (2.6.2) are drawn on the $\phi-$axis for different values of μ. This figure shows the transformation from conventional NPSW structures to NPSS structures without the formation of NPDL structure.

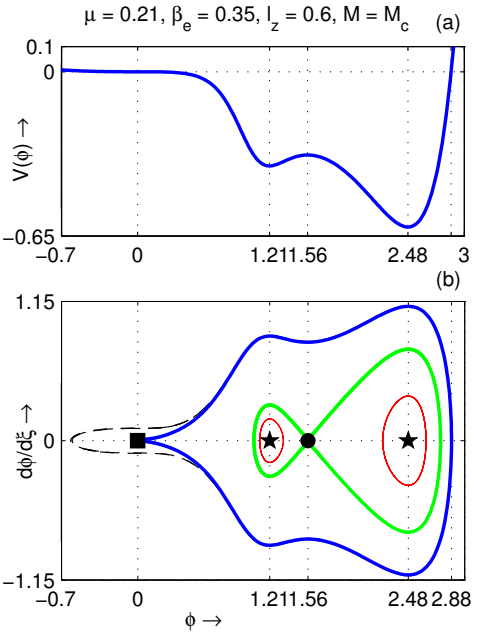

Figure 2.16: (a) $V(\phi)$ and (b) the phase portrait of the system are drawn on the same ϕ-axis at $M = M_c$. The separatrix of lower panel of this figure as shown in blue curve contains another separatrix as shown in green curve and this separatrix (shown in blue curve) corresponds to a PPSS.

following equation:

$$\frac{d^2P}{d\xi^2} = F(\phi) = n_i - 1 - \frac{l_z^2}{M^2} n_i G(\phi). \tag{2.3.25}$$

From the expression n_i as given in (2.2.8), we see that n_i is a function of ϕ. Again, from the expression H as given in (2.3.10), we can conclude that H is a function of ϕ. So, from equation (2.3.22), one can conclude that P is a function of ϕ and ϕ is a function of ξ. Therefore, from the chain rule of composite function, one can write

$$\frac{d^2P}{d\xi^2} = \frac{d^2\phi}{d\xi^2}\frac{dP}{d\phi} + \frac{d^2P}{d\phi^2}\left(\frac{d\phi}{d\xi}\right)^2. \tag{2.3.26}$$

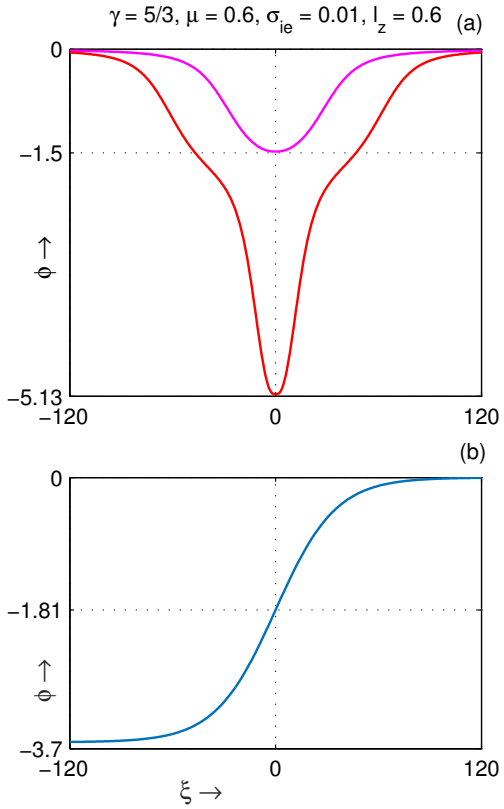

Figure 2.17: ϕ is plotted against ξ for $\gamma = 5/3, \mu = 0.6, \sigma_{ie} = 0.01, l_z = 0.6$ for different values of β_e at the corresponding acoustic speed M_c. (a) The magenta curve corresponds to $\beta_e = 0.228$ which is an NPSW whereas the red curve corresponds to $\beta_e = 0.227$ which is a negative potential supersoliton. (b) The cyan curve corresponds to $\beta_e = 0.22751$ which is an NPDL.

Using (2.3.26), the equation (2.3.25) can be written in the following form:

$$\frac{dQ}{d\phi} + \frac{2}{R}\frac{dR}{d\phi}Q = \frac{2}{R}F(\phi), \tag{2.3.27}$$

where $Q = \left(\frac{d\phi}{d\xi}\right)^2$ and $R = \frac{dP}{d\phi}$ and we have used the following identity

$$\frac{d^2\phi}{d\xi^2} = \frac{1}{2}\frac{d}{d\phi}\left[\left(\frac{d\phi}{d\xi}\right)^2\right].$$

Considering (2.3.27) as a first order and first degree linear ordinary differential equation in Q with integrating factor R^2, the general solution of the equation (2.3.27)

can be put in the following form:

$$\frac{1}{2}\Big(\frac{d\phi}{d\xi}\Big)^2 \times \Big(\frac{dP}{d\phi}\Big)^2 = \int \frac{dP}{d\phi}F(\phi)d\phi + C_1, \tag{2.3.28}$$

where C_1 is a constant of integration. Using the boundary condition (2.3.7), we get

$$0 = \int \frac{dP}{d\phi}F(\phi)d\phi\Big|_{\phi=0} + C_1. \tag{2.3.29}$$

Using the equation (2.3.29), the equation (2.3.28) can be written as

$$\frac{1}{2}\Big(\frac{d\phi}{d\xi}\Big)^2 + V(\phi) = 0, \tag{2.3.30}$$

where

$$V(\phi) = V(M,\phi) = -\frac{\int_0^\phi \frac{dP}{d\phi}F(\phi)d\phi}{\Big(\frac{dP}{d\phi}\Big)^2}. \tag{2.3.31}$$

2.4 Criteria for the Existence of Solitary Structures at the Acoustic Speed

The mechanical analogy of Sagdeev [11] suggests that the energy integral (2.3.30) may support positive or negative potential ion acoustic solitary structures including double layers and supersolitons at the supersonic speed if $\phi = 0$ is the position of unstable equilibrium of a pseudo particle of unit mass associated with the energy integral (2.3.30), i.e., if $V(M,0) = 0$, $V'(M,0) = 0$ and $V''(M,0) < 0$.

Now, differentiating (2.3.31) with respect to ϕ, we get

$$V'(M,\phi) = -\frac{F(\phi)}{dP/d\phi} - 2V(M,\phi)\frac{d^2P/d\phi^2}{dP/d\phi}. \tag{2.4.1}$$

Again, differentiating (2.4.1) with respect to ϕ, we get

$$V''(M,\phi) = -\frac{F'(\phi)}{dP/d\phi} + 3F(\phi)\frac{d^2P/d\phi^2}{(dP/d\phi)^2} + 2V(M,\phi)\Big[3\frac{(d^2P/d\phi^2)^2}{(dP/d\phi)^2} - \frac{d^3P/d\phi^3}{dP/d\phi}\Big]. \tag{2.4.2}$$

Now using equations (2.3.31) and (2.4.1), it is simple to check that $V(M,0)=0$ and $V'(M,0)=0$ for all M, and using equation (2.4.2), we get the following equation:

$$V''(M,0) = -\frac{\mu(1-\beta_e) - \frac{l_z^2}{M^2}\Big\{\gamma\sigma_{ie}\mu(1-\beta_e)+1\Big\}}{(-M^2+\gamma\sigma_{ie})\mu(1-\beta_e)+1}, \tag{2.4.3}$$

where the derivation of (2.4.1), (2.4.2) and (2.4.3) are, respectively, given in Appendix - B, Appendix - C and Appendix - D.

Now the equation (2.4.3) can be put in the following form:

$$V''(M,0) = \frac{M^2 - l_z^2 M_s^2}{M^2 - M_s^2}, \tag{2.4.4}$$

where

$$M_s = \sqrt{\gamma\sigma_{ie} + \frac{1}{\mu(1-\beta_e)}}. \tag{2.4.5}$$

Using the inequality $V''(M,0) < 0$, we get the following bounds for M:

$$M_c < M < M_s, \tag{2.4.6}$$

where

$$M_c = l_z M_s. \tag{2.4.7}$$

Therefore, positive or negative potential ion acoustic solitary structures start to exist when $M > M_c$ and it is not possible to get any solitary structures for $M \geq M_s$. In this chapter, our aim is to investigate the solitary structures at $M = M_c$, i.e., at the acoustic speed. Before going to discuss the existence of solitary structures at $M = M_c$, we want to discuss the following points with respect to a pseudo particle of unit mass associated with the energy integral (2.3.30):

- $V(M,\phi)$ can be regarded as the potential energy of a pseudo particle of unit mass associated with the energy integral (2.3.30).

- The first term of the energy integral (2.3.30) can be regarded as the kinetic energy of a pseudo particle of unit mass associated with the energy integral (2.3.30) with ϕ as the position of the particle at an instant of time ξ.

- It is simple to check that the magnitude of the velocity of the pseudo particle is $\sqrt{-2V(M,\phi)}$ and consequently the velocity of the pseudo particle vanishes if

$$V(M,\phi) = 0. \tag{2.4.8}$$

- The particle is under the action of the force field $-2V'(M,\phi)$ and the force is directed towards the origin $\phi = 0$ if

$$V'(M,\phi) > 0 \quad \text{for} \quad \phi > 0 \tag{2.4.9}$$

and

$$V'(M,\phi) < 0 \quad \text{for} \quad \phi < 0. \tag{2.4.10}$$

- The force acting on the pseudo particle vanishes if

$$V'(M,\phi) = 0. \tag{2.4.11}$$

- Using the equations (2.3.31), (2.4.1) and (2.4.4), it is simple to check that $V(M_c,0) = 0$, $V'(M_c,0) = 0$ and $V''(M_c,0) = 0$. Consequently at the acoustic speed, we cannot conclude that $\phi = 0$ is the position of unstable equilibrium of a pseudo particle of unit mass associated with the energy integral (2.3.30). For this case, i.e., when $V''(M_c,0) = 0$, according to THEOREM 2 of Das *et al.*[70], it is instructive to find the sign of $V'''(M_c,0)$. As the THEOREM 2 of Das *et*

al.[70] plays the key role regarding the existence of any solitary structures at the acoustic speed, we want to state the THEOREM 2 of Das *et al.*[70].

- THEOREM 2 of Das *et al.*[70]: If $V(M_c, 0) = 0$, $V'(M_c, 0) = 0$, $V''(M_c, 0) = 0$ and $V'''(M_c, 0) \neq 0$, then there exists a strictly positive real number $\phi_\epsilon (> 0)$ such that $V'''(M_c, 0)V''(M_c, \phi) > 0$ for all $0 < \phi < \phi_\epsilon$ and $V'''(M_c, 0)V''(M_c, \phi) < 0$ for all $-\phi_\epsilon < \phi < 0$.

  From this theorem one can conclude the following interesting points:

  (a) For $V'''(M_c, 0) < 0$, $V(M_c, \phi)$ is locally convex in a right neighbourhood of the point $\phi = 0$ $(0 < \phi < \phi_\epsilon)$ whereas $V(M_c, \phi)$ is locally concave in a left neighbourhood of the point $\phi = 0$ $(-\phi_\epsilon < \phi < 0)$.

  (b) For $V'''(M_c, 0) > 0$, $V(M_c, \phi)$ is locally concave in a right neighbourhood of the point $\phi = 0$ $(0 < \phi < \phi_\epsilon)$ whereas $V(M_c, \phi)$ is locally convex in a left neighbourhood of the point $\phi = 0$ $(-\phi_\epsilon < \phi < 0)$.

With respect to the sign of $V'''(M_c, 0)$, one can consider the following three cases.

Case - I $(V'''(M_c, 0) < 0)$: For this case, Das *et al.* [70] have proved in THEOREM 3 of their paper [70] that there may exist either a solitary wave or a double layer in the positive potential side but there does not exist any solitary wave or double layer in the negative potential side. In fact, for this case, we have seen that $V(M_c, \phi)$ is locally convex in a right neighbourhood of the point $\phi = 0$. Consequently if a pseudo particle associated with the energy integral (2.3.30) is slightly displaced along the positive direction of ϕ axis from the position $\phi = 0$, then the particle immediately falls into the small right neighbourhood of the point $\phi = 0$ and due to convexity of $V(M_c, \phi)$ in this region, the particle will be moving away from $\phi = 0$ and it will be

continuing its motion until its velocity vanishes, i.e., until ϕ assumes the value ϕ_m, where $\phi_m(> 0)$ is the least strictly positive real number such that $V(M_c, \phi_m) = 0$. Now, in this situation, i.e., for $V(M_c, \phi_m) = 0$, we have the following two possibilities for the formation of PPSW structures at $M = M_c$:

(a) The force acting on the particle at $\phi = \phi_m$ is directed towards the point $\phi = 0$. Consequently, we have an oscillation of the particle within the interval $(0,\ \phi_m)$ and this nonlinear oscillation generates positive potential solitary waves.

(b)The force acting on the particle at $\phi = \phi_m$ vanishes, i.e., the velocity and the force acting on the particle are simultaneously equal to zero at $\phi = \phi_m$ and consequently the particle cannot be reflected back at the origin. In this case, one can get a positive potential double layer solution of (2.3.30).

Therefore, for $V'''(M_c, 0) < 0$, one can get a positive potential solitary wave or positive potential double layer at $M = M_c$ according to whether the following conditions hold good:

$$V(M_c, \phi_m) = 0 \ \&\ V'(M_c, \phi_m) > 0 \text{ for } \phi_m > 0, \tag{2.4.12}$$

or

$$V(M_c, \phi_m) = 0 \ \&\ V'(M_c, \phi_m) = 0 \text{ for } \phi_m > 0, \tag{2.4.13}$$

where we have used (2.4.8) and (2.4.9) to get (2.4.12), and also we have used (2.4.8) and (2.4.11) to get (2.4.13).

These conditions as given in (2.4.12) or (2.4.13) are supplemented by the condition

$$V(M_c, \phi_m) < 0 \ \text{ for } 0 < \phi < \phi_m, \tag{2.4.14}$$

where the inequality (2.4.14) has been added to define the energy integral (2.3.30) within $0 < \phi < \phi_m$ at $M = M_c$.

On the other hand, for this case, we have also seen that $V(M_c, \phi)$ is locally concave in a left neighbourhood of the point $\phi = 0$. Consequently if a pseudo particle associated with the energy integral (2.3.30) is slightly displaced along the negative direction of ϕ axis from the position $\phi = 0$, then the particle immediately falls into the small left neighbourhood of the point $\phi = 0$ and due to concavity of $V(M_c, \phi)$ in this region, the particle will come back again at $\phi = 0$. Therefore, it is not possible to get any solitary structure on the negative potential side.

Case - II ($V'''(M_c, 0) > 0$) : For this case, using THEOREM 4 of Das *et al.* [70], it is possible to get a negative potential solitary wave if there exists a $\phi_m < 0$ such that following conditions hold good

$$V(M_c, \phi_m) = 0 \ \& \ V'(M_c, \phi_m) < 0 \text{ for } \phi_m < 0, \tag{2.4.15}$$

whereas one can get a negative potential double layer at $M = M_c$ if there exists a $\phi_m < 0$ such that

$$V(M_c, \phi_m) = 0 \ \& \ V'(M_c, \phi_m) = 0 \text{ for } \phi_m < 0, \tag{2.4.16}$$

where we have used (2.4.8) and (2.4.10) to get (2.4.15), and also we have used (2.4.8) and (2.4.11) to get (2.4.16).

Now, to define the energy integral (2.3.30) within $\phi_m < \phi < 0$ at $M = M_c$, the conditions (2.4.15) or (2.4.16) must be supplemented by the condition

$$V(M_c, \phi_m) < 0 \ \text{ for } \phi_m < \phi < 0. \tag{2.4.17}$$

On the other hand, from THEOREM 4 of Das *et al.* [70], it can be concluded that it is not possible to get any solitary structure in the positive potential side.

Case - III ($V'''(M_c, 0) = 0$) : For this case, we have the following three sub cases depending on the sign of $V^{iv}(M_c, 0)$.

- (A) $\underline{V^{iv}(M_c, 0) < 0 :}$ Here $V(M_c, \phi)$ is maximum at $\phi = 0$ and consequently the pseudo particle associated with the energy integral (2.3.30) is in a position of unstable equilibrium at $\phi = 0$. Consequently, one can get a PPSW, PPDL, NPSW, NPDL at $M = M_c$ according to whether the following pair of conditions are simultaneously true: (2.4.12) and (2.4.14), (2.4.13) and (2.4.14), (2.4.15) and (2.4.17), (2.4.16) and (2.4.17).

- (B) $\underline{V^{iv}(M_c, 0) > 0 :}$ Here $V(M_c, \phi)$ is minimum at $\phi = 0$ and consequently the pseudo particle associated with the energy integral (2.3.30) is in a position of stable equilibrium at $\phi = 0$. Therefore, it is not possible to get any solitary structures at $M = M_c$.

- (C) $\underline{V^{iv}(M_c, 0) = 0 :}$ In this case, the general prescription is to consider the sign of the next order derivative of $V(M,\ \phi)$ at $(M,\ \phi) = (M_c,\ 0)$. Considering the sign of $V^v(M_c, 0)$, one can study the existence of solitons at $M = M_c$. In the present chapter, we are restricted upto the fourth order derivative of $V(M,\ \phi)$ with respect to ϕ at the point $(M,\ \phi) = (M_c,\ 0)$.

We have used the criteria discussed in this section to investigate the existence of solitary structures at the acoustic speed. Here, we have used THEOREM 1 - THEOREM 5 of Das *et al.* [70] to establish the criteria discussed in this section.

2.5 Existence Domains

Now M_c is a function of $\gamma(= 5/3)$, l_z, σ_{ie}, β_e and μ, i.e., $M_c = M_c(\gamma,\ \sigma_{ie},\ \beta_e,\ \mu,\ l_z)$. One can take the variation of M_c with respect to β_e or μ because $\gamma(= 5/3)$ is a fixed parameter and σ_{ie} can also be taken as fixed for specific plasma system. Here our aim

is to find the existence and the nature of solitary structures along the curve $M = M_c$ with respect to the parameter β_e or μ.

To discuss the existence and the nature of the solitary structure at $M = M_c$, the general prescription is to consider the variation of $V'''(M_c, 0)$ with respect to some parameter of the system. In figure 2.1 of the present chapter, we have considered the variation of $V'''(M_c, 0)$ against β_e. From figure 2.1, we see that a part of the graph is above the β_e-axis, i.e., $V'''(M_c, 0) > 0$ for $0 \leq \beta_e < \beta_{e2}(\approx 0.255)$, the other part is below the β_e-axis, i.e., $V'''(M_c, 0) < 0$ for $\beta_{e2} < \beta_e \leq 0.57$, $V'''(M_c, 0) = 0$ for $\beta_e = \beta_{e2}$ and consequently we have considered the following three cases depending on the sign of $V'''(M_c, 0)$.

Case - I $(V'''(M_c, 0) > 0)$: As $V'''(M_c, 0) > 0$ for $0 \leq \beta_e < \beta_{e2}$, from the discussion as given in Section 2.4, it is expected that the system supports negative potential solitary structures and different types solitary structures at $M = M_c$ have been confirmed from figure 2.2. In this figure (figure 2.2), $V(\phi)$ is plotted against ϕ for different values of β_e, where $0 \leq \beta_e < \beta_{e2}$, i.e., $V'''(M_c, 0) > 0$. This figure shows the existence of NPSW before the formation of NPDL at $M = M_c$, the existence of NPDL at $M = M_c$, the existence of NPSS after the formation of NPDL at $M = M_c$ and the existence of NPSW structure after the formation of NPDL at $M = M_c$. Again from this figure, we see that the numerical value of the amplitude of different negative potential solitary structures increases with decreasing β_e within the interval $0 \leq \beta_e < \beta_{e2}$. On the other hand, as $\beta_e \to \beta_{e2}$ with $\beta_e < \beta_{e2}$, the amplitude of negative potential solitary stuctures (including negative potential double layer and negative potential supersolitons) approaches to zero. To make a clear difference between the topology of different solitary structures, we have considered the phase portraits of the

dynamical system corresponding to the different solitary structures in Section 2.6.

Case - II ($V'''(M_c, 0) < 0$) : As $V'''(M_c, 0) < 0$ for $\beta_{e2} < \beta_e \leq 0.57$, from the discussion as given in Section 2.4, it is expected that the system supports positive potential solitary structures and different types solitary structures at $M = M_c$ have been confirmed from figure 2.3. In this figure (figure 2.3), $V(\phi)$ is plotted against ϕ for different values of β_e, where $\beta_{e2} < \beta_e \leq 0.57$, i.e., $V'''(M_c, 0) < 0$. This figure shows the existence of positive potential soliton at $M = M_c$. Again from this figure, we see that the numerical value of the amplitude of different positive potential solitary structures decreases with decreasing β_e within the interval $\beta_{e2} < \beta_e \leq 0.57$, consequently, the amplitude of positive potential solitary stuctures approaches to zero as $\beta_e \to \beta_{e2}$ with $\beta_e > \beta_{e2}$.

Case - III ($V'''(M_c, 0) = 0$) : At $\beta_e = \beta_{e2}$, $V'''(M_c, 0) = 0$, so at this point the general prescription is to find $V^{iv}(M_c, 0)$. If $V^{iv}(M_c, 0) > 0$, then $\phi = 0$ is a position of stable equilibrium at $M = M_c$ and consequently it is not possible to get any solitary structures. If $V^{iv}(M_c, 0) < 0$, then $\phi = 0$ is a position of unstable equilibrium at $M = M_c$ and consequently one can get a solitary structure if other conditions for the existence of solitary structure hold good. If $V^{iv}(M_c, 0) = 0$ then we go to the next higher order derivative of Sagdeev potential and consider the cases as given for the third order derivative of Sagdeev potential. For the present case, we have seen $V^{iv}(M_c, 0) > 0$ and consequently the system does not support any solitary structure at $\beta_e = \beta_{e2}$.

All the three cases, viz., $V'''(M_c, 0) > 0$, $V'''(M_c, 0) < 0$ and $V'''(M_c, 0) = 0$ can also be investigated by considering variation of $V'''(M_c, 0)$ with respect to μ. For example, in figure 2.4, we have plotted $V'''(M_c, 0)$ against μ. This figure shows the

sign of $V'''(M_c, 0)$ with respect to μ. Specifically, this figure shows that $V'''(M_c, 0) < 0$ for $\mu < \mu_c(\approx 0.5175)$, $V'''(M_c, 0) = 0$ for $\mu = \mu_c$ and $V'''(M_c, 0) > 0$ for $\mu > \mu_c$. So, according to the criteria, it is expected to obtain negative potential solitary structures at $M = M_c$ or positive potential solitary structures at $M = M_c$ according to whether $\mu > \mu_c$ or $\mu < \mu_c$. To confirm the above mentioned facts, we draw figure 2.5 and figure 2.6.

In figure 2.5, $V(\phi)$ is plotted against ϕ for different values of μ at $M = M_c$ and the values of μ are taken from figure 2.4 for which $V'''(M_c,\ 0) > 0$. This figure has been drawn to make a correspondence with the figure 2.4 for $V'''(M_c,\ 0) > 0$. Here red curve ($\mu = 0.6$), magenta curve ($\mu = 0.625$), green curve ($\mu = 0.65$) all correspond to conventional NPSW structures whereas pink curve ($\mu = 0.675$) and black curve ($\mu = 0.7$) indicate the formation of NPSS structures without the formation of NPDL structure. It is also observed that NPSS structure collapse for $\mu > 0.77$ without the formation of NPSW structure. From this figure, we observe that the amplitude of NPSW including NPSS increases for increasing μ, i.e., amplitude of the NPSW including NPSS decreases for decreasing μ and ultimately it collapses at $\mu = \mu_c$.

In figure 2.6, $V(\phi)$ is plotted against ϕ for different values of μ at $M = M_c$ and the values of μ are taken from figure 2.4 for which $V'''(M_c,\ 0) < 0$. This figure has been drawn to make a correspondence with the figure 2.4 for $V'''(M_c,\ 0) < 0$. Here green curve ($\mu = 0.45$), red curve ($\mu = 0.4$), magenta curve ($\mu = 0.35$) and blue curve ($\mu = 0.3$) all correspond to conventional PPSW structures. It is simple to check that $V'''(M_c,\ 0) < 0$ for all PPSW structures as drawn in this figure. From this figure, we observe that the amplitude of the PPSW increases for decreasing μ, i.e., amplitude of the PPSW decreases for increasing μ and ultimately it collapses at $\mu = \mu_c$.

Again figure 2.7 shows the existence of PPSS structure without the formation of PPDL structure. In fact, in figure 2.7, $V(\phi)$ is plotted against ϕ for different values of μ with $\sigma_{ie} = 0.01$, $\beta_e = 0.35$, $l_z = 0.6$ and $M = M_c$. Here magenta curve ($\mu = 0.34$), red curve ($\mu = 0.3$), green curve ($\mu = 0.26$) and blue curve ($\mu = 0.21$) indicate the existence of PPSW structures ($\mu = 0.34, 0.3, 0.26$) including PPSS structure ($\mu = 0.21$) without the formation of PPDL structure. One can easily check that the amplitude of the PPSW decreases with increasing μ and ultimately it collapses at $\mu = \mu_c \approx 0.783$ where $V'''(M_c, 0) = 0$ whereas amplitude of PPSS structure increases with decreasing μ and ultimately it breaks for $\mu < 0.18$. From this figure, we observe that the amplitude of PPSW including PPSS increases for decreasing μ. For definiteness, for the occurrence of PPSW structures, one can draw $V'''(M_c, 0)$ with respect to μ for $\sigma_{ie} = 0.01$, $\beta_e = 0.35$, $l_z = 0.6$. From this figure, it is simple to observe that $V'''(M_c, 0) < 0$ or $V'''(M_c, 0) > 0$ according to whether $\mu < \mu_c \approx 0.783$ or $\mu > \mu_c$ and at $\mu = \mu_c$, $V'''(M_c, 0) = 0$. So, it is possible to get PPSW structures within $0 < \mu < \mu_c$. Here, actual graphical analysis shows that the range of μ for the existence of PPSW structures is $0.18 \leq \mu < \mu_c$.

Now, we see that $V'''(M_c,\ 0) = 0$ at $\mu = \mu_c$ whereas $V^{iv}(M_c,\ 0) > 0$ at $\mu = \mu_c$. Therefore, the potential energy $V(M_c, \phi)$ is minimum at $\mu = \mu_c$ and $\phi = 0$, and consequently there is no question of existence of any solitary structures at $M = M_c$, i.e., the system does not support any solitary structure at $\mu = \mu_c$.

In Section 2.6, we have considered the phase portraits of the dynamical system corresponding to the different solitary structures to distinguish between the topology of different solitary structures at $M = M_c$.

2.6 Phase Portraits

From figures 2.2, 2.3, 2.5, 2.6 and 2.7, one can conclude that the system supports NPSWs, PPSWs, NPDLs, NPSSs and PPSSs. But there are two groups of NPSSs: (a) formation of NPSS after the formation of NPDL (see figure 2.2), (b) formation of NPSS without the formation of NPDL(see figure 2.5). To draw the phase portraits of the different solitary structures, we differentiate the energy integral (2.3.30) with respect to ϕ to get the following equation:

$$\frac{d^2\phi}{d\xi^2} = -V'(M_c, \phi). \tag{2.6.1}$$

This equation can be resolved into the following two coupled first-order first degree differential equations:

$$\frac{d\phi_1}{d\xi} = \phi_2, \ \frac{d\phi_2}{d\xi} = -V'(M_c, \phi_1), \tag{2.6.2}$$

where $\phi_1 = \phi$.

With the help of the equations as given in (2.6.2), we have studied the phase portraits of different solitary structures. We have already defined the solitary structure including double layer and supersoliton with the help of the mechanical analogy of Sagdeev [11] as considered in Section 2.4 for the case of sonic solitary structures. In phase portraits, any solitary structure including double layer and supersoliton can be represented by a separatrix that appears to start and end at the origin $(0, 0)$. More specifically, with respect to the separatrix, one can describe different solitary structures as follows:

(a) The separatrix corresponding to a soliton appears to pass through the origin $(0, 0)$ and it encloses only one stable fixed point but it does not enclose any other separatrix.

(b) The separatrix corresponding to a double layer appears to start and end at the origin $(0, 0)$. It also appears to pass through a non-zero saddle but it does not enclose any other separatrix.

(c) The separatrix corresponding to a supersoliton appears to start and end at the origin $(0, 0)$. It also appears to pass through a non-zero saddle and it encloses at least two stable fixed points and another separatrix not passing through the origin $(0, 0)$.

(d) Moreover, according to Dubinov & Kolotkov [113, 161–163] , the definition of a supersoliton can be structured if we consider the derivative of the electric potential ϕ, i.e., the signature of the electric field. They have shown that the derivative of ϕ always has at least two maxima (minima).

To describe the existence and the shape of different solitary structures, we draw figures 2.8 - 2.12, figure 2.14 and figure 2.16. Again, we have used figure 2.13 to describe the transformation of the supersoliton structures after the formation of double layer whereas the figure 2.15 has been used to describe the transformation of the supersoliton structures without the formation of double layer.

Figures 2.8 (b) - 2.12 (b) are, respectively, the phase portraits of PPSW, NPSW, NPDL, NPSS and NPSW after the formation of NPDL. Figure 2.14 (b) is the phase portrait of NPSS without the formation of NPDL whereas Figure 2.16 (b) is the phase portrait of PPSS without the formation of PPDL. In the upper panel (or marked as (a)) of each of these figures, $V(\phi)$ is plotted against ϕ, whereas the lower panel (or marked as (b)) of each figure shows the phase portrait of the system (2.6.2). The curve $V(\phi)$ and the phase portrait have been drawn on the same horizontal axis $\phi(= \phi_1)$. The small solid square at the origin indicates the point of inflexion which separates the convex and concave portion of the curve $V(\phi)$ against ϕ. On the other hand,

the small solid circle and the small solid star correspond to an unstable equilibrium point and a stable equilibrium point of the system (2.6.2) respectively. An unstable equilibrium point corresponds to a saddle point whereas a stable equilibrium point corresponds to a non-saddle fixed point. From figures 2.8 - 2.12, 2.14, 2.16, we see that each maximum (minimum) point of $V(\phi)$ indicates to a saddle point (an equilibrium point other than a saddle point) of the system (2.6.2).

In figure 2.8(b), the phase portrait of a PPSW has been drawn whereas the curve $V(\phi)$ is drawn against ϕ in figure 2.8(a), which shows the formation of a PPSW. Here from the phase portrait, we see that there is only one separatrix that appears to pass through the point of inflexion $(0, 0)$, and encloses a stable equilibrium point, viz., $(0.79457, 0)$ on the positive potential side of the $\phi-$axis. This separatrix corresponds to a PPSW.

In figure 2.9(b), the phase portrait of an NPSW has been drawn whereas the curve $V(\phi)$ is drawn against ϕ in figure 2.9(a), which shows the formation of an NPSW. Here from the phase portrait, we see that there is only one separatrix that appears to pass through the point of inflexion $(0, 0)$, and encloses a stable equilibrium point, viz., $(-0.88328, 0)$ on the negative potential side of the $\phi-$axis. This separatrix corresponds to an NPSW.

In figure 2.10(b), the phase portrait of an NPDL has been drawn and from this figure, we see that the separatrix corresponding to an NPDL appears to pass through the point of inflexion $(0, 0)$ and again, it appears to pass through the non-zero saddle point (unstable fixed point) at $(-1.8089, 0)$. The separatrix corresponding to an NPDL also encloses the two stable equilibrium points $(-0.9214, 0)$ and $(-4.0122, 0)$. In figure 2.10(a), the curve $V(\phi)$ is drawn against ϕ. Figure 2.10(a) and the separatrix

of figure 2.10(b) together give a one-one correspondence as shown with a heavy blue line in both the lower panel and the upper panel.

In figure 2.11(b), the phase portrait of a negative potential supersoliton has been drawn. From this figure, we have the following observations:

- There are two separatrices as shown in blue curve and green curve.
- The blue separatrix appears to pass through the point of inflexion $(0, 0)$.
- The green separatrix appears to pass through the non-zero saddle point (unstable equilibrium point) $(-1.75, 0)$.
- The blue separatrix envelopes the green separatrix.
- The blue separatrix encloses two non-saddle fixed points (stable equilibrium points), viz., $(-0.9685, 0)$ and $(-4, 0)$.

Therefore, according to Dubinov & Kolotkov [161–163], the blue separatrix confirms the existence of an NPSS after the formation of NPDL. On the other hand, in the upper panel, the curve $V(\phi)$ is drawn against ϕ and this curve corresponds with the blue separatrix in the phase portrait of the lower panel.

In figure 2.12(b), we have plotted the phase portrait of an NPSW after the formation of NPDL and NPSS structures and in figure 2.12(a), $V(\phi)$ is plotted against ϕ which shows the formation of an NPSW. Here from the phase portrait, we see that there is only one separatrix that appears to pass through the point of inflexion $(0, 0)$, and encloses a non-saddle fixed point (stable equlibrium point), viz., $(-3.7686, 0)$ on the negative ϕ - axis. Consequently this separatrix confirms the existence of a conventional NPSW after NPDL.

In figure 2.13, we have plotted the point of inflexion (small solid square) at $(0, 0)$, the unstable fixed point (small solid circle) and the stable fixed points (small solid stars) for $\mu = 0.6$, $l_z = 0.6$ and $\beta_e = 0.22751 - \epsilon$ at the acoustic speed M_c. Here, $\epsilon = 0$ indicates an NPDL. We see that as the value of ϵ increases, equivalently the value of β_e decreases, the distance between the unstable fixed point (small solid circle) and the stable fixed point (small solid star) nearest to it decreases and eventually these two points overlap on each other and disappear from the system. This transformation shows a complete cycle of solitary structures of negative polarity, viz., NPSW $\rightarrow$ NPDL $\rightarrow$ NPSS $\rightarrow$ NPSW.

In figure 2.14(b), phase portrait of a NPSS has been drawn. This supersoliton is formed after the formation of an NPSW without the formation of a double layer. In this figure, we see that the dynamical system defined by the coupled equations as given in (2.6.2) contains two separatrices: blue separatrix appears to pass through the point of inflexion $(0, 0)$ and it encloses the green separatrix and two stable fixed points, viz., $(-9.8035, 0)$ and $(-3.864, 0)$ on the negative ϕ - axis. The green separatrix appears to pass through the unstable fixed point $(-6.2646, 0)$. In the upper panel, $V(\phi)$ is drawn against ϕ which is in a one-one correspondence with the blue separatrix in the phase portrait of the lower panel.

In figure 2.15, the transformation from NPSW structures to NPSS structures without the formation of NPDL is shown. Here, we have plotted the point of inflexion at $(0, 0)$ (small solid square), the unstable fixed point (small solid circle) and the stable fixed point (small solid star) for $\beta_e = 0.2$, $l_z = 0.6$ at the acoustic speed M_c for increasing values of μ starting from $\mu = 0.6$ and ending at $\mu = 0.7$ as shown in the figure. Here, $\mu = 0.6$, $\mu = 0.625$ and $\mu = 0.65$ indicate NPSWs where the dynamical

system (2.6.2) contains only one stable fixed point (small solid star). Again, $\mu = 0.675$ and $\mu = 0.7$ correspond to NPSS structures where we see the existence of one unstable fixed point (small solid circle) apart from the point of inflexion (small solid square) at the origin and two stable fixed points (small solid stars).

In figure 2.16(b), the phase portrait of a PPSS has been drawn. This supersoliton is formed after the formation of a PPSW without the formation of PPDL. In this figure, we see that the dynamical system defined by (2.6.2) contains two separatrices: one appears to start and end at the point of inflexion $(0, 0)$. This blue separatrix encloses the second separatrix shown in green curve and it also encloses more than one stable fixed points, viz., $(1.2106, 0)$ and $(2.4829, 0)$ on the positive potential side. In the upper panel, $V(\phi)$ is plotted against ϕ which shows a correspondence with the blue separatrix in the phase portrait of the lower panel.

Finally, in figure 2.17 (a), we have plotted the ϕ versus ξ graph for a negative potential soliton just before the formation of double layer (magenta curve) for $\beta_e = 0.228$ and for a negative potential supersoliton just after the formation of double layer (red curve) for $\beta_e = 0.227$ whereas in figure 2.17 (b), we have plotted the ϕ versus ξ graph for a negative potential double layer (cyan curve) for $\beta_e = 0.22751$. From figure 2.17 (a), we see that there is a jump-type discontinuity between the amplitudes of the solitons just before and just after the formation of double layer. From figure 2.17 (a), we also notice the formation of dias or platform in the profile of supersoliton symmetrical about $\xi = 0$. Both the points have already been reported by Das *et al.* [69] for dust acoustic waves in a collisionless unmagnetized dusty plasma (figure 4 of Das *et al.* [69]).

2.7 Conclusions

Considering a collisionless magnetized nonthermal dusty plasma system consisting of nonthermal electrons, static negatively charged dust grains and warm adiabatic ions immersed in a constant magnetic field directed along z-axis, IA solitary structures have been investigated at the acoustic speed.

In Chapter-1, we have investigated the existence of different solitary structures including double layers and supersolitons for $M > M_c$ ($\Leftrightarrow U > M_c C_s$) whereas in the present chapter, we have investigated the existence of different solitary structures at $M = M_c$ ($\Leftrightarrow U = M_c C_s$), where M is the normalized velocity or dimensionless velocity of the wave frame, U ($= MC_s$) is the actual velocity of the wave frame and M_c ($M_c C_s$) is the lower bound of M (U) for the existence of solitary structures, i.e., solitary structures begin to exist for $M > M_c$ ($U > M_c C_s$). This is the first problem in magnetized plasma where we have investigated the existence of different solitary structures at $M = M_c$ ($U = M_c C_s$), i.e., at the lower bound of the Mach number (wave frame).

In Chapter-1, we have observed the coexistence of supersonic ($M > M_c$) solitary structures of positive and negative polarities, but in the present chapter, we have seen that the coexistence of sonic ($M = M_c$) solitary structures of opposite polarities is impossible. In Chapter-1, we did not observe the existence of positive potential supersolitons whereas we have found the existence of positive potential supersolitons in the present chapter. In the present chapter, we have observed the transition of solitary structures from solitons to supersolitons without the formation of double layer but we did not find any such transition of solitary structures in Chapter-1

In the case of sonic solitary structures ($M = M_c$), the origin $(0, 0)$ of the $\phi - V(\phi)$

plane is a point of inflexion for the curve $V(\phi)$ against ϕ whereas for the case of supersonic solitary structures ($M > M_c$), the origin $(0, 0)$ of the $\phi - V(\phi)$ plane is a point of maximum for the same curve. More specifically, for the case of supersonic solitary structures ($M > M_c$), $V(\phi)$ is locally convex at $\phi = 0$ or $V(\phi)$ attains a maximum value at $\phi = 0$.

In the case of supersonic solitary structures ($M > M_c$), the origin $(0, 0)$ is a saddle point of the phase portrait of the dynamical system defined by the coupled equation as given in (2.6.2) whereas for the case of sonic solitary structures ($M = M_c$), the origin $(0, 0)$ is not a saddle point. But in any case, a solitary structure can be represented by the separatrix of the phase portrait of the dynamical system defined by the coupled equation as given in (2.6.2), where the separatrix appears to pass through the origin $(0, 0)$.

For the present sonic solitary structures, we have the following important observations on the solitary structures:

- The system supports PPSWs, NPSWs, NPDLs, NPSSs after the formation of NPDL, NPSSs without the formation of NPDL, PPSSs without the formation of PPDL at the acoustic speed for feasible values of the parameters. But the system does not support PPDL at the acoustic speed.

- The system does not support coexistence of solitary waves of opposite polarities.

- There exists a critical value β_{e2} of β_e such that the system may support negative potential solitary structures for $0 \leq \beta_e < \beta_{e2}$ whereas the system may support positive potential solitary structures for $\beta_{e2} < \beta_e \leq \beta_{eT} \approx 0.57$. For $\beta_e = \beta_{e2}$, there does not exist any solitary structure.

For $0 \leq \beta_e < \beta_{e2}$, negative potential solitary structure transforms from negative potential conventional soliton to negative potential double layer to negative potential supersoliton to negative potential conventional soliton again as the parameter β_e decreases from β_{e2}.

For $0 \leq \beta_e < \beta_{e2}$, the amplitude of the negative potential solitary structure including double layer and supersoliton of same polarity decreases with increasing β_e and as $\beta_e \to \beta_{e2}$ with $\beta_e < \beta_{e2}$, the NPSW structure collapses.

For $\beta_{e2} < \beta_e \leq \beta_{eT}$, we have only positive potential soliton and if β_e decreases from $\beta_e = \beta_{eT}$ within the interval $\beta_{e2} < \beta_e \leq \beta_{eT}$ then the amplitude of the PPSW decreases and as $\beta_e \to \beta_{e2}$ with $\beta_e > \beta_{e2}$, the positive potential soliton collapses.

So, the solitons of both polarities collapse at $\beta_e = \beta_{e2}$.

- There exists a critical value μ_c of μ such that the system may support positive potential solitary structures for $0 < \mu < \mu_c$ whereas the system may support negative potential solitary structures for $\mu_c < \mu \leq \mu_c^{(1)}$. For $\mu = \mu_c$, there does not exist any solitary structure and $\mu_c^{(1)}$ is another critical value of μ such that the negative potential supersoliton disappears from the system if $\mu > \mu_c^{(1)}$.

  For $0 < \mu < \mu_c$, we have only positive potential soliton and if μ increases from $\mu > 0$ within the interval $0 < \mu < \mu_c$ then the amplitude of the positive potential soliton decreases and as $\mu \to \mu_c$ with $\mu < \mu_c$, the positive potential soliton collapses.

  For $\mu_c < \mu \leq \mu_c^{(1)}$, negative potential solitary structure changes from negative potential conventional soliton to negative potential supersoliton without the

formation of NPDL as the parameter μ increases within the interval $\mu_c < \mu \leq \mu_c^{(1)}$.

For $\mu_c < \mu \leq \mu_c^{(1)}$, the amplitude of the negative potential solitary structures including supersoliton of same polarity decreases if μ decreases from $\mu = \mu_c^{(1)}$ within the interval $\mu_c < \mu \leq \mu_c^{(1)}$ and as $\mu \to \mu_c$ with $\mu > \mu_c$, the negative potential solitary structure collapses.

So, the solitons of both polarities collapse at $\mu = \mu_c$.

- Regarding the amplitude of the solitary structures, we have the following observations:

  The amplitude of the negative potential soliton increases for increasing μ whereas the amplitude of the negative potential soliton decreases for increasing β_e.

  The amplitude of the negative potential supersoliton increases for increasing μ whereas the amplitude of the negative potential supersoliton decreases for increasing β_e.

  The amplitude of the positive potential soliton decreases for increasing μ whereas the amplitude of the positive potential soliton increases for increasing β_e.

- We have drawn the phase portraits of different solitary structures to know the topology of the structure at the acoustic speed. Regarding these structures, we have the following observations:

  A conventional soliton in phase portrait is represented by a separatrix that appears to pass through the origin enclosing only one stable equilibrium point but this separatrix does not enclose any other separatrix.

A supersoliton in phase portrait is represented by a separatrix that appears to pass through the origin enclosing more than one stable equilibrium points and this separatrix encloses at least one other separatrix. This makes a clear difference between a conventional soliton and a supersoliton.

There is no qualitative difference between soliton before the formation of NPDL and soliton after the formation of NPDL (Figure 2.9 and Figure 2.12).

With the help of phase portrait, we have shown the smooth transition of the different solitary structures: NPSW (prior to the formation of NPDL) $\rightarrow$ NPDL $\rightarrow$ NPSS $\rightarrow$ NPSW (after the formation of NPDL) (Figure 2.13)

We have also shown the smooth transition from NPSW to NPSS without the formation of NPDL (Figure 2.15). This type of transformation can also be verified for positive polarity. For the first time, in magnetized plasma, we have seen this type of transformation of solitary structures for supersonic wave in Chapter-3.

In astrophysical and laboratory plasmas, the concept of supersolitons was introduced by Dubinov and Kolotkov [161–163] in multi-species plasmas. Dubinov and Kolotkov [161] have investigated the ion acoustic NPSWs and positive potential supersolitons (PPSSs) in an unmagnetized plasma consisting of electrons, positrons, negatively charged dust particles and two species of positively and negatively charged ions. Dubinov and Kolotkov [163] have experimentally observed the ion acoustic negative potential supersolitons (NPSSs) in multi-species plasmas. Dubinov and Kolotkov [162] investigated the IA solitary waves (PPSW and NPSS) in a collisionless unmagnetized plasma consisting of electrons, positrons, and two species of positively and negatively charged ions.

Dubinov and Kolotkov [120] have reported that space plasma observations often show intensive bursts of the electric field, occurring in the form of electrostatic supersolitons. They have given example of the space missions $S3-3$ [172], Viking [94], Polar [173], and FAST [174] which were used for the registration of electrostatic solitary structures in the magnetospheric plasma, such as ion-acoustic solitons, double layers and phase holes. Dubinov and Kolotkov [120] have also reported that the records of the mentioned missions are widely available in the literature and often contain certain patterns which can be interpreted as supersolitons. Dubinov and Kolotkov [120] also reported the existence of supersolitons in the auroral regions and lower layers of the Earth's magnetosphere.

Finally, we look forward to future satellite observations, advanced enough to distinguish the signature of different solitary structures at the acoustic speed.

Appendix A : Derivation of Equation (2.3.16):

From equation (2.3.15), we get

$$-M + u = -\frac{M}{n_i}. \tag{2.7.1}$$

Substituting this expression of $-M + u$ in equation (2.3.13), we get the following equation

$$-\frac{M}{n_i}\frac{du_{iz}}{d\xi} + l_z\frac{dH}{d\xi} = 0 \tag{2.7.2}$$

The equation (2.7.2) can be written as

$$\frac{du_{iz}}{d\xi} - \frac{l_z}{M}n_i\frac{dH}{d\xi} = 0 \tag{2.7.3}$$

Substituting the expression of H as given by (2.3.10) into the equation (2.7.3), we get the following equation

$$\frac{du_{iz}}{d\xi} - \frac{l_z}{M}\left(\gamma\sigma_{ie}n_i^{\gamma-1}\frac{dn_i}{d\xi} + n_i\frac{d\phi}{d\xi}\right) = 0 \tag{2.7.4}$$

From equation (2.2.8), we see that n_i is a function of ϕ and consequently we have the following results:

$$
\begin{aligned}
&(A) \quad \int n_i d\phi \ \text{ is a function of } \phi,\\
&(B) \quad \frac{d}{d\phi}\Big(\int n_i d\phi\Big) = n_i,\\
&(C) \quad \frac{d}{d\xi}\Big(\int n_i d\phi\Big) = \frac{d}{d\phi}\Big(\int n_i d\phi\Big)\frac{d\phi}{d\xi} = n_i\frac{d\phi}{d\xi},\\
&(D) \quad \frac{dn_i^{\gamma}}{d\xi} = \gamma n_i^{\gamma-1}\frac{dn_i}{d\xi}.
\end{aligned}
$$

Using the above results, the equation (2.7.4) can be written in the following form:

$$
\frac{du_{iz}}{d\xi} - \frac{l_z}{M}\Big[\sigma_{ie}\frac{dn_i^{\gamma}}{d\xi} + \frac{d}{d\xi}\Big(\int n_i d\phi\Big)\Big] = 0. \tag{2.7.5}
$$

From this equation, one can easily get the following equation:

$$
\frac{d}{d\xi}\Big[u_{iz} - \frac{l_z}{M}\Big(\sigma_{ie}n_i^{\gamma} + \int n_i d\phi\Big)\Big] = 0. \tag{2.7.6}
$$

The above equation is the equation (2.3.16).

Appendix B : Derivation of Equation (2.4.1):

Differentiating equation (2.3.31) with respect to ϕ, we get:

$$
\begin{aligned}
V'(M,\phi) &= -\frac{d}{d\phi}\left[\frac{\int_0^{\phi} P'(\phi)F(\phi)d\phi}{\Big(P'(\phi)\Big)^2}\right]\\
&= -\frac{P'(\phi)F(\phi)}{\Big(P'(\phi)\Big)^2} - \left[\left\{\int_0^{\phi} P'(\phi)F(\phi)d\phi\right\}\frac{(-2)P''(\phi)}{\Big(P'(\phi)\Big)^3}\right]\\
&= -\frac{F(\phi)}{P'(\phi)} + 2\frac{P''(\phi)}{P'(\phi)}\frac{\int_0^{\phi} P'(\phi)F(\phi)d\phi}{\Big(P'(\phi)\Big)^2}\\
&= -\frac{F(\phi)}{P'(\phi)} - 2V(M,\phi)\frac{P''(\phi)}{P'(\phi)},
\end{aligned} \tag{2.7.7}
$$

where we have used the identity $\frac{d}{d\phi}\Big(\int_0^{\phi} P'(\phi)F(\phi)d\phi\Big) = P'(\phi)F(\phi)$ to simplify (2.7.7). The above equation is the equation (2.4.1).

Appendix C : Derivation of Equation (2.4.2):

Differentiating equation (2.7.7) with respect to ϕ, we get:

$$\begin{aligned} V''(M,\phi) &= \frac{d}{d\phi}\Big[-\frac{F(\phi)}{P'(\phi)} - 2V(M,\phi)\frac{P''(\phi)}{P'(\phi)}\Big] \\ &= -\frac{F'(\phi)}{P'(\phi)} + \frac{F(\phi)P''(\phi)}{\Big(P'(\phi)\Big)^2} - 2V(M,\phi)\frac{P'''(\phi)}{P'(\phi)} \\ &\quad +2V(M,\phi)\frac{\Big(P''(\phi)\Big)^2}{\Big(P'(\phi)\Big)^2} - 2V'(M,\phi)\frac{P''(\phi)}{P'(\phi)}. \end{aligned} \tag{2.7.8}$$

Substituting the expression of $V'(M,\phi)$ as given by (2.7.7) into the equation (2.7.8), we get the following equation

$$V''(M,\phi) = -\frac{F'(\phi)}{P'(\phi)} + 3\frac{F(\phi)P''(\phi)}{\Big(P'(\phi)\Big)^2} + 2V(M,\phi)\left\{3\frac{\Big(P''(\phi)\Big)^2}{\Big(P'(\phi)\Big)^2} - \frac{P'''(\phi)}{P'(\phi)}\right\}.$$

The above equation is the equation (2.4.2).

Appendix D : Derivation of Equation (2.4.3):

From the equations (2.2.8), (2.3.10), (2.3.18), (2.3.22) and (2.3.25), we get the following results:

$$n_i(0) = 1, \tag{2.7.9}$$

$$n_i'(0) = \mu(1-\beta_e), \tag{2.7.10}$$

$$H(0) = \frac{\gamma}{\gamma-1}\sigma_{ie}, \tag{2.7.11}$$

$$H'(0) = \gamma\sigma_{ie}\mu(1-\beta_e) + 1, \tag{2.7.12}$$

$$G(0) = 0, \tag{2.7.13}$$

$$G'(0) = 1 + \gamma\sigma_{ie}\mu(1-\beta_e), \tag{2.7.14}$$

$$P(0) = \frac{M^2}{2} + \frac{\gamma}{\gamma-1}\sigma_{ie}, \tag{2.7.15}$$

$$P'(0) = -M^2 + \gamma\sigma_{ie}\mu(1-\beta_e) + 1, \tag{2.7.16}$$

$$F(0) = 0, \tag{2.7.17}$$

$$F'(0) = \mu(1-\beta_e) - \frac{l_z^2}{M^2}\Big[1 + \gamma\sigma_{ie}\mu(1-\beta_e)\Big]. \tag{2.7.18}$$

Using the above results, from equations (2.3.31), (2.4.1), (2.4.2), we get the following results:

$$V(M,0) = 0,$$

$$V'(M,0) = 0,$$

$$V''(M,0) = -\frac{\mu(1-\beta_e) - \frac{l_z^2}{M^2}\Big\{\gamma\sigma_{ie}\mu(1-\beta_e) + 1\Big\}}{(-M^2 + \gamma\sigma_{ie})\mu(1-\beta_e) + 1}.$$

The last equation is the equation (2.4.3).

Chapter 3

Combined effect of Kappa and Cairns distributed electrons on ion acoustic solitary structures in a collisionless magnetized dusty plasma *

Starting from one dimensional Kappa distribution for electrons, we have systematically developed the combined Kappa-Cairns distribution. We have found the effective bounds of both nonthermal parameters κ and β_e for the combined Kappa-Cairns distribution. This distribution can generate more highly energetic particles in comparison with both Kappa and Cairns distributions. We have investigated ion acoustic solitary structures in a collisionless magnetized plasma composed of negatively charged static dust grains, adiabatic warm ions and a population of highly energetic electrons generated from the combined Kappa-Cairns distribution. Sagdeev pseudo potential technique has been considered to investigate the arbitrary amplitude steady state solitary structures including double layers and supersolitons. We have developed a computational scheme to draw the existence domains showing the nature of existence of different solitary structures. Different solitary structures of both positive and negative polarities have been observed for different values of κ and β_e . We have seen two important transitions of solitary structures for negative polarity, viz., soliton before the formation of double layer $\rightarrow$ double layer $\rightarrow$ supersoliton $\rightarrow$ soliton after the formation of double layer, and soliton before the formation of supersoliton $\rightarrow$ supersoliton $\rightarrow$ soliton. For the second case, we have a supersoliton structure without the formation of double layer and this case is completely new one for magnetized plasma. Different solitary structures supported by the system have been investigated with the help of compositional parameter spaces and the phase portraits of the dynamical systems describing different solitary structures.

*This chapter has been published in ***Astrophysics and Space Science*** **365**, 72 (2020); https://doi.org/10.1007/s10509-020-03786-6

3.1 Introduction

Alfvén [34] reported that the velocity distribution functions in many cosmic plasmas are non-Maxwellian as well as highly anisotropic due to the presence of an excess of highly energetic particles, for example, double stars, novae, supernovae, pulsars etc. have been regarded to possess an excess of high-energy particle population. There is no general mechanism to construct the velocity distribution function of energetic particles in the space plasma, consequently different non-Maxwellian velocity distributions have been constructed in phase space to describe the behaviour of the energetic particles on the basis of the assumption that the relaxation time of the energetic particles is not so small to reach thermal equilibrium [35]. Kappa distribution and the nonthermal velocity distribution function of Cairns *et al.* [1] are two widely used non-Maxwellian models for energetic particles.

There are enormous evidence for the existence of a population of highly energetic electrons in space plasmas, resulting in a long high-energy tailed non-Maxwellian distribution [36]. Such a population of suprathermal electrons is generally modelled by a Kappa distribution which has the property that the number of particles in phase space far away from the point $v = 0$ is much greater than the number of particles in the same region for the case of a Maxwellian - Boltzmann distribution, where v is the velocity of the particle in phase space, and consequently the number of highly energetic particles is much larger in Kappa distribution in comparison with Maxwellian - Boltzmann distribution. Decades ago, Binsack [37] used Kappa distribution in his Ph.D. thesis where he mentioned that actually it (Kappa distribution) was introduced by Prof. S. Olbert in his studies of plasmas on IMP-1 [38]. By the same time Vasyliunas [39] also used this distribution. Later, this Kappa distribution was considered

by many authors in various studies of plasma physics [40–57].

On the other hand, for Cairns distributed nonthermal velocity distribution function of the energetic electrons [1], it can be easily shown that for increasing values of the nonthermal parameter (β_e), the distribution function develops wings, symmetrical with respect to the vertical axis $v = 0$, which become stronger as β_e increases, and consequently, nonthermal velocity distribution generates energetic particles for increasing values of β_e in finite region of phase space in the neighbourhood of $v = 0$. Therefore, for increasing β_e, distribution function develops wings, which become stronger as β_e increases, and at the same time the center density in phase space drops, the latter as a result of the normalization of the area under the integral. Consequently, we should not take values of $\beta_e > 4/7$ as that stage might stretch the credibility of the Cairns model too far [60]. Therefore, nonthermal velocity distribution of Cairns *et al.* [1] produces flattening at moderate values of v. So, Cairns distribution of nonthermal electrons [1] can describe the flattening of the distribution with respect to Maxwell - Boltzmann distribution as the background distribution. Cairns distribution has been used by several authors to discuss different wave structures in different plasma systems [17, 61, 64–71, 73–77].

To consider the flattening of the Kappa distribution in the neighbourhood of $v = 0$, one can consider Cairns distribution with respect to Kappa distribution as the background distribution. The combined Kappa-Cairns distribution is aimed to describe the possible deviation from Kappa distribution in the neighbourhood of $v = 0$. So, in the combined Kappa-Cairns distribution, we have considered Kappa distribution as the background electron distribution and the deviation of this background distribution can be described by Cairns distribution. Therefore, our aim is to consider the combined Kappa-Cairns distribution in those heliospheric environments in which

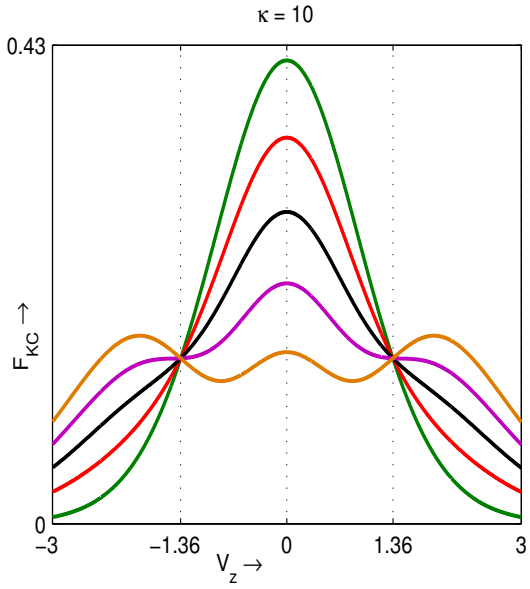

Figure 3.1: This figure shows flattening of the combined Kappa-Cairns distribution described by the nonthermal Cairns distribution with respect to Kappa distribution as the background distribution. Here, the green curve, red curve, black curve, magenta curve and orange curve correspond to the nonthermal parameter $\beta_e = 0$, $\beta_e = 0.2$, $\beta_e = 0.4$, $\beta_e = 0.6$ and $\beta_e = 0.8$ respectively with κ=10.

flattening of the distribution can be discussed by Cairns distribution with respect to Kappa distribution as the background distribution. Figure 3.1 shows the flattening of the combined Kappa-Cairns distribution described by the nonthermal Cairns distribution with respect to Kappa distribution as the background distribution. We have explained this figure in the next section (Section 3.2).

Numerous studies have shown that Kappa distributions (or combinations thereof) are frequently observed in several space, geophysical and other plasmas, where the deviation from Maxwell is more evident in the high-energy tails of the observed distributions. Kappa distributions have been employed to describe space plasma population in the inner heliosphere, including solar wind [79, 80], the planetary magnetospheres,

including magnetosheath [37–39], the outer heliosphere and inner heliosheath [81] etc., which can be described by the combined Kappa-Cairns distributions for even better accuracy.

High-energy tail distributions (κ distributions) do not show major temperature anisotropies but this property of high-energy tail κ distributions is not consistent with various space plasma observations [82]. In fact, the space plasma observations indicate the major temperature anisotropy in astrophysical environments. Again, Pierrard *et al.* [83] reported that the electron temperatures are generally higher in the slow solar wind than in high-speed stream. An excess of parallel temperature has been observed to dominate the observations and it is significantly larger in high-speed streams than in the slower solar wind, while an excess of perpendicular temperature is more common in low-speed and high-density conditions. In both the cases, the temperature anisotropy is high and Kappa distribution cannot describe such particle population. The Combined Kappa-Cairns distribution is a more generalized distribution which may be relevant to serve this purpose.

The satellite observations by Vela 2 and Vela 3 [39] reports that the plasma sheet electrons typically have a broad quasi-thermal energy spectrum, peaked anywhere between a few hundred ev and a few kev, with a non-Maxwellian high-energy tail [108]. Now, the particle distribution in the neighbourhoods of the peaks can be well described by Cairns distribution whereas the particle population along the tail can be described by Kappa distribution. Alongside, there are many space plasma environments where the linear and nonlinear plasma phenomena [1, 39, 54, 109, 110] cannot be precisely described by Cairns distribution or any such non-Maxwellian distribution.

To consider the combined effect of Kappa and Cairns distributed nonthermal electrons, Aoutou *et al.* [175] modelled a non-Maxwellian velocity distribution function which can describe the joint effect of Kappa distribution as well as Cairns distribution. Younsi & Tribeche [176] used this distribution to study the nonlinear dust acoustic waves. Abid *et al.* [109] have numerically analyzed some basic properties of the combined Kappa-Cairns velocity distribution of the lighter species (electrons, ions, positrons) and they call this distribution as Vasyliunas Cairns distribution. But neither Aoutou *et al.* [175] nor Abid *et al.* [109] have considered exact bounds of the parameters κ and β_e when these parameters are considered as parameters of the combined Kappa-Cairns distribution.

With the aim of producing more energetic particles in a collisionless magnetized plasma system, we have considered the combined effect of Kappa and Cairns distribution. In fact, we modify the Kappa distribution by imposing the nonthermal characteristics of Cairns distribution thereon. We have discussed different important properties of this new distribution and finally, we have investigated ion acoustic solitary structures in a collisionless magnetized dusty plasma consisting of negatively charged static dust grains, adiabatic warm ions and combined Kappa-Cairns distributed electrons giving special emphases on the following points. This problem is completely new in literature.

- We have systematically derived combined Kappa-Cairns distribution and this distribution reduces to the one dimensional Kappa distribution as defined by several authors [43, 110, 112] when $\beta_e = 0$. On the other hand, if $\kappa \to \infty$, the combined Kappa-Cairns distribution reduces to nonthermal distribution of Cairns *et al.* [1] whereas if $\beta_e = 0$ and $\kappa \to \infty$, the combined Kappa-Cairns

distribution is simplified to the isothermal distribution.

- For combined effect of Kappa and Cairns distribution, we have found the lower bound of the parameter κ for which combined effect of Kappa and Cairns distribution is well defined as a velocity distribution in phase space.

- We have analytically studied the dependence of the upper bound (β_{eT}) of β_e as a function of κ, i.e., we have shown that β_e is restricted by the inequality $0 \leq \beta_e \leq \beta_{eT}$, where β_{eT} is a function of κ.

- We have shown that as κ tends to ∞, the upper bound β_{eT} of β_e is equal to $4/7$, i.e., when the combined distribution reduces to the nonthermal distribution, the maximum value of the nonthermal parameter is $4/7$ which has already been reported by Verheest & Pillay [60].

- We have derived the expression of the number density of electrons that follow the combined Kappa-Cairns velocity distribution in phase space.

- For the first time in magnetized plasma, we have considered the combined effect of Kappa and Cairns distribution on the solitary structures of the ion acoustic wave in a collisionless magnetized dusty plasma.

- For the first time in magnetized plasma, considering the number density of electrons for combined Kappa-Cairns distribution, we have used Sagdeev pseudo potential method to investigate the arbitrary amplitude ion acoustic solitary structures in a collisionless magnetized dusty plasma.

- For the present plasma system, considering different bounds of Mach number, we have drawn different compositional parameter spaces with respect to the

nonthermal parameter β_e. These compositional parameter spaces clearly show the existence domains of different types of solitary structures for different values of κ and other parameters of the system.

- From the different compositional parameter spaces with respect to the nonthermal parameter β_e, we have seen the existence of different solitary structures, viz., negative potential solitary waves (NPSWs), positive potential solitary waves (PPSWs), negative potential double layers (NPDLs), coexistence of positive and negative potential solitary waves and negative potential solitary waves after the formation of NPDL for different ranges of β_e and κ. But the existence of negative potential solitary waves after the formation of NPDL confirms the existence of negative potential supersolitons (NPSSs) also. For large value of Kappa, the above mentioned solitary structures are qualitatively same as discussed in Chapter-1. In this connection, we would like to mention that Dubinov & Kolotkov [113] first elaborately investigated supersoliton structures in unmagnetized plasma. After that several authors [69, 71–77, 114–120] investigated supersoliton structures in different unmagnetized and magnetized plasma systems.

- For the first time in magnetized plasma, we have observed both types of negative potential supersolitons, viz., negative potential supersoliton after the formation of negative potential double layer of same polarity and negative potential supersoliton without the formation of double layer. Although in an unmagnetized plasma, Verheest *et al.* [114] have shown the existence of supersoliton without the formation of double layer of same polarity.

- For the first time in magnetized plasma, we have analyzed a new transition

of solitary structures: soliton → supersoliton → soliton. This type of transition was not found in Chapter-1, where we considered only Cairns distributed nonthermal electrons. We have also found the well-known transition of solitary structures: soliton → double layer → supersoliton → soliton in the present plasma system.

In this chapter, we have used the same set of hydrodynamic equations (1.2.1) - (1.2.3) of **Chapter-1** consisting of the continuity equation, the equation of motion and the pressure equation of ion fluid along with the same quasi-neutrality condition (1.2.4) of **Chapter-1**, but we have considered the combined effect of Kappa-Cairns distribution on the density function of nonthermal electrons instead of nonthermal electrons as prescribed in the paper of Cairns *et al.* [1]. Again for easy readability of this chapter, the complete set of basic equations has been given in section 3.3 of this chapter also.

3.2 Combined Kappa-Cairns Distribution

The one dimensional Kappa distribution function for electrons can be written in the following form [43, 110, 112]:

$$f_{\kappa e}(v_z^2) = \frac{n_{e0}}{(\pi\kappa\theta^2)^{1/2}} \frac{\Gamma(\kappa)}{(\kappa - \frac{1}{2})} \Big(1 + \frac{v_z^2}{\kappa\theta^2}\Big)^{-\kappa}, \tag{3.2.1}$$

where the effective thermal velocity θ is given by

$$\theta = \sqrt{\frac{2\kappa - 3}{\kappa} \frac{K_B T_e}{m_e}}. \tag{3.2.2}$$

Here K_B is the Boltzmann constant, m_e is the mass of an electron, n_{e0} is the unperturbed or equilibrium number density of electrons, T_e is the average temperature of electrons, v_z is the velocity of electrons in phase space and $\Gamma(x)$ is the Gamma function.

When we compare between the Kappa and the Maxwell - Boltzmann velocity distribution of electrons, then we observe that the Kappa distribution describes the existence of highly energetic particles along the long-tailed one humped symmetrical velocity distribution about the origin $v_z = 0$ but this distribution is unable to describe a population of fast energetic electrons in a finite region of the phase space in the neighbourhood of $v_z = 0$. The observations of electric field structures by the Freja Satellite [58] in the auroral zone influenced Cairns and others [1] to model a velocity distribution of non-Maxwellian electrons which can describe the presence of fast energetic electrons together with a population of Maxwellian distributed electrons. In fact, Cairns [1] distribution describes the fast energetic electrons in a finite region of the phase space in the neighbourhood of $v_z = 0$. Specifically, in the Maxwellian distribution, the number of electrons in the neighbourhood of $v_z = 0$ is maximum whereas in the Cairns [1] distribution, the number of electrons in the neighbourhood of $v_z = 0$ decreases with increasing values of the nonthermal parameter. The Cairns [1] distribution can be written as follows:

$$f_C(v_z^2) = \frac{n_{e0}\left[1 + \alpha_e\left(\frac{v_z}{v_{te}}\right)^4\right]}{(1+3\alpha_e)\sqrt{2\pi}v_{te}} \exp[-\frac{v_z^2}{2v_{te}^2}], \tag{3.2.3}$$

where $v_{te} = \sqrt{\frac{K_B T_e}{m_e}}$ and $\alpha_e \geq 0$.

Therefore, the combined Kappa-Cairns velocity distribution function can be written in the following form:

$$f_{\kappa C}(v_z^2) = A n_{e0}\left[1 + \alpha_e\left(\frac{v_z}{v_{te}}\right)^4\right]\left(1 + \frac{v_z^2}{\kappa\theta^2}\right)^{-\kappa}, \tag{3.2.4}$$

where

$$A = \frac{1}{\sqrt{\pi\kappa\theta^2}} \frac{\Gamma\left(\kappa\right)}{\Gamma\left(\kappa - \frac{5}{2}\right)} \frac{1}{\kappa_1\kappa_2 + 3\alpha_e\kappa_1^2} \tag{3.2.5}$$

with

$$\kappa_1 = \kappa - \frac{3}{2}\ ,\ \kappa_2 = \kappa - \frac{5}{2}. \tag{3.2.6}$$

Plotting the combined Kappa-Cairns distribution ($f_{\kappa C}(v_z^2)$) as given in the equation (3.2.4) against velocity (v_z) in phase space for different values of α_e or $\beta_e\Big[= 4\alpha_e/(1+3\alpha_e)\Big]$, one can analyze the different characteristics of combined Kappa-Cairns distribution. Here α_e or β_e is the nonthermal parameter that determines the proportion of the fast energetic particles in a finite region of phase space in the neighbourhood of $v_z = 0$. For $\alpha_e = 0$ ($\alpha_e = 0 \Leftrightarrow \beta_e = 0$), the equation (3.2.4) becomes the usual Kappa distribution in one dimension whereas for $\kappa \to \infty$, the distribution function (3.2.4) reduces to the nonthermal distribution of Cairns *et al.* [1]. It is simple to check that β_e is an increasing function of α_e. Using the inequality $\alpha_e \geq 0$, it is simple to check that $0 \leq \beta_e < 4/3$. However, we cannot take the entire region of β_e ($0 \leq \beta_e < 4/3$). In fact, for any fixed value of κ, if we plot $f_{\kappa C}(v_z^2)$ against v_z, then we see that for increasing β_e, distribution function $f_{\kappa C}(v_z^2)$ develops wings which become stronger as β_e increases but as $\int_{-\infty}^{\infty} f_{\kappa C}(v_z^2)dv_z = 1$, the center density in phase space drops, and for $\beta_e > \beta_{eT}$, the combined Kappa-Cairns velocity distribution function $f_{\kappa C}(v_z^2)$ attains three maximum values at three different points $v_z = -V$, $v_z = 0$ and $v_z = V$ in phase space and consequently this property of the combined Kappa-Cairns distribution function is qualitatively different from Kappa velocity distribution function as Kappa velocity distribution function has only one maximum at $v = 0$, where β_{eT} and V are given by the following equations:

$$\beta_{eT} = \frac{4}{3 + \dfrac{4(\kappa_1/\kappa)^2}{1-(2/\kappa)}}, \tag{3.2.7}$$

$$\frac{V}{v_{te}} = \sqrt{\frac{\frac{2\kappa_1}{\kappa} + 2\sqrt{1-\frac{2}{\kappa}}\sqrt{\frac{1}{\beta_{eT}} - \frac{1}{\beta_e}}}{1-\frac{2}{\kappa}}}. \tag{3.2.8}$$

Here our aim is to construct a distribution function which can produce more energetic particles in comparison with the Maxwell - Boltzmann velocity distribution function or the Kappa distribution without changing the qualitative behaviour, i.e., the new distribution function has only one maximum. So, we see that the combined Kappa-Cairns distribution describes the non-isothermal distribution having a deviation from the Kappa distribution if β_e is restricted by the following inequality:

$$0 \leq \beta \leq \beta_{eT}. \tag{3.2.9}$$

If $\kappa \to \infty$, then the above inequality reduces to the following inequality: $0 \leq \beta_e \leq 4/7$, i.e., the effective range of β_e is $0 \leq \beta_e \leq 4/7$. Verheest & Pillay [60] have already reported that for nonthermal velocity distribution function of Cairns *et al.* [1], the effective range of β_e is $0 \leq \beta_e \leq 4/7$. Again, for $\kappa \to \infty$, the value of V is equal to $v_{te} \times \sqrt{2 + \sqrt{7 - 4(\beta_e)^{-1}}}$ which has already been reported in Chapter-1 for the nonthermal distribution of electrons as prescribed by Cairns *et al.* [1]. So, the value of the nonthermal parameter β_e for combined Kappa-Cairns distribution function is restricted by the inequality (3.2.9). For $\kappa = 10$, the nonthermal parameter β_e is restricted by the inequality: $0 \leq \beta_e \leq \frac{320}{529} \approx 0.6049$, but in figure 3.1, we have plotted $F_{KC}\Big(= \frac{v_{te} f_{\kappa C}(v_z^2)}{n_{e0}}\Big)$ against $V_z\Big(= \frac{v_z}{v_{te}}\Big)$ for $\beta_e = 0$, $\beta_e = 0.2$, $\beta_e = 0.4$, $\beta_e = 0.6$ and $\beta_e = 0.8$. We see that $\beta_e = 0$, $\beta_e = 0.2$, $\beta_e = 0.4$ and $\beta_e = 0.6$ lie within the admissible range of β_e whereas the curve for $\beta_e = 0.8$ shows that the combined Kappa-Cairns velocity distribution function $f_{\kappa C}(v_z^2)$ attains maximum values at three different points in phase space. So, this property of the combined

Kappa-Cairns distribution function for $\beta_e = 0.8$ is qualitatively different from that of the Kappa distribution. So, it is instructive to consider only that range of β_e for which combined Kappa-Cairns distribution function has a global maximum at $v_z = 0$. Again, from the figure 3.1, we note that the flattening of the combined Kappa-Cairns distribution function increases with increasing values of β_e lying within the interval $0 \leq \beta \leq \beta_{eT}$.

The steady state solution of the Vlasov - Boltzmann equation for electrons following the combined Kappa-Cairns distribution (3.2.4) is given by

$$f_e(v_z, \phi) \;=\; f_{\kappa C}\Big(v_z^2 - \frac{2e\phi}{m_e}\Big). \tag{3.2.10}$$

Consequently the density of electrons following the combined Kappa-Cairns distribution (3.2.4) is given by

$$n_e = \int_{-\infty}^{\infty} f_e(v_z, \phi) dv_z. \tag{3.2.11}$$

Substituting the expression of $f_e(v_z, \phi)$ as given in equation (3.2.10) into the right hand side of the equation (3.2.11), we get the following expression of n_e:

$$\frac{n_e}{n_{e0}} = \Big[1 - \beta_{e1}^{(\kappa)}\Big(\frac{e\phi}{K_B T_e}\Big) + \beta_{e2}^{(\kappa)}\Big(\frac{e\phi}{K_B T_e}\Big)^2\Big]\Big(1 - \frac{1}{\kappa_1}\frac{e\phi}{K_B T_e}\Big)^{-\kappa+\frac{1}{2}}, \tag{3.2.12}$$

where

$$\beta_{e1}^{(\kappa)} = \beta_e^{(\kappa)}\Big(1 + \frac{3}{2\kappa_2}\Big), \tag{3.2.13}$$

$$\beta_{e2}^{(\kappa)} = \beta_e^{(\kappa)}\Big(1 + \frac{1}{\kappa_1} + \frac{3}{4\kappa_1\kappa_2}\Big), \tag{3.2.14}$$

$$\beta_e^{(\kappa)} = \frac{4\alpha_e\kappa_1\kappa_2}{\kappa_1\kappa_2 + 3\alpha_e\kappa_1^2} = \frac{4\alpha_e}{1 + 3\alpha_e\frac{\kappa_1}{\kappa_2}}. \tag{3.2.15}$$

Again it is simple to check the following limiting values of $\beta_e^{(\kappa)}$, $\beta_{e1}^{(\kappa)}$ and $\beta_{e2}^{(\kappa)}$ for $\kappa \to \infty$.

$$\lim_{\kappa\to\infty} \beta_e^{(\kappa)} = \frac{4\alpha_e}{1+3\alpha_e} = \beta_e, \tag{3.2.16}$$

$$\lim_{\kappa\to\infty} \beta_{e1}^{(\kappa)} = \lim_{\kappa\to\infty} \beta_e^{(\kappa)} = \beta_e, \tag{3.2.17}$$

$$\lim_{\kappa\to\infty} \beta_{e2}^{(\kappa)} = \lim_{\kappa\to\infty} \beta_e^{(\kappa)} = \beta_e, \tag{3.2.18}$$

$$\lim_{\kappa\to\infty} \Big(1 - \frac{1}{\kappa_1}\frac{e\phi}{K_B T_e}\Big)^{(-\kappa+\frac{1}{2})} = \exp\Big(\frac{e\phi}{K_B T_e}\Big). \tag{3.2.19}$$

Therefore, making limit as $\kappa \to \infty$ in equation (3.2.12), we get the following expression of n_e:

$$\frac{n_e}{n_{e0}} = \Big[1 - \beta_e\Big(\frac{e\phi}{K_B T_e}\Big) + \beta_e\Big(\frac{e\phi}{K_B T_e}\Big)^2\Big] \exp\Big(\frac{e\phi}{K_B T_e}\Big). \tag{3.2.20}$$

The above equation gives the density of nonthermal electrons as prescribed by Cairns *et al.* [1]. Again, making limit as $\beta_e \to 0$, the expression of n_e as given in equation (3.2.20) is further simplified into the following form:

$$n_e = n_{e0} \exp\Big(\frac{e\phi}{K_B T_e}\Big). \tag{3.2.21}$$

The equation (3.2.21) expresses the density of isothermal electrons.

In the present chapter, we have used equation (3.2.12) to express the density of the combined Kappa-Cairns distributed electrons, which describes the highly energetic particles in a long-tailed non-Maxwellian distribution along with the fast energetic electrons in a finite region of the phase space in the neighbourhood of $v_z = 0$. It is also important to note that for combined Kappa-Cairns distributed nonthermal electrons, the value of the nonthermal parameter β_e is resticted by the inequality

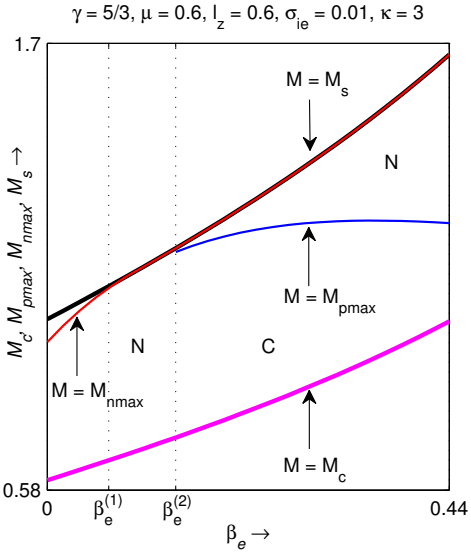

Figure 3.2: M_c, M_{pmax}, M_{nmax}, M_s are plotted against β_e. The magenta curve, blue curve, red curve and black curve correspond to the curves, $M = M_c$, $M = M_{pmax}$, $M = M_{nmax}$ and $M = M_s$, respectively.

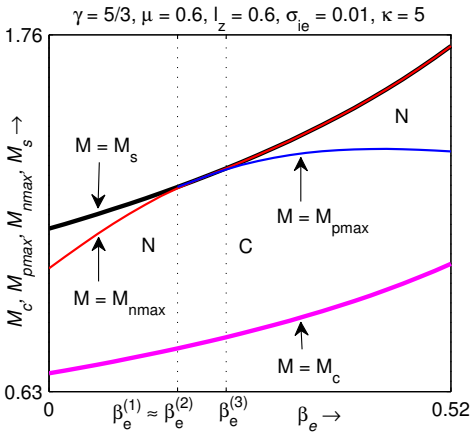

Figure 3.3: M_c, M_{pmax}, M_{nmax}, M_s are plotted against β_e. The magenta curve, blue curve, red curve and black curve correspond to the curves, $M = M_c$, $M = M_{pmax}$, $M = M_{nmax}$ and $M = M_s$, respectively.

(3.2.9) for any fixed value of κ. Again, from the expression of A as given in equation (3.2.5), we can conclude that the parameter κ is restricted by the inquality $\kappa > \frac{5}{2}$. Therefore, for any fixed $\kappa > \frac{5}{2}$, one can use the combined Kappa-Cairns distribution if the nonthermal parameter β_e is resticted by the inequality (3.2.9). This distribution has already been considered by several authors [109, 175, 176]. But they have not considered the actual bounds of the nonthermal parameters κ and β_e for combined Kappa-Cairns distribution.

3.3 Basic Equations

In the present chapter, we have considered the nonlinear behaviour of IA waves in a plasma consisting of negatively charged static dust grains, warm adiabatic ions and

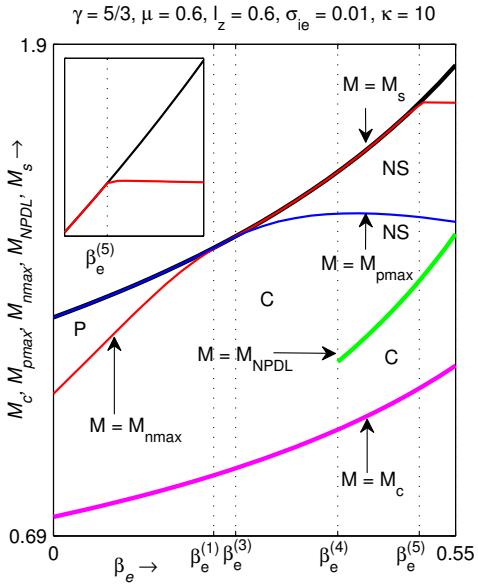

Figure 3.4: M_c, M_{pmax}, M_{nmax}, M_{NPDL}, M_s are plotted against β_e. The magenta curve, blue curve, red curve, green curve and black curve correspond to the curves, $M = M_c$, $M = M_{pmax}$, $M = M_{nmax}$, $M = M_{NPDL}$ and $M = M_s$, respectively.

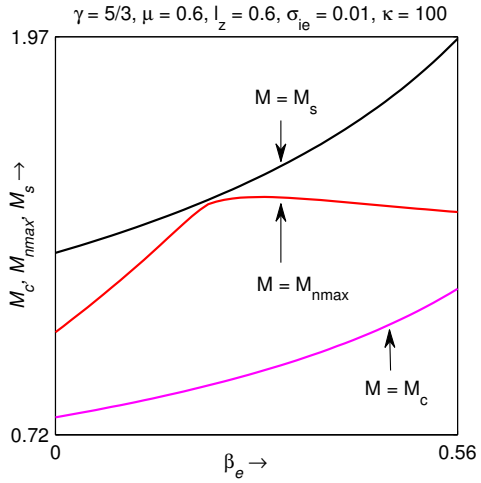

Figure 3.5: M_c, M_{nmax}, M_s are plotted against β_e. The magenta curve, red curve and black curve correspond to the curves, $M = M_c$, $M = M_{nmax}$ and $M = M_s$ respectively.

combined Kappa-Cairns distributed nonthermal electrons, and the plasma is under the action of a uniform static magnetic field ($\overrightarrow{B} = B_0\widehat{z}$) directed along $z-$axis. Now, normalizing number density of electrons (n_e) by n_{i0} (unperturbed ion number density) and electrostatic potential ϕ by $\frac{K_B T_e}{e}$, equation (3.2.12) can be written in the following form:

$$n_e = \mu\Big(1 - \beta_{e1}^{(\kappa)}\phi + \beta_{e2}^{(\kappa)}\phi^2\Big)\Big(1 - \frac{\phi}{\kappa_1}\Big)^{-\kappa+\frac{1}{2}}, \tag{3.3.1}$$

where $\mu = \dfrac{n_{e0}}{n_{i0}}$.

Now, equations (1.2.1) - (1.2.4) of Chapter-1 along with the equilibrium charge neutrality condition (1.2.5) of Chapter-1 can describe the nonlinear behaviour of IA waves in the present plasma system if the number density of electrons (n_e) of equation

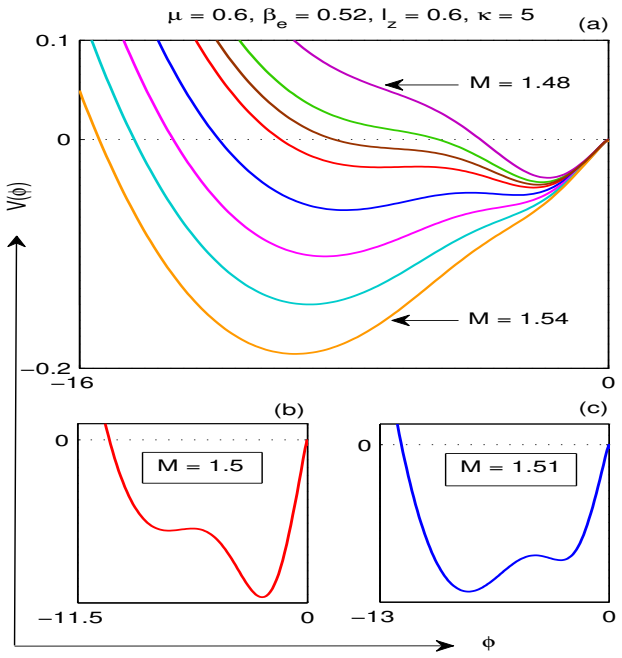

Figure 3.6: (a) $V(\phi)$ is plotted against ϕ for different values of M, for $\mu = 0.6$, $\beta_e = 0.52$, $l_z = 0.6$, $\gamma = 5/3$, $\sigma_{ie} = 0.01$ and $\kappa = 5$. The dark magenta, dark green, brown, red, blue, magenta, sea green and orange curves correspond to $M = 1.48$, $M = 1.49$, $M = 1.495$, $M = 1.5$, $M = 1.51$, $M = 1.52$, $M = 1.53$, and $M = 1.54$ respectively. Amongst these, the red, blue and magenta curves indicate supersolitons and the rest are solitons. The red curve and the blue curve showing supersoliton structures are elucidated in (b) and (c) respectively.

(1.2.6) of Chapter-1 is replaced by equation (3.3.1) of the present chapter. Again, using continuity equation (1.2.1) of ion fluid as given in Chapter-1, the pressure equation (1.2.3) of ion fluid as given in Chapter-1 can be simplified into the following form:

$$p_i = n_i^{\gamma}. \tag{3.3.2}$$

Using the equations (3.3.1) and (3.3.2), the continuity equation of ions, the equation of motion of ion fluid and the quasi-neutrality condition can be expressed as follows:

$$\frac{\partial n_i}{\partial t} + \overrightarrow{\nabla} \cdot (n_i \overrightarrow{u}_i) = 0, \tag{3.3.3}$$

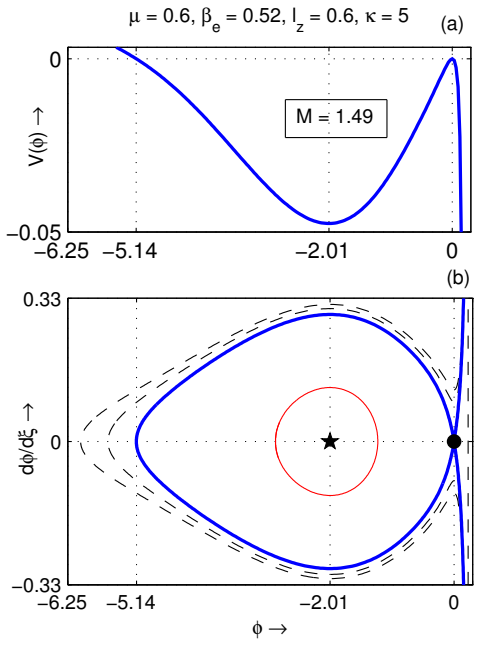

Figure 3.7: (a) $V(\phi)$ and (b) the phase portrait of the system are drawn on the same ϕ-axis for $M = 1.49$ and for $\kappa = 5$. This figure confirms the existence of NPSW before the formation of supersolitons.

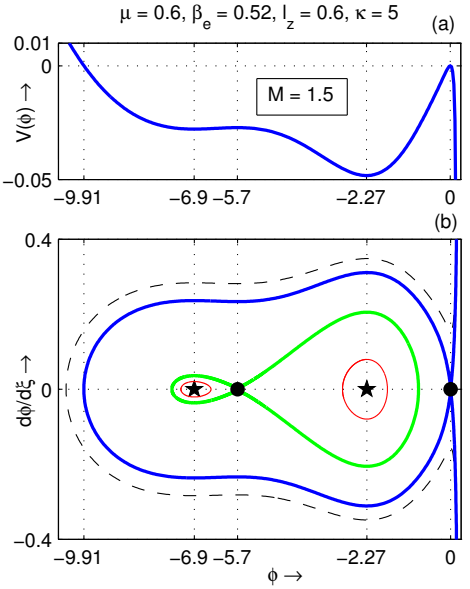

Figure 3.8: (a) $V(\phi)$ and (b) the phase portrait of the system are drawn on the same ϕ-axis for $M = 1.5$ and for $\kappa = 5$. We see that there are two unstable equilibrium points corresponding to two maximum values of $V(\phi)$ at $\phi = 0$ and at $\phi = -5.76$. This figure confirms the existence of supersoliton.

$$\left(\frac{\partial}{\partial t} + \vec{u}_i \cdot \vec{\nabla}\right)\vec{u}_i + \vec{\nabla} H = \vec{u}_i \times \hat{z}, \tag{3.3.4}$$

$$n_i = \mu\left(1 - \beta_{e1}^{(\kappa)}\phi + \beta_{e2}^{(\kappa)}\phi^2\right)\left(1 - \frac{\phi}{\kappa_1}\right)^{-\kappa+\frac{1}{2}} + 1 - \mu, \tag{3.3.5}$$

where

$$H = H(\phi) = \frac{\gamma\sigma_{ie}}{\gamma - 1}(n_i)^{\gamma-1} + \phi. \tag{3.3.6}$$

Here, x, y and z are the spatial variables each of which is normalized by the ion gyroradius $r_g = C_s/\omega_c$; t is the time normalized by the inverse of ion gyrofrequency $(\omega_c)^{-1}$, where $C_s = \sqrt{\frac{K_B T_e}{m_i}}$ and $\omega_c = \frac{eB_0}{m_i c}$. The ion fluid velocity components are u_{ix}, u_{iy} and u_{iz} along x, y and z axes respectively, each of which is normalized by C_s; p_i is the ion pressure normalized by $n_{i0}K_B T_i$; ϕ is the electrostatic potential normalized

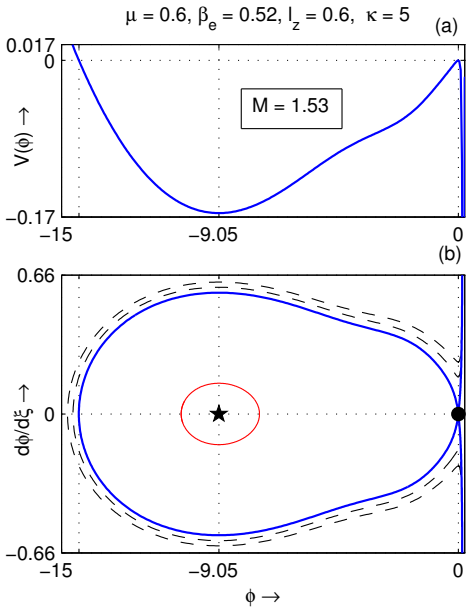

Figure 3.9: (a) $V(\phi)$ and (b) the phase portrait of the system are drawn on the same ϕ-axis for $M = 1.53$ and for $\kappa = 5$. This figure confirms the existence of NPSW after the formation of supersoliton.

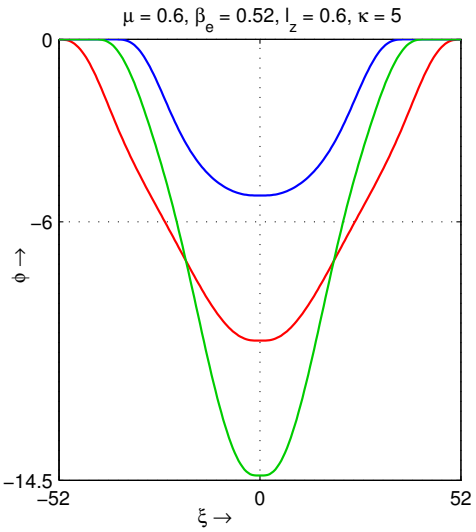

Figure 3.10: ϕ is plotted against ξ for $M = 1.49$ (NPSW before the formation of NPSS) (blue dash-dot curve) $M = 1.5$ (red solid curve) (NPSS) and $M = 1.53$ (blue solid curve) (NPSW after the formation of NPSS) for $\kappa = 5$, $\gamma = 5/3$, $\sigma_{ie} = 0.01$ and other mentioned parameter values.

by $\frac{K_B T_e}{e}$. Here, K_B is the Boltzmann constant; $-e$ is the charge of an electron; m_i is the ion mass; n_{d0} is the unperturbed number density of dust particulates; Z_d is the number of electrons residing on a dust grain surface; $\gamma(= \frac{5}{3})$ is the adiabatic index; $\sigma_{ie} = \dfrac{T_i}{T_e}$, $\mu = \dfrac{n_{e0}}{n_{i0}}$, where T_i is the average temperature of ions and n_{e0} (n_{i0}) is the unperturbed number density of electrons (ions) respectively. We have used same assumption of Choi *et al.* [90] to consider the quasi-neutrality condition (3.3.5) instead of Poisson equation. Several authors [111, 127] have considered the same assumption to study the nonlinear behaviour of IA / DIA waves in magnetized plasma. Using the equations (3.3.3) - (3.3.5), the dimensionless linear dispersion relation for IA wave can be written as

$$\frac{k_z^2}{\omega^2} + \frac{k_\perp^2}{\omega^2 - 1} = M_s^{-2}, \tag{3.3.7}$$

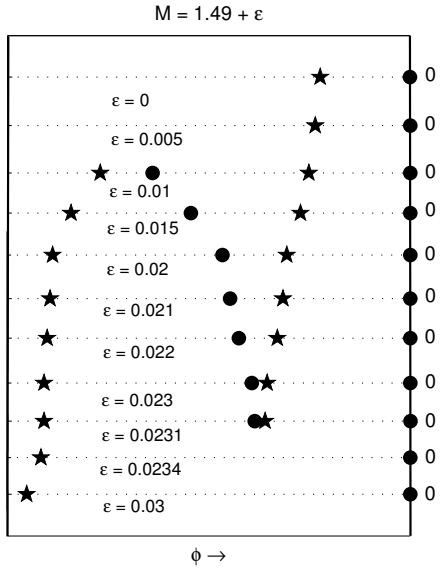

Figure 3.11: Unstable equilibrium points (small solid circles) and stable equilibrium points (small solid stars) for the dynamical system are drawn on the ϕ-axis for different values of $M = 1.49 + \epsilon$. This figure clearly shows the transition from soliton to super-soliton to soliton again.

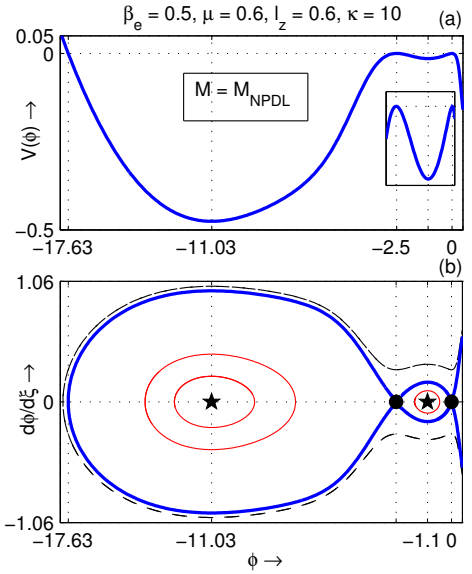

Figure 3.12: (a) $V(\phi)$ and (b) the phase portrait of the system are drawn on the same ϕ-axis for $M = M_{NPDL}$ and for $\kappa = 10$. We see that there are two unstable equilibrium points corresponding to two maximum values of $V(\phi)$ at $\phi = 0$ and at $\phi = -2.54$. This figure confirms the existence of NPDL.

where

$$M_s = \sqrt{\gamma\sigma_{ie} + \frac{1}{\mu}\left\{\frac{\kappa - \frac{1}{2}}{\kappa - \frac{3}{2}} - \beta_{e1}^{(\kappa)}\right\}^{-1}}. \tag{3.3.8}$$

For low frequency IA wave, we have $\omega << \omega_c \Leftrightarrow \frac{\omega}{\omega_c} << 1 \Leftrightarrow \omega << 1$ as ω is normalized by ω_c, i.e., $\frac{\omega}{\omega_c}$ is replaced by ω, and consequently the equation (3.3.7) assumes the following form:

$$\frac{\omega}{k_z} = \left(M_s^{-2} + k_\perp^2\right)^{-1/2}. \tag{3.3.9}$$

The equation (3.3.9) is exactly same as equation (1.2.9) of Chapter-1 if $\kappa \to \infty$.

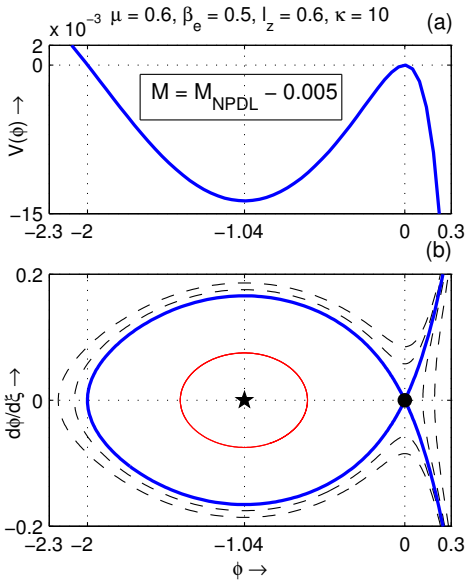

Figure 3.13: (a) $V(\phi)$ and (b) the phase portrait of the system are drawn on the same ϕ-axis for $M = M_{NPDL} - 0.005$ and for $\kappa = 10$. This figure confirms the existence of NPSW just before the formation of NPDL.

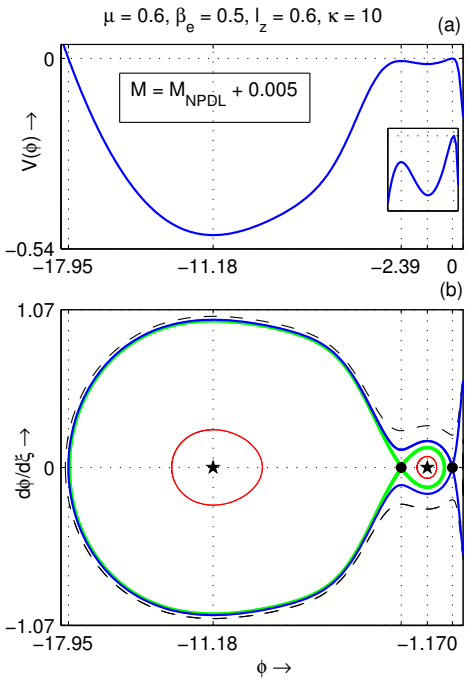

Figure 3.14: (a) $V(\phi)$ and (b) the phase portrait of the system are drawn on the same ϕ-axis for $M = M_{NPDL} + 0.005$ and for $\kappa = 10$. We see that there are two unstable equilibrium points corresponding to two maximum values of $V(\phi)$ at $\phi = 0$ and at $\phi = -2.39$. This figure confirms the existence of supersoliton.

3.4 Energy Integral

To investigate the time independent nonlinear IA waves propagating along a direction having direction cosines (l_x, l_y, l_z), we consider a wave frame moving with a constant velocity M normalized by C_s along a direction having direction cosines (l_x, l_y, l_z). Therefore, here we consider the following transformation:

$$\xi = l_x x + l_y y + l_z z - Mt \quad \text{with} \quad l_x^2 + l_y^2 + l_z^2 = 1. \tag{3.4.1}$$

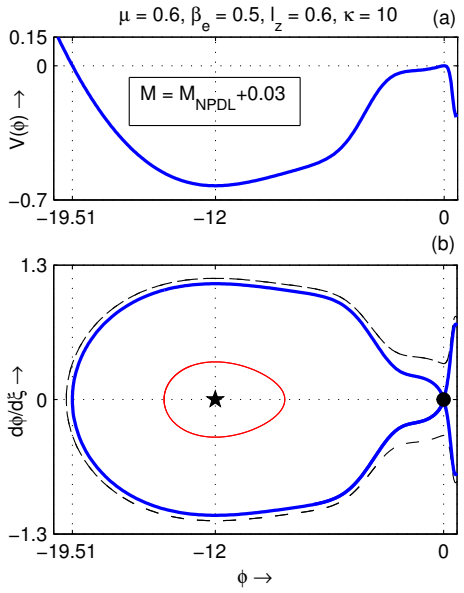

Figure 3.15: (a) $V(\phi)$ and (b) the phase portrait of the system are drawn on the same ϕ-axis for $M = M_{NPDL} + 0.03$ and for $\kappa = 10$. This figure confirms the existence of NPSW after the formation of NPDL and NPSS.

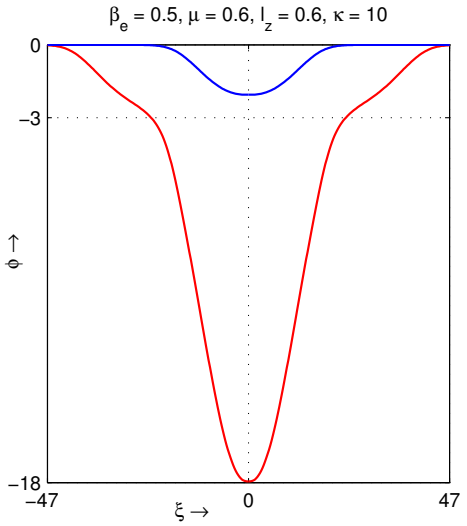

Figure 3.16: ϕ is plotted against ξ for $M = M_{NPDL} + 0.005$ (solid curve) and $M = M_{NPDL} - 0.005$ (dashed curve) for $\kappa = 10$ and other indicated parameter values. The jump discontinuity between the amplitudes of NPSWs immediately before and after the formation of NPDL is evident in this figure.

Consequently all the dependent variables depend only on the single variable ξ. Now, lifting the continuity equation (3.3.3) in the wave frame and using the boundary conditions

$$\Big(n_i, u_{ix}, u_{iy}, u_{iz}, \phi, \frac{d\phi}{d\xi}\Big) \to \big(1, 0, 0, 0, 0, 0\big) \text{ as } |\xi| \to \infty, \tag{3.4.2}$$

we get the following equation:

$$l_x u_{ix} + l_y u_{iy} + l_z u_{iz} = M\Big(1 - \frac{1}{n_i}\Big). \tag{3.4.3}$$

Now, lifting the z component of equation of motion (3.3.4) in the wave frame and using the boundary conditions (3.4.2), the solution of the z component of the equation of motion (3.3.4) for the unknown u_{iz} can be simplified as follows:

$$u_{iz} = \frac{l_z}{M}\Big[\sigma_{ie}\Big\{(n_i)^{\gamma} - 1\Big\} + \int_0^{\phi} n_i d\phi\Big], \tag{3.4.4}$$

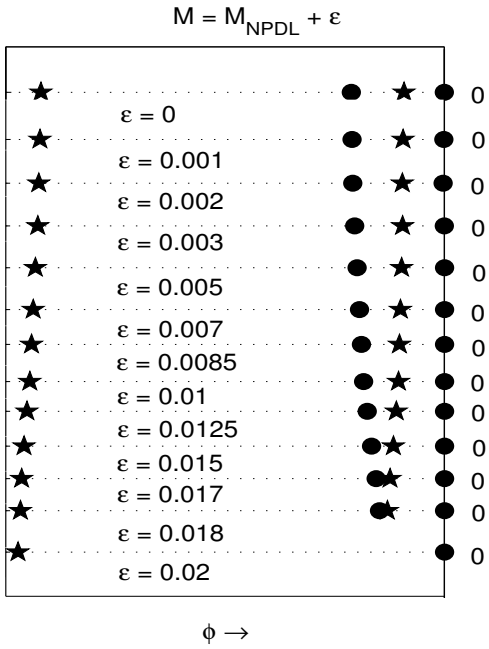

Figure 3.17: Unstable equilibrium points (small solid circles) and stable equilibrium points (small solid stars) for the dynamical system are drawn on the ϕ-axis for different values of $M = M_{NPDL} + \epsilon$ for $\kappa = 10$. This figure clearly shows the transition from double layer to supersoliton to conventional soliton again for negative polarity.

where we have used equation (3.4.3) to simplify the equation (3.4.4) and n_i is given by the equation (3.3.5).

Using the transformation (3.4.1), we get the following solutions for the unknowns u_{ix} and u_{iy} from the x and y components of the equation of motion (3.3.4):

$$\begin{pmatrix} u_{ix} \\ u_{iy} \end{pmatrix} = \begin{pmatrix} G_1(\phi) & -\frac{dP}{d\xi} \\ \frac{dP}{d\xi} & G_1(\phi) \end{pmatrix} \begin{pmatrix} \frac{l_x}{l_x^2 + l_y^2} \\ \frac{l_y}{l_x^2 + l_y^2} \end{pmatrix}, \tag{3.4.5}$$

where

$$G_1(\phi) \equiv G_1(M, \phi) = M - \frac{M}{n_i} - \frac{l_z^2}{M} G(\phi), \tag{3.4.6}$$

$$G(\phi) = \sigma_{ie}\Big(n_i^{\gamma} - 1\Big) + \int_0^{\phi} n_i d\phi, \tag{3.4.7}$$

$$P \equiv P(M, \phi) = \frac{M^2}{2(n_i)^2} + \frac{\gamma\sigma_{ie}}{\gamma - 1}(n_i)^{\gamma-1} + \phi, \tag{3.4.8}$$

and we have used equation (3.4.6) to simplify the equation (3.4.5) and n_i is given by the equation (3.3.5).

Differentiaing the first equation of (3.4.5) with respect to ξ and using this expression of $\frac{du_{ix}}{d\xi}$ in the x component of the equation of motion (3.3.4), we get the following equation:

$$\frac{d^2P}{d\xi^2} = \frac{n_i G_1(\phi)}{M}. \tag{3.4.9}$$

Using the identity

$$\frac{d^2P}{d\xi^2} = \frac{1}{2}\frac{dP}{d\phi}\frac{d}{d\phi}\Big(\frac{d\phi}{d\xi}\Big)^2 + \frac{d^2P}{d\phi^2}\Big(\frac{d\phi}{d\xi}\Big)^2, \tag{3.4.10}$$

the equation (3.4.9) can be written in the following form:

$$\frac{d\Gamma}{d\phi} + \frac{2}{\chi}\frac{d\chi}{d\phi}\Gamma = \frac{2}{\chi}f(\phi), \tag{3.4.11}$$

where

$$\Gamma = \Big(\frac{d\phi}{d\xi}\Big)^2, \chi \equiv \chi(M, \phi) = \frac{dP}{d\phi}, \tag{3.4.12}$$

$$f(\phi) \equiv f(M, \phi) = \frac{n_i G_1(\phi)}{M}. \tag{3.4.13}$$

The equation (3.4.11) is a linear differential equation in Γ having integrating factor χ^2 and consequently the general solution of (3.4.11) can be put in the following form:

$$\frac{1}{2}\Big(\frac{d\phi}{d\xi}\Big)^2 + V(\phi) = 0, \tag{3.4.14}$$

where

$$V(\phi) = V(M, \phi) = -\frac{\int_0^{\phi} \chi f(\phi) d\phi}{\chi^2}, \tag{3.4.15}$$

and we have used (3.4.2) to simplify (3.4.14) and the equation (3.4.14) is known as the energy integral with Sagdeev pseudo potential $V(\phi)(= V(M, \phi))$.

3.5 Different Bounds of Mach Number M

The mechanical analogy of (3.4.14) has been extensively discussed in the paper of Das *et al.* [65]. According to the mechanical analogy of Sagdeev [11], the equation (3.4.14) describes a PPSW (NPSW) if the following conditions hold simultaneously:

- (a) $V(M, 0) = 0$, $V'(M, 0) = 0$ and $V''(M, 0) < 0$,
- (b) $V(M, \phi_m) = 0$, $V'(M, \phi_m) > 0$ ($V'(M, \phi_m) < 0$) for some M with $\phi_m > 0$ for the existence of a PPSW ($\phi_m < 0$ for the existence of a NPSW),
- (c) $V(M, \phi) < 0$ for $\min\{0, \phi_m\} < \phi < \max\{0, \phi_m\}$.

Again, for a PPDL (NPDL) solution of (3.4.14), the second condition (b) is replaced by the following condition:

- (b1) $V(M, \phi_m) = 0$, $V'(M, \phi_m) = 0$, $V''(M, \phi_m) < 0$ for some M with $\phi_m > 0$ for the existence of a PPDL ($\phi_m < 0$ for the existence of a NPDL).

Using the conditions (a), (b) or (b1), (c), we have discussed the different bounds of Mach number M for the existence of different solitary structures:

- M_c & M_s: M_c is the Lower bound of the Mach number for the existence of the solitary structures of any polarity, i.e., solitary structure of any polarity

starts to exist for $M > M_c$. In fact the condition $M > M_c$ is the necessary condition for the existence of solitary structures and the expression of M_c can be obtained from the condition (a). It is simple to check that the conditions $V(M,0) = 0$ and $V'(M,0) = 0$ are trivially satisfied for any M whereas the condition $V''(M,0) < 0$ imposses the following restriction on M:

$$M_c < M < M_s, \tag{3.5.1}$$

where

$$M_c = l_z M_s, \tag{3.5.2}$$

and M_s is given by the equation (3.3.8). Therefore, for the existence of solitary structures of any polarity, we must have $M_c < M < M_s$ and consequently, M_s is the upper bound of the Mach number for the existence of the solitary structure of any polarity.

- M_{PPDL} & M_{NPDL}: The Mach number M_{PPDL} (M_{NPDL}) corresponds to a positive (negative) potential double layer solution of the energy integral (3.4.14). To find the double layer solution, one can use condition (b1). The other two conditions are same for all solitary structures. Let $M = M_d$ and $\phi_m = \phi_d \neq 0$ be the solutions of the equations $V(M,\phi_m) = 0$ and $V'(M,\phi_m) = 0$, i.e., $V(M_d,\phi_d) = 0$ and $V'(M_d,\phi_d) = 0$ for non-zero ϕ_d. Using the equations $V(M_d,\phi_d) = 0$ and $V'(M_d,\phi_d) = 0$, we get the following expression of M_d:

$$M_d = \sqrt{\frac{l_z^2 n_i(\phi_d) G(\phi_d)}{n_i(\phi_d) - 1}}, \tag{3.5.3}$$

where $G(\phi)$ is given by the equation (3.4.7). The equation $V(M_d,\phi_d) = 0$ gives

the following equation:

$$\int_0^{\phi_d} \chi(M_d, \phi) f(M_d, \phi) d\phi = 0, \tag{3.5.4}$$

Solving equations (3.5.3) and (3.5.4) numerically for ϕ_d and M_d, we can proceed our investigation for finding M_{PPDL} and M_{NPDL}. If $V''(M_d, \phi_d) < 0$, then this M_d corresponds to M_{PPDL} (M_{NPDL}) of a PPDL (NPDL) if $\phi_d > 0$ ($\phi_d < 0$) and ϕ_d is the smallest (largest) real satisfying the conditions $V(M_d, \phi_d) = 0$ and $V'(M_d, \phi_d) = 0$. In fact, we have followed the same analysis as given in Chapter-1 to get ϕ_d and M_d.

- M_{pmax} & M_{nmax}: Here M_{pmax} (M_{nmax}) is the upper bound of the Mach number for the existence of all positive (negative) potential solitary structures including positive (negative) potential double layers and positive (negative) potential supersolitons. This upper bound can be determined by considering the theory as discussed in Chapter-1. In fact, to derive the inequality (3.5.1), we have assumed the condition $\chi(M, 0) \neq 0$, otherwise $V(M, \phi)$ is not well defined at $\phi = 0$. But to make $V(\phi)$ well defined, we must consider $\chi(M, \phi) \neq 0$ throughout the entire possible range of ϕ. So, we can consider the equation $\chi(M, \phi) = 0$ instead of considering $\chi(M, \phi) \neq 0$ and the equation $\chi(M, \phi) = 0$ gives

$$\frac{M^2}{M_s^2} = K(\phi), \tag{3.5.5}$$

where

$$K(\phi) = \frac{1}{M_s^2}\Big[\gamma \sigma_{ie} n_i^{\gamma+1} + n_i^3 \Big(\frac{dn_i}{d\phi}\Big)^{-1}\Big]. \tag{3.5.6}$$

Obviously the equation (3.5.5) is well defined only when $K(\phi) > 0$ for all ϕ. From equation (3.5.6), we see that $K(\phi)$ is independent of M. Therefore, $\frac{dP}{d\phi} = 0$

holds good only when M assumes the value $M_s\sqrt{K(\phi)}$ and consequently for the existence of positive [negative] potential solitary structure, M cannot exceed the value $M_s\sqrt{K(\phi_{pmin})}$ $[M_s\sqrt{K(\phi_{nmin})}]$, where $K(\phi)$ attains its global minimum at $\phi = \phi_{pmin}$ $[\phi = \phi_{nmin}]$ in the positive [negative] side of ϕ - axis, i.e., for $\phi_{pmin} \geq 0$ $[\phi_{nmin} \leq 0]$. Now, if $\phi_{pmin} = 0$ $[\phi_{nmin} = 0]$, then M cannot exceed the value M_s because $\sqrt{K(\phi_{pmin})} = \sqrt{K(0)} = 1$ $[\sqrt{K(\phi_{nmin})} = \sqrt{K(0)} = 1]$, i.e., $M < M_s$ and consequently $M_{pmax} = M_s$ $[M_{nmax} = M_s]$. So, we consider the case $\phi_{pmin} > 0$ for positive potential side and the case $\phi_{nmin} < 0$ for negative potential side. For simplicity, let us consider the positive side only, then we have the following two cases: Case I - $K(\phi_{pmin}) > 1$ and Case II - $0 \leq K(\phi_{pmin}) \leq 1$.

Case I : If $K(\phi_{pmin}) > 1$, then the upper bound of M for the existence of the positive potential solitary structures is given by $M_{pmax} = M_s$. In fact, there does not exist any ϕ_{pmin} for which M can assume the value $M_s\sqrt{K(\phi_{pmin})}$ because $M = M_s\sqrt{K(\phi_{pmin})} \Rightarrow \frac{M}{M_s} = \sqrt{K(\phi_{pmin})} > 1 \Rightarrow M > M_s$ which contradicts the fact $M_c < M < M_s$ and consequently $\frac{dP}{d\phi} \neq 0$ for $\phi = \phi_{pmin}$. So, $V(\phi)$ is well defined as a real valued function of ϕ if it is well defined at $\phi = 0$. Therefore, for this case, we have $M_{pmax} = M_s$.

Case II : If $0 \leq K(\phi_{pmin}) \leq 1$, then $M = M_s\sqrt{K(\phi_{pmin})}$ is the minimum value of M at which there is a singularity of $V(\phi)$ at $\phi = \phi_{pmin}$, i.e., $\left.\frac{dP}{d\phi}\right|_{\phi=\phi_{pmin}} = 0$ when $M = M_s\sqrt{K(\phi_{pmin})}$. Therefore, M cannot exceed the value $M_s\sqrt{K(\phi_{pmin})}$, i.e., $M < M_s\sqrt{K(\phi_{pmin})}$. So, for this case, we have $M_{pmax} = M_s\sqrt{K(\phi_{pmin})}$.

Combining Case (I), Case (II) and the earlier discussions, we get the following

formula for M_{pmax}:

$$M_{pmax} = M_s \min\left\{1, \sqrt{K(\phi_{pmin})}\right\}. \tag{3.5.7}$$

Similarly, considering the negative side of ϕ axis, one can derive the following formula for M_{nmax}:

$$M_{nmax} = M_s \min\left\{1, \sqrt{K(\phi_{nmin})}\right\}. \tag{3.5.8}$$

3.6 Existence Domains

With the help of the formulas of M_c, M_s, M_{pmax}, M_{nmax} and the numerical analogy for M_{PPDL} and M_{NPDL} as described by the equations (3.5.2), (3.3.8), (3.5.7), (3.5.8) and the equations (3.5.3) and (3.5.4) respectively, one can draw the compositional parameter spaces or the existence domain with respect to any parameter of the system and this existence domain clearly shows the occurrence of different solitary structures including double layers. Also, if a compositional parameter space shows the existence of solitary waves after the formation of double layers, then the existence of supersoliton is implied but if the system supports supersolitons without the formation of double layer then it is not possible to predict the existence of supersoliton from the compositional parameter spaces. In fact, to confirm the existence of supersoliton structures in either cases, it is essential to consider the phase portraits of the dynamical system describing different solitary structures. In this section, we have considered different compositional parameter spaces with respect to the nonthermal parameter β_e.

In figures 3.2 - 3.5, the magenta curve, the blue curve, the red curve, the black curve and the green curve represent the curves $M = M_c$, $M = M_{pmax}$, $M = M_{nmax}$, $M = M_s$ and $M = M_{NPDL}$, i.e., the curve along which NPDLs exist, respectively.

Here, P, N, C and NS are, respectively, the regions of existence of PPSWs, existence of NPSWs, coexistence of PPSWs and NPSWs and existence of NPSWs after the formation of NPDLs. Based on these notations and terminologies, the figures of the compositional parameter spaces are self-explanatory if we define the following cut-off values of the nonthermal parameter β_e : (a) $\beta_e^{(1)}$: The curve $M = M_{nmax}$ coincides with the curve $M = M_s$ for $\beta_e \geq \beta_e^{(1)}$. (b) $\beta_e^{(2)}$: The curve $M = M_{pmax}$ exists for all $\beta_e \geq \beta_e^{(2)}$. (c) $\beta_e^{(3)}$: The curve $M = M_{pmax}$ differs from the curve $M = M_s$ for all $\beta_e > \beta_e^{(3)}$, i.e., the curve $M = M_{pmax}$ coincides with the curve $M = M_s$ for all $\beta_e^{(2)} \leq \beta_e \leq \beta_e^{(3)}$. (d) $\beta_e^{(4)}$: The curve $M = M_{NPDL}$ exists for all $\beta_e \geq \beta_e^{(4)}$. (e) $\beta_e^{(5)}$: The curve $M = M_{nmax}$ differs from the curve $M = M_s$ for all $\beta_e > \beta_e^{(5)}$, i.e., The curve $M = M_{nmax}$ coincides with the curve $M = M_s$ for all $\beta_e^{(1)} \leq \beta_e \leq \beta_e^{(5)}$.

Again it is important to note that the upper bound of β_e is β_{eT}, where the expression of β_{eT} is given by the equation (3.2.7). For $\kappa = 3$, $\kappa = 5$, $\kappa = 10$ and $\kappa = 100$, the values β_{eT} are approximately 0.67, 0.64, 0.60 and 0.57 respectively. Figures 3.2 - 3.5 are the qualitatively different compositional parameter spaces showing the nature of existence of different solitary structures.

Figure 3.2 is the existence domain with respect to β_e for $\kappa = 3$ along with the values of the other parameters as mentioned in the figure concerned. We have the following observations from this figure: (i) The system supports NPSWs throughout the range of β_e, i.e., for all $0 \leq \beta_e \leq \beta_{eT}$ but for the clearness of the figure, the figure 3.2 has been drawn for $0 \leq \beta_e \leq 0.44$. (ii) The system starts to support PPSWs at $\beta_e = \beta_e^{(2)} = 0.142$, i.e., PPSWs exist for all $\beta_e^{(2)} \leq \beta_e \leq \beta_{eT}$. (iii) The system supports coexistence of PPSWs and NPSWs for all $\beta_e^{(2)} \leq \beta_e \leq \beta_{eT}$. (iv) The curve $M = M_{nmax}$ coincides with the curve $M = M_s$ for $\beta_e^{(1)} \leq \beta_e \leq \beta_{eT}$ where $\beta_e^{(1)} = 0.065$, and differs from $M = M_s$ for $0 \leq \beta_e < \beta_e^{(1)}$. (iv) The system does not support double

layers or supersolitons of any polarity.

Figure 3.3 exhibits the existence regions of different solitary structures the system supports for $\kappa = 5$ along with the values of the other parameters indicated in the figure concerned. This existence domain seems to look similar to figure 3.2, but we have found an interesting property of this existence domain as well as of the system. (i) The system supports NPSWs for all $0 \leq \beta_e \leq \beta_{eT}$ but here the figure 3.3 has been drawn for $0 \leq \beta_e \leq 0.52$. (ii) The system supports coexistence of PPSWs and NPSWs for all $\beta_e^{(2)} \leq \beta_e \leq \beta_{eT}$ where $\beta_e^{(2)} = 0.167$. (iii) The curve $M = M_{nmax}$ (red) starts to coincide with the curve $M = M_s$ (black) at $\beta_e = \beta_e^{(1)} = 0.166$. (iv) The curve $M = M_{pmax}$ (blue) coincides with $M = M_s$ (black) for $\beta_e^{(2)} \leq \beta_e \leq \beta_e^{(3)} = 0.23$. The curve $M = M_{pmax}$ differs from $M = M_s$ for $\beta_e^{(3)} < \beta_e \leq \beta_{eT}$. (v) The system does not support positive potential double layers or positive potential supersolitons. (vi) Although the system does not support negative potential double layers, but in this existence domain, we have observed the existence of negative potential supersolitons, i.e., the system supports NPSSs without the formation of NPDLs. This characteristic of the system has been confirmed and precisely described through the phase portraits of the corresponding dynamical systems in the next Section 3.7.

Figure 3.4 shows the existence domain with respect to β_e for $\kappa = 10$ along with the values of the other parameters as mentioned in the figure concerned. From this figure, we have the following observations: (i) The system supports NPSWs for all admissible values of β_e, i.e., for all $0 \leq \beta_e \leq \beta_{eT}$ but here the figure 3.3 has been drawn for $0 \leq \beta_e \leq 0.55$. (ii) For this existence domain, $\beta_e^{(2)} = 0$, i.e., the system supports PPSWs for all $0 \leq \beta_e \leq \beta_{eT}$. (iii) The system supports coexistence of PPSWs and NPSWs for all $0 \leq \beta_e \leq \beta_{eT}$. The region of this coexistence is bounded by the curve $M = M_c$ (magenta) and the curve $M = M_{nmax}$ (red) for $0 \leq \beta_e \leq \beta_e^{(3)} = 0.25$.

For $\beta_e^{(3)} < \beta_e \leq \beta_{eT}$, the coexistence region is bounded by $M = M_c$ and $M = M_{pmax}$ (blue). (iv) The system starts to support NPDLs along the curve $M = M_{NPDL}$ (green) whenever $\beta_e \geq \beta_e^{(4)} = 0.39$, i.e., NPDLs exist for all $\beta_e^{(4)} \leq \beta_e \leq \beta_{eT}$ along the curve $M = M_{NPDL}$. (v) The system supports NPSSs after the formation of NPDLs. (vi) The system exhibits the existence of NPSWs after the formation of NPDLs. (vii) The curve $M = M_{nmax}$ (red) coincides with the curve $M = M_s$ (black) for $\beta_e^{(1)} \leq \beta_e \leq \beta_e^{(5)}$ where $\beta_e^{(1)} = 0.22$ and $\beta_e^{(5)} = 0.502$. The curve $M = M_{nmax}$ differs from $M = M_s$ for $0 \leq \beta_e < \beta_e^{(1)}$ and for $\beta_e^{(5)} < \beta_e \leq \beta_{eT}$. In fact, we have observed that as κ increases, the value of $\beta_e^{(5)}$ decreases. In other words, $\beta_e^{(5)}$ gradually tends to $\beta_e^{(1)}$, where $M = M_{nmax}$ starts to coincide with $M = M_s$, and eventually, both of these two cut-off marks of β_e disappear from the existence domain, i.e., $M = M_{nmax}$ does not coincide with $M = M_s$ for any value of β_e and consequently, the curve $M = M_{nmax}$ lies completely below the curve $M = M_s$. In fact, with the increasing value of κ, this existence domain (figure 3.4) tends to match the existence domain as shown in FIG. 1.2 of Chapter-1, where we have considered the Cairns nonthermal distribution for the electrons. This fact is clear from figure 3.5, where we have drawn the curves $M = M_c$, $M = M_s$ and $M = M_{nmax}$ only for $\kappa = 100$, keeping the other parameter values same as in figure 3.4. This figure is not the complete existence domain for $\kappa = 100$. The qualitative behaviour of the curves $M = M_{pmax}$ and $M = M_{NPDL}$ remain unchanged. So, the figure along with the figure 3.4 indicates that the compositional parameter space (figure 3.4) tends to the compositional parameter space as shown in FIG. 1.2 of Chapter-1. Again, it is also important to note that $\beta_e^{(2)}$ decreases with increasing κ and finally, it assumes the lower bound of β_e, which is equal to 0.

3.7 Phase Portraits

Supersoliton structure was first introduced by Dubinov & Kolotkov [113]. At the same time, Das *et al.* [69] observed the dias-type solitary structures whose properties are same as the supersolition structure of Dubinov & Kolotkov [113]. Actually, to distinguish between a supersoliton and a conventional soliton, it is important to draw the phase portraits of the dynamical system describing different nonlinear waves. Specifically, according to Dubinov & Kolotkov [113], the separatrix corresponding to a supersoliton encloses one or more inner separatrices and several stable and unstable equilibrium points whereas the separatrix corresponding to a conventional soliton encloses only one stable equilibrium point and consequently there is no other separatrix within the separatrix corresponding to the conventional soliton. Subsequently, several authors [71–77, 114–119, 177] investigated supersoliton structures in different unmagnetized and magnetized plasma system. Recently, Dubinov & Kolotkov [120] have clearly discussed the supersoliton structures in their review works on super-nonlinear waves in astrophysical and laboratory plasmas.

From the existence domains or the compositional parameter spaces, this is convenient to confirm the existence of solitary structures including double layers also. But the existence of supersolitons cannot be confirmed from the existence domains. If we consider the existence domain shown in figure 3.3, we can only say that the system supports solitary waves of both polarities but no other solitary structures of the negative polarity. Particularly, from the existence domain as shown in figure 3.3, it is not possible to predict the occurrence of the negative potential supersoliton. But, for this existence domain, if we plot $V(\phi)$ against ϕ for a sequence of values of the Mach number M then we get figure 3.6. This figure shows that the Mach number

$M = 1.48$ corresponds to a negative potential soliton (shown is violet curve), and as we increase the value of M, the shape of the solitary structure gradually changes from a soliton to a supersoliton. In figure 3.6(a), the first three $V(\phi)$-curves (violet, green and brown) correspond to negative potential solitons wheareas the next three curves (red, blue and magenta) correspond to negative potential supersolitons, and the last two curves (sky-blue and yellow) correspond to negative potential solitons again. Specifically, figue 3.6(b) and figure 3.6(c) respectively show the same red and blue curves in 3.6(a) which clearly show up to be supersolitons. But to distinguish between a soliton and supersoliton, it is instructive to draw the phase portraits, i.e., the structure of supersoliton can be established even more firmly if we draw the phase portraits of the dynamical systems of the solitary structures concerned. Again, if we consider the existence domain shown in figure 3.4, we see that the system supports NPDLs, and also the existence of solitary structures beyond the existence of NPDLs can be surmised from this existence domain. Now, if solitary waves exist after the formation of a double layer, we can be sure about the existence of supersolitons between the double layer and the solitary waves after the formation of double layers. But, existence domains cannot indicate the range of the Mach number M which corresponds to the existence of supersoliton as well as the range of M which corresponds to solitary waves after the occurrence of double layers. Plotting $\phi - V(\phi)$ curves can give an idea in this regard but to confirm the existence of a supersoliton and a soliton after the occurrence of supersolitons, we need to follow the mechanism of phase portraits.

Moreover, if we consider the transition of solitary structures: soliton $\rightarrow$ double layer $\rightarrow$ supersoliton $\rightarrow$ soliton (e.g., fig.3.4), there is a finite jump between the amplitudes of solitons just before and just after the formation of the double layer.

Likewise, if we consider the transition of solitary structures: soliton → supersoliton → soliton without the formation of a double layer (e.g., fig.3.3), we observe that there is a finite jump between the amplitudes of solitons just before and just after the formation of supersolitons. We have also observed that there is a finite jump between the amplitudes of a supersoliton and a soliton before the formation of supersolitons. This phenomenon cannot be explained by the existence domains or $\phi - V(\phi)$ graphs only, but the phase portraits of the dynamical systems corresponding to the concerned solitary structures can describe this well. So, to know the topology of the different nonlinear structure of IA waves, it is necessary to consider the phase portraits of the dynamical system describing the nonlinear waves. Now, to get first order and first degree coupled differential equations describing the nonlinear behaviour of IA waves, we differentiate the energy integral (3.4.14) with respect to ϕ and finally we get the following equations:

$$\frac{d\phi_1}{d\xi} = \phi_2, \ \frac{d\phi_2}{d\xi} = -V'(\phi_1), \quad \text{where} \quad \phi_1 = \phi. \tag{3.7.1}$$

With the help of the existence domain as shown in figure 3.3, we have plotted $V(\phi)$ aganist ϕ and the phase portraits of the corresponding dynamical system in the upper panel (marked (a)) and lower panel (marked (b)) respectively of each of the figures 3.7 - 3.9, to describe the shapes of the solitary structures. We see that there is a one-one correspondence between the curve $V(\phi)$ against ϕ in the upper panel and the separatrix (shown in bold blue line) in the lower panel in each case. Each solid circle in the lower panel corresponds to an unstable equilibrium point where the potential energy $V(\phi)$ of a pseudo particle under the action of a force field $-V'(\phi)$ is maximum and each solid star corresponds to a stable equilibrium point where the potential energy $V(\phi)$ of the pseudo particle is minimum. Therefore, in each of the

figures 3.7 - 3.9, each maximum point of $V(\phi)$ corresponds to an unstable equilibrium point and each minimum point of $V(\phi)$ corresponds to a stable equilibrium point of the dynamical system corresponding to different solitary structures.

Figure 3.7(b) shows the phase portrait of the dynamical system corresponding to an NPSW which appears before the formation of NPSSs. In this figure, we see that there is only one separatrix which appears to start and end at the unstable equilibrium point at the origin $(0, 0)$ and this separatrix encloses only one stable equilibrium point on the negative potential side, viz., $(-5.14, 0)$. In figure 3.7 (a), $V(\phi)$ is plotted against ϕ which corresponds to the separatrix. This confirms the existence of an NPSW for $\kappa = 5$ before the formation of NPSSs.

Figure 3.8(b) shows the phase portrait of the dynamical system corresponding to a negative potential supersoliton. In this figure, we see that there are two separatrices: one seems to begin and end at the unstable equilibrium point at the origin (shown in bold blue curve) which encloses another separatrix that appears to pass through a non-zero unstable fixed point $(-5.76, 0)$ and encloses two stable equilibrium points $(-6.9, 0)$ and $(-2.27, 0)$. In figure 3.8(a), $V(\phi)$ is plotted against ϕ which corresponds to the separatrix of 3.8(b). This confirms the existence of NPSS for $\kappa = 5$ without the formation of NPDL whereas in Chapter-1, we have observed existence of NPSS after the formation of NPDL for $\kappa \to \infty$.

Figure 3.9 shows the phase portrait of the dynamical system corresponding to an NPSW which appears after the formation of NPSSs. In this figure, we see that there is only one separatrix which seems to begin and end at the unstable equilibrium point at the origin $(0, 0)$ and this separatrix encloses only one stable equilibrium point on the negative potential side, viz., $(-9.05, 0)$. In figure 3.9 (a), $V(\phi)$ is plotted against ϕ which corresponds to this mentioned separatrix. This shows the existence of an

NPSW after the formation of supersolitons for $\kappa = 5$.

We have mentioned earlier in this section that figure 3.6 shows the occurrence of solitons, supersolitons and solitons again after the formation of supersolitons, of negative polarity, sequentially, for the increasing values of M, for $\kappa = 5$ and the other parameter values as mentioned in the same figure. So, we observe the following transition of solitary structures: NPSW $\rightarrow$ NPSS $\rightarrow$ NPSW after the formation of NPSSs and here we get NPSSs without the formation of NPDL. Figure 3.10 and 3.11 help us to understand this transition better. In figure 3.10, ϕ is plotted against ξ for three distinct values of the Mach number M. $M = 1.49$ corresponds to the blue curve which represents a negative potential soliton. $M = 1.5$ corresponds to the red curve which exhibits a dias-type solitary structure that follows the definition of a supersoliton given by Dubinov & Kolotkov [113]. $M = 1.53$ corresponds to a negative potential soliton after the occurrence of negative potential supersolitons which is the green curve in figure 3.10. In figure 3.11, we have drawn the stable and unstable equilibrium points of the dynamical system for increasing values of M starting from $M = 1.49$. We see that there are two equilibrium points for first two values of M which corresponds to only one separatrix that seems to pass through the unstable equilibrium point at the origin and encloses only one stable equilibrium point. Then there are four fixed points for the next seven values of M, each of which corresponds to a supersoliton, i.e., the system contains one separatrix that appears to pass through the unstable equilibrium point at the origin and encloses another separatrix. We see that the distance between the non-zero unstable equilibrium point and the stable equilibrium point nearest to the origin decreases for increasing values of M, and finally both of them disappear from the system. In other words, the system is left with only one separatrix passing through the unstable equilibrium point at the

origin and enclosing a single stable equilibrium point which corresponds to a soliton (after the formation of supersolitons). We have numerically observed that our system exhibits this transition: NPSW $\rightarrow$ NPSS $\rightarrow$ NPSW after the formation of NPSSs without the formation of an NPDL in the range $4.9 \leq \kappa \leq 5.05$.

Figure 3.12(b) shows the phase portrait of the dynamical system corresponding to an NPDL for $\kappa = 10$ and other indicated values of parameters. Here we see only one separatrix that seems to begin and end at the unstable equilibrium point at the origin $(0, 0)$ and again seems to pass through another non-zero equilibrium point, viz., $(-2.5, 0)$, and encloses two stable equilibrium points, viz., $(-11.03, 0)$ and $(-1.1, 0)$. In figure 3.12(a), $V(\phi)$ is plotted against ϕ which corresponds to the blue separatrix in figure 3.14(b). This confirms the existence of an NPSS for $\kappa = 10$.

Figure 3.13(b) shows the phase portrait of the dynamical system corresponding to an NPSW for $\kappa = 10$ which appears just before the double layer for the same parameter values. Here we see only one separatrix that seems to begin and end at the unstable equilibrium point at the origin and encloses only one stable equilibrium point, viz., $(-1.04, 0)$, on the negative potential side. In figure 3.13(a), $V(\phi)$ is plotted against ϕ which corresponds to the mentioned separatrix in the lower panel. This confirms the existence of NPSW just before the formation of NPDL for $\kappa = 10$ and other indicated parameter values.

Figure 3.14(b) shows the phase portrait of the dynamical system corresponding to a negative potential supersoliton for $\kappa = 10$ and other indicated values of parameters. Here we see there are two separatrices: one seems to begin and end at the unstable equilibrium point at the origin $(0, 0)$ (shown in bold blue curve) and the other one is enclosed in the first one (shown in bold green curve). This second separatrix seems to pass through a non-zero unstable equilibrium point, viz., (-2.39,0), and encloses

two stable equilibrium points, viz., $(-11.18, 0)$ and $(-1.17, 0)$. In figure 3.14(a), $V(\phi)$ is plotted against ϕ which corresponds to the blue separatrix in figure 3.14(b). This confirms the structure of an NPDL for $\kappa = 10$.

Figure 3.15(b) shows the phase portrait of the dynamical system corresponding to a solitary structure which is qualitatively the same (shown in figure 3.13) as an NPSW, for $\kappa = 10$ and other indicated values of parameters. Here we see only one separatrix that appears to pass through the unstable equilibrium point at the origin $(0, 0)$ and encloses only one stable equilibrium point, viz., $(-12, 0)$. In figure 3.15(a), $V(\phi)$ is plotted against ϕ which corresponds to the separatrix in figure 3.15(b). This confirms the structure of an NPSW after the formation of NPDL for $\kappa = 10$ as an NPSW, for $\kappa = 10$ and other indicated values of parameters. Here we see only one separatrix that seems to pass through the unstable equilibrium point at the origin $(0, 0)$ and encloses only one stable equilibrium point, viz., $(-12, 0)$. In figure 3.15(a), $V(\phi)$ is plotted against ϕ which corresponds to the separatrix in figure 3.15(b). This confirms the structure of an NPSW after the formation of NPDL for $\kappa = 10$.

In figure 3.16, ϕ is plotted against ξ for $M = M_{NPDL} - 0.005$ and $M = M_{NPDL} + 0.005$ for $\kappa = 10$. In figure 3.17, we draw the unstable and stable equilibrium points of the dynamical system for increasing values of M starting from $M = M_{NPDL}$, for $\kappa = 10$. Here, we see that the pair of two patricular equilibrium points, one, the stable equilibrium point nearest to the origin and the other one, the non-zero unstable equilibrium point, appear closer with increasing values of M, and eventually both of them vanish from the system. Thus, the system contains only one separatrix passing through the origin and enclosing only one stable equilibrium point which corresponds to a conventional soliton. The transition from double layer to supersoliton to soliton for negative polarity is evident from this figure.

3.8 Conclusions

We have developed a distribution function from Kappa and Cairns distribution functions and we call this distribution as combined Kappa-Cairns distribution. But, for the first time, this combined distribution was introduced by Aoutou *et al.* [175]. We have studied IA solitary structures in a collisionless magnetized plasma consisting of warm adiabatic ions, static negatively charged dust grains and combined Kappa-Cairns distributed electrons, immersed in a static uniform magnetic field directed along the $z-$ axis. This combined Kappa-Cairns distribution is well defined for $\kappa > 2.5$ for non-zero β_e. But for $\beta_e = 0$, the combined distribution reduces to Kappa distribution and consequently the restriction on κ becomes $\kappa > 1.5$. We have also shown that this combined distribution reduces to (i) Cairns nonthermal distribution if $\kappa \to \infty$, and (ii) the isothermal distribution if $\kappa \to \infty$ and $\beta_e = 0$.

We have seen that there is a restriction on the nonthermal parameter β_e that makes the combined Kappa-Cairns distribution well-defined. We have analytically studied the dependence of the upper bound β_{eT} of β_e on κ. For a given value of $\kappa(> 2.5)$, one can easily get the corresponding β_{eT} as we have formulated β_{eT} as a function of κ only. As $\kappa \to \infty$, β_{eT} takes the value 4/7, i.e., when the combined distribution reduces to Cairns nonthermal distribution, the upper bound β_e is 4/7 which follows the result reported by Verheest & Pillay [60].

Following the theory and mechanism given in Section 3.5, we have determined different bounds of the Mach number M. Considering these bounds of M, we have drawn a number of compositional parameter spaces with respect to the nonthermal parameter β_e. The existence of different solitary structures is evident and specified from these compositional parameter spaces. (i) For $2.5 < \kappa < 4.9$, the system supports PPSWs,

NPSWs and coexistence of them. In this range, the system does not support double layers or supersolitons of any polarity for any set of values of the other parameters of the system. (ii) For $4.9 \leq \kappa \leq 5.05$, the system supports PPSWs, NPSWs, coexistence of PPSWs and NPSWs and negative potential supersolitons (NPSSs) without the formation of double layer of negative polarity. In this range of κ, we have also observed the following transition of solitary structures: NPSW $\rightarrow$ NPSS $\rightarrow$ NPSW after the formation of NPSSs. The system does not support NPDLs, PPDLs or positive potential supersolitons in this range of κ. (iii) For $\kappa > 5.05$, the system supports PPSWs, NPSWs, coexistence of solitary waves of both polarities, NPDLs, NPSSs, NPSWs after the formation of NPDL and NPSSs. We see a conventional transition of solitary structures: NPSW $\rightarrow$ NPDL $\rightarrow$ NPSS $\rightarrow$ NPSW after the formation of NPDL. (iv) For the case of κ distribution, i.e., when $\beta_e = 0$, the system does not support double layer or supersoliton of any polarity.

In the compositional parameter spaces, the existence of solitary waves after a double layer (wherever exists) implies the existence of supersolitons, but the range of the Mach number M for the existence of supersolitons cannot be determined from the compositional parameter spaces. Moreover, for the case where the system supports supersolitons without the formation of a double layer, the compositional parameter space fails to indicate the existence of supersolitons. In this situation, the phase portrait of the dynamical system of the solitary structure concerned has been the best scheme to confirm and describe the existence and topology of a supersoliton. In our present work, we have drawn several phase portraits of the dynamical system of different solitary structures to meet the same purpose. This has also been helpful to understand the two types of transitions of solitary structures we have observed in our sytem.

In conformity with the construction of the combined Kappa-Cairns distribution function, we expect that this combined distribution can generate much more highly energetic particles in the neighbourhood of $v = 0$ as well as in the tail of the distribution curve in the phase space. For the same reason, the combined Kappa-Cairns distribution can be regarded more effective and useful than the Kappa and Cairns distribution functions, keeping in mind the fact that both Kappa and Cairns distribution functions can be derived from the combined Kappa-Cairns distribution function. We hope that this distribution function will be accepted and useful in various fields of plasma studies and beyond. Also, the formation of ion acoustic supersolitons without the formation of an ion acoustic double layer is a new observation in magnetized plasma which adds a new result to the study of IA waves in magneized dusty plasma. So, our present work is hoped to make some significant contributions to the theory of nonlinear wave propagation in a magnetized dusty plasma.

Finally, we hope that next generation satellite observations may be able to distinguish the signature of the existence of different solitary structures in space plasma as described in our present chapter.

Chapter 4

Small amplitude ion acoustic solitary waves in a collisionless magnetized dusty plasma [§]

In this chapter, we have derived a KdV-ZK (Korteweg-de Vries-Zakharov-Kuznetsov) equation to investigate the oblique propagation of weakly nonlinear and weakly dispersive ion acoustic (IA) waves in a collisionless magnetized plasma consisting of warm adiabatic ions, static negatively charged dust grains and combined Kappa-Cairns distribution of electrons. The plasma system is same as the plasma system as defined in Chapter-3 but here we have considered the Poisson equation instead of quasi-neutrality condition along with the different conservation equations to describe the nonlinear behaviour of IA waves. It is found that a factor (B_1) of the coefficient of the nonlinear term of the KdV-ZK equation vanishes along different families of curves in different parameter planes. In this situation, i.e., when $B_1 = 0$, we have derived a modified KdV-ZK (MKdV-ZK) equation to describe the nonlinear behaviour of ion acoustic waves. We have investigated the solitary wave solutions of these evolution equations propagating obliquely to the direction of the magnetic field. We have also discussed the effect of different parameters of the present plasma system on the amplitude of these solitary wave solutions defined by the KdV-ZK and MKdV-ZK equations.

[§]To be communicated.

4.1 Introduction

Nonthermally distributed energetic particles are observed in a number of astrophysical environments [58, 92–107]. Specifically, the observations of electric field structures by the FAST [98–100, 103, 107] Satellite, Viking Satellite [94, 96], Freja Satellite [58] and GEOTAIL [97] and POLAR [101, 102, 107] missions in the Earth magnetosphere, indicate the existence of fast energetic electrons. The electrostatic wave structures observed by the Freja Satellite [58] can be described by Cairns [1] distributed nonthermal electrons. Several authors [1, 17, 18, 20, 22, 24, 64, 65, 67–71, 73–77, 178–180] have investigated ion acoustic (IA) / dust acoustic (DA) / dust ion acoustic (DIA) waves in various plasmas considering nonthermal Cairns [1] distributed electrons.

On the other hand, Kappa distributions have been used to describe space plasma population in the inner heliosphere, including solar wind [79, 80], the planetary magnetospheres, including magnetosheath [37–39], the outer heliosphere and inner heliosheath [81]. Several authors [37–57] have used Kappa distribution in various studies of plasma physics. Although there are many space plasma environments where the linear and nonlinear plasma phenomena [1, 39, 54, 109, 110] cannot be precisely described by Cairns distribution or any such non-Maxwellian distribution.

To consider the combined effect of Kappa and Cairns distributed nonthermal electrons, Aoutou et al. [175] modelled a non-Maxwellian velocity distribution function which can describe the joint effect of Kappa distribution as well as Cairns distribution. Younsi and Tribeche [176] used this distribution to study the nonlinear dust acoustic waves. Abid *et al.* [109] have numerically analyzed some basic properties of the combined Kappa-Cairns velocity distribution of the lighter species (electrons,

ions, positrons) and they call this distribution as Vasyliunas Cairns distribution. In Chapter-3, we have systematically developed the combined Kappa-Cairns distribution and we have obtained the effective bounds of both nonthermal parameters κ and β_e for the combined Kappa-Cairns distribution. This distribution can generate more highly energetic particles in comparison with both Kappa and Cairns distributions.

The existence of dusty plasma is very common in various astrophysical environments such as the planetary rings, asteroid zones, comets, the interstellar medium, Earth's ionosphere and Earth's magnetosphere [84–90, 92] as well as laboratory experiments [181, 182]. Several authors [69, 124–140] have studied DIA / IA solitary structures in different unmagnetized / magnetized dusty plasmas. Some authors [69, 130, 136, 138–140] considered the nonthermal electrons in different unmagnetized or magnetized dusty plasmas.

Considering electrons as isothermal, several authors [14–16] investigated the existence and stability of solitary waves in magnetized plasmas. On the other hand, several authors [17–24] studied the existence and stability of small amplitude solitary waves in a magnetized plasma by considering Cairns distributed nonthermal electrons. In the present chapter, we have investigated the existence of small amplititude ion acoustic solitary structures in a collisionless magnetized dusty plasma consisting of negatively charged static dust grains, adiabatic warm ions and combined Kappa-Cairns distributed electrons. The present chapter is different from Chapter-3 in the following directions :

- In Chapter-3, we have considered quasi-neutrality condition instead of Poisson equation to describe the nonlinear behaviour of IA waves whereas in the present chapter, we have considered the Poisson equation instead of quasi-neutrality

condition.

- In Chapter-3, we have investigated arbitrary amplitude IA solitary structures by considering the Sagdeev pseudo potential method whereas in the present chapter, we have used reductive perturbation method to investigate the small amplitude IA solitary structures.

In this chapter, we have used the same set of hydrodynamic equations (1.2.1) - (1.2.3) of **Chapter-1**, but we have used the combined effect of Kappa-Cairns distribution on the density function of nonthermal electrons as given in equation (3.3.1) of **Chapter-3** instead of nonthermal electrons as prescribed in the paper of Cairns *et al.* [1] and we have also used the Poisson equation instead of quasi-neutrality condition. For easy readability of this chapter, the complete set of basic equations has been given in section 4.2 of this chapter also.

4.2 Basic Equations

We consider the following governing equations to describe the nonlinear behaviour of ion acoustic (IA) waves in a collisionless magnetized dusty plasma consisting of warm adiabatic ions, static negatively charged dust grains and combined Kappa-Cairns distributed electrons. We have assumed that the direction of the constant magnetic field is along z-axis. We have also assumed that the characteristic frequency is much less than the ion cyclotron frequency and the particle pressure is much less than the magnetic pressure.

$$\frac{\partial n_i}{\partial t} + \overrightarrow{\nabla}.(n_i \overrightarrow{u_i}) = 0, \tag{4.2.1}$$

$$\left(\frac{\partial}{\partial t} + \overrightarrow{u_i}.\overrightarrow{\nabla}\right)\overrightarrow{u_i} + \gamma\sigma_{ie} n_i^{\gamma-2}\overrightarrow{\nabla} n_i + \overrightarrow{\nabla}\phi - \omega_c(\overrightarrow{u_i} \times \hat{z}) = \overrightarrow{0}, \tag{4.2.2}$$

$$\nabla^2\phi = 1 - n_i + n_e - \mu, \tag{4.2.3}$$

$$n_e = \mu\big(1 - \beta_{e1}^{(\kappa)}\phi + \beta_{e2}^{(\kappa)}\phi^2\big)\left(1 - \frac{\phi}{\kappa_1}\right)^{-\kappa_3}, \tag{4.2.4}$$

where we have used the following symbols / notations / terminologies:

$$\overrightarrow{\nabla} = \hat{x}\frac{\partial}{\partial x} + \hat{y}\frac{\partial}{\partial y} + \hat{z}\frac{\partial}{\partial z}\ ,\ \nabla^2 = \frac{\partial^2}{\partial x^2} + \frac{\partial^2}{\partial y^2} + \frac{\partial^2}{\partial z^2}\ ,$$

$$\overrightarrow{u_i} = (u_{ix}\ ,\ u_{iy}, u_{iz})\ ,\ \sigma_{ie} = \frac{T_i}{T_e}\ ,\ \omega_c = \frac{eB_0}{m_i c}\ ,$$

$$\beta_{e1}^{(\kappa)} = \beta_e^{(\kappa)}\big(1 + \frac{3}{2\kappa_2}\big)\ ,\ \beta_{e2}^{(\kappa)} = \beta_e^{(\kappa)}\big(1 + \frac{1}{\kappa_1} + \frac{3}{4\kappa_1\kappa_2}\big)\ ,$$

$$\beta_e^{(\kappa)} = \frac{4\beta_e}{4 - 3\beta_e\big(1 - \frac{\kappa_1}{\kappa_2}\big)}\ ,$$

$$\kappa_1 = \kappa - \frac{3}{2}\ ,\ \kappa_2 = \kappa - \frac{5}{2}\ ,\ \kappa_3 = \kappa - \frac{1}{2}.$$

The equations (4.2.1), (4.2.2), (4.2.3) and (4.2.4) are, respectively, the equation of continuity of ions, the equation of motion of ion fluid, the Poisson equation and the number density of combined Kappa-Cairns distributed electron. Here n_i, n_e, $\overrightarrow{u_i} = (u_{ix}, u_{iy}, u_{iz})$, ϕ, (x, y, z) and t are, respectively, the ion number density, the combined Kappa-Cairns distributed electron number density, the ion fluid velocity, the electrostatic potential, the spatial variables, and time. These are normalized by n_{i0}, n_{i0}, c_s, $\frac{K_B T_e}{e}$, λ_D and ω_{pi}^{-1} respectively. Here n_{i0} is the unperturbed ion number density, $c_s\Big(=\sqrt{\frac{K_B T_e}{m_i}}\Big)$ is the ion acoustic speed, $\lambda_D\Big(=\sqrt{\frac{K_B T_e}{4\pi n_{i0} e^2}}\Big)$ is Debye length of the present plasma system and $\omega_{pi}^{-1}\Big(=\sqrt{\frac{m_i}{4\pi n_{i0} e^2}}\Big)$ is the ion plasma period with K_B is the Boltzmann constant, $T_i(T_e)$ is the average temperature of ion (electron), m_i

is the mass of an ion, $-e$ is the charge of an electron and $\gamma\Big(=\frac{5}{3}\Big)$ is the ratio of two specific heats. We have already discussed the origin of the nonthermal parameters $\beta_{e1}^{(\kappa)}$, $\beta_{e2}^{(\kappa)}$, $\beta_{e}^{(\kappa)}$ and β_e and their restrictions in Chapter-3, and $\mu = \frac{n_{e0}}{n_{i0}}$.

To derive the equation (4.2.3), we have used the following unperturbed charge neutrality condition

$$\frac{Z_d n_{d0}}{n_{i0}} = 1 - \mu, \tag{4.2.5}$$

where Z_d is the number of electrons residing on a dust grain surface and n_{d0} is the unperturbed dust number density.

Using the equation (4.2.4), the Poisson equation (4.2.3) can be expressed as

$$\nabla^2\phi = 1 - n_i + \sum_{r=1}^{\infty} a_r^{(\kappa)}\phi^r, \tag{4.2.6}$$

where the expression of $a_r^{(\kappa)}$ is given the following equation:

$$a_r^{(\kappa)} = \mu \begin{cases} \dfrac{b_1}{\kappa_1} - \beta_{e1}^{(\kappa)} & \text{for } \; r = 1, \\ \dfrac{b_r}{\kappa_1^r} - \beta_{e1}^{(\kappa)}\dfrac{b_{r-1}}{\kappa_1^{r-1}} + \beta_{e2}^{(\kappa)}\dfrac{b_{r-2}}{\kappa_1^{r-2}} & \text{for } \; r = 2, 3, 4, ... \end{cases} \tag{4.2.7}$$

with

$$b_r = \frac{\Gamma(\kappa - \frac{1}{2} + r)}{\Gamma(\kappa - \frac{1}{2})\Gamma(r+1)} \quad \text{for } \; r = 1, 2, 3, ... \tag{4.2.8}$$

So, the equations (4.2.1), (4.2.2), and (4.2.6) can be taken as the basic equations describing the nonlinear behaviour of ion acoustic waves propagating obliquely to the direction of the magnetic field. To derive the different evolution equations, we have used the equations (4.2.1), (4.2.2), and (4.2.6).

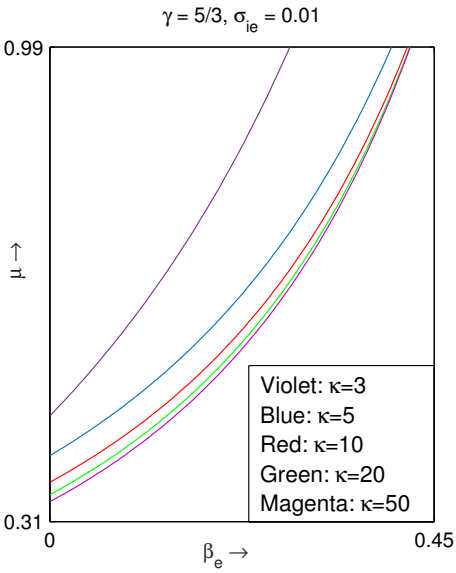

Figure 4.1: μ is plotted against β_e for different values of κ when $B_1 = 0$.

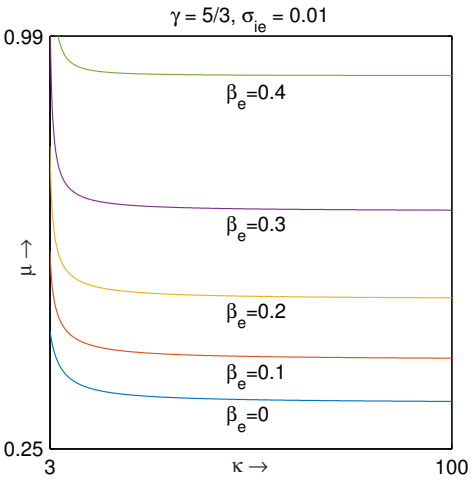

Figure 4.2: μ is plotted against κ for different values of β_e when $B_1 = 0$.

4.3 Evolution Equations

We have used the following stretchings of space coordinates and time to derive different evolution equations :

$$(\xi, \eta, \zeta) = \epsilon^{\frac{1}{2}}(x, y, z - Vt), \tau = \epsilon^{\frac{3}{2}}t, \tag{4.3.1}$$

where ϵ is a small parameter measuring the weakness of the dispersion and V is a constant.

Using above-mentioned stretchings (4.3.1), the equation of continuity of ions (4.2.1), parallel component of equation of motion of ion fluid (4.2.2), perpendicular component of equation of motion of ion fluid (4.2.2) and the Poisson equation (4.2.6) can be written in the following forms:

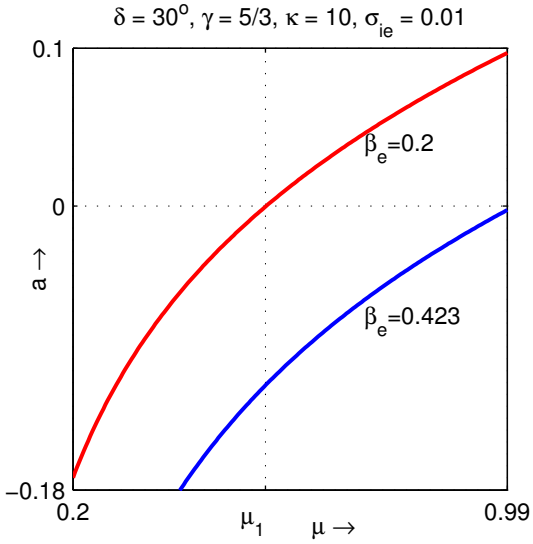

Figure 4.3: Amplitude (a) of the KdV solitary wave is plotted against μ for different values of β_e and fixed values of the other parameters.

- Equation of continuity of ions:

$$-V\epsilon^{\frac{1}{2}}\frac{\partial n_i}{\partial \zeta}+\epsilon^{\frac{3}{2}}\frac{\partial n_i}{\partial \tau}+\epsilon^{\frac{1}{2}}\overrightarrow{\nabla}_{\perp\xi}.(n_i\overrightarrow{u_i}_{\perp})+\epsilon^{\frac{1}{2}}\frac{\partial}{\partial \zeta}(n_i u_{iz})=0, \tag{4.3.2}$$

- Parallel component of equation of motion of ion fluid:

$$\left(-V\epsilon^{\frac{1}{2}}\frac{\partial}{\partial \zeta}+\epsilon^{\frac{3}{2}}\frac{\partial}{\partial \tau}+\epsilon^{\frac{1}{2}}\overrightarrow{u_i}_{\perp}.\overrightarrow{\nabla}_{\perp\xi}+\epsilon^{\frac{1}{2}}u_{iz}\frac{\partial}{\partial \zeta}\right)u_{iz}+\epsilon^{\frac{1}{2}}\gamma\sigma_{ie}n_i^{\gamma-2}\frac{\partial n_i}{\partial \zeta}+\epsilon^{\frac{1}{2}}\frac{\partial \phi}{\partial \zeta}=0, \tag{4.3.3}$$

- Perpendicular component of equation of motion of ion fluid:

$$\left(-V\epsilon^{\frac{1}{2}}\frac{\partial}{\partial \zeta}+\epsilon^{\frac{3}{2}}\frac{\partial}{\partial \tau}+\epsilon^{\frac{1}{2}}\overrightarrow{u_i}_{\perp}.\overrightarrow{\nabla}_{\perp\xi}+\epsilon^{\frac{1}{2}}u_{iz}\frac{\partial}{\partial \zeta}\right)\overrightarrow{u_i}_{\perp}$$
$$+\epsilon^{\frac{1}{2}}\gamma\sigma_{ie}n_i^{\gamma-2}\overrightarrow{\nabla}_{\perp\xi}n_i+\epsilon^{\frac{1}{2}}\overrightarrow{\nabla}_{\perp\xi}\phi-\omega_c\overrightarrow{u_i}_{\perp}\times\hat{z}=\overrightarrow{0}, \tag{4.3.4}$$

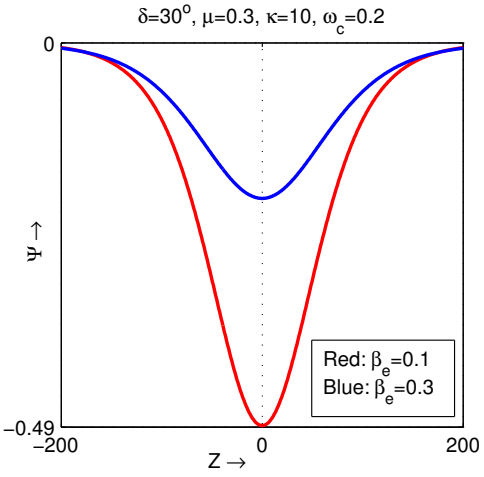

Figure 4.4: Profile of negative potential solitary wave defined by the KdV - ZK equation is plotted for different values of β_e.

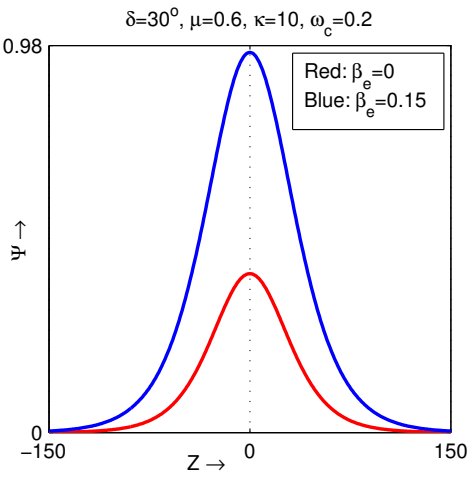

Figure 4.5: Profile of positive potential solitary wave defined by the KdV - ZK equation is plotted for different values of β_e.

- Poisson equation:

$$\epsilon\nabla_\xi^2\phi = 1 - n_i + \sum_{r=1}^{\infty} a_r^{(\kappa)}\phi^r, \tag{4.3.5}$$

where $\overrightarrow{\nabla}_{\perp\xi} = \hat{x}\frac{\partial}{\partial\xi} + \hat{y}\frac{\partial}{\partial\eta}$, $\nabla_\xi^2 = \frac{\partial^2}{\partial\xi^2} + \frac{\partial^2}{\partial\eta^2} + \frac{\partial^2}{\partial\zeta^2}$ and $\overrightarrow{u_i}_\perp = \hat{x}u_{ix} + \hat{y}u_{iy}$.

4.3.1 KdV-ZK Equation

We have applied the following perturbation expansions of the dependent variables to derive the KdV-ZK equation :

$$P = P^{(0)} + \sum_{i=1}^{\infty}\epsilon^i P^{(i)}, Q = Q^{(0)} + \sum_{i=1}^{\infty}\epsilon^{\frac{i}{2}+1}Q^{(i)}, \tag{4.3.6}$$

where $P = n_i,\ \phi,\ u_{iz}$ with $n_i^{(0)} = 1$, $\phi^{(0)} = 0$, $u_{iz}^{(0)} = 0$ and $Q = u_{ix},\ u_{iy}$ with $u_{ix}^{(0)} = 0$, $u_{iy}^{(0)} = 0$. Substituing perturbation expansions (4.3.6) in the equations (4.3.2) - (4.3.5) and equating the coefficients of different powers of ϵ on both sides of each equation,

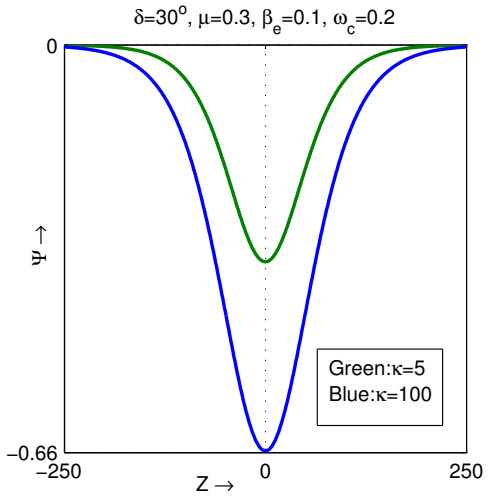

Figure 4.6: Profile of negative potential solitary wave defined by the KdV - ZK equation is plotted for different values of κ.

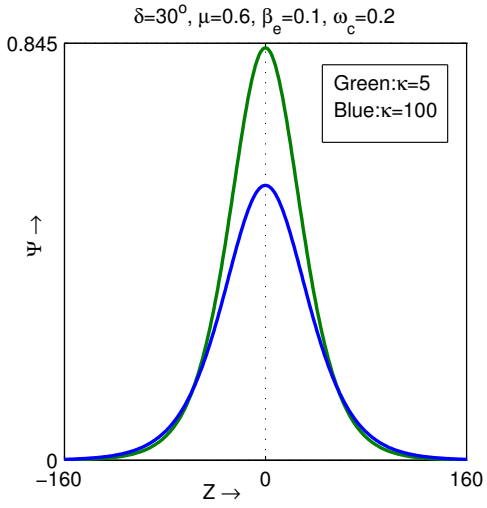

Figure 4.7: Profile of positive potential solitary wave defined by the KdV - ZK equation is plotted for different values of κ.

we obtain a set of equations. From the equation of continuity of ions, we get the following equations at the order $\epsilon^{\frac{3}{2}}$, ϵ^2 and $\epsilon^{\frac{5}{2}}$ respectively.

$$-V\frac{\partial n_i^{(1)}}{\partial \zeta}+\frac{\partial u_{iz}^{(1)}}{\partial \zeta}=0, \tag{4.3.7}$$

$$\overrightarrow{\nabla}_{\perp\xi}.\overrightarrow{u_i}_{\perp}^{(1)}=0, \tag{4.3.8}$$

$$-V\frac{\partial n_i^{(2)}}{\partial \zeta}+\frac{\partial u_{iz}^{(2)}}{\partial \zeta}+\overrightarrow{\nabla}_{\perp\xi}.\overrightarrow{u_i}_{\perp}^{(2)}+\frac{\partial n_i^{(1)}}{\partial \tau}+\frac{\partial}{\partial \zeta}(n_i^{(1)}u_{iz}^{(1)})=0. \tag{4.3.9}$$

From the parallel component of equation of motion of ion fluid, we get the following equations at the order $\epsilon^{\frac{3}{2}}$ and $\epsilon^{\frac{5}{2}}$ respectively.

$$-V\frac{\partial u_{iz}^{(1)}}{\partial \zeta}+\gamma\sigma_{ie}\frac{\partial n_i^{(1)}}{\partial \zeta}+\frac{\partial \phi^{(1)}}{\partial \zeta}=0, \tag{4.3.10}$$

$$-V\frac{\partial u_{iz}^{(2)}}{\partial \zeta}+\gamma\sigma_{ie}\frac{\partial n_i^{(2)}}{\partial \zeta}+\frac{\partial \phi^{(2)}}{\partial \zeta}+\frac{\partial u_{iz}^{(1)}}{\partial \tau}+u_{iz}^{(1)}\frac{\partial u_{iz}^{(1)}}{\partial \zeta}+\gamma(\gamma-2)\sigma_{ie}n_i^{(1)}\frac{\partial n_i^{(1)}}{\partial \zeta}=0. \tag{4.3.11}$$

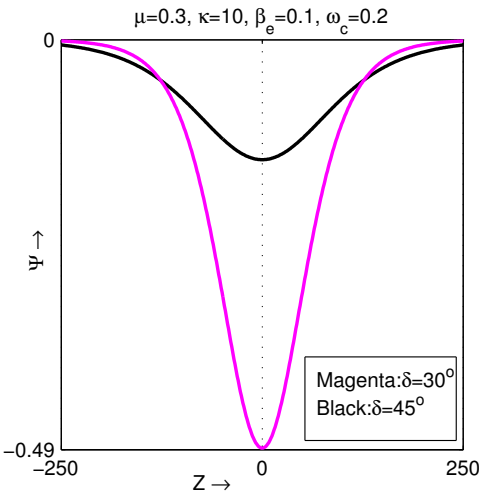

Figure 4.8: Profile of negative potential solitary wave defined by the KdV - ZK equation is plotted for different values of δ.

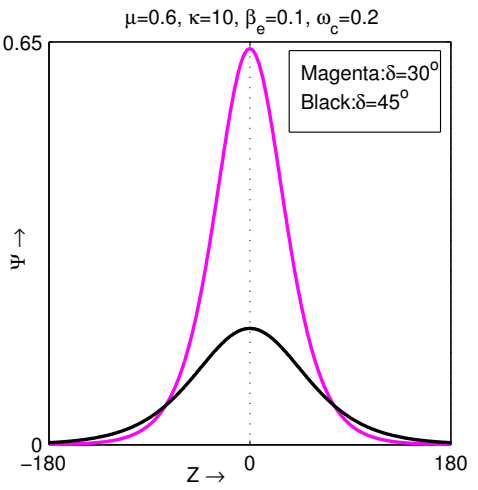

Figure 4.9: Profile of positive potential solitary wave defined by the KdV - ZK equation is plotted for different values of δ.

In fact, there is no equation at the order ϵ^2 for the parallel component of equation of motion of ion fluid.

From the perpendicular component of equation of motion of ion fluid, we get the following equations at the order $\epsilon^{\frac{3}{2}}$ and ϵ^2 respectively.

$$\gamma\sigma_{ie}\overrightarrow{\nabla}_{\perp\xi}n_i^{(1)} + \overrightarrow{\nabla}_{\perp\xi}\phi^{(1)} - \omega_c\overrightarrow{u_i}_{\perp}^{(1)} \times \hat{z} = \overrightarrow{0}, \tag{4.3.12}$$

$$-\omega_c\overrightarrow{u_i}_{\perp}^{(2)} \times \hat{z} - V\frac{\partial\overrightarrow{u_i}_{\perp}^{(1)}}{\partial\zeta} = \overrightarrow{0}. \tag{4.3.13}$$

From the Poisson equation, we get the following equations at the order ϵ and ϵ^2 respectively.

$$-n_i^{(1)} + a_1^{(\kappa)}\phi^{(1)} = 0, \tag{4.3.14}$$

$$\nabla_\xi^2\phi^{(1)} = -n_i^{(2)} + a_1^{(\kappa)}\phi^{(2)} + a_2^{(\kappa)}(\phi^{(1)})^2. \tag{4.3.15}$$

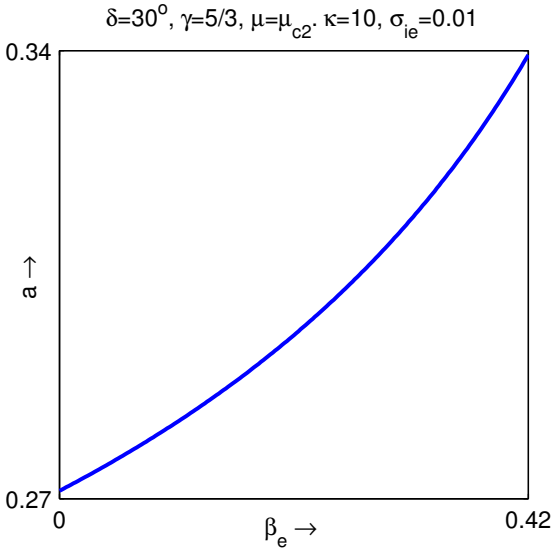

Figure 4.10: Amplitude of the MKdV solitary wave is plotted against β_e when $B_1 = 0$.

At the lowest order (i.e., $o(\epsilon) = \frac{3}{2}$), we get the following two equations from the continuity equation and the parallel component of equation of motion of ion fluid:

$$n_i^{(1)} = \frac{1}{(V^2 - \gamma\sigma_{ie})}\phi^{(1)} \quad \text{and} \quad u_{iz}^{(1)} = \frac{V}{(V^2 - \gamma\sigma_{ie})}\phi^{(1)}. \tag{4.3.16}$$

At the lowest order (i.e., $o(\epsilon) = \frac{3}{2}$), from the perpendicular components of the equation of motion of ion fluid, we get the following expressions of $u_{ix}^{(1)}$ and $u_{iy}^{(1)}$:

$$u_{ix}^{(1)} = -\frac{V^2}{\omega_c(V^2 - \gamma\sigma_{ie})}\frac{\partial\phi^{(1)}}{\partial\eta} \quad \text{and} \quad u_{iy}^{(1)} = \frac{V^2}{\omega_c(V^2 - \gamma\sigma_{ie})}\frac{\partial\phi^{(1)}}{\partial\xi}. \tag{4.3.17}$$

Now, it is simple to check that the continuity equations (4.3.8) at the order $\mathbf{o}(\epsilon) = \mathbf{2}$ is identically satisfied, whereas the perpendicular component (4.3.13) at the order $\mathbf{o}(\epsilon) = \mathbf{2}$ gives the following expressions of $u_{ix}^{(2)}$ and $u_{iy}^{(2)}$:

$$u_{ix}^{(2)} = \frac{V^3}{\omega_c^2(V^2 - \gamma\sigma_{ie})}\frac{\partial^2\phi^{(1)}}{\partial\zeta\partial\xi}, \tag{4.3.18}$$

$$u_{iy}^{(2)} = \frac{V^3}{\omega_c^2(V^2 - \gamma\sigma_{ie})}\frac{\partial^2\phi^{(1)}}{\partial\zeta\partial\eta}. \tag{4.3.19}$$

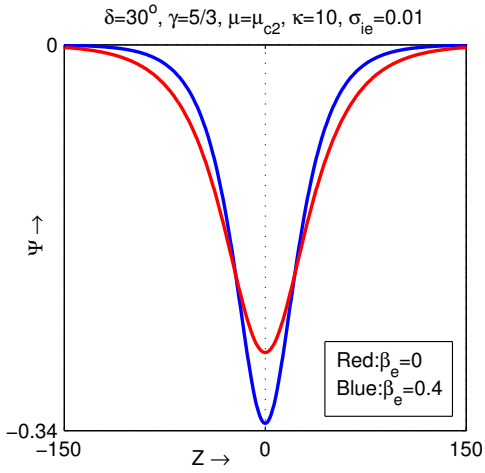

Figure 4.11: Profile of negative potential solitary wave defined by the MKdV - ZK equation is plotted for different values of β_e when $B_1 = 0$.

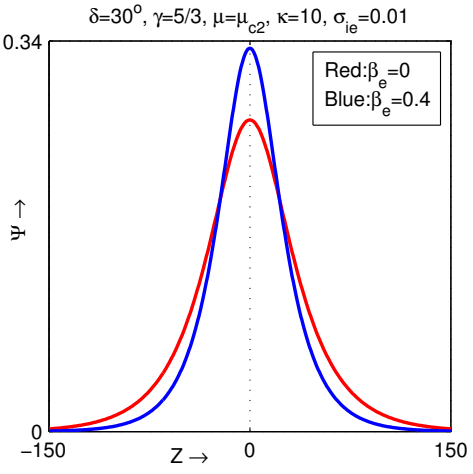

Figure 4.12: Profile of positive potential solitary wave defined by the MKdV - ZK equation is plotted for different values of β_e when $B_1 = 0$.

From equations (4.3.18) and (4.3.19), we get the following expression of $\overrightarrow{\nabla}_{\perp\xi}.\overrightarrow{u_i}^{(2)}_{\perp}$:

$$\overrightarrow{\nabla}_{\perp\xi}.\overrightarrow{u_i}^{(2)}_{\perp} = \frac{V^3}{\omega_c^2(V^2-\gamma\sigma_{ie})}\frac{\partial}{\partial\zeta}\left(\nabla^2_{\perp\xi}\phi^{(1)}\right). \tag{4.3.20}$$

Now eliminating $\dfrac{\partial u_{iz}^{(2)}}{\partial\zeta}$ from the equation of continuity and the parallel component of the equation of motion at the order $o(\epsilon) = \frac{5}{2}$, we get the following expression of $\dfrac{\partial n_i^{(2)}}{\partial\zeta}$:

$$\begin{aligned}\frac{\partial n_i^{(2)}}{\partial\zeta} &= \frac{1}{V^2-\gamma\sigma_{ie}}\frac{\partial\phi^{(2)}}{\partial\zeta} + \frac{2V}{(V^2-\gamma\sigma_{ie})^2}\frac{\partial\phi^{(1)}}{\partial\tau} + \frac{3V^2+\gamma(\gamma-2)\sigma_{ie}}{(V^2-\gamma\sigma_{ie})^3}\phi^{(1)}\frac{\partial\phi^{(1)}}{\partial\zeta} \\ &+ \frac{V^4}{\omega_c^2(V^2-\gamma\sigma_{ie})^2}\frac{\partial}{\partial\zeta}\left(\nabla^2_{\perp\xi}\phi^{(1)}\right),\end{aligned} \tag{4.3.21}$$

where we have used the equations (4.3.16) and (4.3.20) to simplify the expression.

Now we shall use the Poisson equations at different orders to get the dispersion relation and the evolution equation:

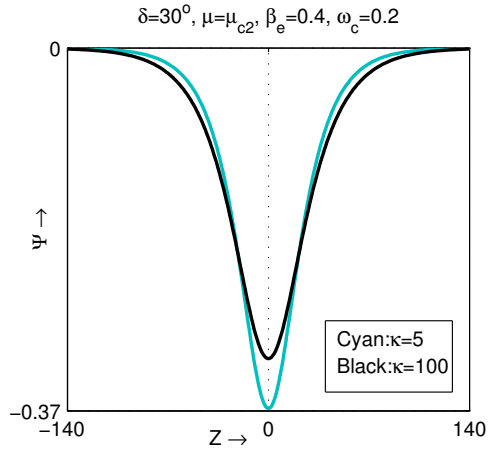

Figure 4.13: Profile of negative potential solitary wave defined by the MKdV - ZK equation is plotted for different values of κ.

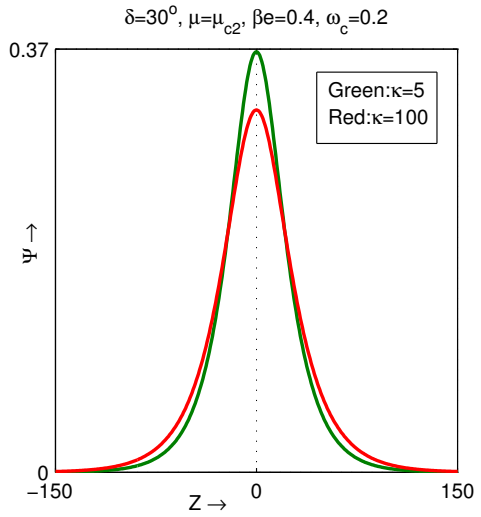

Figure 4.14: Profile of positive potential solitary wave defined by the MKdV - ZK equation is plotted for different values of κ.

- **Poisson equation at the order ϵ:** Eliminating $n_i^{(1)}$ from the lowest order Poisson equation (4.3.14) and the first equation of (4.3.16), we get the following equation:

$$(V^2 - \gamma\sigma_{ie})a_1^{(\kappa)} = 1. \tag{4.3.22}$$

This equation determines the unknown V. This equation is also known as dispersion relation.

- **Poisson equation at the order ϵ^2:** Differentiating the Poisson equation (4.3.15) with respect to ζ and eliminating $\dfrac{\partial n_i^{(2)}}{\partial \zeta}$ from this equation and the

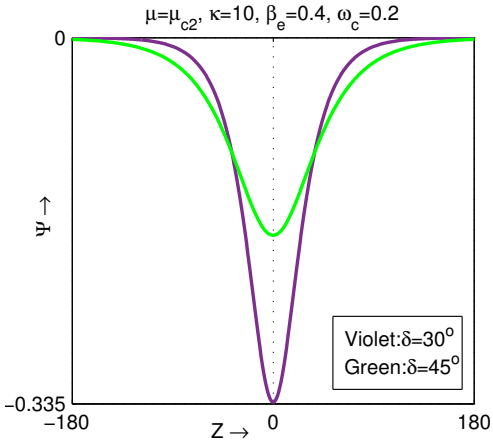

Figure 4.15: Profile of negative potential solitary wave defined by the MKdV - ZK equation is plotted for different values of δ.

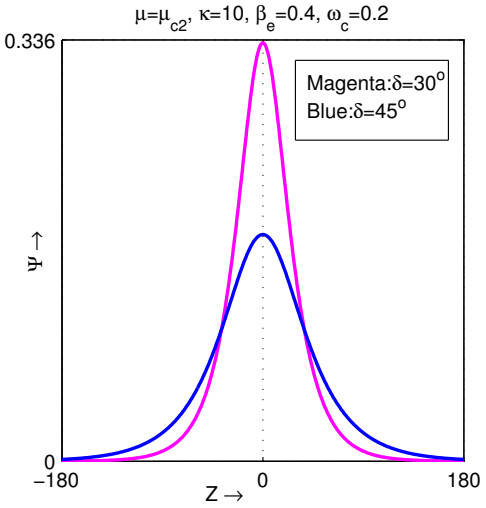

Figure 4.16: Profile of positive potential solitary wave defined by the MKdV - ZK equation is plotted for different values of δ.

equation (4.3.21), we obtain the following equation:

$$\frac{2V}{(V^2-\gamma\sigma_{ie})^2}\frac{\partial\phi^{(1)}}{\partial\tau}+\left\{\frac{3V^2+\gamma(\gamma-2)\sigma_{ie}}{(V^2-\gamma\sigma_{ie})^3}-2a_2^{(\kappa)}\right\}\phi^{(1)}\frac{\partial\phi^{(1)}}{\partial\zeta}+\frac{\partial^3\phi^{(1)}}{\partial\zeta^3}$$
$$+\left\{1+\frac{V^4}{\omega_c^2(V^2-\gamma\sigma_{ie})^2}\right\}\frac{\partial}{\partial\zeta}\left(\nabla_{\perp\xi}^2\phi^{(1)}\right)+\left\{\frac{1}{V^2-\gamma\sigma_{ie}}-a_1^{(\kappa)}\right\}\frac{\partial\phi^{(2)}}{\partial\zeta}=0. \tag{4.3.23}$$

- **KdV - ZK:** Due to the dispersion relation (4.3.22), one can remove the last term of the above equation (4.3.23) and consequently the resulting equation becomes

$$\frac{2V}{(V^2-\gamma\sigma_{ie})^2}\frac{\partial\phi^{(1)}}{\partial\tau}+\left\{\frac{3V^2+\gamma(\gamma-2)\sigma_{ie}}{(V^2-\gamma\sigma_{ie})^3}-2a_2^{(\kappa)}\right\}\phi^{(1)}\frac{\partial\phi^{(1)}}{\partial\zeta}+\frac{\partial^3\phi^{(1)}}{\partial\zeta^3}$$
$$+\left\{1+\frac{V^4}{\omega_c^2(V^2-\gamma\sigma_{ie})^2}\right\}\frac{\partial}{\partial\zeta}\left(\nabla_{\perp\xi}^2\phi^{(1)}\right)=0. \tag{4.3.24}$$

Simplifying the equation (4.3.24), we have derived the following KdV-ZK equation:

$$\frac{\partial \phi^{(1)}}{\partial \tau} + AB_1\phi^{(1)}\frac{\partial \phi^{(1)}}{\partial \zeta} + \frac{1}{2}A\frac{\partial^3 \phi^{(1)}}{\partial \zeta^3} + \frac{1}{2}AD\frac{\partial}{\partial \zeta}\left(\nabla^2_{\perp\xi}\phi^{(1)}\right) = 0, \tag{4.3.25}$$

where

$$A = \frac{1}{V}(V^2 - \gamma\sigma_{ie})^2, \tag{4.3.26}$$

$$B_1 = \frac{3V^2 + \gamma(\gamma-2)\sigma_{ie}}{2(V^2 - \gamma\sigma_{ie})^3} - a_2^{(\kappa)}, \tag{4.3.27}$$

$$D = 1 + \frac{V^4}{\omega_c^2(V^2 - \gamma\sigma_{ie})^2} \tag{4.3.28}$$

and the constant V is given by the equation (4.3.22).

Using the equation (4.3.22), the expression of B_1 can be written as

$$B_1 = \frac{1}{2}\mu\gamma(\gamma+1)\sigma_{ie}\left(c_1^{(k)}\right)^3(\mu + \mu_{c1})(\mu - \mu_{c2}), \tag{4.3.29}$$

where

$$\mu_{c1} = \sqrt{\frac{9}{\left\{2\gamma(\gamma+1)\sigma_{ie}c_1^{(k)}\right\}^2} + \frac{2c_2^{(k)}}{\gamma(\gamma+1)\sigma_{ie}\left(c_1^{(k)}\right)^3}} + \frac{3}{2\gamma(\gamma+1)\sigma_{ie}c_1^{(k)}}, \tag{4.3.30}$$

$$\mu_{c2} = \sqrt{\frac{9}{\left\{2\gamma(\gamma+1)\sigma_{ie}c_1^{(k)}\right\}^2} + \frac{2c_2^{(k)}}{\gamma(\gamma+1)\sigma_{ie}\left(c_1^{(k)}\right)^3}} - \frac{3}{2\gamma(\gamma+1)\sigma_{ie}c_1^{(k)}}, \tag{4.3.31}$$

$$c_1^{(k)} = \frac{a_1^{(k)}}{\mu} \quad \text{and} \quad c_2^{(k)} = \frac{a_2^{(k)}}{\mu}. \tag{4.3.32}$$

The nonlinear behaviour of IA waves can be described by the KdV-ZK equation (4.3.25) only when the factor (B_1) of the coefficient of the nonlinear term of the KdV-ZK equation does not vanish i.e., when $B_1 \neq 0$ because $A \neq 0$. But when $B_1 = 0$,

the coefficient of the nonlinear term of the KdV-ZK equation (4.3.25) vanishes along different family of curves in the compositional parameter planes. Then the nonlinear behaviour of IA waves cannot be described by the KdV-ZK equation. In this situation, we have derived the MKdV-ZK equation to describe the nonlinear behaviour of IA waves. From the expression of B_1 as given in (4.3.29), it is clear that when $B_1 = 0$, μ takes the value μ_{c2} ($-\mu_{c1}$) if $c_1^{(k)} > 0$ and $c_1^{(k)}c_2^{(k)} > 0$ ($c_1^{(k)} < 0$ and $c_1^{(k)}c_2^{(k)} < 0$). But it can be easily checked that $c_1^{(k)}c_2^{(k)} > 0$ along with $c_1^{(k)} > 0$ and consequently μ takes the value μ_{c2} when $B_1 = 0$. In fact, there are different families of curves in different parameter planes along which $B_1 = 0$. Here we consider two different families of curves along which $B_1 = 0$. In figure 4.1, μ is plotted against β_e for different values of κ when $B_1 = 0$ whereas in figure 4.2, μ is plotted against κ for different values of β_e when $B_1 = 0$. Therefore, at each point on each curve of both figures 4.1 and figure 4.2, the value of B_1 is equal to zero. Therefore, when the values of the parameters lie on the curves as indicated in figure 4.1 and figure 4.2, it is not possible to describe the nonlinear behaviour of IA waves through the KdV - ZK equation. In the next section, we have derived a modified KdV - ZK equation, which effectively describes the nonlinear behaviour of IA waves when $B_1 = 0$.

4.3.2 MKdV-ZK Equation

We have applied the following perturbation expansions of the dependent variables to derive the MKdV-ZK equation when $B_1 = 0$:

$$P = P^{(0)} + \epsilon^{\frac{i}{2}} F^{(i)}, Q = Q^{(0)} + \epsilon^{\frac{i+1}{2}} Q^{(i)}, \tag{4.3.33}$$

where repeated index means summation over that index, $P = n_i, \phi, u_{iz}$ with $n_i^{(0)} = 1$, $\phi^{(0)} = 0$, $u_{iz}^{(0)} = 0$ and $Q = u_{ix}, u_{iy}$ with $u_{ix}^{(0)} = 0$, $u_{iy}^{(0)} = 0$. Substituing perturbation expansions (4.3.33) in the equations (4.3.2) - (4.3.5) and equating the coefficients of the different power of ϵ on both sides of each equation, we obtain a set of equations. From the equation of continuity of ions, we get the following equations at the order ϵ, $\epsilon^{\frac{3}{2}}$ and ϵ^2 respectively.

$$-V\frac{\partial n_i^{(1)}}{\partial \zeta} + \frac{\partial u_{iz}^{(1)}}{\partial \zeta} = 0, \tag{4.3.34}$$

$$-V\frac{\partial n_i^{(2)}}{\partial \zeta} + \frac{\partial u_{iz}^{(2)}}{\partial \zeta} + \overrightarrow{\nabla}_{\perp\xi}.\overrightarrow{u_i}_{\perp}^{(1)} + \frac{\partial}{\partial \zeta}\left(n_i^{(1)}u_{iz}^{(1)}\right) = 0, \tag{4.3.35}$$

$$\begin{aligned} -V\frac{\partial n_i^{(3)}}{\partial \zeta} + \frac{\partial u_{iz}^{(3)}}{\partial \zeta} + \overrightarrow{\nabla}_{\perp\xi}.\overrightarrow{u_i}_{\perp}^{(2)} + \frac{\partial n_i^{(1)}}{\partial \tau} &+ \frac{\partial}{\partial \zeta}\left(n_i^{(1)}u_{iz}^{(2)} + n_i^{(2)}u_{iz}^{(1)}\right) \\ &+ \overrightarrow{\nabla}_{\perp\xi}.\left(n_i^{(1)}\overrightarrow{u_i}_{\perp}^{(1)}\right) = 0. \end{aligned} \tag{4.3.36}$$

From the parallel component of equation of motion of ion fluid, we get the following equations at the order ϵ, $\epsilon^{\frac{3}{2}}$ and ϵ^2 respectively.

$$-V\frac{\partial u_{iz}^{(1)}}{\partial \zeta} + \gamma\sigma_{ie}\frac{\partial n_i^{(1)}}{\partial \zeta} + \frac{\partial \phi^{(1)}}{\partial \zeta} = 0, \tag{4.3.37}$$

$$-V\frac{\partial u_{iz}^{(2)}}{\partial \zeta} + \gamma\sigma_{ie}\frac{\partial n_i^{(2)}}{\partial \zeta} + \frac{\partial \phi^{(2)}}{\partial \zeta} + u_{iz}^{(1)}\frac{\partial u_{iz}^{(1)}}{\partial \zeta} + \gamma(\gamma-2)\sigma_{ie}n_i^{(1)}\frac{\partial n_i^{(1)}}{\partial \zeta} = 0, \tag{4.3.38}$$

$$\begin{aligned} -V\frac{\partial u_{iz}^{(3)}}{\partial \zeta} &+ \gamma\sigma_{ie}\frac{\partial n_i^{(3)}}{\partial \zeta} + \frac{\partial \phi^{(3)}}{\partial \zeta} + \frac{\partial u_{iz}^{(1)}}{\partial \tau} + \left(\overrightarrow{u_i}_{\perp}^{(1)}.\overrightarrow{\nabla}_{\perp\xi}\right)u_{iz}^{(1)} \\ &+ \frac{\partial}{\partial \zeta}\left\{u_{iz}^{(1)}u_{iz}^{(2)} + \gamma(\gamma-2)\sigma_{ie}n_i^{(1)}n_i^{(2)}\right\} \\ &+ \frac{\gamma(\gamma-2)(\gamma-3)}{2}\sigma_{ie}\left(n_i^{(1)}\right)^2\frac{\partial n_i^{(1)}}{\partial \zeta} = 0. \end{aligned} \tag{4.3.39}$$

From the perpendicular component of equation of motion of ion fluid, we get the following equations at the order ϵ and $\epsilon^{\frac{3}{2}}$ respectively.

$$\overrightarrow{\nabla}_{\perp\xi}\left(\phi^{(1)}+\gamma\sigma_{ie}n_i^{(1)}\right)-\omega_c\overrightarrow{u_i}_{\perp}^{(1)}\times\hat{z}=\overrightarrow{0}, \tag{4.3.40}$$

$$\overrightarrow{\nabla}_{\perp\xi}\left(\phi^{(2)}+\gamma\sigma_{ie}n_i^{(2)}\right)-\omega_c\overrightarrow{u_i}_{\perp}^{(2)}\times\hat{z}-V\frac{\partial\overrightarrow{u_i}_{\perp}^{(1)}}{\partial\zeta}-\gamma(\gamma-2)\sigma_{ie}n_i^{(1)}\overrightarrow{\nabla}_{\perp\xi}n_i^{(1)}=\overrightarrow{0}. \tag{4.3.41}$$

From the Poisson equation, we get the following equations at the order $\epsilon^{\frac{1}{2}}$, ϵ and $\epsilon^{\frac{3}{2}}$ respectively.

$$-n_i^{(1)}+a_1^{(\kappa)}\phi^{(1)}=0, \tag{4.3.42}$$

$$-n_i^{(2)}+a_1^{(\kappa)}\phi^{(2)}+a_2^{(\kappa)}\left(\phi^{(1)}\right)^2=0, \tag{4.3.43}$$

$$\nabla_\xi^2\phi^{(1)}=-n_i^{(3)}+a_1^{(\kappa)}\phi^{(3)}+2a_2^{(\kappa)}\phi^{(1)}\phi^{(2)}+a_3^{(\kappa)}(\phi^{(1)})^3. \tag{4.3.44}$$

From the equation of continuity of ions and the parallel component of the equation of motion of ion fluid both at the order ϵ, we get

$$n_i^{(1)}=\frac{1}{(V^2-\gamma\sigma_{ie})}\phi^{(1)} \quad \text{and} \quad u_{iz}^{(1)}=\frac{V}{(V^2-\gamma\sigma_{ie})}\phi^{(1)}. \tag{4.3.45}$$

From the perpendicular component of the equation of motion of ion fluid at order ϵ, we get the following expressions of $u_{ix}^{(1)}$ and $u_{iy}^{(1)}$:

$$u_{ix}^{(1)}=-\frac{V^2}{\omega_c(V^2-\gamma\sigma_{ie})}\frac{\partial\phi^{(1)}}{\partial\eta} \quad \text{and} \quad u_{iy}^{(1)}=\frac{V^2}{\omega_c(V^2-\gamma\sigma_{ie})}\frac{\partial\phi^{(1)}}{\partial\xi} \tag{4.3.46}$$

From the above two equations, we get the following equation:

$$\overrightarrow{\nabla}_{\perp\xi}.\overrightarrow{u_i}_{\perp}^{(1)}=0. \tag{4.3.47}$$

From the equation of continuity of ions and the parallel component of the equation of motion of ion fluid both at the order ϵ, we get

$$n_i^{(2)} = \frac{1}{V^2-\gamma\sigma_{ie}}\phi^{(2)} + \frac{3V^2+\gamma(\gamma-2)\sigma_{ie}}{2(V^2-\gamma\sigma_{ie})^3}\big(\phi^{(1)}\big)^2, \tag{4.3.48}$$

$$u_{iz}^{(2)} = \frac{V}{V^2-\gamma\sigma_{ie}}\phi^{(2)} + \frac{V}{2}\frac{V^2+\gamma^2\sigma_{ie}}{(V^2-\gamma\sigma_{ie})^3}\big(\phi^{(1)}\big)^2. \tag{4.3.49}$$

From the perpendicular component of the equation of motion of ion fluid at order $\epsilon^{\frac{3}{2}}$, we get the following expressions of $u_{ix}^{(2)}$ and $u_{iy}^{(2)}$:

$$u_{ix}^{(2)} = -\frac{1}{\omega_c}\frac{\partial\chi^{(2)}}{\partial\eta} + \frac{V^3}{\omega_c^2(V^2-\gamma\sigma_{ie})}\frac{\partial^2\phi^{(1)}}{\partial\zeta\partial\xi}, \tag{4.3.50}$$

$$u_{iy}^{(2)} = \frac{1}{\omega_c}\frac{\partial\chi^{(2)}}{\partial\xi} + \frac{V^3}{\omega_c^2(V^2-\gamma\sigma_{ie})}\frac{\partial^2\phi^{(1)}}{\partial\zeta\partial\eta}, \tag{4.3.51}$$

where

$$\chi^{(2)} = \phi^{(2)} + \gamma\sigma_{ie}n^{(2)} - \frac{1}{2}\gamma(\gamma-2)\sigma_{ie}\Big(n^{(1)}\Big)^2. \tag{4.3.52}$$

From the equations (4.3.50) and (4.3.51), we get the following equation:

$$\overrightarrow{\nabla}_{\perp\xi}.\overrightarrow{u_i}_{\perp}^{(2)} = \frac{V^3}{\omega_c^2(V^2-\gamma\sigma_{ie})}\frac{\partial}{\partial\zeta}\Big(\nabla_{\perp\xi}^2\phi^{(1)}\Big). \tag{4.3.53}$$

Now eliminating the term $\dfrac{\partial u_{iz}^{(3)}}{\partial\zeta}$ from equation of continuity of ions and parallel component of the equation of motion of ion fluid at the order $o(\epsilon) = \frac{5}{2}$, we get the following expression of $\dfrac{\partial n_i^{(3)}}{\partial\zeta}$:

$$\begin{aligned}\frac{\partial n_i^{(3)}}{\partial\zeta} &= \frac{1}{V^2-\gamma\sigma_{ie}}\frac{\partial\phi^{(2)}}{\partial\zeta} + \frac{2V}{(V^2-\gamma\sigma_{ie})^2}\frac{\partial\phi^{(2)}}{\partial\tau} + \frac{V^4}{\omega_c^2(V^2-\gamma\sigma_{ie})^2}\frac{\partial}{\partial\zeta}\Big(\nabla_{\perp\xi}^2\phi^{(1)}\Big)\\ &+ \frac{15V^4+(\gamma^2+13\gamma-18)\gamma\sigma_{ie}V^2+(\gamma-2)(2\gamma-3)\gamma^2\sigma_{ie}^2}{2(V^2-\gamma\sigma_{ie})^5}\big(\phi^{(1)}\big)^2\frac{\partial\phi^{(1)}}{\partial\zeta}\\ &+ \frac{3V^2+\gamma(\gamma-2)\sigma_{ie}}{(V^2-\gamma\sigma_{ie})^3}\frac{\partial}{\partial\zeta}\Big(\phi^{(1)}\phi^{(2)}\Big).\end{aligned} \tag{4.3.54}$$

Now we shall use the Poisson equations at different orders to get the dispersion relation and the evolution equation:

- **Poisson equation at the order $\epsilon^{1/2}$:** Eliminating $n_i^{(1)}$ from the Poisson equation (4.3.42) at the order $o(\epsilon) = \frac{1}{2}$ and the first equation of (4.3.45), we get the following equation:

$$(V^2 - \gamma\sigma_{ie})a_1^{(k)} = 1. \tag{4.3.55}$$

  This equation is same as the equation (4.3.22).

- **Poisson equation at the order ϵ:** Replacing the value of $n_i^{(2)}$ as given by the equation (4.3.48) into the left-hand side of the Poisson equation (4.3.43) at the order $o(\epsilon) = 1$, we get

$$-\frac{1}{V^2 - \gamma\sigma_{ie}}\left\{1 - (V^2 - \gamma\sigma_{ie})a_1^{(k)}\right\}\phi^{(2)} - B_1\big(\phi^{(1)}\big)^2. \tag{4.3.56}$$

  The first term of the above expression vanishes due to the dispersion relation (4.3.22) whereas the second term of the above expression is equal to zero due to the critical condition $B_1 = 0$ and consequently the Poisson equation at the order ϵ is identically satisfied.

- **Poisson equation at the order $\epsilon^{3/2}$:** Differentiating the Poisson equation (4.3.44) with respect to ζ and removing $\frac{\partial n_i^{(3)}}{\partial \zeta}$ from this equation and the equation (4.3.54), we obtain the following equation:

$$\begin{aligned}&\frac{1}{2}A\left\{\frac{1}{V^2 - \gamma\sigma_{ie}} - a_1^{(k)}\right\}\frac{\partial\phi^{(3)}}{\partial\zeta} + AB_1\frac{\partial}{\partial\zeta}\left(\phi^{(1)}\phi^{(2)}\right) + \frac{\partial\phi^{(1)}}{\partial\tau}\\ &+AB_2(\phi^{(1)})^2\frac{\partial\phi^{(1)}}{\partial\zeta} + \frac{1}{2}A\frac{\partial^3\phi^{(1)}}{\partial\zeta^3} + \frac{1}{2}AD\frac{\partial}{\partial\zeta}\left(\nabla_{\perp\xi}^2\phi^{(1)}\right) = 0,\end{aligned} \tag{4.3.57}$$

where

$$B_2 = \frac{15V^4 + (\gamma^2 + 13\gamma - 18)\gamma\sigma_{ie}V^2 + (\sigma_{ie} - 2)(2\sigma_{ie} - 3)\gamma{\sigma_{ie}}^2}{4(V^2 - \gamma\sigma_{ie})^3} - \frac{3}{2}a_3^{(k)} \tag{4.3.58}$$

and the expressions of A and D are same as given in equations (4.3.26) and (4.3.28) respectively.

Due to the dispersion relation (4.3.22), one can remove the first term of the above equation (4.3.57). Again one can remove the second term of the above equation with the help of the critical condition $B_1 = 0$. Simplifying the above equation (4.3.57), we have derived the following MKdV-ZK equation :

$$\frac{\partial\phi^{(1)}}{\partial\tau} + AB_2(\phi^{(1)})^2\frac{\partial\phi^{(1)}}{\partial\zeta} + \frac{1}{2}A\frac{\partial^3\phi^{(1)}}{\partial\zeta^3} + \frac{1}{2}AD\frac{\partial}{\partial\zeta}\left(\nabla^2_{\perp\xi}\phi^{(1)}\right) = 0. \tag{4.3.59}$$

4.4 Solitary Wave Solutions

The evolution equations (4.3.25) and (4.3.59) can be written in more compact form as follows:

$$\frac{\partial\phi^{(1)}}{\partial\tau} + AB_r(\phi^{(1)})^r\frac{\partial\phi^{(1)}}{\partial\zeta} + \frac{1}{2}A\frac{\partial^3\phi^{(1)}}{\partial\zeta^3} + \frac{1}{2}AD\frac{\partial}{\partial\zeta}\left(\nabla^2_{\perp\xi}\phi^{(1)}\right) = 0, \tag{4.4.1}$$

where $r = 1$ and 2. We shall consider the following change of the independent variables for a solitary wave solution of the equation (4.4.1) propagating at an angle δ with the external uniform static magnetic field directed along the z-axis:

$$Z = \xi\sin\delta + \zeta\cos\delta - U\tau, \tag{4.4.2}$$

and for travelling wave solutions of (4.4.1), we take $\phi^{(1)} = \Psi(Z)$ in the equation (4.4.1). Under the above mentioned change of coordinates and using the equation (4.4.2), the equation (4.4.1) transforms to the following equation:

$$-U\frac{d\Psi}{dZ} + a_r\Psi^r\frac{d\Psi}{dZ} + E\frac{d^3\Psi}{dZ^3} = 0. \tag{4.4.3}$$

The expressions of a_r and E are given by the following equations:

$$a_r = AB_r\cos\delta, E = \frac{1}{2}A\cos\delta(\cos^2\delta + D\sin^2\delta). \tag{4.4.4}$$

Using the boundary conditions: Ψ, $\frac{d\Psi}{dZ}$, $\frac{d^2\Psi}{dZ^2} \to 0$ as $|Z| \to \infty$, the solitary wave solution of (4.4.3) can be written as follows:

$$\Psi = a\text{sech}^{\frac{2}{r}}\left(\frac{Z}{\chi}\right), \tag{4.4.5}$$

where a and χ are given by the following equations:

$$a^r = \frac{(r+1)(r+2)U}{2a_r}, \chi^2 = \frac{4E}{r^2U}, \tag{4.4.6}$$

for $r = 1$ and 2.

4.5 KdV - Solitons

KdV soliton is defined by equation (4.4.5) for $r = 1$, where the amplitude (a) and width (χ) of the KdV soliton are, respectively, given by the first equation and second equation of (4.4.6) for $r = 1$. In this section, we shall analyse the effect of different parameters of the present plasma system on the amplitude of the solitary wave defined by the KdV - ZK equation.

In figure 4.3, amplitde (a) of the solitary wave is plotted against μ for fixed values of the other parameters of the system. From this figure, we observe the following points:

- At $\mu = \mu_1$ (for red curve) the amplitude of the soliton is equal to zero, and KdV - ZK equation defines positive potential solitary wave for $\mu > \mu_1$, whereas this equation defines negative potential solitary wave for $\mu < \mu_1$

- The amplitude of positive potential solitary wave increases with increasing μ whenever μ lies within the interval $\mu_1 < \mu < 1$

- The amplitude of negative potential solitary wave decreases with increasing μ whenever μ lies within the interval $0 < \mu < \mu_1$

- The blue curve of this figure (figure 4.3) shows that the point μ_1 disappears from the system for $\beta_e > \beta_{ec}(= 0.423)$, i.e., there exists critical value β_{ec} of β_e such that KdV - ZK equation defines negative potential solitary wave only for the entier range of μ lying within $0 < \mu < 1$ whenever $\beta_e > \beta_{ec}$.

In figures 4.4 - 4.9, profiles of different KdV solitary waves have been drawn to investigate the effects of different parameters of the system on the KdV solitary structures.

- In figure 4.4, profile of negative potential solitary wave defined by KdV - ZK equation is plotted for different values of β_e. This figure shows that the amplitude of the negative potential KdV solitary wave decreases with increasing values of β_e whereas figure 4.5 shows that the amplitude of the positive potential KdV solitary wave increases with increasing values of β_e.

- In figure 4.6, profile of negative potential solitary wave defined by KdV - ZK equation is plotted for different values of κ. Figure 4.6 shows that the amplitude of the negative potential KdV solitary wave increases with increasing values of

κ whereas figure 4.7 describes that the amplitude of the positive potential KdV solitary wave decreases with increasing values of κ.

- Figure 4.8 shows that the amplitude of the negative potential KdV solitary wave decreases with increasing values of δ whereas figure 4.9 describes that the amplitude of the positive potential KdV solitary wave decreases with increasing values of δ.

4.6 MKdV - Solitons

MKdV soliton is defined by equation (4.4.5) for $r = 2$, where the amplitude (a) and width (χ) of the MKdV soliton are, respectively, given by the first equation and the second equation of (4.4.6) for $r = 2$. In this section, we shall analyse the effect of different parameters of the present plasma system on the amplitude of the solitary wave defined by the MKdV - ZK equation.

- In figure 4.10, amplitde (a) of the MKdV solitary wave is plotted against β_e for fixed values of the other parameters of the system. This figure shows that the amplitde (a) of the MKdV solitary wave increases with increasing values of β_e lying within the inteval $0 \leq \beta_e \leq \beta_{e1}$. For the given values of the parameters as indicated in the figure 4.10, the value of β_{e1} is equal to 0.42 (approximately). The interval $0 \leq \beta_e \leq \beta_{e1}$ actually gives the entire range of β_e for the validity of the MKdV solitons. In fact it can be proved taht if $\beta_e > \beta_{e1}$ then the value of μ is greater or equal to one which contradicts the fact that μ is restricted in the interval $0 < \mu < 1$.

In figures 4.11 - 4.16, profiles of different MKdV solitons have been drawn to investigate the effects of different parameters of the system on the MKdV solitary structures.

- Figure 4.11 shows that the amplitude of the negative potential MKdV solitary wave increases with increasing values of β_e and the same result holds good for the case of positive potential also, i.e., figure 4.12 shows that the amplitude of positive potential MKdV solitary wave increases with increasing values of β_e.

- In figure 4.13, profile of negative potential solitary wave defined by MKdV - ZK equation is plotted for different values of κ. Figure 4.13 shows that the amplitude of the negative potential MKdV solitary wave decreases with increasing values of κ and the smae result is true for the case of positive potential solitary wave. In fact, figure 4.14 describes that the amplitude of the positive potential MKdV solitary wave decreases with increasing values of κ.

- Figure 4.15 shows that the amplitude of the negative potential MKdV solitary wave decreases with increasing values of δ and also figure 4.16 describes that the amplitude of the positive potential MKdV solitary wave decreases with increasing values of δ.

4.7 Conclusions

- To discuss the nonlinear behaviour of the small amplitude ion acoustic wave in a collisionless magnetized plasma consisting of warm adiabatic ions, static negatively charged dust grains and combined Kappa-Cairns distribution of electrons,

we have derived the following KdV - ZK equation:

$$\frac{\partial\phi^{(1)}}{\partial\tau} + AB_1\phi^{(1)}\frac{\partial\phi^{(1)}}{\partial\zeta} + \frac{1}{2}A\frac{\partial^3\phi^{(1)}}{\partial\zeta^3} + \frac{1}{2}AD\frac{\partial}{\partial\zeta}\left(\nabla^2_{\perp\xi}\phi^{(1)}\right) = 0 \qquad (4.7.1)$$

- We have observed that a factor (B_1) of the coefficient of the nonlinear term of the KdV-ZK equation vanishes along a family of curves in different parameter planes and for this case, following MKdV-ZK equation can effectively describe the nonlinear behaviour of the ion acoustic wave:

$$\frac{\partial\phi^{(1)}}{\partial\tau} + AB_2(\phi^{(1)})^2\frac{\partial\phi^{(1)}}{\partial\zeta} + \frac{1}{2}A\frac{\partial^3\phi^{(1)}}{\partial\zeta^3} + \frac{1}{2}AD\frac{\partial}{\partial\zeta}\left(\nabla^2_{\perp\xi}\phi^{(1)}\right) = 0. \qquad (4.7.2)$$

- We have derived the solitary wave solutions of both KdV - ZK and MKdV - ZK equations propagating obliquely to the direction of the magnetic field. Again it is easy to check that the MKdV-ZK equation admits the coexistence of both negative and positive potential solitary waves because $\phi^{(1)}$ is solution of the MKdV-ZK equation $\Leftrightarrow -\phi^{(1)}$ is also a solution of the same MKdV-ZK equation.

Numerically we have observed the following points:

1. For KdV solitons

   - the amplitude of the negative potential soliton decreases with increasing β_e whareas the amplitude of the positive potential soliton increases with increasing β_e,
   - the amplitude of the negative potential soliton increases with increasing κ whareas the amplitude of the positive potential soliton decreases with increasing κ,

- the amplitude of the negative potential soliton decreases with increasing δ and also the amplitude of the positive potential soliton decreases with increasing δ.

2. For MKdV solitons

- the amplitude of the soliton increases with increasing β_e for both positive potential and negative potential solitons,
- the amplitude of the soliton decreases with increasing κ for both positive potential and negative potential solitons,
- the amplitude of the soliton decreases with increasing δ for both positive potential and negative potential solitons.

Chapter 5

Arbitrary amplitude ion acoustic solitary structures in a collisionless magnetized dusty plasma consisting of nonthermal electrons and isothermal positrons [‡]

The present chapter is an extension of Chapter-1 in the following direction: instead of considering three-component collisionless magnetized plasma consisting of adiabatic warm ions, nonthermal electrons and static negatively charged dust grains, we have considered a collisionless magnetized four-component plasma consisting of adiabatic warm ions, nonthermal electrons, isothermal positrons and static negatively charged dust grains immersed in a static uniform magnetic field directed along a fixed direction. Arbitrary amplitude ion acoustic solitary structures have been investigated in the present plasma system. We have observed that the system supports positive potential solitary waves, negative potential solitary waves, coexistence of solitary waves of both polarities, negative potential double layers, negative potential supersolitons, positive potential supersolitons for different values of the parameters of the system. We have investigated the effect of different parameters of the system on the solitary structures.

[‡]To be communicated.

5.1 Introduction

Paul and Bandyopadhyay [138] studied dust ion acoustic solitary structures in an unmagnetized collisionless dusty plasma consisting of warm adiabatic ions, static negatively charged dust grains, nonthermally distributed electrons and isothermally distributed positrons. In this chapter, we have considered the plasma system of Paul and Bandyopadhyay [138] by considering a static uniform magnetic field directed along a fixed direction. Paul and his co-workers [75, 77, 138, 140] have extensively reported the existence of this plasma system in different astrophysical plasmas. Paul and Bandyopadhyay [138] employed Sagdeev pseudo potential method to investigate the existence of various solitary structures including double layers and supersolitons. The nonlinear behaviour of the ion acoustic (IA) waves in the present magnetized plasma system has been investigated by considering variations of the different parameters of the system. We have observed different solitary structures in the present magnetized plasma system in comparison with the observations of the solitary structures as given in the paper of Paul and Bandyopadhyay [138]. There are several works [183–194] on multi-component magnetized plasmas consisting of positrons. There are several works [195–199] where isothermal distribution has been considered for the lighter species of the plasma system but the plasma system has been considered to be unmagnetized in each case.

Following the same analysis as given in Chapter-1 and Chapter-3, we have derived the energy integral for the ion acoustic wave propagating obliquely to the direction of the magnetic field and using the energy integral, we have anlyzed the solitary structures of the present plasma system by considering the $\phi - V(\phi)$ curve and the phase portrait of the dynamical system describing the nonlinear behaviour of the ion acoustic wave, where ϕ is the normalized eletrostatic potential and $V(\phi)$ is the

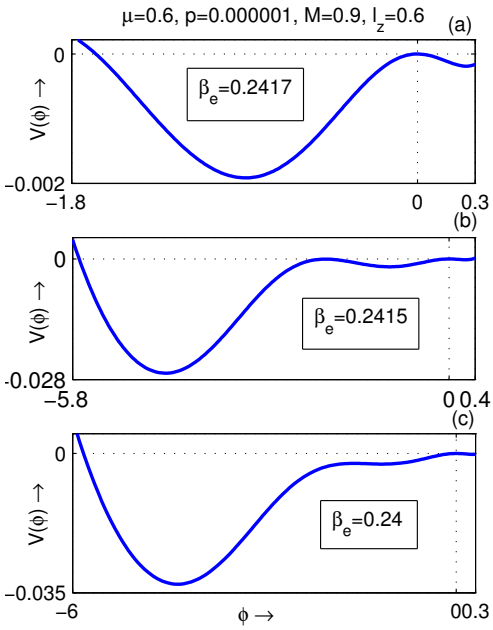

Figure 5.1: $V(\phi)$ is plotted against ϕ for $\gamma = 5/3, \sigma_{ie} = 0.01, \mu = 0.6, p = 0.000001, l_z = 0.6, M = 0.9$ for three different values of β_e. (a) $\beta_e = 0.2417$ corresponds to an NPSW; (b) $\beta_e = 0.2415$ corresponds to an NPDL; (c) $\beta_e = 0.24$ corresponds to an NPSS.

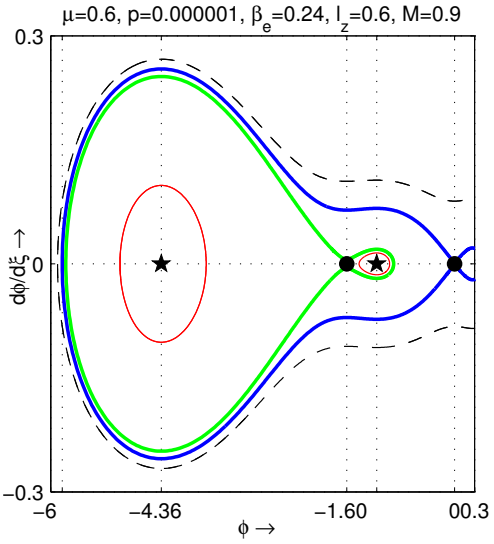

Figure 5.2: This figure shows the phase portrait corresponding to a NPSS for $\gamma = 5/3, \sigma_{ie} = 0.01, \mu = 0.6, p = 0.000001, \beta_e = 0.24, l_z = 0.6, M = 0.9$. Each small solid circle corresponds to an unstable equilibrium point whereas each small solid star corresponds to a stable equilibrium point. The blue separatrix appears to pass through the origin and encloses another separatrix shown in green curve and two stable equilibrium points. This phase portrait confirms the formation of an NPSS.

Sagdeev pseudo potential associated with the energy integral for the present plasma system.

5.2 Basic Equations

In the present paper, we have considered a collisionless magnetized dusty plasma consisting of adiabatic warm ions, Cairns [1] distributed nonthermal electrons, isothermal positrons and static negatively charged dust particulates, immersed in a uniform

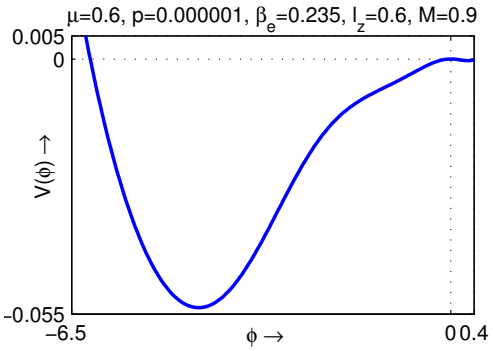

Figure 5.3: $V(\phi)$ is plotted against ϕ for $\gamma = 5/3, \sigma_{ie} = 0.01, \mu = 0.6, p = 0.000001, \beta_e = 0.235, l_z = 0.6, M = 0.9$. This curve exhibits the formation of an NPSW after the formation of an NPDL.

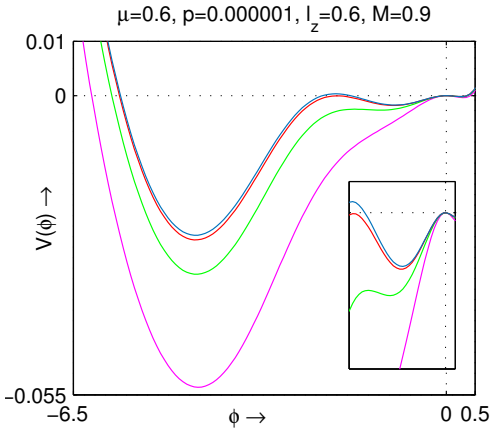

Figure 5.4: $V(\phi)$ is plotted against ϕ for different values of β_e for $\gamma = 5/3, \sigma_{ie} = 0.01, \mu = 0.6, p = 0.000001, l_z = 0.6, M = 0.9$. The cyan curve corresponds to $\beta_e = 0.2417$ and shows the formation of an NPSW; the red curve corresponds to $\beta_e = 0.2415$ and shows the formation of an NPDL; the green curve corresponds to $\beta_e = 0.24$ and shows the formation of an NPSS; the magenta curve corresponds to $\beta_e = 0.235$ and shows the formation of an NPSW after the formation of an NPDL.

static magnetic field directed along $z-$axis. The the basic equations can be written as follows:

$$\frac{\partial n_i}{\partial t} + \overrightarrow{\nabla} \cdot (n_i \overrightarrow{u}_i) = 0, \tag{5.2.1}$$

$$\left(\frac{\partial}{\partial t} + \overrightarrow{u}_i \cdot \overrightarrow{\nabla}\right) \overrightarrow{u}_i + \frac{\sigma_{ie}}{n_i} \overrightarrow{\nabla} p_i = -\overrightarrow{\nabla}\phi + \overrightarrow{u}_i \times \widehat{z}, \tag{5.2.2}$$

$$\frac{\partial p_i}{\partial t} + (\overrightarrow{u}_i \cdot \overrightarrow{\nabla}) p_i + \gamma p_i (\overrightarrow{\nabla} \cdot \overrightarrow{u}_i) = 0, \tag{5.2.3}$$

$$n_i = n_e + 1 + p - \mu - n_p. \tag{5.2.4}$$

Equations (5.2.1), (5.2.2) and (5.2.3) are, respectively, the equation of continuity, equation of motion and the pressure equation for ion fluid. We have considered the

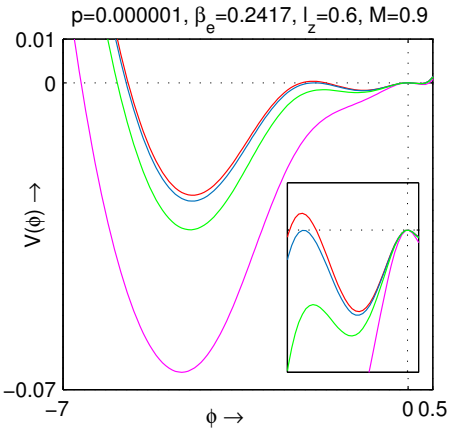

Figure 5.5: $V(\phi)$ is plotted against ϕ for different values of μ for $\gamma = 5/3, \sigma_{ie} = 0.01, p = 0.000001, \beta_e = 0.1, l_z = 0.6, M = 0.9$. The red curve corresponds to $\mu = 0.6$ and shows the formation of an NPSW; the cyan curve corresponds to $\mu = 0.60017$ and shows the formation of an NPDL; the green curve corresponds to $\mu = 0.601$ and shows the formation of an NPSS; the magenta curve corresponds to $\mu = 0.605$ and shows the formation of an NPSW after the formation of an NPDL.

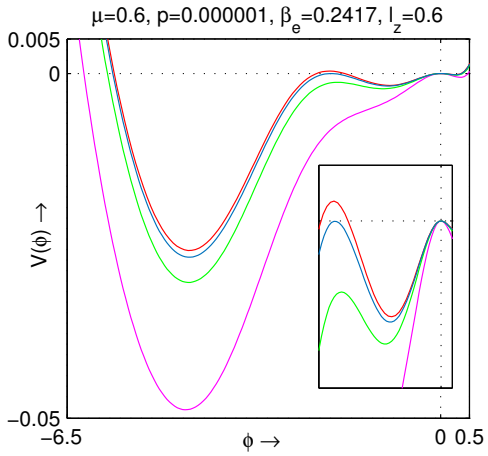

Figure 5.6: $V(\phi)$ is plotted against ϕ for different values of M for $\gamma = 5/3, \sigma_{ie} = 0.01, \mu = 0.6, p = 0.000001, \beta_e = 0.2417, l_z = 0.6$. The red curve corresponds to $M = 0.9$ and shows the formation of an NPSW; the cyan curve corresponds to $M = 0.90021$ and shows the formation of an NPDL; the green curve corresponds to $M = 0.901$ and shows the formation of an NPSS; the magenta curve corresponds to $M = 0.91$ and shows the formation of an NPSW after the formation of an NPDL.

quasi-neutral condition (5.2.4) to get a consistent system of equations, i.e., instead of Poisson equation, we have used the quasi-neutrality condition to make a closed and consistent system of equations. The quasi-neutrality condition is considered on the basis of the assumption that the length scale of the solitary structure is greater than the Debye length or the gyroradius [90, 111].

The equilibrium charge neutrality condition is given by

$$\frac{Z_d n_{d0}}{n_{i0}} = 1 + p - \mu, \tag{5.2.5}$$

where

$$p = \frac{n_{p0}}{n_{i0}} \quad \text{and} \quad \mu = \frac{n_{e0}}{n_{i0}}. \tag{5.2.6}$$

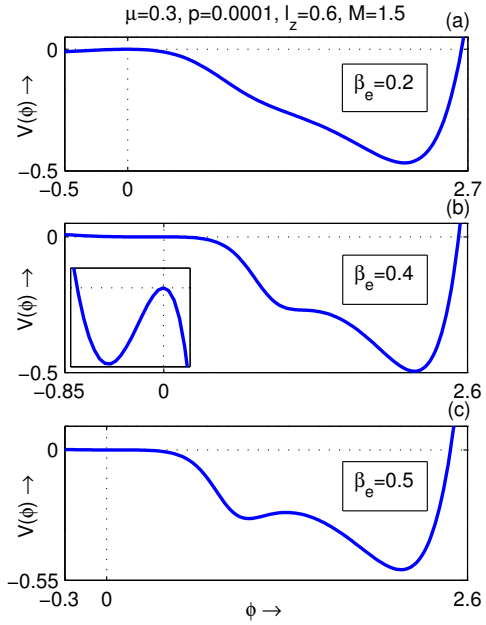

Figure 5.7: $V(\phi)$ is plotted against ϕ for $\gamma = 5/3, \sigma_{ie} = 0.01, \mu = 0.3, p = 0.0001, l_z = 0.6, M = 1.5$ for three different values of β_e. (a) $\beta_e = 0.2$ corresponds to a PPSW; (b) $\beta_e = 0.4$ corresponds to the coexistence of a PPSS and an NPSW; (c) $\beta_e = 0.5$ corresponds to a PPSS.

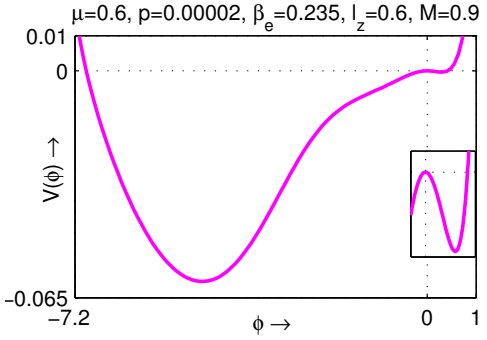

Figure 5.8: $V(\phi)$ is plotted against ϕ for $\gamma = 5/3, \sigma_{ie} = 0.01, \mu = 0.6, p = 0.00002, \beta_e = 0.235, l_z = 0.6, M = 0.9$. This curve exhibits the formation of the coexistence of a PPSW and an NPSW.

Here, n_{i0}, n_{e0}, n_{p0} and n_{d0} are, respectively, the unperturbed number densities of ions, nonthermal electrons, isothermal positrons and dust grains, Z_d is the number of electrons residing on a dust grain surface. In the basic equations, n_i, n_e, n_p, $\overrightarrow{u}_i = (u_{ix}, u_{iy}, u_{iz})$, p_i, ϕ, (x, y, z), and t are, respectively, the ion number density, the electron number density, the positron number density, the ion fluid velocity, the ion fluid pressure, the electrostatic potential, the spatial variables and time, and they have been nomalized by n_{i0}, n_{i0}, n_{i0}, C_s $(= \sqrt{\frac{K_B T_e}{m_i}})$, $n_{i0} K_B T_i$, $\frac{K_B T_e}{e}$, C_s/ω_c and $(\omega_c)^{-1}$ respectively, where ω_c is the ion gyrofrequency. Here, m_i is the mass of an ion, γ is the adiabatic index and $\sigma_{ie} = \frac{T_i}{T_e}$.

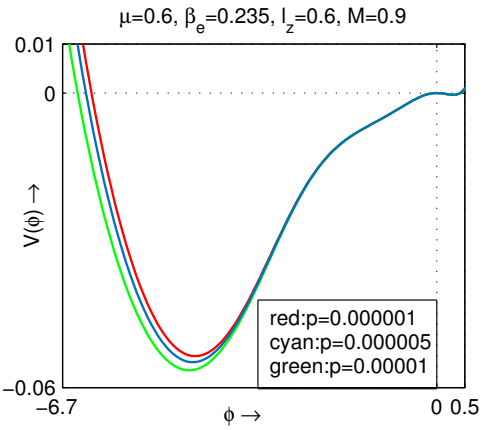

Figure 5.9: $V(\phi)$ is plotted against ϕ for different values of p for $\gamma = 5/3, \sigma_{ie} = 0.01, \mu = 0.6, \beta_e = 0.235, l_z = 0.6, M = 0.9$. The red curve corresponds to an NPSW for $p = 0.000001$, the cyan curve corresponds to an NPSW for $p = 0.000005$, the green curve corresponds to an NPSW for $p = 0.00001$. The amplitude of the NPSWs increases with increasing p.

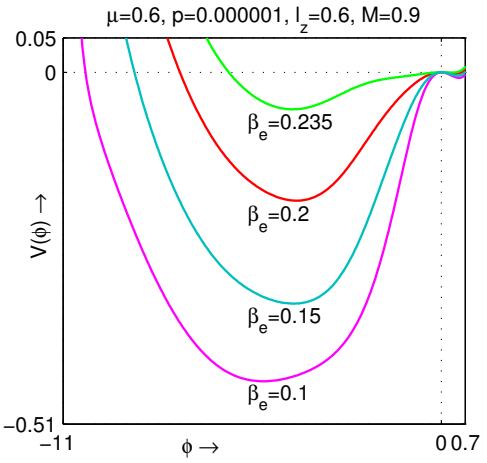

Figure 5.10: $V(\phi)$ is plotted against ϕ for different values of β_e for $\gamma = 5/3, \sigma_{ie} = 0.01, \mu = 0.6, p = 0.000001, l_z = 0.6, M = 0.9$. The green curve corresponds to an NPSW for $\beta_e = 0.235$, the red curve corresponds to an NPSW for $\beta_e = 0.2$, the teal curve corresponds to an NPSW for $\beta_e = 0.15$, and the magenta curve corresponds to an NPSW for $\beta_e = 0.1$. The amplitude of the NPSWs decreases with increasing β_e.

Under the above mentioned normalization of the field variables, the number density of nonthermal electrons (n_e) and the number density of isothermal positrons (n_p) can be written as

$$n_e = \mu(1 - \beta_e\phi + \beta_e\phi^2)e^{\phi}, \tag{5.2.7}$$

and

$$n_p = pe^{-\phi}. \tag{5.2.8}$$

The linear dispersion relation for IA waves is given by

$$\frac{k_\perp^2}{\omega^2 - \omega_c^2} + \frac{k_z^2}{\omega^2} = C_s^{-2} M_s^{-2}, \tag{5.2.9}$$

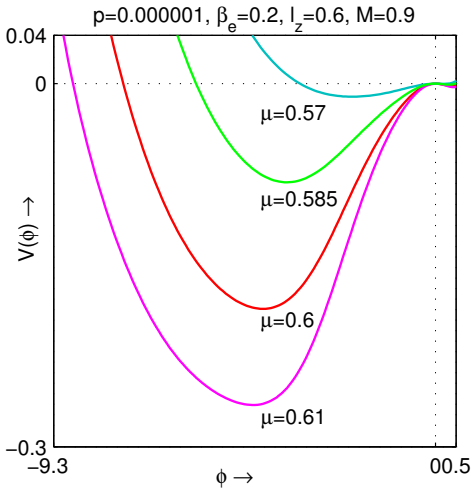

Figure 5.11: $V(\phi)$ is plotted against ϕ for different values of μ for $\gamma = 5/3, \sigma_{ie} = 0.01, p = 0.000001, \beta_e = 0.2, l_z = 0.6, M = 0.9$. The teal curve corresponds to an NPSW for $\mu = 0.57$, the green curve corresponds to an NPSW for $\mu = 0.585$, the red curve corresponds to an NPSW for $\mu = 0.61$, and the magenta curve corresponds to an NPSW for $\mu = 0.61$. The amplitude of the NPSWs increases with increasing μ.

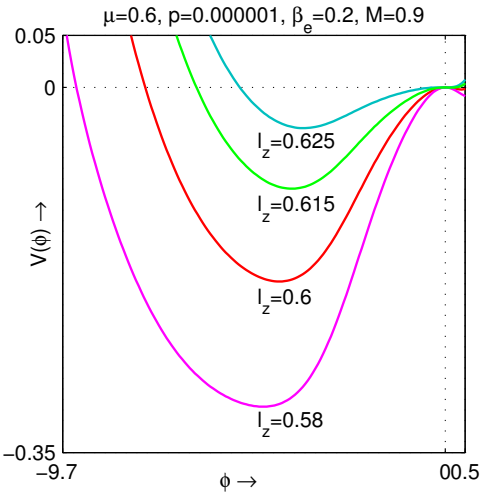

Figure 5.12: $V(\phi)$ is plotted against ϕ for different values of l_z for $\gamma = 5/3, \sigma_{ie} = 0.01, \mu = 0.6, p = 0.000001, \beta_e = 0.2, M = 0.9$. The teal curve corresponds to an NPSW for $l_z = 0.625$, the green curve corresponds to an NPSW for $l_z = 0.615$, the red curve corresponds to an NPSW for $l_z = 0.6$, and the magenta curve corresponds to an NPSW for $l_z = 0.58$. The amplitude of the NPSWs decreases with increasing l_z.

where

$$M_s = \sqrt{\gamma\sigma_{ie} + \frac{1-p}{p+\mu(1-\beta_e)}}, \tag{5.2.10}$$

$$k_\perp^2 = k_x^2 + k_y^2, \tag{5.2.11}$$

$$k_\perp^2 + k_z^2 = k^2, \tag{5.2.12}$$

k is the wave number and ω is the wave frequency.

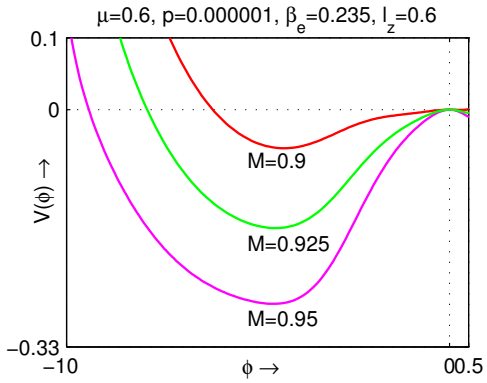

Figure 5.13: $V(\phi)$ is plotted against ϕ for different values of M for $\gamma = 5/3, \sigma_{ie} = 0.01, \mu = 0.6, p = 0.000001, \beta_e = 0.2, l_z = 0.6$. The red curve corresponds to an NPSW for $M = 0.9$, the green curve corresponds to an NPSW for $M = 0.925$, the magenta curve corresponds to an NPSW for $M = 0.95$. The amplitude of the NPSWs increases with increasing M.

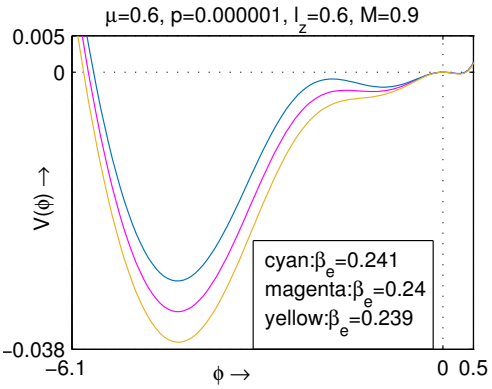

Figure 5.14: $V(\phi)$ is plotted against ϕ for different values of β_e for $\gamma = 5/3, \sigma_{ie} = 0.01, \mu = 0.6, p = 0.000001, l_z = 0.6, M = 0.9$. The cyan curve corresponds to an NPSS for $\beta_e = 0.241$, the magenta curve corresponds to an NPSS for $\beta_e = 0.24$, the yellow curve corresponds to an NPSS for $\beta_e = 0.239$. The amplitude of the negative potential supersolitons decreases with increasing β_e.

5.3 Energy Integral

Assuming that all the dependent variables depend only on a single variable $\xi = l_x x + l_y y + l_z z - Mt$, where M is independent of the spatial variables and time, we study the obliquely propagating arbitrary amplitude time independent IA solitary structures by lifting the basic equations (5.2.1), (5.2.2), (5.2.3) and (5.2.4) in the wave frame moving with a constant velocity M normalized by C_s.

Solving the above mentioned set of equations for the velocity components u_{ix}, u_{iy} and u_{iz}, we get:

$$u_{ix} = L_x\left\{M - \frac{M}{n_i} - \frac{l_z^2}{M}G(\phi)\right\} - L_y\frac{dS}{d\xi}, \tag{5.3.1}$$

$$u_{iy} = L_y\left\{M - \frac{M}{n_i} - \frac{l_z^2}{M}G(\phi)\right\} + L_x\frac{dS}{d\xi}, \tag{5.3.2}$$

$$u_{iz} = \frac{l_z}{M}G(\phi), \tag{5.3.3}$$

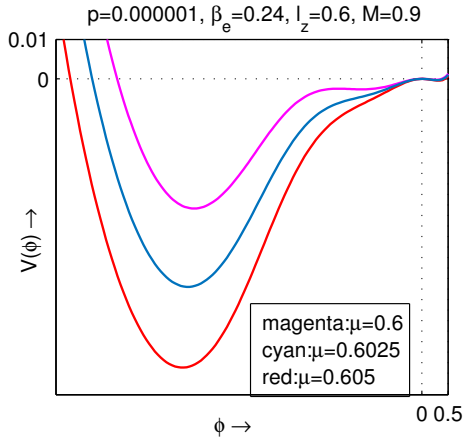

Figure 5.15: $V(\phi)$ is plotted against ϕ for different values of μ for $\gamma = 5/3, \sigma_{ie} = 0.01, p = 0.000001, \beta_e = 0.24, l_z = 0.6, M = 0.9$. The magenta curve corresponds to an NPSS for $\mu = 0.6$, the cyan curve corresponds to an NPSS for $\mu = 0.6025$, the red curve corresponds to an NPSS for $\mu = 0.605$. The amplitude of the negative potential supersolitons increases with increasing μ.

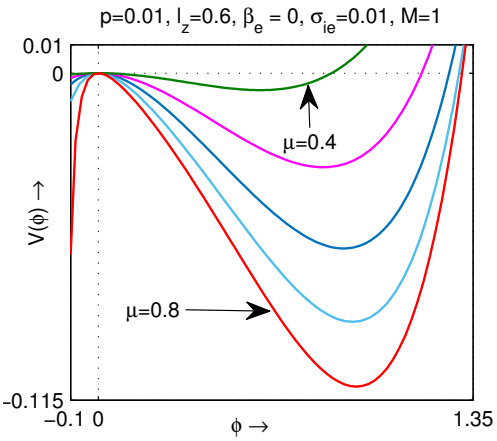

Figure 5.16: $V(\phi)$ curves are drawn against ϕ for different values of μ. $\mu = 0.4$ corresponds to the green curve, $\mu = 0.5$ corresponds to the magenta curve, $\mu = 0.6$ corresponds to the cyan curve, $\mu = 0.7$ corresponds to the sky-blue curve, and $\mu = 0.8$ corresponds to the red curve. This figure shows that the amplitude of PPSW increases with increasing μ.

where

$$L_x = \frac{l_x}{l_x^2 + l_y^2}, \quad L_y = \frac{l_y}{l_x^2 + l_y^2}, \tag{5.3.4}$$

$$G = G(\phi) = \sigma_{ie}\{n_i^{\gamma} - 1\} + \int_0^{\phi} n_i d\phi, \tag{5.3.5}$$

$$S = S(M, \phi) = \frac{M^2}{2n_i^2} + \frac{\gamma \sigma_{ie}}{\gamma - 1} n_i^{\gamma - 1} + \phi \tag{5.3.6}$$

and we have used the following boundary conditions:

$$\left(n_i, u_{ix}, u_{iy}, u_{iz}, \phi, \frac{d\phi}{d\xi}\right) \to (1, 0, 0, 0, 0, 0) \text{ as } |\xi| \to \infty. \tag{5.3.7}$$

Following the same analysis as given in Chapter-1 and Chapter-3, we get

$$\frac{d^2 S}{d\xi^2} = f(\phi) = n_i - 1 - \frac{l_z^2}{M^2} n_i G(\phi). \tag{5.3.8}$$

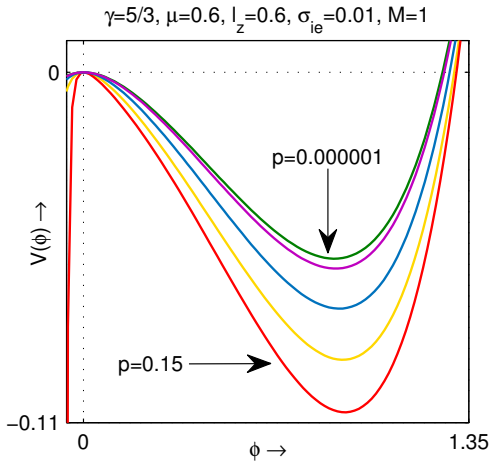

Figure 5.17: $V(\phi)$ curves are drawn against ϕ for different values of p. $p = 0.000001$ corresponds to the green curve, $p = 0.0001$ corresponds to the magenta curve, $p = 0.001$ corresponds to the cyan curve, $p = 0.01$ corresponds to the yellow curve, and $p = 0.15$ corresponds to the red curve. This figure shows that the amplitude of PPSW increases for increasing p.

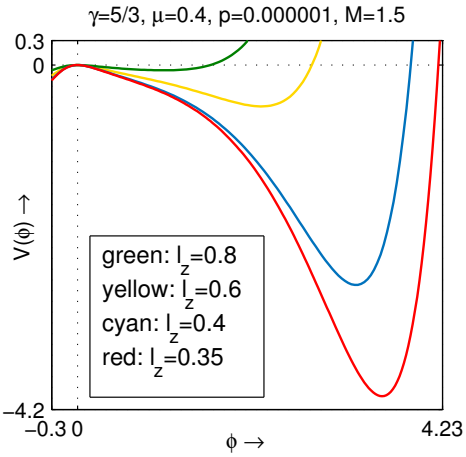

Figure 5.18: $V(\phi)$ curves are drawn against ϕ for different values of l_z. This figure shows that the amplitude of PPSW decreases for increasing l_z.

Using the identity

$$\frac{d^2S}{d\xi^2} = \frac{1}{2}\frac{dS}{d\phi}\frac{d}{d\phi}\left(\frac{d\phi}{d\xi}\right)^2 + \frac{d^2S}{d\phi^2}\left(\frac{d\phi}{d\xi}\right)^2 \tag{5.3.9}$$

in equation (5.3.8) and we obtain

$$\frac{d\Gamma}{d\phi} + \frac{2}{R}\frac{dR}{d\phi}\Gamma = \frac{2}{R}f(\phi), \tag{5.3.10}$$

where $\Gamma = \left(\frac{d\phi}{d\xi}\right)^2$ and $R = \frac{dS}{d\phi}$.

Equation (5.3.10) is a linear differential equation in Γ and the general solution is given by

$$\left(\frac{d\phi}{d\xi}\right)^2 \times \left(\frac{dS}{d\phi}\right)^2 = \int 2\frac{dS}{d\phi}f(\phi)d\phi + C, \tag{5.3.11}$$

where C is a constant of integration.

Using the boundary condition (5.3.7), we obtain the following energy integral:

$$\frac{1}{2}\Big(\frac{d\phi}{d\xi}\Big)^2 + V(\phi) = 0, \tag{5.3.12}$$

where

$$V(\phi) = V(M,\phi) = -\frac{\int_0^{\phi} \frac{dP}{d\phi} f(\phi) d\phi}{\Big(\frac{dP}{d\phi}\Big)^2}. \tag{5.3.13}$$

5.4 Graphical Analysis of Solitary Structures

In this section, we have consideded the existence of different solitary structures with the help of the analysis of the Sagdeev pseudo potential $V(\phi)$ by considering the well-known theory of Sagdeev pseudo potential [11] for the existence of solitary structures. In fact, according to this theory, the system supports positive (negative) potential solitary wave if

(i) $\phi = 0$ is the position of unstable equilibrium, i.e., $V(0) = V'(0) = 0$ and $V''(0) < 0$,

(ii) there exists some $\phi_m > 0$ ($\phi_m < 0$) such that $V(\phi_m) = 0$, $V'(\phi_m) > 0$ ($V'(\phi_m) < 0$),

(iii) $V(\phi) < 0$ for all $\min\{0, \phi_m\} < \phi < \max\{0, \phi_m\}$.

For the existence of positive (negative) potential double layer, the condition (ii) is replaced by the following condition:

(ii) $V(\phi_m) = 0$, $V'(\phi_m) = 0$ ($V''(\phi_m) < 0$).

We have also considered the effect of different parameters of the system on the solitary stucture given different values to the parameters of the system and observed the variations of the wave structure.

In figure 5.1(a), we have plotted $V(\phi)$ against ϕ for $\mu = 0.6, p = 0.000001, \beta_e = 0.2417, l_z = 0.6, M = 0.9$. This figure shows the formation of an NPSW. In figure 5.1(b), we have plotted $V(\phi)$ against ϕ for $\mu = 0.6, p = 0.000001, \beta_e = 0.2415, l_z = 0.6, M = 0.9$. This figure shows the formation of an NPDL. In figure 5.1(c), we have plotted $V(\phi)$ against ϕ for $\mu = 0.6, p = 0.000001, \beta_e = 0.24, l_z = 0.6, M = 0.9$. This figure shows the formation of an NPSS, but to confirm the supersoliton structure, in figure 5.2, we draw the phase portrait of the dynamical system described by the coupled differential equations:

$$\frac{d\phi_1}{d\xi} = \phi_2, \ \frac{d\phi_2}{d\xi} = -V'(\phi_1), \quad \text{where} \quad \phi_1 = \phi. \tag{5.4.1}$$

These coupled differential equations can be easily obtained by differentiating the energy integral (5.3.12) with respect to ϕ. In figure 5.2, each small solid circle corresponds to an unstable equilibrium point whereas each small solid star corresponds to a stable equilibrium point. The blue separatrix appears to pass through the origin and encloses another separatrix shown in green curve and two stable equilibrium points. So, following the definition of supersoliton given by Dubinov and Kolotkov [142], this phase portrait confirms the formation of an NPSS. In figure 5.3, we have drawn the $\phi - V(\phi)$ curve for an NPSW after the formation of an NPDL for $\mu = 0.6, p = 0.000001, \beta_e = 0.235, l_z = 0.6, M = 0.9$. From the figures 5.1 and 5.3, we see that for fixed values of μ, p, l_z and M, as we gradually decrease the value of β_e, we see the formation of NPSW, NPDL, NPSS and NPSW after the formation of NPDL. This particular transition of negative potential solitary structures can be described by considering the figure 5.4. In this figure (figure 5.4), we see that for $\beta_e = 0.2417$,

$\beta_e = 0.2415$, $\beta_e = 0.24$ and $\beta_e = 0.235$, the system respectively generates an NPSW (cyan curve), an NPDL (red curve), an NPSS (green curve) and an NPSW (magenta curve) after the formation of an NPDL.

In figure 5.5, for $p = 0.000001, \beta_e = 0.1, l_z = 0.6, M = 0.9$, we see that for $\mu = 0.6$, $\mu = 0.60017$, $\mu = 0.601$ and $\mu = 0.605$, the system respectively generates an NPSW (red curve), an NPDL (cyan curve), an NPSS (green curve) and an NPSW (magenta curve) after the formation of an NPDL.

In figure 5.6, for $\mu = 0.6, p = 0.000001, \beta_e = 0.1, l_z = 0.6$, we see that for $M = 0.9$, $M = 0.90021$, $M = 0.901$ and $M = 0.91$, the system respectively generates an NPSW (red curve), an NPDL (cyan curve), an NPSS (green curve) and an NPSW (magenta curve) after the formation of an NPDL.

In figure 5.7(a), $V(\phi)$ is plotted against ϕ for $\mu = 0.3, p = 0.0001, \beta_e = 0.2, l_z = 0.6, M = 1.5$. This figure shows the formation of a PPSW. In figure 5.7(b), $V(\phi)$ is plotted against ϕ for $\mu = 0.3, p = 0.0001, \beta_e = 0.4, l_z = 0.6, M = 1.5$. This figure shows the formation of the coexistence of a PPSS and an NPSW. In figure 5.7(c), $V(\phi)$ is plotted against ϕ for $\mu = 0.3, p = 0.0001, \beta_e = 0.5, l_z = 0.6, M = 1.5$. This figure shows the formation of a PPSS.

In figure 5.8, $V(\phi)$ is plotted against ϕ for $\mu = 0.6, p = 0.00002, \beta_e = 0.235, l_z = 0.6, M = 0.9$. This figure shows the formation of the coexistence of an NPSW and a PPSW. In fact, we have observed that for the fixed values of the parametes as given in figure 5.8, the system does not support any negative potential solitary structure for $p > 0.00002$, rather the system supports only positive potential solitary structures. So, $p = 0.00002$ can be considered as a critical value of p for the existence of negative potential solitary structures for $\mu = 0.6, \beta_e = 0.235, l_z = 0.6, M = 0.9$.

In figure 5.9, $V(\phi)$ is plotted against ϕ for different values of p with $\mu = 0.6, \beta_e = 0.235, l_z = 0.6, M = 0.9$. Here, $p = 0.000001$, $p = 0.000005$ and $p = 0.00001$ correspond to the red curve, the teal curve and the green curve, respectively. All the three curves exhibit three distinct NPSWs. From this figure, we see that the amplitude of the NPSWs increases with increasing p.

In figure 5.10, $V(\phi)$ is plotted against ϕ for different values of β_e with $\mu = 0.6, p = 0.000001, l_z = 0.6, M = 0.9$. Here, $\beta_e = 0.235$, $\beta_e = 0.2$, $\beta_e = 0.15$ and $\beta_e = 0.1$ correspond to the green curve, the red curve, the teal curve and the magenta curve, respectively. All the four curves exhibit four distinct NPSWs. From this figure, we see that the amplitude of the NPSWs decreases with increasing β_e.

In figure 5.11, $V(\phi)$ is plotted against ϕ for different values of μ with $p = 0.000001, \beta_e = 0.235, l_z = 0.6, M = 0.9$. Here, $\mu = 0.57$, $\mu = 0.585$, $\mu = 0.6$ and $\mu = 0.61$ correspond to the teal curve, the green curve, the red curve and the magenta curve, respectively. All the four curves exhibit four distinct NPSWs. From this figure, we see that the amplitude of the NPSWs increases with increasing μ.

In figure 5.12, $V(\phi)$ is plotted against ϕ for different values of l_z with $\mu = 0.6, p = 0.000001, \beta_e = 0.235, M = 0.9$. Here, $l_z = 0.625$, $l_z = 0.615$, $l_z = 0.6$ and $l_z = 0.58$ correspond to the teal curve, the green curve, the red curve and the magenta curve, respectively. All the four curves exhibit four distinct NPSWs. From this figure, we see that the amplitude of the NPSWs decreases with increasing l_z.

In figure 5.13, $V(\phi)$ is plotted against ϕ for different values of M with $\mu = 0.6, p = 0.000001, \beta_e = 0.235, l_z = 0.6$. Here, $M = 0.9$, $M = 0.925$ and $M = 0.95$ correspond to the red curve, the green curve and the magenta curve, respectively. All the three curves exhibit three distinct NPSWs. From this figure, we see that the amplitude of the NPSWs decreases with increasing M.

In figure 5.14, $V(\phi)$ is plotted against ϕ for different values of β_e with $\mu = 0.6, p = 0.000001, l_z = 0.6, M = 0.9$. Here, $\beta_e = 0.241$, $\beta_e = 0.24$ and $\beta_e = 0.239$ correspond to the cyan curve, the magenta curve and the yellow curve, respectively. All the three curves exhibit three distinct negative potential supersolitons. From this figure, we see that the amplitude of the NPSSs decreases with increasing β_e.

In figure 5.15, $V(\phi)$ is plotted against ϕ for different values of μ with $p = 0.000001, \beta_e = 0.24, l_z = 0.6, M = 0.9$. Here, $\mu = 0.6$, $\mu = 0.6025$ and $\mu = 0.605$ correspond to the magenta curve, the cyan curve and the red curve, respectively. All the three curves exhibit three distinct NPSSs. From this figure, we see that the amplitude of the NPSSs increases with increasing μ.

To examine the effect of the nonthermal electron density on the present plasma system, we draw figure 5.16, where we have plotted $V(\phi)$ against ϕ for different values of μ, with the fixed values of the other parameters as shown in the figure. Particularly, this figure is drawn for isothermal electrons, i.e., $\beta_e = 0$. The green curve in this figure is the PPSW for $\mu = 0.4$. For increasing values of μ, we observe that the amplitude of the soliton monotonically increases. The magenta curve, cyan curve, sky-blue curve and the red curve correspond to $\mu = 0.5$, $\mu = 0.6$, $\mu = 0.7$ and $\mu = 0.8$, respectively. Such formation of PPSWs along with the nature that the amplitude of the soliton increases with increasing value of μ is found in the left neighbourhood of $\mu = 0.4$ as well as in the right neighbourhood of $\mu = 0.8$.

Again, the amplitude of the soliton is found to increase as the isothermal positron density increases. This is shown in figure 5.17. This figure is also drawn for isothermal electrons. In this figure, we have plotted $V(\phi)$ against ϕ for different values of p. Here, $p = 0.000001$ corresponds to the green curve, $p = 0.0001$ corresponds to the magenta curve, $p = 0.001$ corresponds to the cyan curve, $p = 0.01$ corresponds to the

yellow curve, and $p = 0.15$ corresponds to the red curve. This figure shows that the amplitude of PPSW increases with increasing p.

Figure 5.18 shows the existence of PPSWs for different values of l_z. This figure shows that the amplitude of PPSW decreases with increasing l_z.

5.5 Conclusions

We have studied the nonlinear behaviour of ion acoustic solitary structures in a collisionless magnetized dusty plasma system which is immersed in a static magnetic field directed along z-axis. Electron species is nonthermal whereas positron species is isothermal. The system also contains adiabatic warm ions and negatively charged static dust particulates. We have used the Sagdeev pseudo potential method to determine and analyze the nonlinear behaviour of the ion acoustic wave. We have observed that the system supports NPSWs, NPDLs, NPSSs, NPSWs after the formation of NPDL, PPSWs, coexistence of PPSS and NPSW, PPSS, coexistence of PPSW and NPSW. The phase portrait of the dynamical system describing the nonlinear behaviour of ion acoustic wave has been drawn to confirm the existence of NPSS.

The parameters of the system are μ, p, β_e, l_z and M. We have observed the nature of the solitary structures with respect to each of the parameters of the system. For NPSWs,

- the amplitude of NPSW increases with increasing p,
- the amplitude of NPSW decreases with increasing β_e,
- the amplitude of NPSW increases with increasing μ,

- the amplitude of NPSW decreases with increasing l_z and
- the amplitude of NPSW increases with increasing M.

We have also examined the variations of the amplitude of negative potential supersolitons (NPSS) with respect to β_e and μ individually. We have seen that the amplitude of NPSS decreases with increasing β_e whereas the amplitude of NPSSs increases with increasing μ.

We have studied the variations of the amplitude of PPSWs with respect to μ, p and l_z for both isothermal electrons and isothermal positrons, i.e., we have considered $\beta_e = 0$. For PPSWs,

- the amplitude of PPSW increases for increasing μ,
- the amplitude of PPSW increases with increasing p and
- the amplitude of PPSW decreases with increasing l_z.

We have also determined a critical value p_c of positron concentration p such that the system supports only positive potential solitary structures and no negative potential solitary structures for $p > p_c$. For $\mu = 0.6, \beta_e = 0.235, l_z = 0.6, M = 0.9$, the value of p_c is 0.00002.

References

[1] R A Cairns, A A Mamum, R Bingham, R Boström, R O Dendy, C M C Nairn, and P K Shukla. *Geophys. Res. Lett.*, 22:2709, 1995.

[2] J E Allen. *Phys. Scr.*, 57:436, 1998.

[3] John Scott Russell. *Report on Waves: Made to the Meetings of the British Association in 1842-43*. 1845.

[4] J Boussinesq. *Comptes Rendus Acad. Sci.*, 72:755, 1871.

[5] L Rayleigh. *Phil. Mag.*, 1:257, 1876.

[6] D J Korteweg and G De Vries. *Phil. Mag.*, 39:422, 1895.

[7] J H Adlam and J E Allen. *Phil. Mag.*, 3:448, 1958.

[8] W H Munk. *Ann. N. Y. Acad. Sci.*, 51:376, 1949.

[9] N J Zabusky and M D Kruskal. *Phys. Rev. Lett.*, 15:240, 1965.

[10] H Washimi and T Taniuti. *Phys. Rev. Lett.*, 17:996, 1966.

[11] R. Z. Sagdeev. *Reviews of Plasma Physics Vol-4 (ed. M. A. Leontovich)*. New York, NY: Consultant Bureau, 1966.

[12] P K Shukla and M Y Yu. *J. Math. Phys.*, 19:2506, 1978.

[13] J L Bona, W G Pritchard, and L R Scott. *Phys. Fluids*, 23:438, 1980.

[14] E W Laedke and K H Spatschek. *J. Plasma Phys.*, 28:469, 1982.

[15] E Infeld. *J. Plasma Phys.*, 33:171, 1985.

[16] K P Das and F Verheest. *J. Plasma Phys.*, 41:139, 1989.

[17] A A Mamun and R A Cairns. *J. Plasma Phys.*, 56:175, 1996.

[18] A Bandyopadhyay and K P Das. *J. Plasma Physics*, 62.

[19] A Bandyopadhyay and K P Das. *Phys. Scr.*, 63:145, 2001.

[20] A Bandyopadhyay and K P Das. *Phys. Plasmas*, 9:465, 2002.

[21] J Das, A Bandyopadhyay, and K P Das. *Phys. Plasmas*, 14:092304, 2007.

[22] Sk A Islam, A Bandyopadhyay, and K P Das. *J. Plasma Phys.*, 74:765, 2008.

[23] Sk A Islam, A Bandyopadhyay, and K P Das. *Phys. Plasmas*, 16:022307, 2009.

[24] S V Singh, S Devanandhan, G S Lakhina, and R Bharuthram. *Phys. Plasmas*, 23:082310, 2016.

[25] W Malfliet. *Am. J. Phys.*, 60:650, 1992.

[26] R A Cairns, A A Mamun, R Bingham, and P K Shukla. *Phys. Scr.*, T63:80, 1996.

[27] Z Yan and H Zhang. *Phys. Lett. A*, 285:355, 2001.

[28] A A Mamun and P K Shukla. *J. Geophys. Res. Space Phys.*, 107:SIA–15, 2002.

[29] A A Mamun and P K Shukla. *Phys. Plasmas*, 9:1468, 2002.

[30] S Ghosh. *Phys. Plasmas*, 12:094504, 2005.

[31] A E Dubinov, I D Dubinova, and V A Gordienko. *Phys. Plasmas*, 13:082111, 2006.

[32] P Bandyopadhyay, G Prasad, A Sen, and P K Kaw. *Phys. Rev. Lett.*, 101:065006, 2008.

[33] E I El-Awady and W M Moslem. *Phys. Plasmas*, 18:082306, 2011.

[34] H Alfvén. *Cosmic plasma*, volume 82. Taylor & Francis, 1981.

[35] M Djebli and H Marif. *Phys. Plasmas*, 16:063708, 2009.

[36] G Livadiotis. *Kappa distributions: Theory and applications in plasmas*. Elsevier, 2017.

[37] J H Binsack. PhD thesis, Massachusetts Institute of Technology, 1966.

[38] S Olbert. In *Physics of the Magnetosphere*, page 641. Springer, 1968.

[39] V M Vasyliunas. *J. Geophys. Res.*, 73:2839, 1968.

[40] R L Mace and M A Hellberg. *Phys. Plasmas*, 2:2098, 1995.

[41] R L Mace, M A Hellberg, and R A Treumann. *J. Plasma Phys.*, 59:393, 1998.

[42] R L Mace, G Amery, and M A Hellberg. *Phys. Plasmas*, 6:44, 1999.

[43] M A Hellberg and R L Mace. *Phys. Plasmas*, 9:1495, 2002.

[44] A F Viñas, Richard L Mace, and Robert F Benson. *J. Geophys. Res. Space Phys.*, 110:A06202, 2005.

[45] T K Baluku and M A Hellberg. *Phys. Plasmas*, 15:123705, 2008.

[46] N S Saini, I Kourakis, and M A Hellberg. *Phys. Plasmas*, 16:062903, 2009.

[47] A Berbri and M Tribeche. *Phys. Plasmas*, 16:053703, 2009.

[48] A Berbri and M Tribeche. *Phys. Plasmas*, 16:053701, 2009.

[49] T K Baluku, M A Hellberg, I Kourakis, and N S Saini. *Phys. Plasmas*, 17:053702, 2010.

[50] G Livadiotis and D J McComas. *Astrophys. J.*, 741:88, 2011.

[51] S A El-Tantawy, N A El-Bedwehy, and W M Moslem. *Phys. Plasmas*, 18:052113, 2011.

[52] A Danehkar, N S Saini, M A Hellberg, and I Kourakis. *Phys. Plasmas*, 18:072902, 2011.

[53] T K Baluku and M A Hellberg. *Phys. Plasmas*, 19:012106, 2012.

[54] I Kourakis, S Sultana, and M A Hellberg. *Plasma Phys. Control. Fusion*, 54:124001, 2012.

[55] S Sultana, I Kourakis, and M A Hellberg. *Plasma Physics and Control. Fusion*, 54:105016, 2012.

[56] M A Hellberg, T K Baluku, F Verheest, and I Kourakis. *J. Plasma Phys.*, 79:1039, 2013.

[57] G Williams, F Verheest, M A Hellberg, M G M Anowar, and I Kourakis. *Phys. Plasmas*, 21:092103, 2014.

[58] P O Dovner, A I Eriksson, R Boström, and B Holback. *Geophys. Res. Lett.*, 21:1827, 1994.

[59] K Nishihara and M Tajiri. *J. Phys. Soc. Japan*, 50:4047, 1981.

[60] F Verheest and S R Pillay. *Phys. Plasmas*, 15:013703, 2008.

[61] A A Mamun, R A Cairns, and P K Shukla. *Phys. Plasmas*, 3:2610, 1996.

[62] T S Gill, P Bala, H Kaur, N S Saini, S Bansal, and J Kaur. *Eur. Phys. J. D*, 31:91, 2004.

[63] S V Singh and G S Lakhina. *Nonlinear Process. Geophys.*, 11:275, 2004.

[64] S R Pillay and F Verheest. *J. Plasma Phys.*, 71:177, 2005.

[65] A Das, A Bandyopadhyay, and K P Das. *Phys. Plasmas*, 16:073703, 2009.

[66] R Sabry, W M Moslem, and Padma Kant Shukla. *Phys. Plasmas*, 16:032302, 2009.

[67] H R Pakzad. *Phys. Lett. A*, 373:847–850, 2009.

[68] F Verheest, M A Hellberg, and T K Baluku. *Phys. Plasmas*, 19:032305, 2012.

[69] A Das, A Bandyopadhyay, and K P Das. *J. Plasma Phys.*, 78:149, 2012.

[70] A Das, A Bandyopadhyay, and K P Das. *J. Plasma Phys.*, 78:565, 2012.

[71] O R Rufai, R Bharuthram, S V Singh, and G S Lakhina. *Phys. Plasmas*, 21:082304, 2014.

[72] S V Singh and G S Lakhina. *Commun. Nonlinear Sci. Numer. Simul.*, 23:274, 2015.

[73] A Paul and A Bandyopadhyay. *Astrophys. Space Sci.*, 361:172, 2016.

[74] F Verheest and Manfred A Hellberg. *Phys. Plasmas*, 24:022306, 2017.

[75] A Paul, A Das, and A Bandyopadhyay. *Plasma Phys. Rep.*, 43:218, 2017.

[76] A Paul, A Das, and A Bandyopadhyay. *Plasma Phys. Rep.*, 43:218, 2017.

[77] A Paul and A Bandyopadhyay. *Indian J. Phys.*, 92:1187, 2018.

[78] Y Ghai, N S Saini, and B Eliasson. *Phys. Plasmas*, 25:013704, 2018.

[79] M R Collier, D C Hamilton, G Gloeckler, P Bochsler, and R B Sheldon. *Geophys. Res. Lett.*, 23:1191, 1996.

[80] M Maksimovic, V Pierrard, and J F Lemaire. *Astron. Astrophys.*, 324:725, 1997.

[81] R B Decker and S M Krimigis. *Adv. Space Res.*, 32:597, 2003.

[82] M P Leubner. *J. Geophys. Res. Space Phys.*, 88:469, 1983.

[83] V Pierrard, M Lazar, S Poedts, Š Štverák, M Maksimovic, and P M Trávníček. *Sol. Phys.*, 291:2165, 2016.

[84] E C Whipple, T G Northrop, and D A Mendis. *J. Geophys. Res.*, 90:7405, 1985.

[85] C K Goertz. *Rev. Geophys.*, 27:271, 1989.

[86] N N Rao, P K Shukla, and M Y Yu. *Planet. Space Sci.*, 38:543, 1990.

[87] F Verheest. *Planet. Space Sci.*, 40:1, 1992.

[88] N N Rao. *J. Plasma Phys.*, 53:317, 1995.

[89] P K Shukla. *Phys. Plasmas*, 8:1791, 2001.

[90] C R Choi, C-M Ryu, N C Lee, and D-Y Lee. *Phys. Plasmas*, 12:022304, 2005.

[91] R L Merlino. *Plasma Phys. Appl.*, 81:73, 2006.

[92] J R Asbridge, S J Bame, and I B Strong. *J. Geophys. Res.*, 73:5777, 1968.

[93] W C Feldman, R C Anderson, S J Bame, S P Gary, J T Gosling, D J McComas, M F Thomsen, G Paschmann, and M M Hoppe. *J. Geophys. Res.*, 88:96, 1983.

[94] R Boström, G Gustafsson, B Holback, G Holmgren, H Koskinen, and P M Kintner. *Phys. Rev. Lett.*, 61:82, 1988.

[95] R Lundin, A Zakharov, R Pellinen, H Borg, B Hultqvist, N Pissarenko, E M Dubinin, S W Barabash, I Liede, and H Koskinen. *Nature*, 341:609, 1989.

[96] R Boström. *IEEE Trans. Plasma Sci.*, 20:756, 1992.

[97] H Matsumoto, H Kojima, T Miyatake, Y Omura, M Okada, I Nagano, and M Tsutsui. *Geophys. Res. Lett.*, 21:2915, 1994.

[98] R E Ergun, C W Carlson, J P McFadden, F S Mozer, G T Delory, W Peria, C C Chaston, M Temerin, et al. *Geophys. Res. Lett.*, 25:2025, 1998.

[99] R E Ergun, C W Carlson, J P McFadden, F S Mozer, G T Delory, W Peria, C C Chaston, M Temerin, et al. *Geophys. Res. Lett.*, 25:2061, 1998.

[100] G T Delory, R E Ergun, C W Carlson, L Muschietti, C C Chaston, W Peria, J P McFadden, and R Strangeway. *Geophys. Res. Lett.*, 25:2069, 1998.

[101] J R Franz, P M Kintner, and J S Pickett. *Geophys. Res. Lett.*, 25:1277, 1998.

[102] C A Cattell, J Dombeck, J R Wygant, M K Hudson, F S Mozer, M A Temerin, W K Peterson, C A Kletzing, et al. *Geophys. Res. Lett.*, 26:425, 1999.

[103] R Pottelette, R E Ergun, R A Treumann, M Berthomier, C W Carlson, J P McFadden, and I Roth. *Geophys. Res. Lett.*, 26:2629, 1999.

[104] F Verheest. *Waves in Dusty Space Plasmas*. Dordrecht, Netherlands: Kluwer Academic, 2000.

[105] P K Shukla and A A Mamun. *Introduction to Dusty Plasma Physics*. Bristol, UK: IoP, 2002.

[106] Y Futaana, S Machida, Y Saito, A Matsuoka, and H Hayakawa. *J Geophys. Res.*, 108:SMP–15, 2003.

[107] J P McFadden, C W Carlson, R E Ergun, F S Mozer, L Muschietti, I Roth, and E Moebius. *J. Geophys. Res.*, 108:8018, 2003.

[108] N. F. Ness. *J. Geophys. Res.*, 70:2989, 1965.

[109] A A Abid, S Ali, J Du, and A A Mamun. *Phys. Plasmas*, 22:084507, 2015.

[110] M A Hellberg, R L Mace, T K Baluku, I Kourakis, and N S Saini. *Phys. Plasmas*, 16:094701, 2009.

[111] C R Choi, C M Ryu, N C Lee, D-Y Lee, and Y Kim. *Phys. Plasmas*, 12:072301, 2005.

[112] J J Podesta. *Phys. Plasmas*, 12:052101, 2005.

[113] A E Dubinov and D Y Kolotkov. *Plasma Phys. Rep.*, 38:909, 2012.

[114] F Verheest, M A Hellberg, and I Kourakis. *Phys. Rev. E*, 87:043107, 2013.

[115] F Verheest, M A Hellberg, and I Kourakis. *Phys. Plasmas*, 20:012302, 2013.

[116] F Verheest, G S Lakhina, and M A Hellberg. *Phys. Plasmas*, 21:062303, 2014.

[117] F Verheest. *J. Plasma Phys.*, 80:787, 2014.

[118] O R Rufai, R Bharuthram, S V Singh, and G S Lakhina. *Phys. Plasmas*, 22:102305, 2015.

[119] O R Rufai, R Bharuthram, S V Singh, and G S Lakhina. *Phys. Plasmas*, 23:032309, 2016.

[120] A E Dubinov and Dmitrii Y Kolotkov. *Rev. Mod. Plasma Phys.*, 2:1–46, 2018.

[121] P K Shukla and V P Silin. *Phys. Scr.*, 45:508, 1992.

[122] Y Chen and M Y Yu. *Phys. Plasmas*, 1:1868, 1994.

[123] S Maitra and R Roychoudhury. *Phys. Plasmas*, 13:112302, 2006.

[124] S Ghosh, S Sarkar, M Khan, and M R Gupta. *Phys. Scr.*, 63:395, 2001.

[125] P K Shukla and A A Mamun. *NJP*, 5:17, 2003.

[126] F Verheest, T Cattaert, and M A Hellberg. *Phys. Plasmas*, 12:082308, 2005.

[127] C R Choi, C-M Ryu, D-Y Lee, N C Lee, and Y-H Kim. *Phys. Lett. A*, 364.

[128] S Mahmood and S Hussain. *Phys. Plasmas*, 14:082303, 2007.

[129] P Chatterjee, T Saha, and C-M Ryu. *Phys. Plasmas*, 15:123702, 2008.

[130] T Saha and P Chatterjee. *Phys. Plasmas*, 16:013707, 2009.

[131] S K El-Labany, E F El-Shamy, and S A El-Warraki. *Phys. Plasmas*, 16:013703, 2009.

[132] S K El-Labany, M Shalaby, E F El-Shamy, and L S El-Sherif. *Planet. Space Sci.*, 57:1246, 2009.

[133] M Shahmansouri and H Alinejad. *Phys. Plasmas*, 19:123701, 2012.

[134] M Adnan, S Mahmood, and A Qamar. *Contrib. Plasma Phys.*, 54:724, 2014.

[135] B Sahu, A Sinha, and R Roychoudhury. *Phys. Plasmas*, 21:103701, 2014.

[136] M Sayyar, H Zahed, S J Pestehe, and S Sobhanian. *Phys. Plasmas*, 23:073704, 2016.

[137] S A El-Tantawy. *Astrophys. Space Sci.*, 361:1, 2016.

[138] A. Paul and A. Bandyopadhyay. *Astrophys. Space Sci.*, 361:172, 2016.

[139] A. Paul, A. Das, and A. Bandyopadhyay. *Plasma Phys. Rep.*, 43:218, 2017.

[140] A. Paul, A. Bandyopadhyay, and K. P. Das. *Phys. Plasmas*, 24:013707, 2017.

[141] A. Das, A. Bandyopadhyay, and K. P. Das. *Phys. Plasmas*, 16:073703, 2009.

[142] A. E. Dubinov and D. Y. Kolotkov. *Plasma Phys. Rep.*, 38:909, 2012.

[143] A Hasegawa and T Sato. *Phys. Fluids*, 25:632, 1982.

[144] S Baboolal, R Bharuthram, and M A Hellberg. *J. Plasma Phys.*, 40.

[145] R Bharuthram and P K Shukla. *Planet. Space Sci.*, 40:973, 1992.

[146] R A Cairns, R Bingham, R O Dendy, C M C Nairn, P K Shukla, and A A Mamun. *J. de Physique*, 5:C6–43, 1995.

[147] S I Popel, M Y Yu, and V N Tsytovich. *Phys. Plasmas*, 3:4313, 1996.

[148] A A Mamun, R A Cairns, and P K Shukla. *Phys. Plasmas*, 3:702, 1996.

[149] A A Mamun. *Phys. Rev. E*, 55:1852, 1997.

[150] S K Maharaj, S R Pillay, R Bharuthram, S V Singh, and G S Lakhina. *Phys. Scr.*, T113:135, 2004.

[151] M Marklund, B Eliasson, and P K Shukla. *Phys. Rev. E*, 76:067401, 2007.

[152] S Ali, W M Moslem, P K Shukla, and R Schlickeiser. *Phys. Plasmas*, 14:082307, 2007.

[153] W F El-Taibany and M Wadati. *Phys. Plasmas*, 14:103703, 2007.

[154] S Ghosh and R Bharuthram. *Astrophys. Space Sci.*, 314:121, 2008.

[155] P Chatterjee and K Roy. *Z. Naturforsch. A*, 63:393, 2008.

[156] E I El-Awady, S A El-Tantawy, W M Moslem, and P K Shukla. *Phys. Lett. A*, 374:3216, 2010.

[157] M Tribeche and L Djebarni. *Phys. Plasmas*, 17:124502, 2010.

[158] H R Pakzad and M Tribeche. *Astrophys. Space Sci.*, 330:95, 2010.

[159] M Tribeche and A Merriche. *Phys. Plasmas*, 18:034502, 2011.

[160] O R Rufai, R Bharuthram, S V Singh, and G S Lakhina. *Phys. Plasmas*, 19:122308, 2012.

[161] A E Dubinov and D Y Kolotkov. *IEEE Trans. Plasma Sci.*, 40:1429, 2012.

[162] A E Dubinov and D Y Kolotkov. *Plasma Phys. Rep.*, 38:909, 2012.

[163] A E Dubinov and D Y Kolotkov. *High Energy Chem.*, 46:349, 2012.

[164] S V Singh, S Devanandhan, G S Lakhina, and R Bharuthram. *Phys. Plasmas*, 20:012306, 2013.

[165] A Paul, A Bandyopadhyay, and K P Das. *Phys. Plasmas*, 24:013707, 2017.

[166] Sandip Dalui, Sankirtan Sardar, and Anup Bandyopadhyay. *Zeitschrift für Naturforschung A*, 76:455, 2021.

[167] F Verheest and M A Hellberg. *Phys. Plasmas*, 17:023701, 2010.

[168] T K Baluku, M A Hellberg, and F Verheest. *Europhys. Lett.*, 91:15001, 2010.

[169] F Verheest and M A Hellberg. *Phys. Plasmas*, 22:012301, 2015.

[170] A Paul, A Bandyopadhyay, and K P Das. *Plasma Phys. Rep.*, 45:466, 2019.

[171] H Alfvén. *Cosmic plasma*, volume 82. D. Reidel Publishing Company, Dordrecht, Holland, 1981.

[172] M Temerin, K Cerny, W Lotko, and F S Mozer. *Phys. Rev. Lett.*, 48:1175, 1982.

[173] F S Mozer, R Ergun, M Temerin, C Cattell, J Dombeck, and J Wygant. *Phys. Rev. Lett.*, 79:1281, 1997.

[174] R E Ergun, C W Carlson, J P McFadden, F S Mozer, L Muschietti, I Roth, and R J Strangeway. *Phys. Rev. Lett.*, 81:826, 1998.

[175] K Aoutou, M Tribeche, and Taha H Zerguini. *Phys. Plasmas*, 15:013702, 2008.

[176] S Younsi and M Tribeche. *Phys. Plasmas*, 15:073706, 2008.

[177] A E Dubinov and D Y Kolotkov. *IEEE Trans. Plasma Sci.*, 40:1429, 2012.

[178] R Sabry, W M Moslem, E F El-Shamy, and P K Shukla. *Phys. Plasmas*, 18:032302, 2011.

[179] S Sardar, A Bandyopadhyay, and K P Das. *Phys. Plasmas*, 23:073703, 2016.

[180] S Sardar, A Bandyopadhyay, and K P Das. *Phys. Plasmas*, 23:123706, 2016.

[181] A Barkan, Robert L Merlino, and N Dangelo. *Phys. Plasmas*, 2:3563, 1995.

[182] J B Pieper and J Goree. *Phys. Rev. Lett.*, 77:3137, 1996.

[183] F B Rizzato. *J. Plasma Phys.*, 40:289, 1988.

[184] S H Cho, H J Lee, and Y S Kim. *Phys. Rev. E*, 61:4357, 2000.

[185] P K Shukla, J T Mendonca, and R Bingham. *Phys. Scr.*, T113:133, 2004.

[186] P K Shukla and M Marklund. *Phys. Scr.*, T113:36, 2004.

[187] I Kourakis, F Verheest, and N F Cramer. *Phys. Plasmas*, 14:022306, 2007.

[188] S A Khan and W Masood. *Phys. Plasmas*, 15:062301, 2008.

[189] T S Gill, A S Bains, and N S Saini. *Can. J. Phys.*, 87:861, 2009.

[190] A E Dubinov, D Y Kolotkov, and M A Sazonkin. *Tech. Phys.*, 57:585, 2012.

[191] N Roy, S Tasnim, and A A Mamun. *Phys. Plasmas*, 19:033705, 2012.

[192] M Ferdousi, S Sultana, and A A Mamun. *Phys. Plasmas*, 22:032117, 2015.

[193] U N Ghosh, A Saha, N Pal, and P Chatterjee. *J. Theor. Appl. Phys.*, 9:321, 2015.

[194] A Atteya, M A El-Borie, G D Roston, and A S El-Helbawy. *J. Taibah Univ. Sci.*, 14:1182, 2020.

[195] M Lontano, S V Bulanov, J Koga, M Passoni, and T Tajima. *Phys. Plasmas*, 9:2562, 2002.

[196] A E Dubinov and A A Dubinova. *Plasma Phys. Rep.*, 34:403, 2008.

[197] A E Dubinov, A A Dubinova, and M A Sazonkin. *J. Commun. Technol. Electron.*, 55:907, 2010.

[198] E F El-Shamy, M M Selim, A El-Depsy, M O Abdellahi, O Al-Hagan, A Al-Mogeeth, and L Alelyani. *Phys. Plasmas*, 27:032101, 2020.

[199] El-Depsy A and Selim M M. *IEEE Tran. Plasma Sci.*, 44:2901, 2016.

Debdatta Debnath.
15/02/2022